Geological Survey of Canada
Commission géologique du Canada

BULLETIN 376

STRATIGRAPHY, METAMORPHISM, STRUCTURE, AND THEIR TECTONIC IMPLICATIONS IN THE SIFTON AND DESERTERS RANGES, CASSIAR AND NORTHERN ROCKY MOUNTAINS, NORTHERN BRITISH COLUMBIA

C.A. Evenchick

Canada

1988

GEOLOGICAL SURVEY OF CANADA
BULLETIN 376

STRATIGRAPHY, METAMORPHISM, STRUCTURE, AND THEIR TECTONIC IMPLICATIONS IN THE SIFTON AND DESERTERS RANGES, CASSIAR AND NORTHERN ROCKY MOUNTAINS, NORTHERN BRITISH COLUMBIA

C.A. Evenchick

1988

Energy, Mines and Resources Canada

Énergie, Mines et Ressources Canada

Available in Canada through

authorized bookstore agents and other bookstores

or by mail from

Canadian Government Publishing Centre
Supply and Services Canada
Ottawa, Canada K1A 0S9

and from

Geological Survey of Canada offices:

601 Booth Street
Ottawa, Canada K1A 0E8

3303-33rd Street N.W.,
Calgary, Alberta T2L 2A7

100 West Pender Street,
Vancouver, B.C. V6B 1R8

A deposit copy of this publication is also available for reference in public libraries across Canada

Cat. No. M42-376E Canada: $13.00
ISBN 0-660-12882-9 Other countries: $15.60

Price subject to change without notice

Critical Reader
H. Gabrielse

Original manuscript submitted-1986-03
Final version approved for publication-1987-05

Préface

Systematic 1:250 000 scale mapping by officers of the Geological Survey through the 1960s and 1970s revealed that the Northern Rocky Mountain Trench, a major geological feature of the Canadian Cordillera, is part of a system of dextral strike-slip faults. The trench is the locus of hundreds of kilometres of dextral strike-slip fault movement.

The Sifton and Deserters ranges on both sides of the trench were studied by Dr. Evenchick to determine the amount and timing of displacement on faults in the trench, and to compare and contrast the geology across the trench. Her report provides the first detailed account of stratigraphy of the Windermere Supergroup in the northern Rocky Mountains; the significance of basement gneiss and Windermere stratigraphy to Proterozoic tectonics; and the Mesozoic and Cenozoic metamorphic and structural evolution. An analysis of detailed and regional structures has led to a new conceptual model for the transfer of displacement from one transcurrent fault to another that is applicable to other major strike-slip fault systems in the world.

R.A. Price
Assistant Deputy Minister
Geological Survey of Canada

Préface

La cartographie systématique à l'échelle de 1/250 000 entreprise par le personnel de la Commission géologique dans les années 60 et 70 a révélé que le sillon des Rocheuses du Nord, un élément géologique d'envergure de la Cordillère canadienne, fait partie d'un système de décrochements dextre. Le sillon représente le foyer de centaines de kilomètres de déplacement horizontal dextre.

M^{me} Evenchick a étudié les chaînons Sifton et Deserters de part et d'autre du sillon en vue de déterminer l'ampleur et la chronologie du déplacement le long des failles dans le sillon, et de comparer et de contraster la géologie en travers du sillon. Son rapport présente la première étude détaillée de la stratigraphie du supergroupe de Windermere dans la partie nord des Rocheuses, de la contribution du socle gneissique et de la stratigraphie du Windermere à la tectonique protérozoïque, et de l'évolution structurale et métamorphique au cours du Cénozoïque et du Mésozoïque. L'analyse des structures détaillées et régionales a permis d'élaborer un nouveau modèle théorique du transfert du déplacement d'une faille transverse à l'autre, qui peut également s'appliquer aux autres grands systèmes de décrochements du monde.

R.A. Price, sous-ministre adjoint
Commission géologique du Canada

CONTENTS

Figures

Tables

Frontispiece

Camp in the southern Sifton Ranges viewed to the south. The ridge on the right is well layered metaquartzite and amphibolite of unit HIqa, in the hanging wall of the Sifton Fault; the blocky weathering ridges on the left are part of an undeformed Eocene granite body (Balourdet Pluton) that intrudes the Sifton Fault. (GSC 204482-A)

STRATIGRAPHY, METAMORPHISM, STRUCTURE, AND THEIR TECTONIC IMPLICATIONS IN THE SIFTON AND DESERTERS RANGES, CASSIAR AND NORTHERN ROCKY MOUNTAINS, NORTHERN BRITISH COLUMBIA

Abstract

Deserters Range, in the Foreland Belt of the Canadian Cordillera, flanks the Northern Rocky Mountain Trench (NRMT) at 57°N. The Sifton Ranges in the Omineca Belt, flank the NRMT at 58°N. In both ranges, crystalline basement is overlain by complexly deformed metasediments of the Upper Proterozoic Windermere Supergroup. In the Sifton Ranges the age of the basement (1.85 Ga) indicates that pre-Windermere strata were uplifted and eroded prior to Windermere sedimentation. In Deserters Range the age of the basement (728 Ma), and its nonconformable relationship with overlying strata indicate a period of uplift and erosion prior to Windermere sedimentation. The data support a model of late Proterozoic uplift, rifting, sedimentation, and volcanic activity younger than 728 Ma.

Mineral assemblages and geothermobarometry for both ranges indicate amphibolite facies metamorphism. Synmetamorphic deformation resulted in a strong foliation parallel with the bedding which, in the Sifton Ranges, is isoclinally folded.

Movement on the gently-dipping Sifton Fault, in the Sifton Ranges, postdates the peak of metamorphism (mid-Jurassic(?)), and predates the intrusion of an Eocene pluton. It is interpreted to be a contraction fault, and the lineations, shear bands, sheath folds, and analysis of minor folds which are dispersed about a gently-dipping great circle collectively indicate top-to-the-south-southeast displacement. The south-southeast direction of contraction contrasts with the northeast regional contraction characteristic of the Omineca and Foreland belts, and can be explained by a model which relates the Sifton Fault kinematically to dextral transcurrent faults in the region. The Sifton Fault is interpreted to be a ramp that accommodated convergence south-southeast of a left-stepping bend in a dextral transcurrent fault.

Résumé

Le chaînon Deserters, dans la zone de l'avant-pays de la Cordillière canadienne, longe le sillon des Rocheuses du Nord à 57° de latitude nord. Les chaînons Sifton dans la zone d'Ominéca longent le sillon à 58° de latitude nord. Le socle cristallin dans les deux chaînons repose sous les métasédiments fortement déformés du supergroupe de Windermere du Protérozoïque supérieur. D'après l'âge du socle (1,85 Ga) dans les chaînons Sifton, les couches qui ont précédé le Windermere auraient été soulevées et érodées avant le Windermere. Dans le chaînon Deserters, l'âge du socle (728 Ma) et le fait que les couches sus-jacentes y reposent en discordance révèlent qu'une période de soulèvement et d'érosion a précédé la sédimentation du Windermere. Les données portent à croire qu'il y a eu soulèvement, création de fossés, sédimentation et activité volcanique au cours du Protérozoïque récent, il y a moins de 728 Ma.

Les associations minérales et la géothermobarométrie des deux chaînons attestent d'un métamorphisme caractérisé par le faciès des amphibolites. La déformation synmétamorphique a produit une foliation marquée, parallèle à la stratification, qui, dans les chaînons Sifton, est déformée en plis isoclinaux.

Dans les chaînons Sifton, le mouvement le long de la faille de Sifton a eu lieu après l'apogée du métamorphisme (milieu du Jurassique(?)), et avant l'intrusion d'un pluton éocène. La faille du Sifton, à pendage faible, serait une faille de contraction, et l'ensemble des linéations, des zones cisaillées et des plis en gaine, ainsi que l'analyse des plis mineurs dispersés autour d'un grand cercle à pendage faible, indiquent que son compartiment supérieur s'est déplacé vers le sud-sud-est. La contraction vers le sud-sud-est s'oppose à la contraction régionale vers le nord-est qui caractérise la zone d'Oménica et celle de l'avant-pays et s'explique au moyen d'un modèle qui établit un lien cinématique entre la faille de Sifton et les failles transverses dextres trouvées dans la région. La faille de Sifton représenterait une rampe le long de laquelle il y a eu convergence vers le sud-sud-est à partir d'une inflexion vers la gauche dans une faille transverse dextre.

SUMMARY

Deserters Range, in the Foreland Belt of the Canadian Cordillera, flanks the Northern Rocky Mountain Trench (NRMT) at 57°N. The Sifton Ranges in the Omineca Belt, flank the NRMT at 58°N. These areas were chosen for study because they provide an opportunity to compare the geology on both sides of the trench, which is the locus of hundreds of kilometres of dextral strike-slip displacement.

Stratigraphy

In both ranges, crystalline basement dated by U-Pb zircon geochronology is overlain by complexly deformed greenschist and amphibolite facies metasediments assigned to the Upper Proterozoic Windermere Supergroup.

Deserters Range

Basement rocks and metasediments occur in a structural culmination which exposes the lowest stratigraphic level east of the Northern Rocky Mountain Trench and north of the gneiss along the Southern Rocky Mountain Trench 650 km to the southeast. The rocks occur in an east-facing inclined anticline, revealing from west to east, a section from basement rocks through the Misinchinka Group to Cambrian strata. The basement (728 Ma) is granitoid, and is overlain nonconformably by pebble-conglomerate at the base of 200 m of metaquartzite. The metaquartzite is overlain by 400 m of amphibolite intercalated with metaquartzite, followed by a unit of pelitic schist and metaquartzite, and a unit of marble and metaquartzite. The distinctive marble and metaquartzite unit is overlain by amphibole-chlorite schist with minor pelitic schist, calcareous chlorite schist, psammite, marble, and metadiamictite. The overlying unit of resistant impure metaquartzite is 30 to 80 m thick and is overlain by 1000 to 1500 m of amphibole-chlorite schist, metadiamictite in a matrix of chlorite schist, and marble. The overlying Chowika Formation is the most distinctive marker in the Deserters Range. It is 150 m of pure marble that is resistant to weathering and can be easily traced on air photographs. The Chowika Formation is overlain by at least 700 m of recessive green, grey and black chlorite-sericite phyllite with minor resistant members of marble, metaconglomerate, and metasandstone. At the eastern boundary of the study area, the phyllite is overlain by metaquartzite and archaeocyathid-bearing marble of the Lower Cambrian Gog Group.

Sifton Ranges

In the Sifton Ranges, three stratigraphic assemblages with characteristics typical of the Ingenika Group are separated by two faults. Strata in the northwest part of the area are exposed in a gently south-plunging anticline. The area is separated from the main part of the Sifton Ranges to the east by a normal fault. The

SOMMAIRE

Le chaînon Deserters, dans la zone de l'avant-pays de la Cordillère canadienne, longue le sillon des Rocheuses du nord à 57° de latitute nord. Les chaînons Sifton dans la zone d'Oménica longent le sillon à 58° de latitute nord. Ces régions ont été étudiées car elles permettent de comparer la géologie de part et d'autre du sillon, qui représente le foyer de centaines de kilomètres de déplacement horizontal dextre.

Stratigraphie

Dans les deux chaînons, le socle cristallin, dont l'âge a été établi par la datation à l'U-Pb du zircon, repose sous des métasédiments très déformés du faciès des amphibolites et des schistes verts, qui font partie du supergroupe de Windermere du Protérozoïque supérieur.

Chaînon Deserters

Les roches du socle et les métasédiments se trouvent dans une culmination, dans laquelle le niveau stratigraphique inférieur affleure à l'est du sillon des Rocheuses du Nord et au nord du gneiss le long du sillon des Rocheuses du Sud, à 650 kilomètres vers le sud-est. Les roches se trouvent dans un anticlinal incliné, orienté vers l'est, où affleurent, d'ouest en est, une section exposant les roches du socle jusqu'au groupe de Misinchinka inclus puis jusqu'aux couches cambriennes. Le socle granitoïde, qui date de 728 Ma, est recouvert en discordance par un conglomérat à galets qui se trouve au pied d'un métaquartzite de 200 m d'épaisseur. Le métaquartzique est sous-jacent à 400 m d'amphibolite avec du métaquartzite; viennent ensuite une unité de schiste ardoisier et de métaquartzite et une unité de marbre et de métaquartzite. L'unité distinctive de marbre et de métaquartzite est sous-jacente à un schiste à amphibole et à chlorite qui contient de faibles quantités de schiste ardoisier, de chloritoschiste calcaire, de psammite, de marbre et de diamictite métamorphique. L'épaisseur de l'unité sus-jacente de métaquartzique impur résistant varie de 30 à 80 m; cette unité repose sous du schiste à amphibole et à chlorite, de la diamictite métamorphique à matrice de chloritoschiste et du marbre, l'épaisseur du tout variant de 1 000 à 5 000 m. La formation sus-jacente de Chowika est le niveau repère le plus distinctif du chaînon Deserters. Elle se compose de marbre pur résistant d'une épaisseur de 150 m que l'on retrouve facilement dans les photographies aériennes. La formation de Chowika est sous-jacente à au moins 700 m de phyllade à chlorite et à séricite noire, grise et verte, à caractère récessif; on y trouve également des termes résistants peu importants de marbre, de métaconglomérat et de métagrès. À la limite est de la zone étudiée, la phyllade repose sous du quartzite métamorphique et du marbre à archaeocyathidés du groupe de Gog du Cambrien inférieur.

Chaînons Sifton

Dans les chaînons Sifton, trois ensembles stratigraphiques ayant les caractéristiques du groupe d'Ingenika sont séparés les uns des autres par deux failles. Les couches dans la partie nord-ouest de la région affleurent dans un anticlinal qui plonge doucement vers le sud. Une faille normale sépare la région de la partie principale des chaînons Sifton, vers l'est. La faille de Sifton, à pendage faible, divise la partie principale des chaînons en deux: une

main part of the Sifton Ranges is divided by the gently-dipping Sifton Fault into a northern part in the footwall of the fault, and a southern part in the hanging wall of the fault.

In the northwest part of the Sifton Ranges, the base of the sequence is at least 1200 m of quartzofeldspathic metagrit of the Swannell Formation. It is overlain by the Tsaydiz Formation, consisting of 200 m of recessive green phyllite with a sandy marble member near the base. Phyllite of the Tsaydiz Formation is abruptly overlain by the 15 to 25 m of pure marble assigned to the Espee Formation, which is in turn overlain by a unit of metasiltstone and marble 300 to 350 m thick called the Stelkuz Formation. The lower member of the Stelkuz Formation is laminated metasiltstone overlain by 15 m of grey marble and chlorite phyllite interbedded with sandy dolomite marble. The middle member is chlorite phyllite with minor siltstone, and the upper member is dominantly laminated metasiltstone, grading up into metaquartzite of the Lower Cambrian Boya Formation. The Boya Formation is 1 to 3 m thick and is overlain by 20 to 25 m of marble of the Rosella Formation. The Boya and Rosella formations comprise the Lower Cambrian Atan Group, which is overlain by phyllite, calcareous phyllite, and marble of the Cambro-Ordovician Kechika Group.

Strata in the northern part of the Sifton Ranges are exposed in a doubly-plunging antiform (Sifton Antiform) that is truncated by the overlying Sifton Fault. The structurally lowest unit is rusty weathering metaquartzite and pelitic schist. It is overlain by a unit of paragneiss that ranges from 200 to 900 m thick. The paragneiss unit is overlain by pure marble and calc-silicate rock 65 m thick, which grades up into a unit of pelitic schist 150 to 400 m thick. The relatively fine grained clastic units of the lower part of the sequence are overlain by 400 to 1200 m of quartzofeldspathic metagrit, psammite, quartz-pebble conglomerate, pelitic schist, and psammitic schist. The structurally highest unit consists of 200 m of impure marble, psammite, and minor quartzofeldspathic grit.

Rocks in the hanging wall of the Sifton Fault are highly strained and comprise a gently-dipping fault zone in which the apparent stratigraphy is to some extent of tectonic origin. Restoration of the following stratigraphic sequence is based on comparisons with the general Windermere sequence elsewhere in the region and on the inference that 1.85 Ga orthogneiss is basement to the succession. The orthogneiss occurs in the south end of the Sifton Ranges, and forms the core of a north-plunging anticline. It is structurally overlain by an extensive unit of metaquartzite and amphibolite about 1000 m thick. A unit of highly strained schist, psammite, marble and rare amphibolite structually underlies the metaquartzite/amphibolite formation in northern exposures, and is inferred to structually overlie it in the south.

partie nord dans la lèvre inférieure de la faille, et une partie sud dans la lèvre supérieure de la faille.

Dans la partie nord-ouest des chaînons Sifton, la base de la séquence se compose d'au moins 1 200 m de métasable silicofeldspathique de la formation de Swannell. Elle est sous-jacente à la formation de Tsaydiz, qui se compose de phyllade verte récessive sur une épaisseur de 200 m, avec un niveau de marbre sablonneux près de la base. La phyllade de la formation de Tsaydiz repose en discordance sous du marbre pur dont l'épaisseur varie de 15 à 25 m; le marbre, qui fait partie de la formation d'Espee, est sous-jacent à la formation de Stelkuz, qui se compose d'aleurolite métamorphique et de marbre et dont l'épaisseur est de 300 à 350 m. Le niveau inférieur de la formation de Stelkuz est une aleurolite métamorphique laminée qui repose sous 15 m de marbre gris et de phyllade chloriteuse avec des interstratifications de marbre dolomitique sablonneux. Le niveau intermédiaire est une phyllade chloriteuse avec de faibles quantités d'aleurolite, tandis que le terme supérieur se compose surtout d'aleurolite métamorphique laminée, qui se transforme vers le haut en métaquartzite de la formation de Boya du Cambrien inférieur. La formation de Boya, dont l'épaisseur varie de 1 à 3 m, est sous-jacente à entre 20 et 25 m de marbre de la formation de Rosella. Les formations de Boya et de Rosella forment le groupe d'Atan du Cambrien inférieur; ce groupe est sous-jacent au groupe cambro-ordovicien de Kechika qui se compose de phyllade, de phyllade calcaire et de marbre.

Les couches dans la partie nord de chaînons Sifton affleurent dans un antiform à plongement double (antiform de Sifton) qui est tronqué par la faille sus-jacente de Sifton. L'unité structuralement inférieure se compose de métaquartzite et de schiste ardoisier aux surfaces altérées rouillées. Elle est sous-jacente à une unité de paragneiss dont l'épaisseur varie de 200 à 900 m, qui repose sous une unité de marbre pur et de roche à silicate de calcium dont l'épaisseur est de 65 m. Cette dernière se transforme vers le haut en une unité de schiste ardoisier dont l'épaisseur varie de 150 à 400 m. Les unités clastiques à grain relativement fin de la partie inférieure de la séquence reposent sous du métasable quartzofeldspathique, de la psammite, du conglomérat à galets de quartz, du schiste pélitique et du micaschiste psammitique, l'épaisseur de l'ensemble variant de 400 à 1 200 m. L'unité structuralement la plus élevée se compose de marbre impur, de psammite et de faibles quantités de sable quartzofeldspathique; son épaisseur est de 200 m.

Les roches de la lèvre supérieure de la faille de Sifton sont fortement surtendues et forment une zone de failles à pendage faible dans laquelle la stratigraphie apparente aurait une origine en partie tectonique. La reconstitution de la séquence stratigraphique suivante se fonde sur des comparaisons de l'ensemble de la séquence de Windermere ailleurs dans la région et sur la supposition que l'orthogneiss de 1,85 Ga d'années représente le socle sous la séquence. L'orthogneiss se trouve dans l'extrémité sud des chaînons Sifton et forme le noyau d'un anticlinal à plongement vers le nord. Il est structuralement sous-jacent à une vaste unité de métaquartzite et d'amphibolite dont l'épaisseur est d'environ 1 000 m. Une unité de schiste surtendu, de psammite et de marbre, dans laquelle on retrouve rarement de l'amphibolite, est structuralement sous-jacente à la formation de métaquartzite/amphibolite dans les affleurements au nord; cette unité serait structuralement sus-jacente à la formation, dans le sud de la région. L'unité tectonique inférieure de la lèvre supérieure est

The lowest structural unit in the hanging wall is muscovite-chlorite-garnet schist with anastomosing foliations that result in wavy lenses of schist about 1 cm thick; it is inferred to be the highest stratigraphic unit.

Cenozoic rocks

The basement gneiss and metaquartzite/ampibolite unit in the southern Sifton Ranges are intruded by an undeformed biotite granite pluton. Biotite from the pluton has been dated by the K-Ar method at 41.6 Ma. Pegmatite dykes, also with Eocene K-Ar ages, intrude the footwall and hanging wall of the Sifton Fault. Lamprophyre dykes cut all formations in the Sifton Ranges, and the granite pluton at the south end of the range. A K-Ar age on biotite from a lamprophyre dyke that cuts the hanging wall is 37.8 Ma.

The Sifton Formation consists of nonmarine sandstone and poorly sorted massive, or crudely layered pebble to boulder conglomerate. It occurs along the two fault zones bounding the Sifton Ranges.

Age and tectonic implications of the Windermere Supergroup and its basement

An age of 1.85 Ga for orthogneiss basement in the Sifton Ranges indicates that Middle and possibly some Upper Proterozoic rocks were removed by uplift and erosion in pre — and early Windermere time. Detrital zircons with inherited U-Pb ages of about 2 Ga in metasediments of the Yukon Tanana Terrane (Alaska), and in feldspathic grits of the Windermere Supergroup in the Cassiar-Omineca and Cariboo mountains suggest widespread exposure of Early Proterozoic gneiss in the Late Proterozoic; the gneisses may have been a major source for the Windermere Supergroup. Granitic basement (728 Ma) east of the Northern Rocky Mountain Trench, in Deserters Range, is overlain nonconformably by the Windermere Supergroup. In the northern Rocky Mountains, swarms of northerly-trending diabase dykes of probable early Windermere age cut thick pre-Windermere strata and demonstrate Late Proterozoic extension. These data support a model of Late Proterozoic uplift, rifting, sedimentation, and volcanic activity at least locally (in Deserters Range) younger than 728 Ma.

Metamorphism

Metamorphism in the Deserters and Sifton ranges is postulated to be mid-Mesozoic by comparison with other parts of the core zone of the Omineca Belt that have been dated radiometrically. The variety of metamorphic grade and the distribution of isograds in both ranges are inferred to be largely the result of postmetamorphic upright folding which provides structural and metamorphic relief. The Deserters

un schiste à muscovite, à chlorite et à grenat caractérisé par des foliations anastomosées qui produisent des lentilles onduleuses de schiste d'environ 1 cm d'épaisseur; on déduit qu'il s'agit de l'unité stratigraphique la plus élevée.

Roches cénozoïques

Un pluton de granite à biotite non déformé coupe le socle gneissique et l'unité de métaquartzite/amphibolite dans la partie sud des chaînons Sifton. La datation de K-Ar de la biotite tirée du pluton donne un âge de 41,6 Ma. Des filons de pegmatite, qui selon la datation au K-Ar dateraient de l'Éocène, font intrusion dans les lèvres supérieure et inférieure de la faille de Sifton. Des filons de lamprophyre coupent toutes les formations dans les chaînons Sifton, ainsi que le pluton de granite à l'extrémité sud du chaînon. La datation au K-Ar de la biotite tirée d'un filon de lamprophyre qui fait intrusion dans la lèvre supérieure donne un âge de 37,8 Ma.

La formation de Sifton se compose de grès d'origine non marine et de conglomérat à galets ou à gros blocs grossièrement stratifié ou massif et mal trié, également d'origine non marine. Cette formation se trouve le long des deux zones de failles en bordure des chaînons Sifton.

Âge et importance tectonique du supergroupe de Windermere et de son socle

Le socle d'orthogneiss des chaînons Sifton date de 1,85 Ga, ce qui porte à croire que les roches du Protérozoïque moyen ainsi que certaines roches du Protérozoïque supérieur ont été enlevées par soulèvement et érosion avant l'accumulation du Windermere et au début de celle-ci. La datation à l'U-Pb de zircons détritiques tirés des métasédiments du terrane de Tanana au Yukon (Alaska) et des sables feldspathiques du supergroupe de Windermere dans les monts Cassiar-Ominéca et Cariboo, donne des âges d'environ 2 Ga; les gneiss du Protérozoïque inférieur auraient donc affleuré sur de vastes étendues au cours du Protérozoïque supérieur et pourraient avoir contribué pour une grande partie des sédiments du supergroupe de Windermere. Le socle granitique (728 Ma) à l'est du sillon des Rocheuses du Nord, dans le chaînon Deserters, repose en discordance sous le supergroupe de Windermere. Dans la partie nord des Rocheuses, des essaims de filons de diabase à orientation nord, qui dateraient du début du Windermere, ont fait intrusion dans des couches épaisses antérieures au Windermere et représentent une extention du Protérozoïque supérieur. Ces données appuient un modèle de soulèvement, de création de fossés, de sédimentation et d'activité volcanique au cours du Protérozoïque supérieur qui, à certains endroits (dans le chaînon Deserters), dateraient de moins de 728 Ma.

Métamorphisme

Une comparaison avec d'autres parties du noyau de la zone d'Ominéca qui ont été datées par radiométrie porte à croire que le métamorphisme dans les chaînons Deserters et Sifton daterait du milieu du Mésozoïque. Les différents degrés de métamorphisme et la répartition des isogrades dans les deux chaînons résulteraient en grande partie de la formation postmétamorphique de plis droits qui fournissent un relief structural et métamorphique. Les roches les plus fortement métamorphisées des Rocheuses du

Range has the highest grade rocks in the northern Rocky Mountains, and the Sifton Ranges have some of the highest grade metapelites in the northern Omineca Belt. Isolated uplift in the Eocene, which followed the regional Cretaceous uplift experienced by much of the northern Omineca Belt, may provide an explanation for the relatively high grade in the Sifton Ranges.

Deserters Range

Metamorphic grade in Deserters Range is lowest in the east at the highest stratigraphic and structural levels, and increases to the west to the Northern Rocky Mountain Trench, where the lowest stratigraphic and structural levels occur. The pelitic mineral assemblages define five metamorphic zones bounded by two mineral isograds and two reaction isograds. The sequence of zones is: chlorite; biotite; garnet; staurolite — biotite; and kyanite — garnet — biotite. Chloritoid first appears in the chlorite zone. Muscovite, plagioclase, and quartz are present in all assemblages. Phyllite and schist in all zones have a strong foliation that is folded. The growth of phyllosilicates is defined as syn-D1. The textures in thin section from each zone suggest that the growth of garnet cores was syn-D1 and the growth of other porphyroblasts and garnet rims was postkinematic with respect to D1, indicating that metamorphism outlasted D1. A phase of deformation (D2) after the peak of metamorphism crenulated the phyllosilicates that define the S1 foliation, kinked the kyanites, and folded the isograds along with formation contacts on a large scale. A geothermobarometric study of the highest grade rocks yielded temperatures and pressures of about 530°C, and 7 to 8 kb. These data are consistent with the conditions of metamorphism suggested by the pelitic mineral assemblages.

Sifton Ranges

In the northern Sifton Ranges, metamorphic grade increases eastward from chlorite zone in the northwest, to sillimanite zone in the core of the Sifton Antiform. The highest grade isograds are truncated by the Sifton Fault, which has staurolite zone rocks in its immediate hanging wall.

Pelitic mineral assemblages in the footwall of the Sifton Fault define six metamorphic zones separated by a mineral isograd, three reaction isograds, and a fault. The kyanite — sillimanite reaction isograd occurs over a mappable volume and is mapped as a seventh metamorphic zone. The sequence of zones is: chlorite; garnet; staurolite — biotite; kyanite — garnet — biotite; sillimanite — kyanite; sillimanite; and sillimanite — K-feldspar. All assemblages include muscovite, plagioclase, and quartz. Poorly defined snowball textures in garnets are a result of synmetamorphic deformation (defined as D1). The phyllosilicates that define the foliation are either early-, syn — or late-D1. Isoclinal folding and metamorphism were followed by postmetamorphic

Nord se trouvent dans le chaînon Deserters, tandis que les pélites métamorphiques les plus fortement métamorphisées dans la partie nord de la zone d'Ominéca se trouvent dans les chaînons Sifton. Le degré de métamorphisme relativement élevé que l'on trouve dans les chaînons Sifton pourrait être dû à une période de soulèvement isolé au cours de l'Éocène, qui aurait suivi le soulèvement régional subi au Crétacé par une grande partie du secteur nord de la zone d'Ominéca.

Chaînon Deserters

Dans le chaînon Deserters, le degré de métamorphisme le plus faible se trouve à l'est, là où les niveaux stratigraphique et structural sont les plus élevés; le degré de métamorphisme augmente vers l'ouest jusqu'au sillon des Rocheuses du Nord, où l'on trouve les niveaux stratigraphique et structural les plus faibles. Les associations de minéraux pélitiques définissent cinq zones métamorphiques limitées par deux isogrades minéralogiques et deux lignes cotectiques. La suite des zones est la suivante: chlorite; biotite; grenat; staurotide-biotique; et disthène-grenat-biotite. La chloritoïde apparaît pour la première fois dans la zone de chlorite. Toutes les associations contiennent de la muscovite, du plagioclase et du quartz. Dans toutes les zones, la phyllade et le schiste ont une foliation marquée et plissée. Les phyllosilicates se seraient formés pendant la déformation D1. Les textures de chaque zone vues en lames minces portent à croire que la croissance des noyaux de grenat a eu lieu en même temps que la déformation D1, tandis que la croissance d'autres porphyroblastes et des bordures de grenat a eu lieu après la déformation D1; le métamorphisme aurait donc persisté après la déformation D1. Une phase de déformation (D2) a eu lieu après l'apogée de métamorphisme; elle a formé des microplis dans les phyllosilicates qui définissent la foliation S1, plissoté le disthène et plissé les isogrades et les contacts des formations suivant une grande échelle. L'étude géothermobarométrique des roches les plus fortement métamorphisées donne des températures d'environ 530°C et des pressions de 7 à 8 kb. Ces données correspondent aux conditions de métamorphisme que traduisent les associations de minéraux pélitiques.

Chaînons Sifton

Dans le nord des chaînons Sifton, le degré de métamorphisme augmente vers l'est, passant de la zone de chlorite au nord-ouest à la zone de sillimanite dans le noyau de l'antiform de Sifton. Les isogrades de métamorphisme les plus élevées sont tronquées par la faille de Sifton, dont la lèvre supérieure immédiate contient des roches de la zone de staurolite.

Les associations de minéraux pélitiques dans la lèvre inférieure de la faille de Sifton définissent six zones métamorphiques séparées par une isograde minéralogique, trois lignes cotectiques et une faille. La ligne cotectique de sithène-sillimanite se présente sur une étendue à l'échelle de la carte; elle représentait une septième zone métamorphique. La séquence des zones est la suivante: chlorite; grenat; staurolite-biotite; disthène-grenat-biotite; sillimanite-disthène; sillimanite; et sillimanite-feldspath potassique. Toutes les associations contiennent de la muscovite, du plagioclase et du quartz. Des textures en boules de neige mal définies dans les grenats sont le résultat d'une déformation synmétamorphique (D1). Les phyllosilicates qui produisent la foliation sont soient anté-, syn-, ou tardicinématiques par rapport à la déformation D1. La formation de plis isoclinaux et le

upright folding (D2) that produced the Sifton Antiform. The folded isograds are truncated by the Sifton Fault, indicating that the fault postdates the peak of metamorphism. A geothermobarometric study of kyanite — garnet — biotite zone rocks yielded temperatures and pressures of about 600°C, and 6.5 to 7.5 kb. These data are consistent with conditions of metamorphism suggested by the pelitic mineral assemblages.

The metamorphic zones that have been mapped in the hanging wall of the Sifton Fault are: staurolite — biotite; kyanite — garnet — biotite; sillimanite — kyanite; and a (late) thermal overprint in the contact aureole of the Eocene granite pluton at the south end of the range. Isograds are poorly constrained because of the paucity of pelitic compositions that retain prograde assemblages. Only the kyanite — garnet — biotite and the sillimanite isograds appear on the map. Porphyroblasts are fine grained and dispersed in a matrix of finely recrystallized quartz and mica, and as a result, it is rarely possible to demonstrate textural equilibrium. The assemblages are inferred to represent the peak of the same metamorphic event that affected the footwall, and to have quenched prior to displacement on the Sifton Fault, which truncates isograds in its footwall. Metamorphic grade is highest in the metaquartzite/amphibolite unit which, overlying the basement gneiss, is the lowest stratigraphic unit with pelitic compositions. It is also the highest structural unit in the Sifton Ranges, and its position at least 1 km above the Sifton Fault is another argument for postmetamorphic displacement on the Sifton Fault. A geothermobarometric study of the kyanite — garnet — biotite zone rocks yielded temperatures and pressures of about 600 to 660°C, and 5.5 to 7 kb. These data are consistent with the conditions of metamorphism suggested by pelitic mineral assemblages, and both indicate that the hanging wall was metamorphosed at about the same depth as the footwall. The tectonic loading associated with the Sifton Fault may have contributed to the net postmetamorphic uplift and may provide an explanation for why some of the highest grade rocks in the northern Omineca Belt are found in the Sifton Ranges.

Structure and tectonics

Syn — and post-metamorphic deformation is inferred to be Mesozoic and younger on the basis of radiometric dating of metamorphic minerals in other parts of the northern Omineca Belt. Any pre-Mesozoic deformation has been obliterated or is not geometrically distinct from the Mesozoic deformation.

Deserters Range

Bedding (S0), and foliation (S1) parallel with bedding, have gentle to moderate dips in the western part of the range, and moderate to steep dips in the

métamorphisme ont été suivis par la formation de plis droits postmétamorphiques (D2) qui ont produit l'antiform de Sifton. Les isogrades plissées sont tronquées par la faille de Sifton, ce qui révèle que la faille a suivi l'apogée du métamorphisme. L'étude géothermobarométrique des roches de la zone de disthène-grenat-biotite a donné des températures d'environ 600°C et des pressions de 6,5 à 7,6 kb. Ces données correspondent aux conditions de métamorphisme suggérées par les associations de minéraux pélitiques.

Les zones métamorphiques suivantes ont été cartographiées dans la lèvre supérieure de la faille de Sifton; staurolite-biotite; disthène-grenat-biotite; sillimanite-disthène; et une surimpression thermique (tardive) dans l'auréole de métamorphisme du pluton granitique éocène à l'extrémité sud du chaînon. Les isogrades sont mal limitées car les compositions pélitiques qui ont conservé des associations progrades sont peu nomreuses. Seules les isogrades de disthène-grenat-biotite et de sillimanite sont indiquées sur la carte. Les porphyroblastes à grain fin sont dispersés dans une matrice de quartz et de mica finement recristallisés et il est donc rarement possible de démontrer l'équilibre textural. Les associations représentaient l'aposée de l'événement métamorphique qui a touché la lèvre inférieure et elles se seraient refroidies rapidement avant le déplacement le long de la faille de Sifton, qui a tronqué les isogrades dans la lèvre inférieure. Le degré de métamorphisme le plus élevé se trouve dans l'unité de quartzite métamorphique/amphibolite qui recrouvre le socle gneissique et qui représente l'unité stratigraphique la plus basse à composition pélitique. C'est aussi l'unité structurale la plus élevée des chaînons Sifton et sa position à au moins un kilomètre au-dessus de la faille de Sifton est un autre indice en faveur d'un déplacement postmétamorphique le long de la faille de Sifton. L'étude géothermobarométrique des roches de la zone de disthène-grenat-biotite donne des températures variant de 600 à 660°C et des pressions allant de 5,5 à 7 kb. Ces données correspondent bien aux conditions de métamorphisme indiquées par les associations de minéraux pélitiques et elles portent à croire que la lèvre supérieure a été métamorphisée à environ la même profondeur que la lèvre inférieure. La charge tectonique associée à la faille de Sifton pourrait avoir contribué au soulèvement postmétamorphique net et pourrait expliquer pourquoi on trouve dans les chaînons Sifton certaines des roches les plus fortement métamorphisées de la partie nord de la zone d'Ominéca.

Structure et tectonique

La datation radiométrique des minéraux métamorphiques trouvés ailleurs dans la partie nord de la zone d'Ominéca porte à croire que la déformation syn- et postmétamorphique daterait du Mésozoïque et d'après. Toute déformation antérieure au Mésozoïque a été oblitérée ou ne peut être distinguée géométriquement de la déformation mésozoïque.

Chaînon Deserters

La stratification (S0) et la foliation (S1) parallèle à la stratification ont des pendages faibles à modérés dans la partie ouest du chaînon et modérés à forts dans la partie est. Les plis mésoscopiques à zonation complexe et à fabrique pénétrative sont cylindriques, et on y trouve souvent des types harmoniques et disharmoniques. Il n'y a pas eu croissance de minéraux dans les surfaces

eastern part of the range. Mesoscopic folds of compositional layering and penetrative fabric are cylindrical, and both harmonic and disharmonic types are common. There is a lack of mineral growth in the axial surfaces (S2) of crenulations and folds. The strongly foliated and anisotropic character of the assemblage has resulted in the development of angular, open to closed folds, chevron and kink folds in thinly-layered rocks, and rounded similar folds in thickly-layered rocks. The folds have northwest-trending axes coaxial with mineral lineations and mullions, and are indicative of the northeasterly shortening that is typical of the Foreland and Omineca belts. The folds appear to represent mainly one episode of deformation. The earliest deformation recognized is synmetamorphic, but the lack of minor folds associated with the S1 foliation inhibits generalizations about the kinematics of the deformation. Chevron and kink folding of the foliation and of kyanite crystals, and the lack of axial surface foliation to F2 folds, indicate that folding postdates the peak of metamorphism. The bedding, foliation parallel with bedding, and isograds, are folded into a map-scale inclined anticline, the Deserters Anticline. Folds plunge consistently northwest in the northwest, and gently southeast in the southeast, forming a gentle structural and metamorphic culmination.

Sifton Ranges

The Sifton Fault separates two regions of contrasting structural style. Cylindrical folds of compositional layering and penetrative fabric with northwest-trending axes, and a coherent internal stratigraphy are features that discriminate the footwall from the shear zone in the hanging wall.

Two episodes of deformation associated with northeast shortening in the footwall of the fault are evident. Intense early deformation (D1) resulted in transpositon of bedding, folds of bedding (F1), foliation (S1), and folds of the foliation (F1). Tight to isoclinal synmetamorphic F1 folds have northwest-trending axes. They have no map-scale expression because the level of erosion is entirely within a single, structurally upright panel. The F1 folds are refolded by coaxial, open, upright folds (F2) which produced the only map-scale structure in the footwall, the Sifton Antiform.

A third episode of deformation in the Sifton Ranges is defined by the truncation of the Sifton Antiform by the Sifton Fault. The Sifton Fault is the lower contact of a gently-dipping shear zone that covers more than half of the Sifton Ranges. The mylonitic foliation is commonly gently-dipping, but is folded by late upright open folds. A strong lineation in the plane of the foliation plunges consistently north-northwest. Shearbands at microscopic and mesoscopic scales cut the mylonitic foliation at an acute angle and indicate top-to-the-south-southeast displacement. Mesoscopic sheath folds have axes parallel with the lineation, and their sense of rotation

axiales (S2) des crénulations et des plis. La nature fortement foliée et anisotropique de l'association a donné lieu à la formation de plis ouverts ou fermés angulaires, de plis en chevrons et de kinks dans les roches finement stratifiées, et de plis isoclinaux arrondis dans les lits rocheux épais. Les axes des plis, à orientation nord-ouest, sont parallèles aux linéations minérales et aux structures columnaires; ils sont une indication du raccourcissement vers le nord-est qui caractérise les zones de l'avant-pays et d'Ominéca. Les plis représenteraient surtout une phase de déformation unique. La déformation la plus ancienne qui puisse être reconnue est synmétamorphique, mais l'absence de plis mineurs associés à la foliation F1 nous empêche de formuler des idées générales au sujet de la cinématique de la déformation. La formation de plis en chevrons et de kinks dans la foliation et dans les cristaux de disthène, et l'absence d'une foliation dans les surfaces axiales des plis F2 révèlent que le plissement a été postérieur à l'apogée de métamorphisme. La stratification, la foliation parallèle à la stratification et les isogrades sont plissées de façon à former un anticlinal incliné, l'anticlinal de Deserters, qui peut être cartographié. Les plis plongent régulièrement vers le nord-ouest dans le nord-ouest, et doucement vers le sud-est dans le sud-est, formant ainsi une culmination structurale et métamorphique douce.

Chaînons Sifton

La faille de Sifton sépare deux régions aux styles tectoniques constrastants. Des plus cylindriques à zonation complexe et à fabrique pénétrative, dont les axes ont une orientation nord-ouest et une stratigraphie interne cohérente, permettent de distinguer la lèvre inférieure de la zone cisaillée dans la lèvre supérieure.

Deux épisodes de déformation associés au rétrécissement nord-est dans la lèvre inférieure de la faille sont évidents. Une déformation précoce intense (D1) a transposé la stratification, plissé la stratification (F1), produit une foliation (F1) et plissé la foliation (F1). Des plis fermés ou isoclinaux S1 synmétamorphiques ont des axes à orientation nord-ouest. Ils n'ont aucune expression à l'échelle de la carte puisque le niveau d'érosion se trouve entièrement à l'intérieur d'un seul panneau structuralement droit. Les plis F1 ont été plissés à nouveau par des plis droits ouverts coaxiaux (F2) qui ont produit la seule structure à l'échelle de la carte dans la lèvre inférieure, soit l'antiform de Sifton.

Un troisième épisode de déformation dans les chaînons Sifton est défini par le retranchement de l'antiform de Sifton par la faille de Sifton. La faille de Sifton forme le contact inférieur d'une zone cisaillée à pendage faible qui couvre plus de la moitié des chaînons Sifton. La foliation mylonitique, normalement à pendage faible, a été déformée par des plis ouverts, droits, récents. Une linéation marquée dans le plan de la foliation plonge régulièrement vers le nord-nord-ouest. Des bandes cisaillées microscopiques et mésoscopiques coupent la foliation mylonitique à un angle aigu; elles indiquent que le sommet s'est déplacé vers le sud-sud-est. Le sens de rotation des plis en gaine mésoscopiques dont les axes sont parallèles à la linéation indique que le sommet s'est déplacé vers le sud-sud-est. L'analyse à l'échelle de la carte des plis cylindriques mésoscopiques montre que ces plis sont dispersés de façon à former un grand cercle parallèle à la foliation, et que le point séparant les plis aux sens de rotation opposés est parallèle à la linéation moyenne. Le sens de rotation des plis indique que le sommet s'est déplacé vers le

indicates top-to-the-south-southeast displacement. A map-scale analysis of mesoscopic cylindrical folds shows that they are dispersed into a great circle parallel with the foliation, and the point separating folds with opposing senses of rotation is parallel with the mean lineation. The sense of rotation of the folds indicates top-to-the-south-southeast displacement. The simplest interpretation of the structural style in the hanging wall of the Sifton Fault is that the mylonitic foliation, lineation, sheath folds, and shear bands developed as a result of progressive simple shear in a gently-dipping shear zone that displaced the hanging wall south-southeast relative to the footwall. Regional geology and local structures suggest that the fault accommodated south-southeasterly contraction, a direction of compression anomalous to the Omineca Belt.

The gently-dipping fault zone can be related geometrically and kinematically to major dextral transcurrent faults which dissect the region. The model involves two segments of a left-stepping transcurrent fault zone that are joined via a gently-dipping thrust fault with displacement in a direction parallel with the transcurrent fault. In this model, in contrast with other models of contraction at bends in transcurrent faults, the amount of displacement transfered from one transcurrent fault to the other balances with the amount of displacement on the thrust fault. The amount of overlap of hanging wall on footwall measured parallel with the direction of displacement is 80 to 90 km, and is the minimum amount of displacement on the Sifton Fault.

The Sifton Fault model satisfies both local and regional geological constraints and has led to a refinement of the estimates of the displacement on the major transcurrent faults in the northern Omineca Belt. It gives an explanation for the distribution of Eocene K-Ar dates and clastic sediments which are almost restricted to this region. In addition, it provides an alternative to the "crustal extension" model of metamorphic core complexes for the development of elongate ranges with gently-dipping (and fault-related) foliations.

sud-sud-est. L'interprétation la plus simple du style tectonique dans la lèvre supérieure de la faille de Sifton veut que la foliation mylonitique, la linéation, les plis en gaine et les bandes cisaillées se soient formés à la suite d'un cisaillement simple progressif dans une zone cisaillée à pendage faible qui aurait déplacé la lèvre supérieure vers le sud-sud-est, par rapport à la lèvre inférieure. La géologie régionale et les structures locales portent à croite qu'il y a eu contraction vers le sud-sud-est le long de la faille; cette direction de compression est anormale dans la zone d'Ominéca.

La zone de failles à pendage faible peut être reliée géométriquement et cinématiquement aux grandes failles transverses dextres qui divisent la région. Le modèle comprend deux segments d'une zone de failles transverses à inflexion gauche qui sont reliés au moyen d'une faille chevauchante à pendage faible, dont le déplacement a été parallèle à la faille transverse. Dans ce modèle, contrairement aux autres modèles de contraction aux points d'inflexion des failles transverses, l'ampleur du déplacement transféré d'une faille transverse à l'autre est égale à l'ampleur du déplacement le long de la faille chevauchante. Le chevauchement de la lèvre supérieure sur la lèvre inférieure, mesuré parallèlement à la direction de déplacement, est de 80 à 90 kilomètres, soit le déplacement minimum le long de la faille de Sifton.

Le modèle de la faille de Sifton satisfait aux contraintes géologiques tant locales que régionales; il a permis de perfectionner les estimations du déplacement le long des failles transverses majeures dans la partie nord de la zone d'Ominéca. Ce modèle explique la répartition des dates établies au K-Ar et des sédiments clastiques éocènes que l'on trouve presque uniquement dans cette région. En outre, il sert d'alternative au modèle d'extension de la croûte des complexes aux noyaux métamorphiques proposé pour la formation de chaînons allongés caractérisés par des foliations doucement inclinées et reliées aux failles.

INTRODUCTION

The geology of Sifton and Deserters ranges was mapped at a scale of 1:50 000 with the purposes of: 1) investigating the stratigraphy of the Windermere Supergroup in northern British Columbia, and 2) comparing the stratigraphy, structural style, and metamorphism across the Northern Rocky Mountain Trench. These ranges were chosen because assemblages of rock types (granite, metaquartzite, and amphibolite) apparently unique to both ranges were thought to be offset 125 km along faults in the Northern Rocky Mountain Trench (H. Gabrielse, pers. comm. 1980). From reconnaissance mapping by H. Gabrielse, the ranges were known to be underlain by the Upper Proterozoic to Lower Cambrian Windermere Supergroup and the Lower Cambrian Atan and Gog groups. The stratigraphy remained undivided except for the delineation of thick marble units. Structures recognized were the Deserters Anticline, the Sifton Fault, and the doubly plunging antiform in the northern Sifton Ranges. In Deserters Range, a southwestward increase in metamorphic grade culminates near gneissic granite along the Northern Rocky Mountain Trench.

This report presents the first detailed account of Windermere Supergroup geology in the Rocky Mountains north of Peace Reach, Williston Lake. It is one of the first detailed studies of Windermere stratigraphy, structure, and metamorphism in the Omineca Belt north of the Cariboo Mountains (54°N). The other studies include a regional (and locally detailed) examination of the northern Omineca Belt by J.L. Mansy (Mansy and Gabrielse, 1978; Mansy, 1980), and a study of the structure, metamorphism and geochronology of part of the northern Wolverine Complex by R.R. Parrish (1976,1979).

Location, access, field and laboratory studies

Deserters Range, in the Muskwa Ranges of the Northern Rocky Mountains, flanks the Northern Rocky Mountain Trench between latitudes 56°45′ and 56°54′N and longitudes 124°35′ and 124°50′W (Fig. 1). It can be reached by charter aircraft from Mackenzie to Ingenika, followed by a short helicopter flight across Williston Lake. The Sifton Ranges, in the southernmost Cassiar Mountains, bound the west side of the Northern Rocky Mountain Trench between latitudes 57°37′ and 57°59′N, and longitudes 126°00′ and 126°37′W, and can be reached by helicopter in about an hour from either Ingenika, or Dease Lake on Highway 37.

After a four day reconnaissance in 1980 with H. Gabrielse, about 35 weeks were spent in the field during the summers of 1981 to 1983. Fieldwork involved traversing from camps that were supplied and moved weekly by helicopter. Several days of helicopter reconnaissance work and spot checks in key localities completed the investigation. Locations of traverses and spot checks are shown in Figure 2. Laboratory work included the study of thin sections of selected rock samples to determine their metamorphic assemblages and structural characteristics. It also involved the analysis of garnet, biotite, and plagioclase with the electron microprobe in the Department of Geological Sciences at Queen's University.

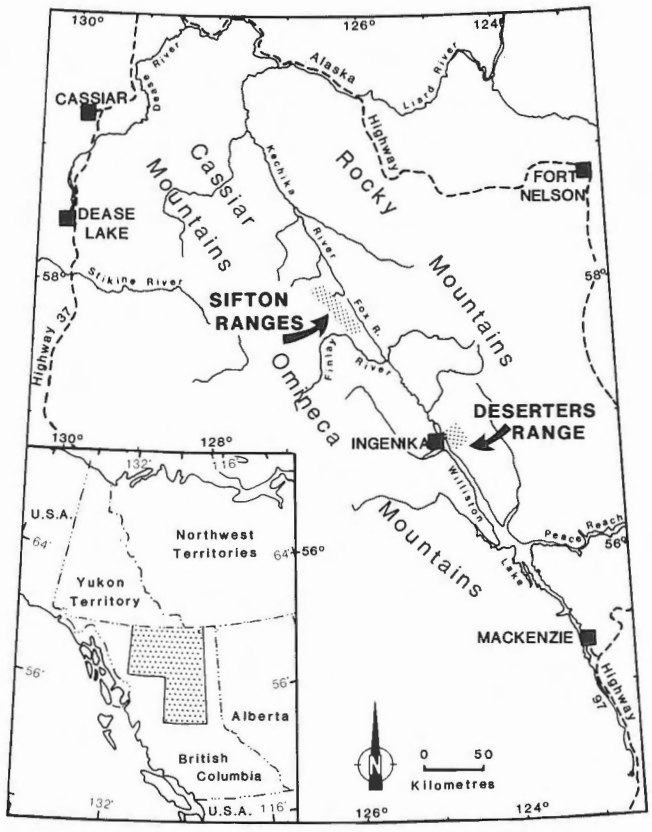

Figure 1. Location map of study area.

Physical features

The area studied in central Deserters Range covers 150 km², and is bounded by Chowika Creek, Ivor Creek, and Williston Lake in the Northern Rocky Mountain Trench (Fig. 2). It includes two northeast-trending ridges which rise from an elevation of 700 m in the trench to 2000 m at ridge crests. The area is well exposed in some creeks and on ridges above treeline which, unfortunately, is only about 150 m below the ridge crests. The ridges are moderately rugged with steep northwest faces and gentle southeast slopes. The eastern parts of both ridges are underlain by phyllite and the resulting scree covers much of the slopes.

The Sifton Ranges study area covers 500 km². It constitutes most of the Sifton Ranges and is bounded by Ludwig and Spinel creeks, Obo River, Fox Pass, and the Northern Rocky Mountain Trench (Fig. 2). The topography is characterized by a central northwest-trending spine, off which northeast-trending ridges branch and afford excellent natural cross-sections of the geology. North-facing slopes are commonly steep to vertical with 100 % exposure. South-facing slopes are commonly grass or scree covered with moderate slopes, allowing access to the excellent ridge exposures. Peak elevation and ruggedness increase to the south, from gentle ridges about 2000 m in elevation to precipitous ridges about 2400 m in elevation. The trench is about 900 m elevation at this latitude. Outcrop is generally sparse or absent below an elevation of 1500 m.

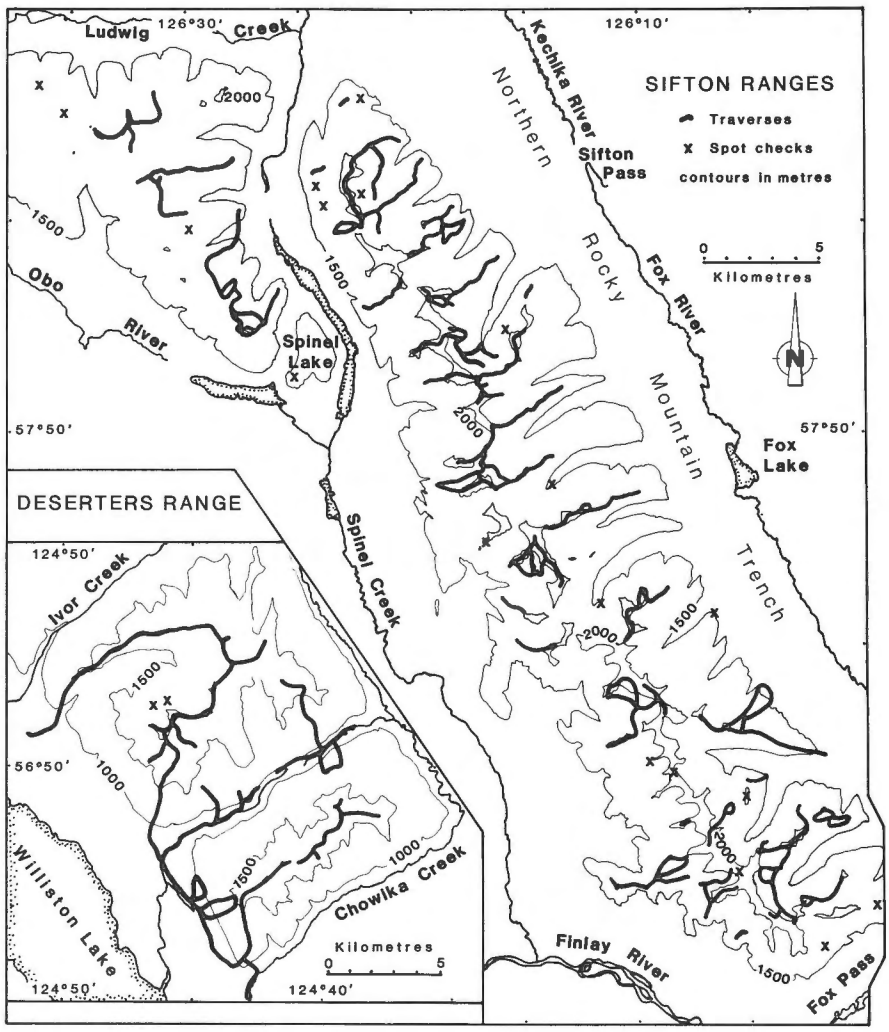

Figure 2. Location map of traverses and spot checks.

Past work

Study of Deserters Range geology began in 1893 with R.G. McConnell's (1896) reconnaissance of ranges bordering the Omineca and Finlay rivers. McConnell established that the Deserters Range was underlain by Precambrian rocks and that conglomerates in the Northern Rocky Mountain Trench were Tertiary. Dolmage (1928) mapped the area of the Finlay River basin, and Rutter and Taylor (1968) mapped the geology along the Finlay River that was later flooded behind the W.A.C. Bennett Dam. In 1941 Hedley and Holland (1941) undertook reconnaissance mapping of the Turnagain and upper Kechika rivers and became the first geologists to report on Sifton Ranges geology. They applied the name Sifton Formation to the Tertiary conglomerate in the trench at Sifton Pass, and noted that the Sifton Ranges were underlain by schist, quartzite, limestone and granite.

H. Gabrielse began Operation Finlay in 1970 to complete the geological reconnaissance mapping of Fort Grahame (now Mesilinka) East-Half (94C), Ware West-Half (94F) and Toodoggone River (94E) map areas. Associated with Operation Finlay were G.H. Eisbacher, who studied the tectonic framework of Upper Cretaceous to Lower Tertiary continental deposits of the Sifton Basin (Eisbacher, 1972, 1974), and J.L. Mansy, who studied the stratigraphy, sedimentation and structure of Upper Proterozoic and Lower Cambrian rocks of northern British Columbia. The work of Gabrielse, Mansy, Dodds, and Eisbacher constitute the most recent and complete accounts of the regional geology of the study area. This work is summarized in a paper on the geology of Fort Grahame map area (Gabrielse, 1975), a paper on the stratigraphy, terminology, and correlation of Upper Proterozoic rocks in Cassiar and Omineca mountains (Mansy and Gabrielse, 1978), and Open File maps of Toodoggone east-half and Ware west-half map areas (Gabrielse et al., 1977a). They assigned strata in the Deserters Range and in anticlinoria in the Cassiar and Omineca mountains to the Upper Proterozoic Misinchinka and Ingenika groups respectively. The Ingenika Group was divided into four formations, and correlation was established between Windermere strata in the Rocky, Cassiar, Omineca, Cariboo and Purcell mountains, although the age and correlation of most strata in the Sifton Ranges remained unresolved. The Sifton Fault was recognized in 1976 as a north-trending, east-dipping fault, and was interpreted to be a west-directed thrust (Gabrielse et al., 1977b). The hanging wall rocks were thought to

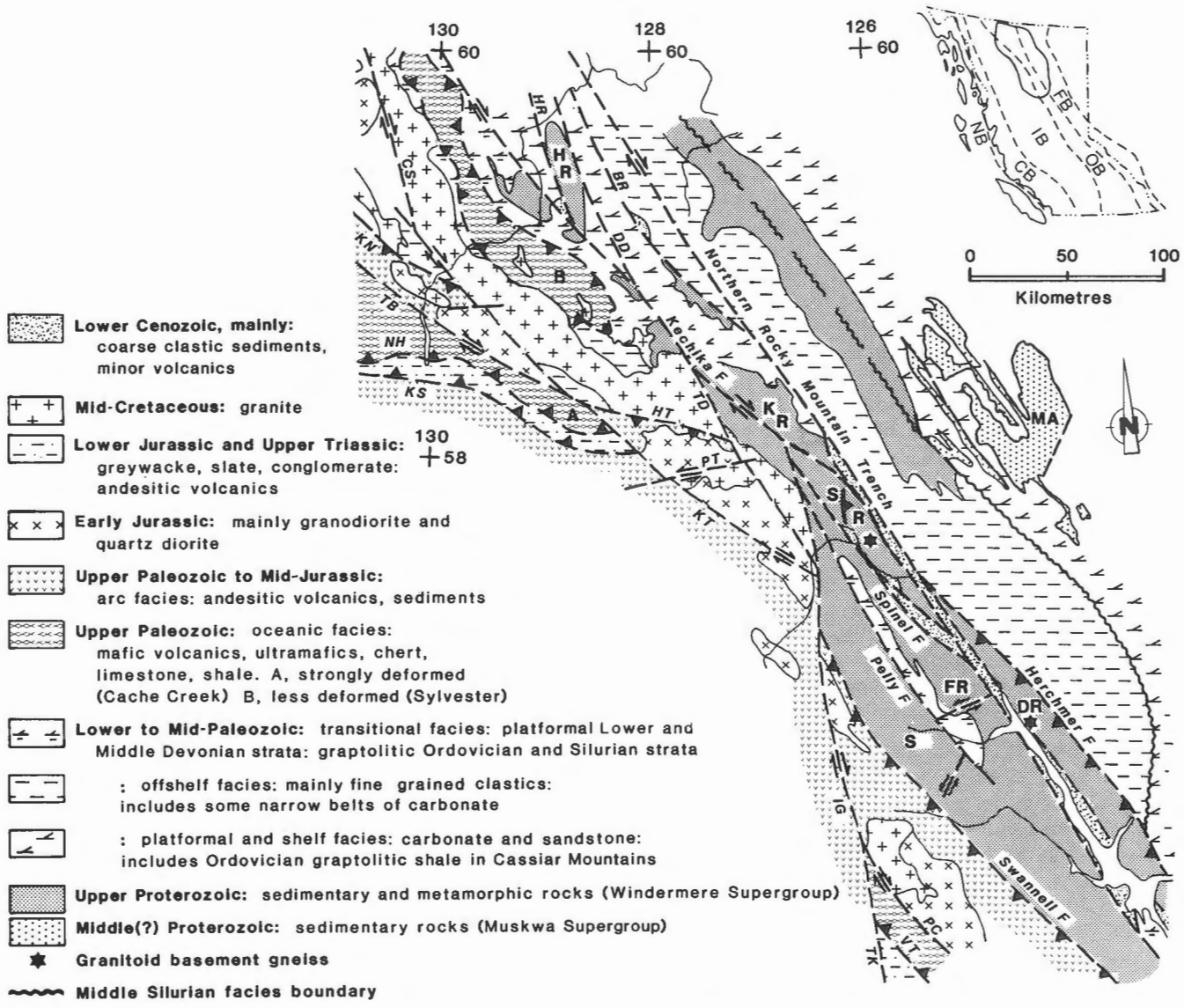

Figure 3. Map of regional geology. Ranges: DR Deserters; FR Finlay; HR Horseranch; KR Kechika; SR Sifton; SW Swannell. MA Muskwa Anticlinorium. Faults: BR Burnt Rose; CS Cassiar; DD Deadwood; HR Horseranch; HT Hottah; IG Ingenika; KN Klinkit; KS King Salmon; KT Kutcho; NH Nahlin; PC Pinchi; PT Pitman; TD Thudaka; TB Thibert; TK Takla; VT Vital (after Gabrielse, 1985). Geological Belts: FB Foreland; OB Omineca; IB Intermontane; CB Coast; NB Insular.

resemble those of the Deserters Range and the footwall rocks were thought to be Upper Proterozoic to Lower Ordovician, based on their stratigraphic position and general lithology. Granite in the Deserters Range was considered first to be part of the Misinchinka Group (Gabrielse, 1975). Biotites from the granite yielded Eocene K-Ar ages (Wanless et al., 1978, p. 21), and when a Tertiary K-Ar age was obtained for a granitic body in the Sifton Ranges which discordantly intrudes Proterozoic strata, the Deserters granite was reinterpreted to be Eocene (Dodds, in Wanless et al., 1979, p.10; Gabrielse, pers. comm. 1980). Samples of granite collected during this study gave a U-Pb zircon age of 728 Ma (Evenchick et al., 1984).

Regional geology

The study areas lie within the Foreland Belt (Deserters Range) and Omineca Belt (Sifton Ranges) of the Canadian Cordillera (Fig. 3). In this region the Northern Rocky Mountain Trench is the boundary between the two belts although the geology in the Deserters Range is more akin to that of the Omineca Belt than to that of the Foreland Belt. The Omineca Belt consists of intrusive rocks and sediments metamorphosed to medium and high grade. It contrasts with the very low grade sediments of the Foreland Belt to the east, and with sedimentary, volcanic and intrusive rocks of the Intermontane Belt to the west.

The Foreland Belt consists of a northeast-tapering wedge of Middle Proterozoic to Late Jurassic miogeoclinal and platformal carbonate and clastic rocks deposited on the western margin of the North American craton. Thin-skinned deformation of the miogeocline and platform, lasting from the Late Jurassic to Paleogene, resulted in uplift, erosion, and deposition of a clastic wedge that was subsequently involved in the deformation. The deformation resulted in about 200 km of northeast shortening in the southern Canadian Rockies (Bally et al., 1966; Price and Mountjoy, 1970; Price, 1981), and about 55 km in the northern Rockies (Gabrielse and Taylor, 1983). Metamorphism in the Foreland Belt is sub-greenschist or low-greenschist facies. Exceptions occur in small areas flanking the Rocky Mountain Trench at both Deserters Range, and 650 km to the southeast, where structural culminations expose Precambrian crystalline basement gneiss and its amphibolite facies cover (Oke and Simony, 1981; Oke, 1982). In the northern Rocky Mountains, Middle to possibly Upper Proterozoic strata are exposed only in the Muskwa Anticlinorium, where they are greater than 6000 m thick and are directly overlain by Lower Cambrian strata (Taylor and Stott, 1973). These strata are bounded on the west by about 3000 m of Upper Proterozoic sediments in a belt lacking exposures of older Proterozoic rock. Upper Proterozoic strata are also exposed along the Northern Rocky Mountain Trench, where they form the hanging wall of the Herchmer Fault.

The Omineca Belt consists of Precambrian crystalline basement, Middle Proterozoic to mid-Paleozoic miogeoclinal strata, and Paleozoic to Mesozoic volcanogenic rocks. The strata are multiply deformed, regionally metamorphosed, and intruded by Jurassic and Cretaceous plutons. In the northern Omineca Belt, Middle Proterozoic strata and Jurassic plutons are absent. The core zone of the northern Omineca Belt consists of fault-bounded, northwest-trending elongate anticlinoria of amphibolite facies Upper Proterozoic strata in Horseranch, Kechika, Sifton, Swannell, and Finlay ranges (Fig. 3). The core zone is characterized by moderately inclined, west-verging isoclinal structures (Gabrielse, 1975). In the Sifton Ranges, the moderate inclination is a result of refolding of recumbent folds by upright folds at least a kilometre in amplitude. Sparse geochronology on metamorphic minerals suggest that a major phase of deformation and regional metamorphism occurred in Middle to Late Jurassic times (Parrish, 1979), similar to timing in the Cariboo Mountains in the southern Omineca Belt. Uplift of the core-zone anticlinoria in the mid-Cretaceous and Eocene is indicated by K-Ar dating of muscovite, biotite and hornblende (Parrish, 1979; Wanless et al., 1978,1979; Stevens et al., 1982). In the Sifton Ranges, isoclinal folds, metamorphic isograds, and postmetamorphic upright folds (mid-Cretaceous (?)) are truncated by the gently dipping Sifton Fault, which is inferred to be related to major dextral transcurrent faulting. The fault is cut by undeformed Eocene granite; its age is thus limited to the interval between mid-Cretaceous(?) and Eocene. An east-trending crenulation cleavage in the Swannell and parts of Finlay ranges, and in the Paleogene sediments within fault zones, may also be associated with regional north-northwest dextral transcurrent faulting in mid-Cretaceous to Cenozoic times (Gabrielse, 1985). Uplift of core-zone anticlinoria, and transcurrent faulting resulted in deposition of Late Cretaceous to Eocene continental deposits of the Sifton Basin (Eisbacher, 1974). The sediments are exposed in linear belts along the Kechika, Spinel, and Northern Rocky Mountain Trench fault zones.

The cover rocks in the Omineca Belt are Upper Proterozoic to Lower Mississippian miogeoclinal strata and are deformed, but not as intensely as those of the core zone. In the regions northwest of Dease River and northeast of Kechika Fault, folds and thrusts verge to the northeast, but southeast of the Dease River and southwest of Kechika Fault vergence is to the southwest (Gabrielse, 1985). West-verging folds and thrusts merge with the sole fault of the Sylvester Allochthon, a stack of thrust sheets of Mississippian to Triassic oceanic rocks that was emplaced to the northeast (Harms, 1984). The age of structures is constrained only by late Early Cretaceous granitic rocks west of Kechika Fault that cut all contractional structures, including the Sylvester Allochthon. Structures are poorly understood in allochthonous and autochthonous terranes in the northwesternmost part of the Omineca Belt in the Yukon.

Core-zone and cover rocks are dissected by a swarm of dextral transcurrent faults that accommodated up to 1000 km of northward displacement, as illustrated by offset shelf to offshelf facies boundaries, structural domains, and plutons (Gabrielse, 1985). Of concern to this study are faults in the Northern Rocky Mountain Trench (>700 km of displacement prior to mid-Cretaceous to Eocene, and 125 km during and/or since the Eocene), the Kechika Fault (>170 km in mid-Cretaceous to Oligocene), and the Spinel Fault Zone (85 km in Late Eocene to Oligocene) (Gabrielse, 1985).

The Omineca Belt is thought to be a metamorphic welt in which metamorphism, deformation, granitic intrusion, and uplift and erosion are a result of tectonic thickening during Mesozoic collision of volcanic-arc and oceanic terranes with the North American craton and its continental terrace wedge (Monger et al., 1982). As a result of oblique convergence, transcurrent faulting has played a major role in this evolution; in the northern Omineca Belt the swarm of faults has had a profound influence on the distribution of rock types, facies, and structural styles. The location and significance of these faults to the south are not clear. Paleomagnetic studies indicate about 2000 km of northward displacement of the Stikine Terrane since the Middle Cretaceous (Irving et al., 1985), but offsets on transcurrent faults east of Stikinia (Gabrielse, 1985) provide geological evidence for only half of that amount of displacement. Most regions of the Omineca Belt are considered to be terranes that are allochthonous though not necessarily exotic to the North American craton (eg. Coney et al., 1980; Monger et al., 1982; Silberling and Jones, 1984). According to the terrane concept, the Deserters Range is part of cratonic North America, and the Sifton Ranges are part of the Cassiar Terrane, a fault block of cratonic North America (Silberling and Jones, 1984).

Acknowledgments

This report formed the basis of a Ph.D. dissertation completed at the Department of Geological Sciences, Queens's University at Kingston. Dugald Carmichael supervised the thesis; Ray Price was also a supervisor in 1980, and continued in that role after leaving Queen's. Their advice and guidance throughout the study, and constructive criticism and editing of the thesis are warmly acknowledged. I am indebted to Hu Gabrielse of the Geological Survey of Canada for suggesting the project, introducing me to the geology of the areas, and for providing continuing enthusiasm, constructive criticism, and moral support. His patient editing of early drafts of the thesis is greatly appreciated.

The study could not have been done without the support of the GSC, which provided much appreciated summer employment, logistical support to carry out the fieldwork, and bore the cost of most of the thin sections. Funds for additional helicopter time, and financial support while at Queen's (for thin sections and time on the electron microprobe) were from NSERC grants to Dugald Carmichael. The support of Natural Sciences and Engineering Research Council of Canada, in the form of a Postgraduate Scholarship (1980/81-1983/84), and of Queen's University, in the form of a Reinhardt Scholarship (1984), are gratefully acknowledged.

Lisel Currie was an excellent assistant and companion for almost half of the fieldwork; her help and enthusiasm added greatly to the work. Jennifer O'Brien provided keen and enjoyable assistance for several weeks in 1983. Jasmine Hobart assisted in fieldwork during summer 1981. Peter Roeder and Dave Kempson gave valuable advice on the operation of the electron microprobe; APL programs composed by Dugald Carmichael were used to manipulate the probe data.

STRATIGRAPHY

Introduction

Sifton and Deserters ranges are underlain by four distinct stratigraphic assemblages (Table 1) with characteristics typical of the Windermere Supergroup.

1) In Deserters Range, strata of the Misinchinka Group nonconformably overlie 728 Ma granitoid basement (Evenchick et al., 1984) and are overlain by Lower Cambrian strata. The sequence includes metadiamictite but lacks thick units of quartzofeldspathic metagrit, one of the most distinctive of Windermere lithologies.

2) West of Spinel Lake (*see* Fig. 2) in the Sifton Ranges, the strata are correlated with formations of the Ingenika Group as described by Mansy and Gabrielse (1978) for the Cassiar and Omineca mountains. The Ingenika Group is overlain by thin metaquartzite and marble of the Lower Cambrian Atan Group.

3) East of Spinel Lake, in the footwall of the Sifton Fault, a dominantly metaclastic sequence is structurally overlain by marble and several thin layers or lenses of quartzofeldspathic metagrit and quartz-pebble metaconglomerate, that are in turn overlain by marble. These units may represent a part of the Swannell Formation stratigraphically lower than that exposed west of Spinel Lake.

4) The hanging wall of the Sifton Fault consists of 1.85 Ga basement orthogneiss (Evenchick et al., 1984) structurally overlain by a unit of metaquartzite and amphibolite with minor pelitic schist. These units are in complex structural relationship with units of marble, schist, and psammite.

These assemblages exhibit a variety of styles and intensity of strain. All have a strong foliation parallel with compositional layering, and metamorphism to amphibolite facies, which have obliterated almost all primary structures except bedding. The thicknesses of units given in the Table of Formations (Table 1) are structural thicknesses. In Deserters Range, the foliation and compositional layering are openly to tightly folded. The large-scale structure is an inclined anticline. Isoclinal folds are conspicuously absent; only one intrafolial fold in marble was found. A stratigraphic section is present from Precambrian basement to Lower Cambrian strata. West of Spinel Lake, layer-parallel and oblique foliation and rare mesoscopic isoclinal folds are present, but folds do not repeat units on map scale. East of Spinel Lake in the footwall of the Sifton Fault, layer-parallel foliation and bedding are isoclinally folded on a large (cliff) scale, but units are not repeated on map scale. The tight to isoclinal folds have been refolded by upright folds. In the hanging wall, a strong layer-parallel foliation occurs in a variety of ductile fault rocks and is inferred to have formed during emplacement of the hanging wall. Compositional layering is lensoidal and discontinuous, and folding is strongly noncylindrical, so that the apparent stratigraphy is at least in part of tectonic origin, and no realistic estimate of primary thickness can be made. Even down-plunge projections of geometry and present thickness are suspect because of the noncylindrical fold style.

Deserters Range

Basement rocks and metasediments (locally in amphibolite facies) occur in a structural culmination which exposes the lowest stratigraphic level east of the Northern Rocky Mountain Trench and north of the gneiss along the Southern Rocky Mountain Trench 650 km to the southeast. To the north, no crystalline basement rocks are exposed, and metamorphic grade is rarely greater than lower greenschist facies. The rocks occur in an east-facing inclined anticline, revealing from west to east, a section from basement rocks through the Windermere Supergroup to Cambrian strata (Fig. 4 in pocket).

Deserters Gneiss (Hg)

Exposed on the east floor and low flanks of the trench between Chowika and Police creeks is light pink- to cream-weathering, mesocratic, medium grained, homogeneous granite (Fig. 5a) with uniform modal mineralogy of 25 % quartz, 30 % plagioclase, 40 % potassium feldspar, 4 % biotite and muscovite, and <1 % zircon, apatite, allanite(?) and monazite(?). A steep northwest-trending mylonitic

Table 1. Table of formations (no stratigraphic correlations are assumed between Precambrian units)

System	Series	Deserters Range		Sifton Ranges		Hanging wall of Sifton Fault	
		Formation and thickness (m)	Lithology	Formation and thickness (m)	Lithology	Formation and thickness (m)	Lithology
Cenozoic	Tertiary			Sifton Fm >250	Poorly sorted pebble to boulder conglomerate		Granite; pegmatite dykes, lamprophyre dykes
Paleozoic	Cambrian Ordovician	Kechika Group	Nodular limestone and siltstone	Kechika Group	Calcareous phyllite, marble		intrusive contact
	Cambrian	Gog Group 70	Metaquartzite; marble	Atan 20-30	Metaquartzite; marble		
Unconformity							
lower Paleozoic and Hadrynian		Misinchinka Group HMcp >700	Chlorite phyllite, minor marble, metasandstone	Ingenika Group Stelkuz Fm 300-350	Laminated metasiltstone; marble; chlorite phyllite	Ingenika Group (?)	
Hadrynian		Hmc 150	Marble; thinbedded base, and massive upper part	Espee Fm 15-25	Marble		
		HMscd 1000-1500	Amphibole chlorite schist; minor amphibolite, marble, psammite, diamictite	Tsaydiz Fm 200	Chlorite schist; minor grit lenses		
		HMs 30-80	Impure metaquartzite	Swannell Fm >1200	Quartz feldspar metagrit; pelitic schist		
		HMcs 150-200	Amphibole chlorite schist and amphibolite; minor pelitic schist and marble	Hlc >200	Impure marble, minor schist and metasandstone		
		HMm 70-100	Pure metaquartzite (15m) between two marble members	Hlg 400-1200	Pelitic schist, metagrit, psammite	Hlws >300	Rusty-weathering wavy pelitic schist; minor psammite
		Hmp 250-400	Pelitic schist and metaquartzite	Hlps 150-400	Pelitic schist	Hlsm >600	Quartz lens schist; psammite; marble
		HMa 400	Metaquartzite, amphibolite, minor pelitic schist	Hlm 40-60	Pure marble, calc silicate	Hlqa >800	Pure metaquartzite, amphibolite; minor pelitic schist, feldspathic metaquartzite, paragneiss
		Hmq 200	Pure metaquartzite; pebble conglomerate at base	Hlp 200-900	Paragneiss, pelitic schist		
		Nonconformity		Hlq >500	Rusty-weathering metaquartzite, pelitic schist, paragneiss, marble		
		Hg	Gneissic granite (728 Ma)				
Aphebian						Unconformity	
						Tochieka gneiss	augen orthogneiss (1.85 Ga); Amphibolite

foliation which varies from poorly to well developed is inferred to be a result of movement on faults within the Northern Rocky Mountain Trench. Two tabular inclusions 1 to 2 m thick and composed of fine grained biotite schist are exposed at elevations of 800 and 850 m on the southwest slope of the ridge referred to informally herein as "Henry's Ridge". The contact of gneissic granite with cover rocks is exposed at an elevation of 900 m in the southernmost of the two creeks draining the southwest slope of "Henry's Ridge". At the contact the granite is altered, cream weathering, relatively massive, and fine grained. The overlying pebble conglomerate weathers to a similar appearance making the contact difficult to recognize. It is most easily seen from one side of the creek looking NW or SE, where gently dipping layering in the cover contrasts with granite that is massive, or has a weakly developed but steep foliation. Closer inspection reveals poorly exposed quartz pebbles in the cover immediately overlying the contact. Neither cover nor basement appears to be more strained at the contact, and bedding in the cover is concordant with the nonconformity. Zircons from the granite dated by R. R. Parrish yield a U-Pb age of 728 $+9/-7$ Ma (Evenchick et al., 1984). The unit is named herein the Deserters Gneiss.

Misinchinka Group

Metaquartzite (HMq)

The Deserters Gneiss is overlain nonconformably by 5 to 15 cm of quartz-pebble metaconglomerate rich in grit-size potassium feldspar clasts and coarse, sand-size zircon and sphene (Fig. 5b). The metaconglomerate is overlain by about a metre of gritty feldspathic metaquartzite, in turn overlain by 200 m of metaquartzite (Fig. 5c) which is thick-bedded and white, with an approximate modal mineralogy of 95 % quartz, 5 % feldspar and muscovite, and <1 % zircon, sphene, opaques, and tourmaline. The metaquartzite forms cliffs where exposed in creeks, and resistant ribs at an elevation of about 1000 m along the southwest slope of "Henry's Ridge". The thickness of the unit is taken from exposures on the southwest-facing slope of "Henry's Ridge", where the bedding has a consistently gentle dip and does not appear to be significantly folded. The upper 20 to 50 m of this unit is exposed in both Police and Chowika creeks as anticlinal crests, and in the creeks draining the southwest slope of "Henry's Ridge".

Amphibolite and metaquartzite (HMa)

The metaquartzite unit is overlain by about 400 m of amphibolite intercalated with metaquartzite and pelitic schist. Amphibolite layers are commonly 1 to 3 or more metres thick and may represent flows or sills, but no primary structures or cross cutting relationships were found. Metaquartzite in this unit is varicoloured, pure, and thin-bedded, forming members 1 to 20 m thick. Kyanite-staurolite-garnet schist occurs sparsely in the upper 50 m. The unit is exposed in creeks and along the southwest ridges of Deception Cone and "Henry's Ridge". It is resistant to weathering and, together with the underlying metaquartzite unit, underlies the steepest west slopes of the ridges (Fig. 6a).

Pelitic schist and metaquartzite (HMp)

The amphibolite unit is overlain by about 250 to 400 m of staurolite-garnet schist, with minor thin-bedded, flaggy, white to rusty-white metaquartzite in members 0.5 to 1 m thick. One particularly thick (about 30 m) and stark white vitreous metaquartzite is mapped as a separate member (HMp1), in part because of its cliff-forming nature. Most of the unit weathers recessively, and forms gentle slopes above the resistant underlying units (Fig. 6a).

Marble and metaquartzite (HMm)

The lowest continuous marble layers mark the base of an excellent structural marker about 70 to 100 m thick. It is a distinctive unit consisting of about 15 m of flaggy to thick-bedded white metaquartzite between two members of thin-bedded, pure marble and actinolite marble. The lower marble member consists of about 20 m of cream weathering marble with minor phyllite, and the upper marble member consists of about 40 m of buff weathering marble in which the top 10 m is interbedded with metaquartzite and amphibolite. The unit is moderately resistant to weathering and forms cliffs above the underlying recessive schist.

Amphibole chlorite schist (HMcs)

About 150 to 200 m of amphibole-chlorite schist and amphibolite, with minor calcareous chlorite schist, minor pelitic schist, psammite and marble is exposed along the tops of both ridges. Metadiamictite on the northern ridge of Deception Cone consists of isolated rounded quartzite cobbles in a chlorite schist matrix.

Impure metaquartzite (HMs)

Grey weathering impure metaquartzite is about 30 to 80 m thick. It consists mainly of quartz and feldspar, with about 10 % carbonate, and 10 % biotite and epidote, and beds vary from 2 to 30 cm thick. It is extremely resistant to weathering, forms the highest topographic features on both ridges, and as such is an important structural marker. On Deception Cone it is exposed as gently dipping erosional remnants that cap the ridge for 2.5 km along the gentle crest of the Deserters Anticline (Fig. 6a). Thickness varies from about 30 m on the ridge west of Deception Cone to about 80 m on "Henry's Ridge" and the ridge north of Deception Cone.

Schist, marble, and metadiamictite (HMscd)

The unit consists of a variety of rock types and ranges from 1000 to 1500 m thick. The lower half is characterized by monotonous amphibolite and amphibole-chlorite schist, with minor members of psammite, metaquartzite, and marble 1 to 2 m thick. The upper part is mainly chlorite

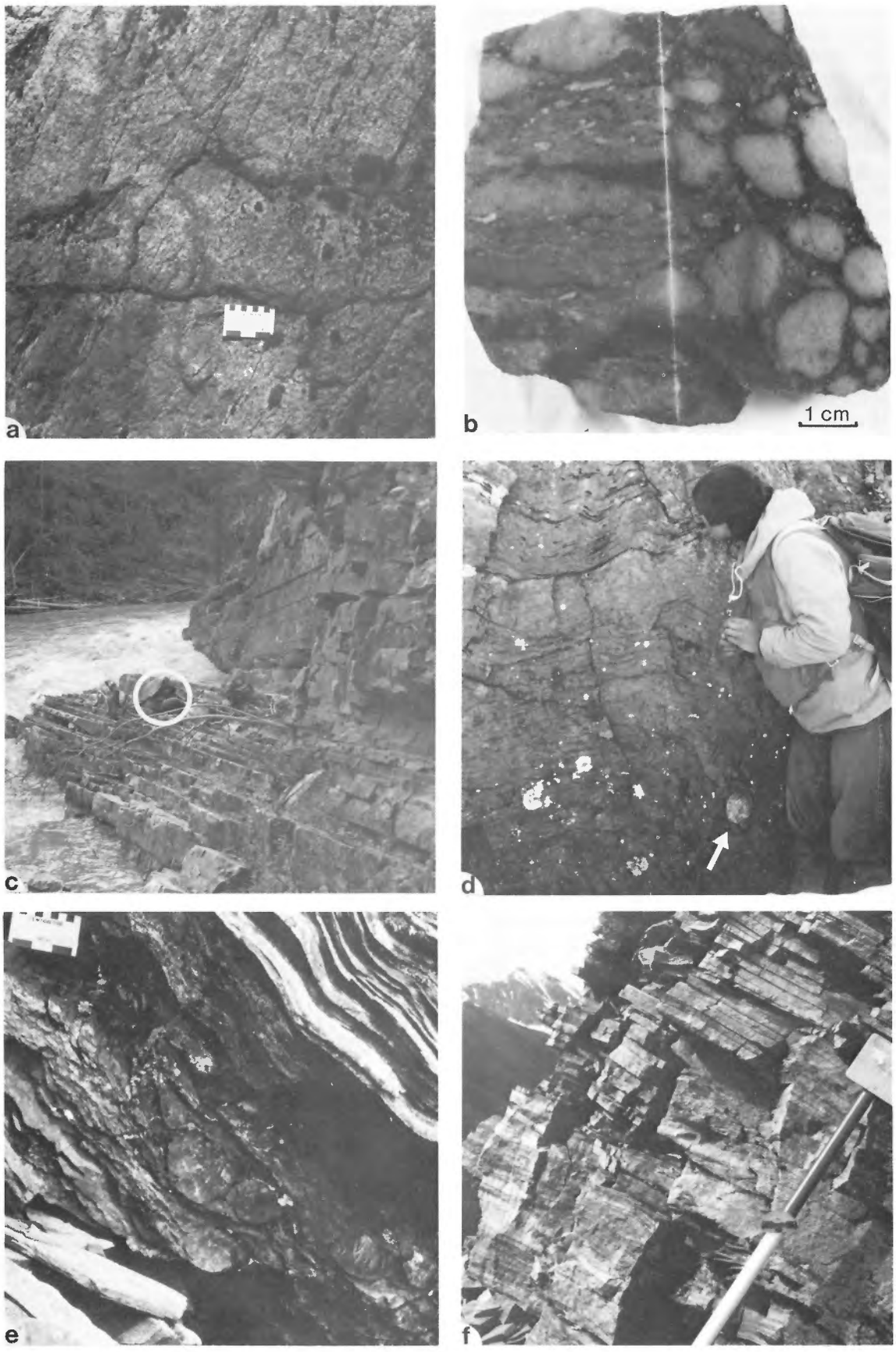
a
b
1 cm
c
d
e
f

schist and phyllite, which at various levels on all ridges forms the matrix of metadiamictite with isolated quartzite cobbles and boulders (Fig. 5d).

Several distinctive rock types within the upper chlorite schists may or may not be continuous members, but are at about the same stratigraphic level on all ridges. On Deception Cone, the lowest distinctive member is 20 m of iron-rich metasediments. It consists of magnetite chlorite schist with magnetite euhedra 1 to 3 mm across, and black magnetite quartz feldspar layers 2 to 4 mm thick interbedded with schist. Schist below and above the magnetite-rich rocks has rusty-weathering spots. In the overlying chlorite phyllite is a 1 to 3 m thick member of quartz and marble pebble to cobble conglomerate. About 80 m above the iron-rich interval is a distinctive marble member (HMscd1) that consists of 5 m of blocky, white weathering calcite marble, 1 m of platy grey calcite marble, and 10 m of sandy dolomite marble. One to 3 m of quartz and marble pebble to cobble conglomerate interbedded with sandy dolomite marble and chlorite phyllite (Fig. 5e) occurs in two intervals less than 200 m above the marble member. On the ridge north of Deception cone the marble member is underlain by schist and overlain by about 10 m of quartz-pebble to cobble conglomerate and brown weathering quartzitic metasandstone with rare opalescent blue quartz grains. On "Henry's Ridge" chlorite phyllite and psammite occur at about the same stratigraphic level as iron-rich metasediments on Deception Cone. Marble is also present at about the same level and is overlain by about 15 m of green weathering gritty metasandstone with rare opalescent blue quartz clasts. The upper part of the formation on all ridges has 10 to 20 m of distinctive platy, grey phyllite interbedded on a scale of about 5 mm with buff weathering sandy dolomite marble. In a northwest-facing cirque on "Henry's Ridge" the formation grades upwards from phyllite interbedded with metaquartzite into phyllite interbedded with sandy dolomite marble at the base of the pure marble of unit HMc. Graded bedding of sandy dolomite marble at this locality represents the only graded bedding seen in both Sifton and Deserters ranges and indicates that the beds at the base of the overlying marble formation are upright.

Figure 5. Photographs of Deserters Range rock types. a) Deserters Gneiss; homogeneous granite with a steep foliation. (GSC 204482-B) b) Metaconglomerate at the base of HMq cut perpendicular to, and parallel with the long axis of pebbles. Large clasts are quartz and small white clasts are K-feldspar. (GSC 204482-C) c) Well bedded metaquartzite of HMq in Chowika Creek. (GSC 204482-D) d) Isolated quartzite cobble in fine grained metasediments of HMscd. (GSC 204482-E) e) Lense of quartzite-cobble conglomerate interbedded with chlorite phyllite in HMscd. (GSC 204482-F) f) Platy and thin-bedded grey marble near the base of the Chowika Formation. (GSC 404482-G)

Chowika Formation (HMc)

A marble unit 150 m thick is the most distinctive marker in the Deserters Range and is easily traced on air photographs (Fig. 6b). Sandy dolomite marble at the base is overlain by mainly thin and irregularly-bedded, platy, grey weathering marble with 10 m of massive light grey marble (Fig. 5f) near the base, 50 to 80 m of massive white, cream and buff weathering marble in the middle of the unit, and dark grey, thin-bedded, and fine grained marble in the upper part. With the exception of one phyllitic interval 5 m thick, the unit is remarkably pure. It forms resistant, well exposed, northwest-trending ribs on all ridges, and illustrates the change from flat dips in the west, shown by other units, to moderate east dips in the east (Fig. 4,6). The unit is named herein the Chowika Formation, after Chowika Creek. The above description refers to the type section on the ridge north of Chowika Creek ("Henry's Ridge").

Chlorite phyllite (HMcp)

The eastern parts of both ridges are underlain by at least 700 m of recessive green, grey, and black chlorite-sericite phyllite with minor resistant members of marble, metaconglomerate, and metasandstone. On "Henry's Ridge" about 450 m above the base of the unit is a grey and buff fine grained marble member (HMcp1) 35 m thick in an anticline-syncline pair (Fig. 6b). It is dominantly massive grey calcite marble and dolomite marble with an upper 5 m of thin-bedded dark grey calcite marble. On Deception Cone two thinner marble members (HMcp1) are only 150 and 200 m above the base of the unit. The lower member consists of about 15 m of rusty and buff weathering, well bedded sandy dolomite marble grading up into platy grey marble. The upper member is about 10 m thick with a thin base of buff weathering sandy dolomite marble, 4 m of thin and wavy-bedded grey marble and an upper 4 m of grey marble with dolomitic marble nodules 3 to 5 cm across. The two marble members are separated by 35 m of grey, silver, and green phyllite, with 1 to 2 m of quartz-cobble conglomerate midway between them. Phyllite associated with marble members on both ridges is silver weathering with limonitic spots. On the southeast and east ridges of Deception Cone, the marble members are overlain by about 100 to 200 m of green chlorite phyllite which is locally interbedded with green coarse sandstone with blue quartz grains. The exposures farthest east on Deception Cone are phyllite and thick-bedded metasandstone with herringbone crossbeds.

Gog Group (lЄG)

A small area 3 km southeast of the right-angle bend in Chowika Creek was mapped to investigate strata in the vicinty of the Herchmer Fault. The footwall consists of wavy banded and nodular limestone and siltstone of the Upper Cambrian and Lower Ordovician Kechika Group. In the hanging wall of the fault, the Lower Cambrian Gog Group is structurally overlain by green and silver phyllite of the Misinchinka Group. This is inferred to be an inverted sequence on the overturned limb of an anticline in the hanging wall of the Herchmer Fault. The Gog Group

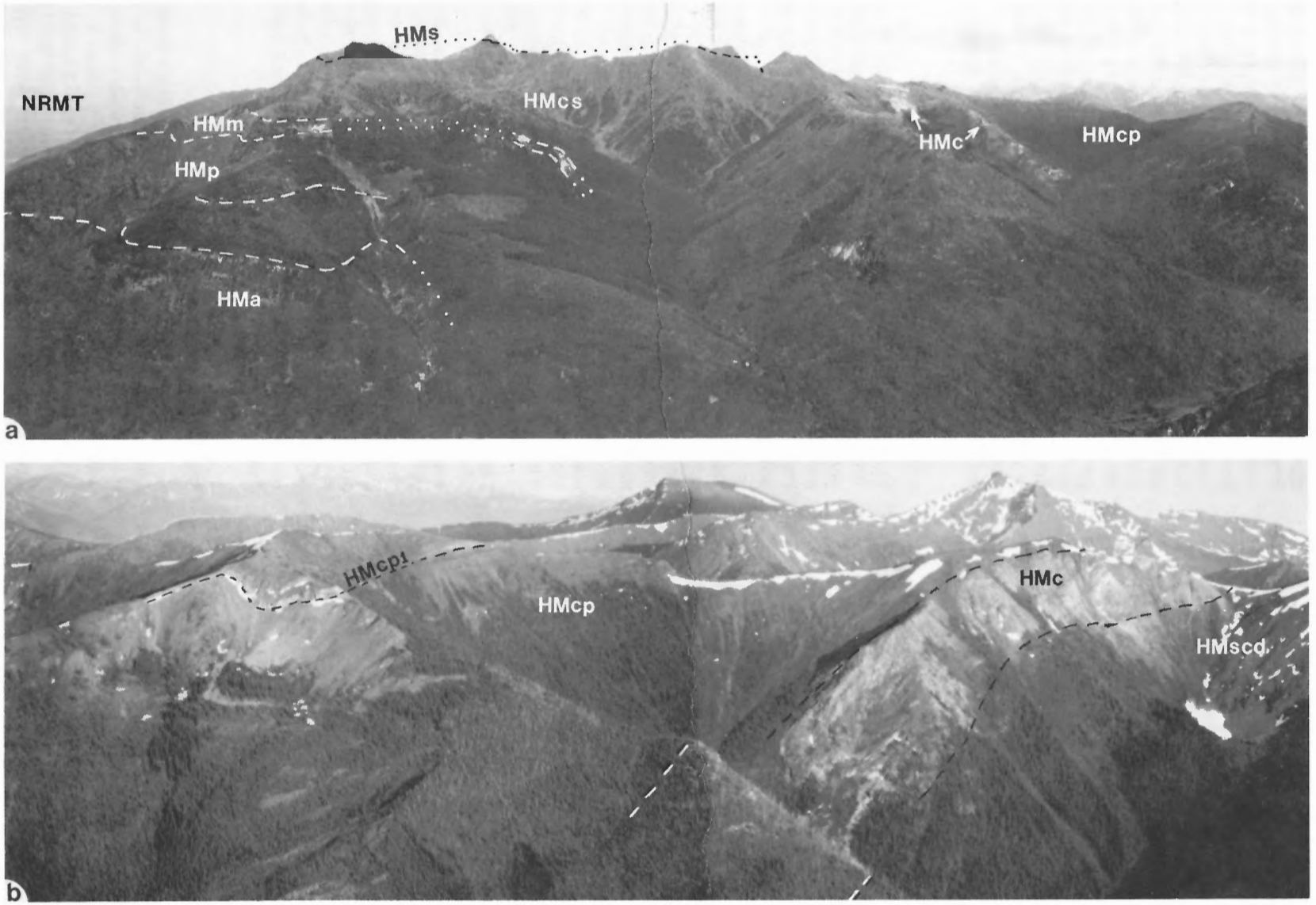

Figure 6. Deserters Range. a) View northwest to gently dipping lower map units on Deception Cone. (GSC 204482-H, I) b) View southeast to marble units on east "Henry's Ridge".

immediately below the Misinchinka Group consists of about 10 m of white and rusty weathering metaquartzite underlain by about 15 m of oolitic and archaeocyathid-bearing rusty orange weathering marble. The marble is in turn underlain by 35 m of white massive metaquartzite and rusty weathering metaquartzite and phyllite interbedded with about 10 m of rusty and grey weathering marble. No outcrop evidence of stratigraphic facing was found, but overturned bedding was recognized by Gabrielse (pers. comm., 1981) 30 km to the south, in Lower Cambrian quartzites in the hanging wall of the Herchmer Fault.

Sifton Ranges, west of Spinel Lake

Much of the region traversed west of Spinel Lake forms the gently to moderately west-dipping limb of an open to closed anticline that plunges gently to the southeast (Fig. 7, in pocket). In the south the closure is well illustrated by the map pattern. In the north, bedding in the Swannell Formation flattens over the closure.

Ingenika Group

Swannell Formation (HIs)

The eastern parts of the two northern ridges are underlain by rusty weathering quartzofeldspathic metagrit of the Swannell Formation. Bedding dips gently over the crest of an open anticline, so that the ridge exposures represent no more than 1200 m of stratigraphic thickness. The formation is characterized by beds of quartzofeldspathic coarse grit 20 to 80 cm thick, with chalky white potassium feldspar clasts and elongate quartz, including some opalescent blue quartz clasts (Fig. 8a). Garnet-chlorite-muscovite schist is interbedded with the metagrit. About 600 m below the top of the formation there are at least two sandy dolomite marble members 5 to 10 m thick.

Tsaydiz Formation (HIt)

The Swannell Formation grades over a few metres into phyllite of the Tsaydiz Formation. A few lenses of gritty feldpathic metasandstone similar to the Swannell grits are present, but the 200 m thick unit is dominated by recessive, rusty weathering, green chlorite phyllite. Near its base on the ridge at 58°56′N, a sandy marble member 25 m thick forms rusty weathering resistant bluffs, and on the ridge to the north a few marble members 1 to 2 m thick are interbedded with the phyllite. The upper 30 to 50 m are grey and green phyllite with sparse lenses of coarse quartzofeldspathic metagrit. This section differs from the type section of the Tsaydiz Formation which lacks marble near the base and is calcareous in its upper part, grading up into marble of the overlying Espee Formation (Mansy and Gabrielse, 1978).

Espee Formation (HIe)

Pure marble of the Espee Formation abruptly overlies phyllite of the Tsaydiz Formation. The unit is 15 to 25 m thick and consists of thin and irregularly bedded, locally laminated and massive, dolomitic marble. It is exposed as resistant cream and grey weathering knobs on all ridges and as cliffs on all slopes. It can be traced from the northernmost ridge southeast through folds to the southernmost ridge, where it closes in the core of a south-plunging anticline (Fig. 8b). Contacts with phyllite in the underlying and overlying formations are sharp.

Stelkuz Formation (HIst)

The Stelkuz Formation is about 300 to 350 m thick and consists of a lower marble and metaclastic unit, overlain by two fine grained metaclastic units. The base of the lowest unit consists of about 20 m of laminated metasiltstone with black chlorite phyllite partings that weather a distinctive dark maroon. The metasiltstone unit is abruptly overlain by about 15 m of rusty weathering, thin-bedded grey marble, overlain in turn by several metres of chlorite phyllite interbedded with thin-bedded sandy dolomite marble. The sequence of resistant weathering Espee Formation overlain by the recessive maroon weathering metasiltsone and resistant weathering marble of the lower Stelkuz Formation is distinctive and well exposed on the northern two ridges. The middle member of the Stelkuz Formation is dominated by chlorite phyllite with minor siltstone. The upper member consists of tan weathering, white and light green laminated metasiltstone (Fig. 8c) with minor metaquartzite and marble. Thin-bedded metaquartzite in the metasiltstone and black phyllite increases in proportion and thickness as it grades into metaquartzite of the Boya Formation.

Atan Group

Boya Formation (lЄAb)

The Boya Formation, a Lower Cambrian metaquartzite, varies from 1.5 m thick in the north to 3 m thick in the central region and less than 1 m thick in the south. It occurs as isolated exposures the length of the area and closes in a faulted anticline in the south. The contact with underlying metasiltstone of the Stelkuz Formation is exposed on the southern and northernmost ridges. The uppermost siltstone beds in the Stelkuz Formation increase in thickness and grain size over an interval of about 0.5 m into thin — to thick-bedded, brown and rusty weathering pink, and white metaquartzite.

Rosella Formation (lЄAr)

The Rosella Formation consists of about 20 to 25 m of marble exposed in discontinuous outcrop the length of the area as resistant, peak-forming bluffs (Fig. 8b). In the north, metaquartzite of the Boya Formation is in sharp contact with rusty weathering green phyllite 1 m thick, which is overlain by 1 m of thin-bedded orange and buff weathering marble. The buff weathering marble is overlain by about 5 m of thin-bedded, grey weathering marble and by 3 to 5 m of platy, rusty weathering marble. This sequence is overlain by more than 7 m of phyllite with minor siltstone interbedded with grey marble. A similar sequence is found at the south end of the area, except that there the Boya Formation is very thin, and the basal

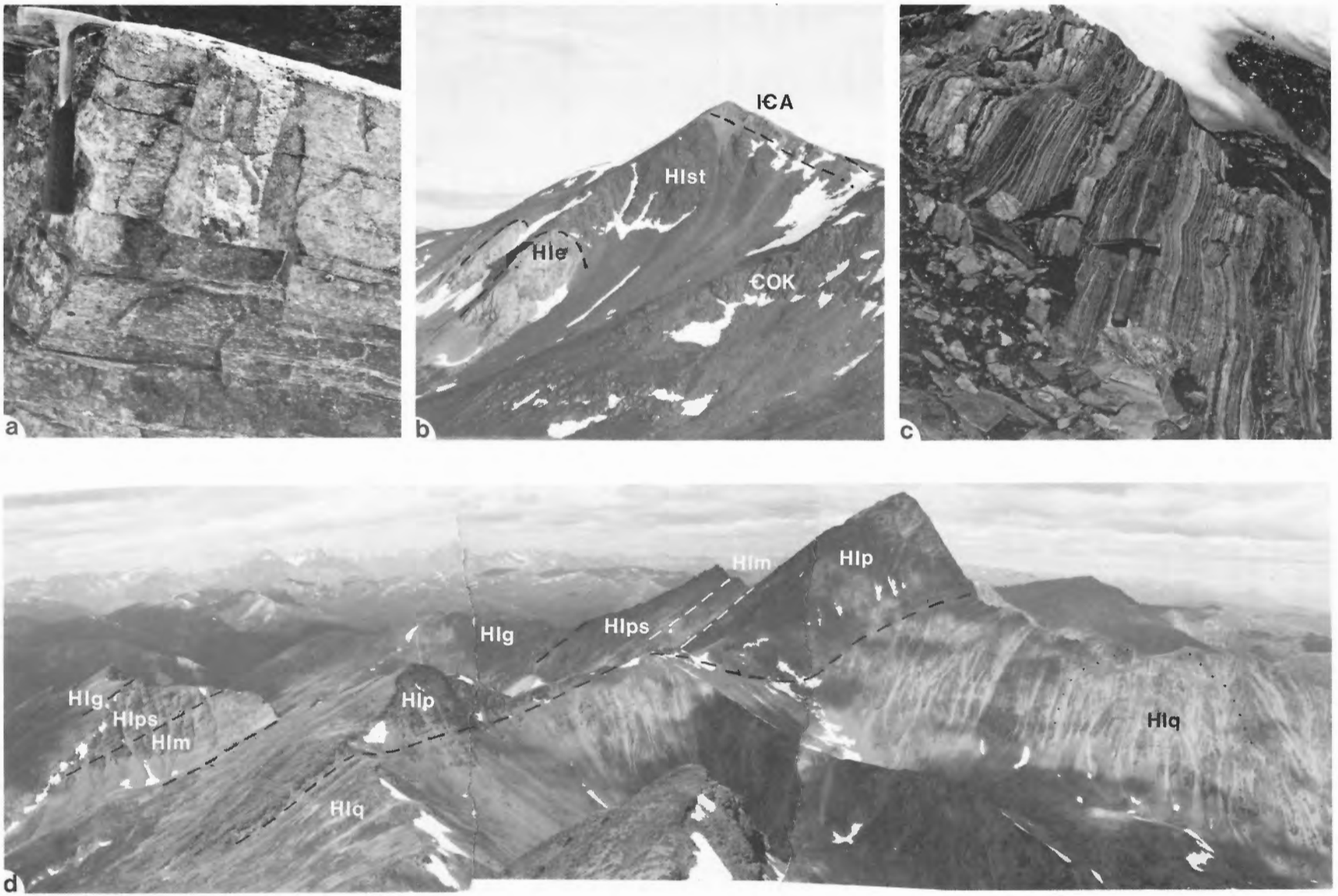

Figure 8. Rocks east and west of Spinel Lake. a) Quartzofeldspathic metagrit of the Swannell Formation (GSC 204482-L). b) View SE to the southern exposures of the Ingenika Group west of Spinel Lake. (GSC 204482-M) c) Laminated metasiltstone characteristic of the Stelkuz Formation. (GSC 204482-N) d) View NW from Mount Slocomb to strata on the west flank of Sifton Antiform exposed on the ridges of "Atche Peak", the most prominent peak in the photograph. The core of the Sifton Antiform is at the extreme right. (GSC 204482-0, P, Q)

Rosella consists of 10 to 15 m of reddish-brown marble overlain by about 5 m of well bedded grey marble. The contact with the Kechika Group is not exposed, but the distinctive weathering characteristics of the Kechika Group on slopes near the highest Rosella suggest that only 1 or 2 m of section are covered by talus.

Kechika Group (ЄOK)

Interbedded phyllite, calcareous chlorite phyllite, and grey, platy, fine grained marble of the Kechika Group form the western high ridges of the area. The unit weathers a distinctive rusty buff and occurs as high rounded ridges. It appears to be at least several hundred metres thick, but tight folding and intense penetrative cleavage preclude reliable measurement.

Sifton Ranges, east of Spinel Lake

Ingenika Group

The stratigraphy in this area is described from lowest to highest structural units. The section is inferred to be stratigraphically upright by the similarity to other Windermere sections with a clastic base and increasing amounts of carbonate in the upper part. Early recumbent folds with no map-scale expression are refolded into an open upright antiform (Sifton Antiform) which results in the map pattern shown in Figure 7.

Metaquartzite and schist (HIq)

The lowest map unit occurs in the core of the doubly plunging antiform in the centre of the range (Fig. 8d). It is at least 500 m thick, weathers a distinctive rusty orange and is very resistant to weathering, forming the most rugged topography in the area. The dominant rock type is thick-bedded, blocky and rusty-weathering metaquartzite with layers of sillimanite-garnet schist 1 to 30 mm thick. The lowest strata include minor garnet-hornblende schist and two white-weathering tremolite marble members each about 10 m thick, the only stratigraphic markers in the unit. The uppermost marble forms isoclinal folds on and south of Mount Slocomb which are refolded into an upright antiform. The Sifton Antiform is well exposed in metaquartzites on the ridge east of "Atche Peak" (Fig. 8d).

Paragneiss (HIp)

Paragneiss 200 to 900 m thick closes to the north and occurs on both limbs of the antiform as resistant dark grey ridges flanking the rusty weathering metaquartzite peaks (Fig. 8d). It is dominantly muscovite-biotite-quartzo-feldspathic gneiss in layers 2 to 50 cm thick with sillimanite-garnet schist layers 1 to 10 mm thick. The thickness and proportion of pelitic schist increases in the upper 5 to 10 m of the unit. A few metres of pelitic schist occur below the upper contact.

Marble and calc-silicate (HIm)

Schist at the top of the paragneiss unit is overlain abruptly by a unit of grey and buff weathering pure marble and resistant, dark weathering calc-silicate rock. The lower 15 m is well-bedded pure marble on the west limb of the Sifton Antiform, but occurs as two members each 20 m thick and separated by 1 m of schist on the east limb. The pure marble is overlain by 25 m of brown-weathering, thick-layered calc-silicate rock, and pure marble interbedded with diopside and scapolite-bearing calc-silicate in layers 5 to 15 mm thick. The unique weathering of this sequence makes it an excellent stratigraphic and structural marker which is almost continuously exposed on ridges on both limbs of the antiform (Fig. 8d), but discontinuously in the valley where the unit plunges out to the north.

Pelitic schist (HIps)

Calc-silicate in the upper part of unit HIm is interbedded with pelitic schist and grades over several metres into a moderately recessive-weathering kyanite-staurolite-garnet schist. The unit is 150 to 400 m thick, weathers dark grey, and overlies the marble and calc-silicate formation along the west limb of the Sifton Antiform (Fig. 8d), around the closure to the north, and on one ridge of the east limb.

Metagrit, schist and metaconglomerate (HIg)

Pelitic schist is overlain by a fine and coarse clastic unit 400 to 1200 m thick that outcrops along the western flank and northern ridges of the area. The unit consists of light grey quartzofeldspathic metagrit, psammite, and minor calc-silicate, in layers 10 to 20 m thick that are resistant to weathering. Those rocks are interbedded with dark grey and rusty-weathering quartz-pebble metaconglomerate, kyanite-staurolite-garnet schist, and psammitic schist that are moderately recessive weathering.

Marble (HIc)

The uppermost map unit consists of more than 200 m of brown-buff, platy, impure marble with layers of psammite and minor quartzofeldspathic metagrit. It is structurally complex, moderately recessive weathering, and is exposed only on the west flank of the range.

Sifton Ranges, hanging wall of the Sifton Fault

Rocks in the hanging wall of the Sifton Fault are highly strained and comprise a gently dipping fault zone in which the apparent stratigraphy is to some extent of tectonic origin (Fig. 7). Restoration of the following stratigraphic sequence is conjectural and based on comparison with the general Windermere sequence elsewhere in the region and on the inference that orthogneiss is basement to the succession. The contact between gneiss and the overlying metaquartzite is not inferred to represent great stratigraphic separation.


a

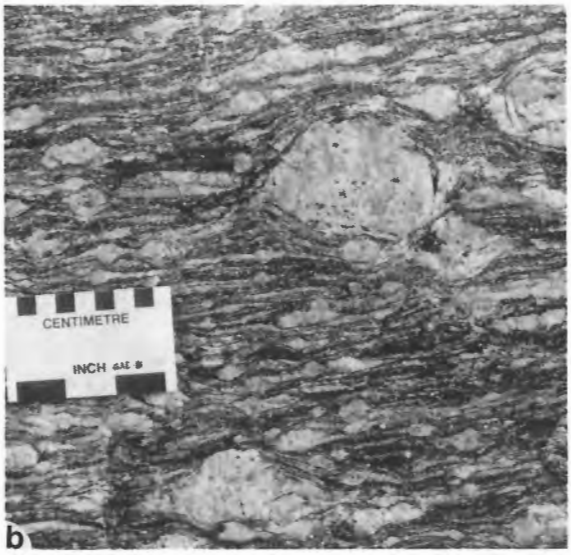
CENTIMETRE
b


c


d


e


f

Tochieka Gneiss (Agn)

Augen orthogneiss occurs in a north-plunging open anticline, and forms dark grey, resistant-weathering cliffs and ledges. The gneiss is strongly foliated leucocratic to mesocratic biotite-feldspar-quartz gneiss with potassium feldspar augen (Fig. 9a,b). The texture ranges from foliated gneiss lacking augen to gneiss with augen up to 3 by 4 cm in cross-section with a great variety in axial ratios. The gneiss is relatively homogeneous and consists of 30 % quartz, 35 % potassium feldspar, 25 % plagioclase, 5-10 % biotite, and minor muscovite, garnet, zircon, and apatite. It is intercalated with layers and boudins of amphibolite (Fig. 9c) which represent about 5 to 10 % of the formation. The lack of metasedimentary rock types and the high potassium feldspar content of the gneiss support the interpretation that it is orthogneiss. Zircons from the gneiss dated by R. R. Parrish using the U-Pb method yield an age of 1.85 ± 0.13 Ga (Parrish and Armstrong, 1983; Evenchick et al., 1984). The unit is regarded as basement to the hanging wall succession, and is referred to herein as the Tochieka Gneiss, after the Fox (formerly Tochieka) River on the east side of the Sifton Ranges. The type section is designated as the peak 1.5 km WSW of Peak 2023, in the central area of exposure of gneiss.

Ingenika(?) Group

Metaquartzite and amphibolite (HIqa)

The Tochieka Gneiss is structurally overlain by an extensive unit of metaquartzite and amphibolite, about 1000 m thick, which weathers white and dark grey and underlies the highest and most rugged topography of the study area. The gneiss/metaquartzite contact is well exposed on the ridge where the gneiss plunges out to the north below metaquartzite, and in a north-facing cirque 2 km ENE of Warner Peak. Lack of a strain gradient at the contact, and the sequence of metaquartzite over Early Proterozoic gneiss support the interpretation that the metaquartzite is a basal quartzite that was deposited on crystalline basement. Metaquartzite is intercalated with amphibolite in layers 2 to 5 cm thick in the basal 20 m of the unit. The remainder has amphibolite intercalations and metaquartzite layering on the scale of metres (Fig. 9d). The unit is about 70 % metaquartzite, >25 % amphibolite, and <5 % feldspathic metaquartzite, pelitic schist and paragneiss. The metaquartzite is pure (Fig. 9e,f), with >95 % quartz, and <5 % muscovite, zircon, garnet, and kyanite. Amphibolite is about 50 to 70 % hornblende, with quartz, plagioclase, and minor sphene, apatite, and in some samples, garnet. Pelitic schist has kyanite, sillimanite, staurolite, and garnet. Potassium feldspar is the dominant feldspar in the feldspathic metaquartzites.

Schist, marble, psammite (HIsm)

A unit of highly strained schist, psammite, marble and rare amphibolite is in complex structural relationship with the metaquartzite/amphibolite formation for the length of the hanging wall exposures. Dominant rock types are biotite schist with abundant quartz lenses (Fig. 10b), pelitic schist, quartzofeldspathic mylonite, and thick, white weathering tremolite marble and buff weathering marble. Marble members in this formation are the only useful structural markers within the hanging wall, forming large scale recumbent isoclines on the ridge west of Fox Lake (Fig. 10a) and synformal closures on the southwest flank of the range. The use of these markers is limited, commonly they are discontinuous as a result of either pinching out along shear zones, or noncylindrical folding, or both. Marble that occurs as isolated blocks may represent either many different marble layers or one or two layers repeated by folding and faulting. The unit structurally underlies the metaquartzite and amphibolite unit in northern exposures, and is inferred to structurally overlie it in the south. It is interpreted to stratigraphically overlie the metaquartzite and amphibolite unit in part on structural grounds, and in part by comparison with other Windermere strata in which carbonate occurs in the upper part of the succession.

Wavy schist (HIws)

The lowest structural unit is inferred to be the highest stratigraphic unit in the hanging wall. The muscovite-biotite-chlorite-garnet schist is extremely rusty and recessive weathering. It has anastomosing foliations that result in wavy lenses of schist about 1 cm thick (Fig. 10c). The schist includes minor layers of quartzofeldspathic mylonitic rock, rare amphibolite, and rare discontinuous layers of marble.

Cenozoic sedimentary and igneous rocks of the Sifton Ranges

Balourdet Pluton (Eg)

Undeformed biotite granite in the southern Sifton Ranges is fine — to medium-grained and leucocratic, with uniform modal mineralogy of 30 % quartz, 25 % plagioclase (oligoclase), 35 % potassium feldspar, 5-10 % biotite, and minor zircon, sphene, apatite, and allanite(?). It occurs as a homogeneous body that cuts the contact between the Tochieka Gneiss and the metaquartzite/amphibolite unit. Rare granitoid dykes cut both footwall and hanging-wall strata, and the pluton is cut by lamprophyre dykes. The K-Ar age of biotite from the pluton is 41.6 ± 2.2 Ma (Wanless et al., 1979). Balourdet Pluton is named after Mt. Balourdet, south of Fox Pass.

Figure 9. Rocks in the hanging wall of Sifton Fault. a), b) Tochieka Gneiss (Agn). (GSC 204482-R, S) c) Boudins of amphibolite and the outcrop characteristics of the Tochieka Gneiss. (GSC 204482-T) d) Cliff exposures of HIqa. The white folded layers are metaquartzite, and the dark layers are amphibolite. (GSC 204482-U) e),f) strongly foliated metaquartzite of unit HIqa. (GSC 204482-V, W)

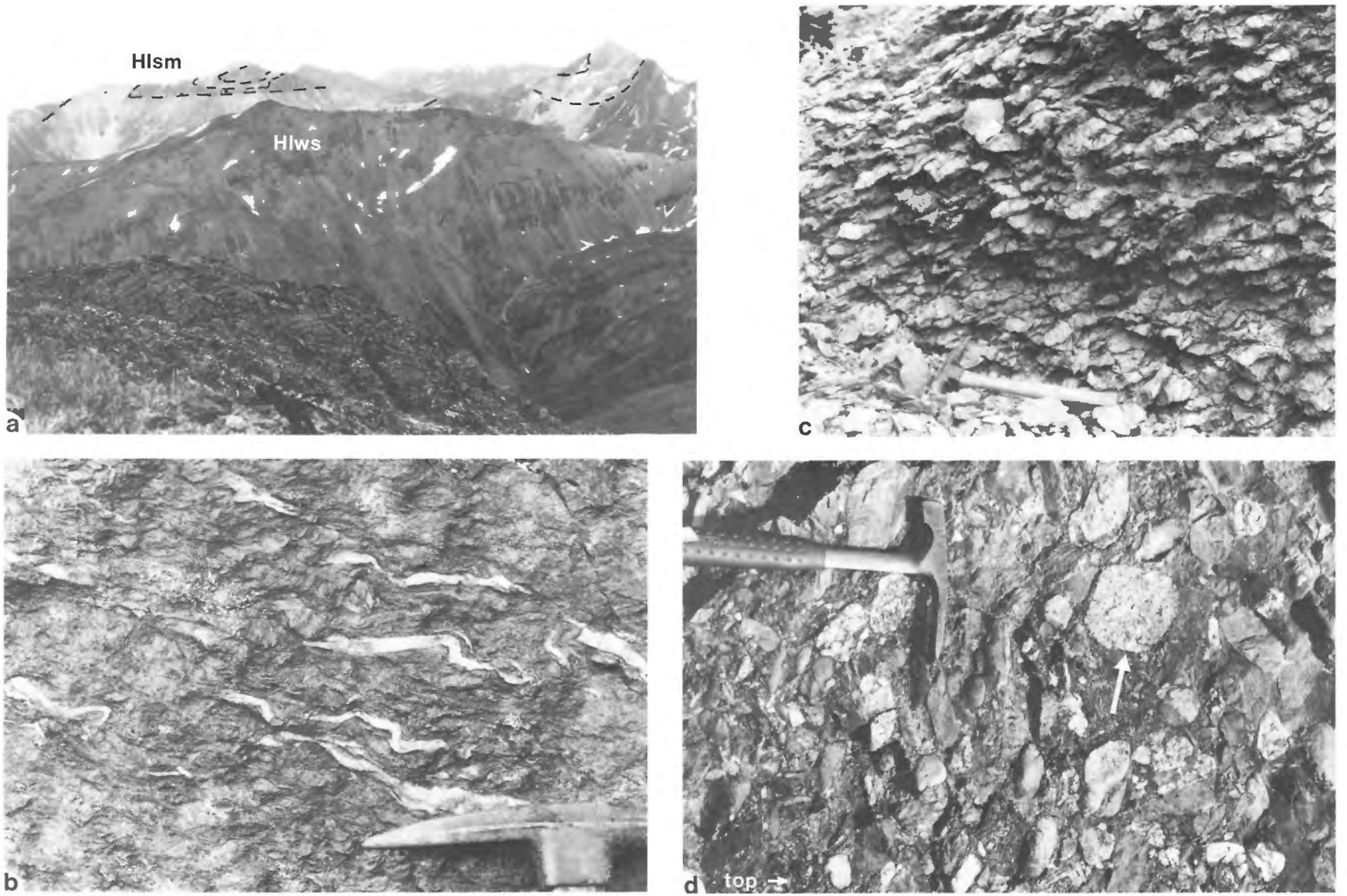

Figure 10. Rocks in the Sifton Ranges. a) View SE to recumbent folds of marble in Hlsm. In the foreground is a typical ridge exposure of rusty weathering wavy schist of unit Hlws. (GSC 204482-X) b) Quartz lense biotite schist of unit Hlsm. (GSC 204482-Y) c) Typical outcrop of wavy schist that comprises much of unit Hlws. (GSC 204482-Z) d) Crudely layered and poorly sorted conglomerate of the Sifton Formation. More than half the clasts are quartzite, and the rest are limestone, greenstone, and rare granite (indicated by arrow). (GSC 204483-A)

Pegmatite dykes

A thick undeformed pegmatite dyke, found in the valley north of "Atche Peak", has books of muscovite up (to 15 cm across) and garnets 2 to 3 mm in diameter. Several pegmatite dykes occur in the hanging wall of the Sifton Fault about 5 km northeast of Warner Peak; K-Ar ages of muscovite and biotite from one of the dykes are 43 ± 2.2 and 51 ± 1.8 Ma respectively (Wanless et al., 1979).

Lamprophyre dykes

All formations in the Sifton Ranges are cut by undeformed, fine — to coarse-grained lamprophyre dykes, 0.3 to 2 m thick, with modal mineralogy 25 % biotite, 25-30 % diopside, 20 % plagioclase, 10 % potassium feldspar, and about 5 % of each of apatite, sphene, quartz, carbonate, and opaques. The dykes are kersantites in the classification of Streckeisen (1979) because they contain essential biotite, and plagioclase is more abundant that potassium feldspar. Some mesocratic to melanocratic dykes are aphanitic. Biotite from a dyke northeast of Fox Peak has been dated by the K-Ar method at 37.8 ± 1.7 Ma (Wanless et al., 1979).

Volcanic rocks (Ev)

Four small isolated outcrops of altered volcanic rocks occur along the fault on the southwest flank of the Sifton Ranges that extends north past the east side of Spinel Lake. In hand specimen they are rusty weathering, fine grained, and green and black on fresh surfaces. Pyroclastic volcanics and andesitic dykes occur south of the study area near the junction of the Spinel Fault Zone and the Northern Rocky Mountain Trench. A whole-rock K-Ar age on an andesitic dyke is 41.6 ± 2.8 Ma (Wanless et al., 1978).

Sifton Formation (Es)

The Upper Cretaceous to Paleogene Sifton Formation (Eisbacher, 1974) is exposed at an elevation of 1700 m on the west flank of the Sifton Ranges. It is part of a belt that extends south along the Spinel Fault Zone to the Northern Rocky Mountain Trench. The formation was studied throughout the Sifton Basin by Eisbacher (1974), and little time was devoted to it in this project. Floras from near the study area are Paleocene to Eocene, but the Sifton Formation in the Kechika Fault Zone includes Late Cretaceous (Santonian-Campanian) strata.

Exposures on the ridge 5 km west of Warner Peak consist mainly of poorly sorted, massive or crudely layered pebble to boulder conglomerate (Fig. 10d). Clasts are grey limestone, white to pink quartzite, two-mica granite, greenstone, and grit with blue quartz. No rock types unique to the Sifton Ranges are present in the conglomerate, but they are typical of those found in the surrounding ranges. Conglomerate is gently dipping and at least 250 m thick. The base is not exposed, but 3 km to the southeast the Sifton Formation appears to overlie the Kechika Group, as it does 23 and 68 km to the southeast in the Cormier Range and the east flank of the Finlay Ranges respectively (Gabrielse et al., 1977a). In the southern Cormier Range, the unconformable contact between Sifton Formation and underlying strata (perhaps equivalent to hanging wall strata), is not believed to be affected by tectonism (H. Gabrielse, pers. comm., 1982). Conglomerates in the Sifton Formation are interpreted by Eisbacher (1974) to be talus, mountain-stream, debris-flow, and alluvial-fan deposits, and the sandstones are interpreted as river and lake deposits. Paleocurrent indicators and the composition of clasts suggest local provenance into south-flowing rivers (Eisbacher, 1974).

Tectonic implications of Cenozoic rocks

According to Eisbacher (1974) the Sifton Formation was deposited in response to extension and normal faulting associated with the initial uplift of the Columbian Orogen in mid-Cretaceous time. A later pulse of compressional brittle deformation caused kink folding of the clastic rocks and their basement.

Deposition of the Sifton Formation is almost restricted to basins surrounding and south of the Sifton Ranges. The age of the Sifton Formation in this area coincides with the age of latest uplift of the Sifton Ranges that is indicated by almost concordant K-Ar ages of biotite, muscovite, and hornblende from metamorphic rocks, and from igneous rocks which intrude the metamorphic rocks (*see* Fig. 46). These data suggest that deposition of the Sifton Formation was a result of Late Cretaceous to Eocene rapid uplift restricted to the Sifton Ranges and other local areas, rather than mid-Cretaceous uplift of the Omineca Belt as was suggested by Eisbacher. Uplift is inferred to have been on steep faults. Crowell (1974a) proposed that clastic sediments may be deposited in a region depressed by the loading of a thrust fault associated with compressional regions of transcurrent faults (*see* structure and tectonics). Small areas of the Sifton Formation also occur along the Kechika Fault to the northwest of the Sifton Ranges. The deformation of the clastic rocks described by Eisbacher may be a result of Eocene or later displacement on the steep faults.

Regional variations and correlations of Windermere stratigraphy

The Windermere Supergroup is a dominantly clastic, Upper Proterozoic succession which overlies the Purcell Supergroup and younger strata or crystalline basement, and underlies Lower Cambrian quartzite. Where basal Lower Cambrian strata are fine grained and argillaceous, the boundary between the Proterozoic and Paleozoic is difficult to determine or cannot be recognized. In a few localities, archaeocyathids have been found in carbonate members in phyllites of the Misinchinka Group, indicating that it includes some Lower Cambrian strata (Gabrielse, 1975).

The distribution of the Windermere Supergroup and a map of locations that are referred to are shown in Figure 11. The Windermere Supergroup is represented east of the Rocky Mountain Trench by (from south to north) the

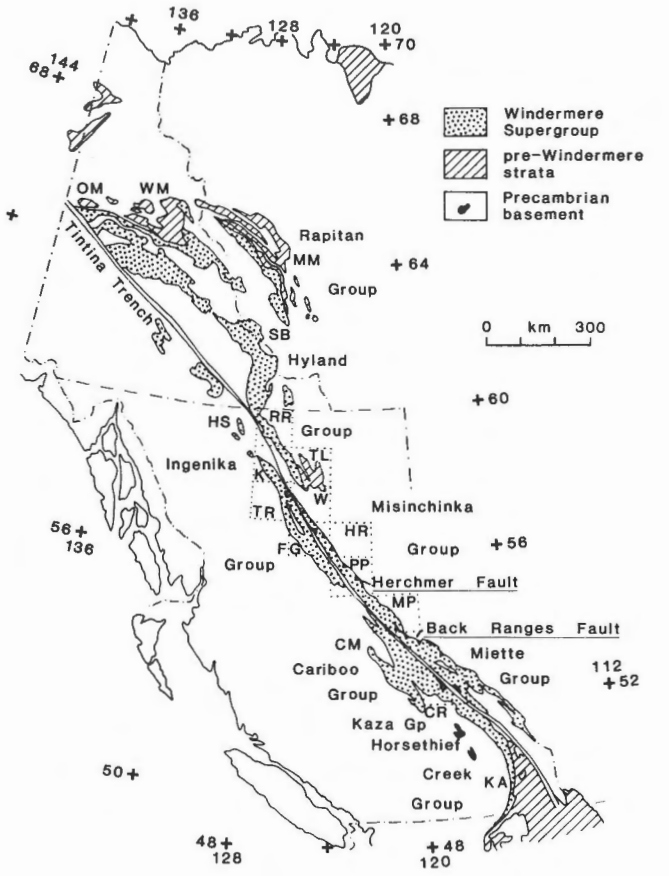

Figure 11. Distribution of the Windermere Supergroup. Map areas: CR Canoe River; FG Fort Grahame; HR Halfway River; K Kechika; MP Monkman Pass; PP Pine Pass; RR Rabbit River; TR Toodoggone; TL Tuchodi Lakes; W Ware. Geological and geographical features: CM Cariboo Mountains; HS Horseranch Range; KA Kootenay Arc; MM Mackenzie Mountains; OM Ogilvie Mountains; SB Selwyn Basin; WM Wernicke Mountains. Map modified after Eisbacher, 1981.

Hector, Miette, and Misinchinka groups. East of the Tintina Trench it includes the Hyland Group (formerly the "Grit Unit" (S.P. Gordey, pers. comm., 1986)), the Rapitan Group and younger Upper Proterozoic strata in Mackenzie and Wernecke mountains, and the upper part of the Tindir Group along the Alaska-Yukon border. West of the Rocky Mountain Trench it includes the Horsethief Creek, Kaza, Cariboo, and Ingenika Groups. Reviews of Windermere stratigraphy and correlations are given by Gabrielse (1972), Campbell et al. (1973), Young et al. (1973), Mansy and Gabrielse (1978), Young et al. (1979), Poulton and Simony (1980), and Eisbacher (1981). Windermere sequences are characterized in a general way by a thick lower unit of coarse and fine clastics with minor carbonate overlain by a unit of fine clastics. Either of the two clastic units may include diamictites. They are overlain by a discontinuous thick carbonate unit which is in turn overlain by fine clastics with minor conglomerate and carbonate.

Deserters Range

The Deserters Range has generally the same sequence of rock types as Windermere assemblages elsewhere, but its lower part includes a thick amphibolite unit and lacks the distinctive thick units of feldspathic gritty sandstone. In most regions, the lower clastic units can be distinguished from the upper fine clastic unit only by their position relative to the thick carbonate unit. However, there is no way of determining if the discontinuous thick carbonate unit found throughout the belt of Windermere Supergroup is everywhere at the same stratigraphic level. A thick carbonate in the upper Miette Group 48 km northwest of Jasper was named the Byng Formation by Slind and Perkins (1966). The discovery, near Mount Robson, of an Ediacaran fauna in a carbonate platform at the same stratigraphic level as the Byng Formation indicates a latest Precambrian age for the thick discontinuous carbonates in the upper Miette Group (Hofmann et al., 1985). The Miette is unconformably overlain by the Gog Group. Thompson (1978) extended correlation of the Byng Formation northwest into the Monkman Pass map area, where it occurs in the footwall of the Back Ranges Fault. Farther northwest, in the Pine Pass map area, a thick carbonate formation occurs in the hanging wall of the Herchmer Fault and there, as in the Deserters Range, a thick succession of fine clastics intervene between the thick carbonate and the Gog Group. These relationships suggest that the carbonate in the hanging wall of the Herchmer Fault is probably not correlative with the Byng Formation.

In the Ware, Fort Grahame, and Halfway River map areas, the Misinchinka Group occurs in a belt 300 km long in the hanging wall of the Herchmer Fault (Gabrielse, 1975; Irish, 1970). This belt may extend 240 km south into the Monkman Pass area where R.I. Thompson (pers. comm., 1985) regards the Back Ranges Fault as an extension of the Herchmer Fault. The study area is located in the northern part of this belt and is a structural culmination in which the lower three-quarters of the section plunges out 15 km to the north, and 10 km to the south. As a result, all of the belt to the north and much of it to the south in Fort Grahame map area is underlain by the uppermost unit of chlorite phyllite. A minor culmination may be present 55 km south of the study area, where a thick carbonate is associated with green and black phyllitic slates, diamictite, platy limestone, gritty feldspathic quartzite, and pebble conglomerate (Gabrielse, 1975). To the southeast, in Halfway River (Irish, 1970), Pine Pass (Stott et al., 1983; Muller, 1961), and Monkman Pass (Thompson, 1978) map areas, the Misinchinka Group consists of a lower unit of phyllite, quartzite and diamictite, a middle unit of carbonate and quartzite, and an upper unit of argillite, quartzite, and siltite. In Halfway River map area, a locality of diamictite and magnetite in chlorite schist is near the contact of phyllite with a limestone unit. A similar association occurs in unit HMscd in the Deserters Range. North of Deserters Range, Windermere rocks are exposed in a belt 200 km long crossing the Ware (Taylor et al., 1979), Tuchodi Lakes (Taylor and Stott, 1973), Kechika (Gabrielse, 1962a) and Rabbit River (Gabrielse, 1962b) map areas. The belt consists of chloritic phyllite, slate,

feldspathic quartz-pebble conglomerate, sandstone, carbonate and local sheared greenstone lenses. A distinctive unit of maroon and green shale occurs near the top of the assemblage over extensive areas. The strata are probably correlative with the Hyland Group in southeastern Yukon Territory (S.P. Gordey, pers. comm., 1986). The thick assemblage is in fault contact with pre-Windermere strata to the east which are overlain directly by Lower Cambrian quartzite.

Diamictites are found throughout the belt of Windermere Supergroup at several stratigraphic levels and are interpreted as either mass-flow or glacial deposits or both. In the Mackenzie and Wernecke mountains there is strong evidence, in the form of dropstones, striated stones on a polished pavement, and facies distribution, that at least some diamictites in the lower part of the Windermere assemblage are of glacial origin (Eisbacher, 1981; Yeo, 1981). Diamictites in Ware map area are interpreted by Taylor et al. (1979) as mass flows and by Fritz (1972) and Eisbacher (1981) as glacial. Diamictites in Deserters Range retain no primary structures so it is not possible to determine their origin. However, if they are glacial, then at least one glacial event in the Windermere is younger than 728 Ma.

The Deserters Range shares the general Windermere association of iron-rich metasediments with diamictite (Yeo, 1981). In the Mackenzie and Wernecke mountains, thick iron-formation is found near the base of the Windermere Supergroup. In the Misinchinka Group in Deserters Range and the Halfway River area, magnetite schists occur near diamictite in the upper part of the succession.

The only area with strata similar to the base of the Deserters section is 650 km to the southeast in Canoe River map area. Near Mount Blackman, a Precambrian basement complex including basement granite dated at 741 $+22/-20$ Ma (Parrish and Armstrong, 1983) is overlain by metaquartzite at the base of a complete section of the Miette Group. These relationships are exposed in two culminations of basement gneiss east of the Rocky Mountain Trench. The Bulldog Gneiss (McDonough and Simony, 1984) is overlain by 50 m of metaquartzite, and about 30 km to the southeast, the Mount Blackman Gneiss is overlain by 200 m of muscovite quartzite (Oke and Simony, 1981; Leonard, 1984). In both areas, gneiss below the contact is strongly sheared, and the contact is thought to be a basement-cover décollement. The contact is poorly exposed and placed at the first appearance of biotite (Oke and Simony, 1981). Amphibolite occurs in the basement gneiss but not in the cover rocks, and the metaquartzite is overlain by a complete Miette succession. The sedimentary contact between the Deserters Gneiss and the overlying metaquartzite in Deserters Range adds strength to the arguement that the tectonic contact in the southern occurrences need not represent great stratigraphic separation, and that the quartzite is basal Windermere.

Sifton Ranges west of Spinel Lake

Correlations of strata in the Sifton Ranges west of Spinel Lake with the Windermere Supergroup are straightforward. The rock types and sequence of strata west of Spinel Lake can be directly correlated with the formations of the Ingenika Group elsewhere in the region as defined by Mansy and Gabrielse (1978), and with uppermost Precambrian and Lower Cambrian strata as described by Fritz (1980, 1984). The Swannell, Tsaydiz, Espee, and Stelkuz formations are lithostratigraphic correlatives of the Kaza Group, Isaac, Cunningham, and Yankee Belle formations respectively of the Cariboo Mountains (Mansy and Gabrielse, 1978; Fritz, 1984). The correlation is based on strong lithological and stratigraphic sequence similarities. Formations of the Ingenika Group are of comparable structural thickness to those reported by Mansy and Gabrielse, with the exception of the Espee Formation which is only 20 m thick, in contrast to measured sections of 290, 134, and 408 m farther south. In addition, the Atan Group is extremely thin, with only 1 to 3 m of Boya Formation and 25 m of Rosella Formation, contrasting with 950 and 266 m of the same formations in nearby areas (Fritz, 1984). The thin Atan Group may be related to the sub-Rosella disconformity recognized in the Cassiar Mountains, and/or to tectonic thinning.

Sifton Ranges east of Spinel Lake

East of Spinel Lake, the dominantly clastic nature of the sequence, the presence of feldspathic quartz-pebble metaconglomerate, and the abundance of marble in the upper structural levels suggest correlation with the Windermere Supergroup. The abundance of coarse clastic material above HIm suggests that the strata are part of the Swannell Formation and stratigraphically underlie, or are equivalent with, parts of the Swannell Formation west of Spinel Lake. This interpretation is supported by the possible correlation of metaquartzite stratigraphically low in the footwall, with metaquartzite low in the Swannell Formation in both the southern Swannell Ranges (Roots, 1954), and in the Butler Range. In the Butler Range, metaquartzite is associated with basement(?) gneiss (Gabrielse, 1975, and pers comm., 1984). The sequence is inferred to be upright from the presence of carbonate in the upper structural levels and metaquartzite in the lowest structural levels.

Hanging wall of the Sifton Fault

The hanging wall stratigraphy is generally similar to that in the Deserters Range, with metaquartzite and amphibolite overlying crystalline basement. No other exposures of Proterozoic basement gneiss are known in the Omineca Belt north of the Cariboo Mountains, but the presence of inherited 2 Ga Pb in detrital zircons in Windermere strata in the Cassiar and Cariboo mountains reveals that Early Proterozoic gneiss was being eroded during the Late Proterozoic (Evenchick et al., 1984). No amphibolite occurs in the assemblages west of Spinel Lake nor in the footwall of the Sifton Fault, nor in the Windermere sequences described by Mansy and Gabrielse (1978). Amphibolite occurs in the Swannell Formation in the Butler Range (Gabrielse, 1975). Although direct correlation with Deserters Range stratigraphy is not likely, the common metaquartzite and amphibolite overlying basement suggest a similar environment of formation of basal Windermere

strata, not necessarily at the same time or place. The marble and fine metaclastics are inferred to be in the upper part of the succession. The structurally low wavy schist unit may correlate roughly with fine clastic strata in the upper part of Windermere succession.

Tectonic implications of stratigraphy in Deserters and Sifton ranges

The base of the Windermere Supergroup is generally not exposed, except in the Kootenay Arc (e.g. Leclair, 1983), the northern Rocky Mountains (Fritz, 1972), and parts of the Yukon (Eisbacher, 1981) where it unconformably overlies thick assemblages of Upper and Middle Proterozoic strata, and probably east of the Southern Rocky Mountain Trench where it overlies crystalline basement. Prior to this study, the few contacts of Windermere Supergroup with crystalline basement have been described as tectonic, and the stratigraphic relationship of the metaquartzite to the basement has been in doubt. The nonconformable relationship demonstrated in Deserters Range (Evenchick, 1983), and the probable unconformable relationship in Sifton Ranges provide insight into Late Proterozoic paleogeography, suggesting uplift, mafic igneous activity and extension younger than 728 Ma. The following important relationships and their implications are noted: 1) In Sifton Ranges, the Windermere Supergroup is underlain by early Proterozoic crystalline basement, the Tochieka Gneiss, but to the north and east, thick pre-Windermere strata are present. The absence of pre-Windermere strata in Deserters and Sifton ranges suggest that Middle and possibly some Upper Proterozic rocks were uplifted and eroded. Considerable post-728 Ma uplift is required to expose the granite basement in Deserters Range prior to deposition of quartzite on the basement. In addition, the presence of inherited 2 Ga Pb in zircons in Windermere strata of the Cassiar and Cariboo mountains (Evenchick et al., 1984) suggests widespread exposure of Early Proterozoic gneisses during the late Proterozoic. Uplifted blocks of orthogneiss and pre-Windermere strata are an appealing source for the grits that characterize the Windermere Supergroup, and a local source for the grits reduces the problem of deriving them from the craton far to the east and over a thick pre-Windermere sequence. 2) The abundance of amphibolite in metaquartzite near the base of the Sifton and Deserters ranges sequences, and of numerous wide, northerly-trending diabase dykes that cut pre-Windermere strata in the northern Rocky Mountains suggest early Windermere mafic igneous activity in an extensional environment. The U-Pb date on zircons from the Deserters Gneiss indicates that igneous activity and extension at least locally postdates 728 Ma.

These relationships are consistent with the following model of rifting that at least locally initiated Windermere sedimentation (Fig. 12). At 728 Ma, a granitic intrusion cooled to below the blocking temperature of zircon; the granite was possibly associated with high heat flow during early extension and thermal uplift (Fig. 12a). Continued uplift and erosion of pre-Windermere rocks eventually exposed the granite and gneissic basement, and both were onlapped by basal conglomerate and quartzite (Fig. 12b).

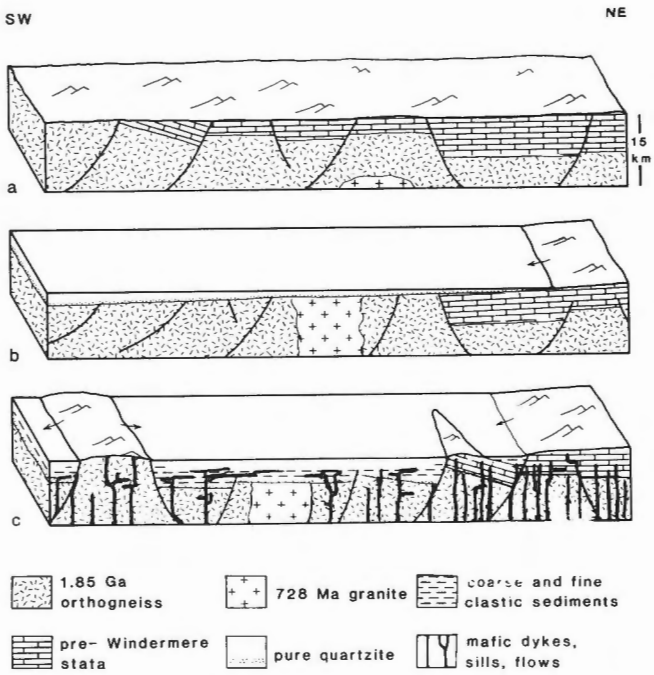

Figure 12. Model of early Windermere environment. a) Extension and thermal uplift accompanied by the intrusion, and subsequent cooling (728 Ma) of granite. b) Uplift and erosion of pre-Windermere strata to expose the granite, followed by deposition of basal conglomerate and quartzite. c) Renewed extension accompanied by mafic igneous activity and deposition of coarse clastic detritus from uplifted blocks of basement gneiss.

Renewed extension accompanied by mafic igneous activity resulted in dyke swarms cutting pre-Windermere strata, amphibolite (sills or flows) associated with quartzite in basal Windermere sequences, and uplifted blocks that shed coarse clastic potassium feldspar-rich detritus into rift basins (Fig. 12c). The study of Windermere Supergroup in less metamorphosed areas of the Cariboo and Omineca mountains has led to the interpretation that the fine clastics overlying the grit units were deposited in a quiet environment below wave base and represent an interval of decrease in relief of the source area and of decrease in basin depth (Mansy and Gabrielse, 1978). The overlying carbonates reflect a phase of shoaling, with the carbonates and overlying fine clastics deposited in shallow marine water after the sedimentary prism built up to wave base (Mansy and Gabrielse, 1978).

Age of the Windermere Supergroup

The commonly cited age for the base of the Windermere Supergroup is 850 Ma (Miller et al., 1973). The age is from K-Ar dates on the Huckleberry volcanics which overlie thick diamictite near the base of the Windermere Supergroup in northern Washington. The reported dates range from 233 to 918 Ma. The rocks dated are altered greenstones, and recent geochemical work by Devlin et al. (1984,1985) suggests that the age derived by Miller is not indicative of the age of extrusion of the volcanics because the K-Ar system was disturbed. The Deserters data help

Table 2. Mineral assemblages in Deserters and Sifton ranges. Maximum-phase assemblages of metapelites, and mineral assemblages in associated psammitic, calcareous and mafic rocks. Minerals after semicolon need not be present.

	Pelitic assemblages										
	kf	sil	ky	st	gn	bi	ctd	ch	mu	pl	qtz
Deserters Range:											
chlorite							+/−	x	x	x	x
biotite					x		x	x	x	x	
garnet					x	x	+/−	x	x	x	x
st-bi				x	x	x		+/−	x	x	x
ky-gn-st			x	x	x	x			x	x	x
Sifton Ranges:											
E & W of Spinel L.											
chlorite						x		x	x	x	x
garnet					x	x		x	x	x	x
st-bi				x	x	x			x	x	x
ky-gn-bi			x	x	x	x			x	x	x
sill-ky		x	x	+/−	x	x			x	x	x
sill		x			x	x			x	x	x
sill-Kf	x	x			x	x			x	x	x
Hanging wall											
bi-gn					x	x			x	x	x
st-bi				x	x	x			x	x	x
ky-gn-bi			x	x	x	x			x	x	x

	Psammite (qtz)	quartzite (qtz)	calcareous (cc, qtz)	mafic (qtz, plag)
Deserters R.				
chlorite	mu, ch, pl		pl, mu; ch	
biotite	pl, bi; mu, ch	mu, bi	pl, bi; mu, ch	act, mu, bi, ep
garnet			pl, bi; mu, ch, tr	hb, act, bi, ep; ch
st-bi	mu; bi, gn, ep, ch	mu, bi	pl, bi; mu, tr	
ky-gn-bi	mu; bi, gn, st, pl	mu; pl, bi		hb; bi, ep
E & W of Spinel Lake				
chlorite	pl, mu, ch; ep		pl, mu, ch; ep	
garnet	pl, mu, bi; gn, ep			
st-bi	pl, mu, bi, gn; st			
ky-gn-bi	pl, bi; mu			
sill-ky	pl, mu; cc		sph; pl, bi, gn, di, sc, hb, ch	
sill	pl, mu, bi; gn, sil		sph, di, pl; gn, bi, sc, hb, ch, ep	
Hanging wall				
st-bi	pl; mu, bi, gn, st	pl, mu, bi; gn;	pl, mu, bi, tr, shp, ep	
ky-gn-bi	pl, bi; gn	bi; mu, pl	bi; pl, mu	hb, bi; mu, sph
sill-ky	pl, bi; mu, gn, Kf, hb, and, cd (gneiss)	mu, bi; pl, gn		

establish a younger age for the base of the Windermere (728 Ma). Similar dates from zircon geochronology are the 741 + 22/−20 Ma age on gneiss associated with basal Windermere near Mount Blackman, southern Rocky Mountains (Parrish and Armstrong, 1983), and an age of about 777 Ma (Roots and Parrish, unpublished data) for volcanic rocks associated with coarse clastic rift-type sediments in the Mount Harper area of the Ogilvie Mountains. Rb-Sr dates of 766 ± 24 and 769 ± 27 Ma on sills and dykes that cut pre-Windermere strata in the Mackenzie Mountains (Armstrong et al., 1982) indicate a 770 Ma phase of extension, consistent with early Windermere rifting. From the construction of tectonic subsidence curves of the post-rift strata of the miogeocline by the backstripping method, Bond and Kominz (1984) suggest that regardless of when rifting started, it ended between 555 and 600 Ma. A younger age for the Windermere Supergroup would reduce the length of the rifting phase, (episodic or protracted) from 250 to 150 Ma or less.

METAMORPHISM

Strata in the study areas reached a peak of metamorphism in greenschist and amphibolite facies (Gabrielse, 1975, 1977a). The purpose of the metamorphic study is to gain an understanding of the pressure and temperature

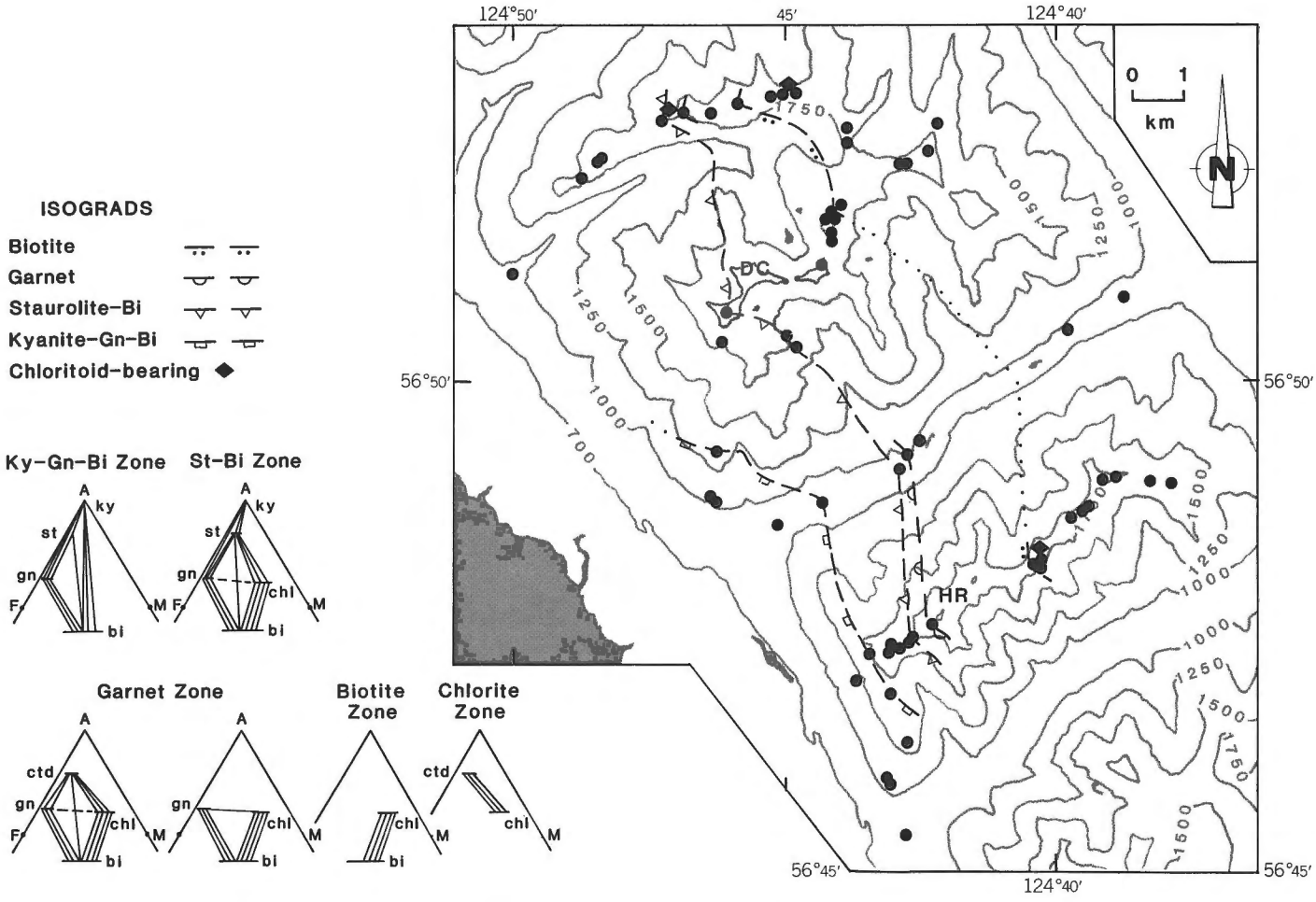

Figure 13. Metamorphic map of the Deserters Range. Points correspond to maximum-phase assemblages. Ornaments are on the high grade side of the isograds. Sub-assemblages for each zone, and reactions (depicted by crossing tie-lines) for each isograd, are shown on the AFM projection of Thompson (1957). DC Deception Cone, HR "Henry's Ridge".

conditions of metamorphism and the relationship of metamorphism to deformation. The position of previously mapped isograds has been refined, new isograds have been defined and mapped, and mineral assemblages and textures have been examined in thin section. The pressure and temperature conditions of metamorphism have been contrained by the study of mineral assemblages, and an analysis of mineral chemistry using the electron microprobe.

Pelitic mineral assemblages are the focus of this study because pelitic schist is the most abundant rock type with the potential for mapping isograds and defining the pressure and temperature conditions of metamorphism. Isograds were mapped in the field and verified or refined by examination of thin sections. Maximum-phase assemblages for each zone are given in Table 2. The table includes mineral assemblages in associated psammitic, calcareous, and mafic rocks. Interpretation of the metamorphic conditions is based on the bathozone scheme advocated by Carmichael (1978) for pelitic rocks. The bathozone diagram has been modified by Carmichael (*in* Archibald et al. 1983) to be consistent with geothermometry of the bathozone 5/4 facies series of Pigage and Greenwood (1982). Most metapelites in the study area approximate the ideal pelitic system SiO_2-Al_2O_3-FeO-MgO-Na_2O-K_2O-H_2O, with MnO and CaO as the principal "impurity" components. They contain quartz, plagioclase (An_{10-50}), and muscovite, permitting graphical display of assemblages on the AFM projection (Thompson, 1957) of the AFMK tetrahedron. Intersecting tie-lines result in changes to the topology of the AFM diagram which graphically illustrate the discontinuous reactions that correspond to mappable isograds in each of the ranges. Discussion is limited to discontinuous reactions because they are sufficient to explain the progressive change in assemblages with increasing metamorphic grade.

No information on the absolute age of metamorphism is provided by this study. Geochronological studies in the Wolverine Complex, 150 km to the southwest of the Sifton Ranges, indicate that regional metamorphism was probably Middle Jurassic (Parrish, 1979). Mid-Cretaceous K-Ar dates on metamorphic rocks and batholiths in the Cassiar

and Omineca mountains suggest regional uplift and cooling at that time (Wanless et al., 1971,1978,1979). Eocene K-Ar dates in restricted areas, including the study area (Wanless et al., 1979; Stevens et al., 1982), reflect another episode of uplift and cooling.

Metapelites in Deserters Range

Metamorphic grade is lowest in the east at the highest stratigraphic and structural levels, and increases to the west to the Northern Rocky Mountain Trench, where the lowest stratigraphic and structural levels occur. The pelitic mineral assemblages define five metamorphic zones bounded by two mineral isograds and two reaction isograds (Fig. 13). In most assemblages, phyllosilicates define the foliation, quartz is granoblastic with undulose extinction, and the accessory minerals are zircon, apatite, tourmaline, epidote, ilmenite and graphite(?). Retrograde chlorite and sericitized plagioclase are minor constituents. Isograds are defined only on four narrow transects and are subparallel with formation contacts, so it is possible that the mineral isograds are controlled in part by the variety of rock types present.

Phyllite and schist in all zones have a strong foliation that is folded (Fig. 14). The deformation resulting in the development of the foliation is referred to as D1, and folding of the foliation is referred to as D2.

Chlorite zone

Metapelites in the chlorite zone consist mainly of **sericite**, **chlorite**, **plagioclase**, and **quartz**. Porphyroblasts of **chloritoid** occur 200 to 500 m east of the biotite isograd on the ridge north of Deception Cone and on "Henry's Ridge". Chlorite and sericite define the foliation in phyllite, and chlorite also occurs as porphyroblasts. Foliation is commonly parallel with bedding, and in some cases is strongly crenulated (Fig. 14a), although the crenulations rarely result in a surface of easy splitting (crenulation cleavage). In rare examples, foliation that crosscuts bedding is crenulated. Primary clasts of quartz and feldspar are evident in the sparse metasandstones in the zone. Straight trails of opaque inclusions in chloritoid porphyroblasts contrast with the strong crenulation of the exterior foliation (Fig. 14b), and indicate that growth of chloritoid postdates development of foliation (D1) and predates crenulation (D2) of the foliation. The topology of the AFM diagram is shown in Figure 13.

Biotite zone

The dominant minerals in the biotite zone are **muscovite**, **biotite**, **chlorite**, **plagioclase**, and **quartz**. The appearance of biotite does not change the AFM topology of the chlorite zone. The biotite isograd may occur by a number of reactions depending on the bulk composition, but none of the equilibria have been calibrated so the isograd is of no quantitative value for determining the metamorphic conditions (Turner, 1981). All phyllosilicates define a foliation which is warped and crenulated. In rare examples biotite occurs also as coarse porphyroblasts with straight inclusion trails, indicating post-D1 and pre-D2 growth of biotite.

Garnet zone

The garnet zone is marked by the first appearance of garnet and the dominant minerals **garnet**, **muscovite**, **biotite**, **chlorite**, **plagioclase**, and **quartz**. **Chloritoid** occurs with the assemblage in one locality near the high grade limit of the garnet zone on the ridge north of Deception Cone, 100 m from the staurolite isograd. The 7-mineral assemblage results in intersecting tie-lines (Fig. 13) which show graphically the discontinuous reaction:

gn + mu + ch + ilm → ctd + bi + plag + qtz + water (1)

This is the highest grade occurrence of chloritoid, and its coexistence with biotite precludes further coexistence of chlorite and garnet. Phyllosilicates define the foliation. Garnet porphyroblasts are 2 to 5 mm in diameter and have straight, sigmoidal, and snowball inclusion trails, that indicate syn — and post-D1, but pre-D2 growth (Fig. 14c) of garnet.

Staurolite-biotite zone

The staurolite-biotite zone is marked by the first appearance of **staurolite**. The full assemblage **garnet-staurolite-muscovite-biotite-chlorite-plagioclase-quartz** occurs only 200 m beyond the staurolite isograd and chlorite is absent up-grade. The appearance of staurolite with biotite and disappearance of chlorite with garnet is depicted in Figure 13 by intersecting tie-lines on the AFM diagram; it corresponds to the discontinuous reaction:

gn + ch + mu + ilm → st + bi + plag + qtz + water. (2)

On the ridge north of Deception Cone, the staurolite reaction isograd is 100 m west of the highest-grade occurrence of chloritoid. These relationships are in accord with experimental and petrological work that shows that the lowest grade reactions that produce staurolite are chloritoid and chlorite + garnet breakdown reactions (Winkler, 1979). Kyanite occurs in a single thin section from a sample halfway through the staurolite zone on "Henry's Ridge". It coexists with garnet, staurolite, and muscovite, but not with biotite, and represents an Fe — and Al-rich bulk composition on the AFM diagram. It is the first appearance of kyanite, but is not a mappable isograd in this area because of the restricted bulk composition required to produce it. It can be appreciated from the AFM topology of the zone that the absence of chlorite-bearing assemblages also indicates relatively Fe-rich bulk compositions.

Phyllosilicates define a foliation which is preserved in garnet cores as either straight, sigmoidal, or snowball trails of inclusions, in garnet rims as "wrapped" helicitic inclusions, and in staurolite as straight inclusion trails (Fig. 14d). The foliation is strongly crenulated where it is not preserved as inclusions (Fig. 14e). The textural zoning in garnet suggests syn-D1 growth of garnet and wrapping of the foliation around the early-formed garnets prior to growth of garnet rims. The rim textures and the presence of staurolite and chloritoid as rim inclusions (Fig. 14e) indicate post-D1 and pre-D2 growth of chloritoid, staurolite, and garnet rims.

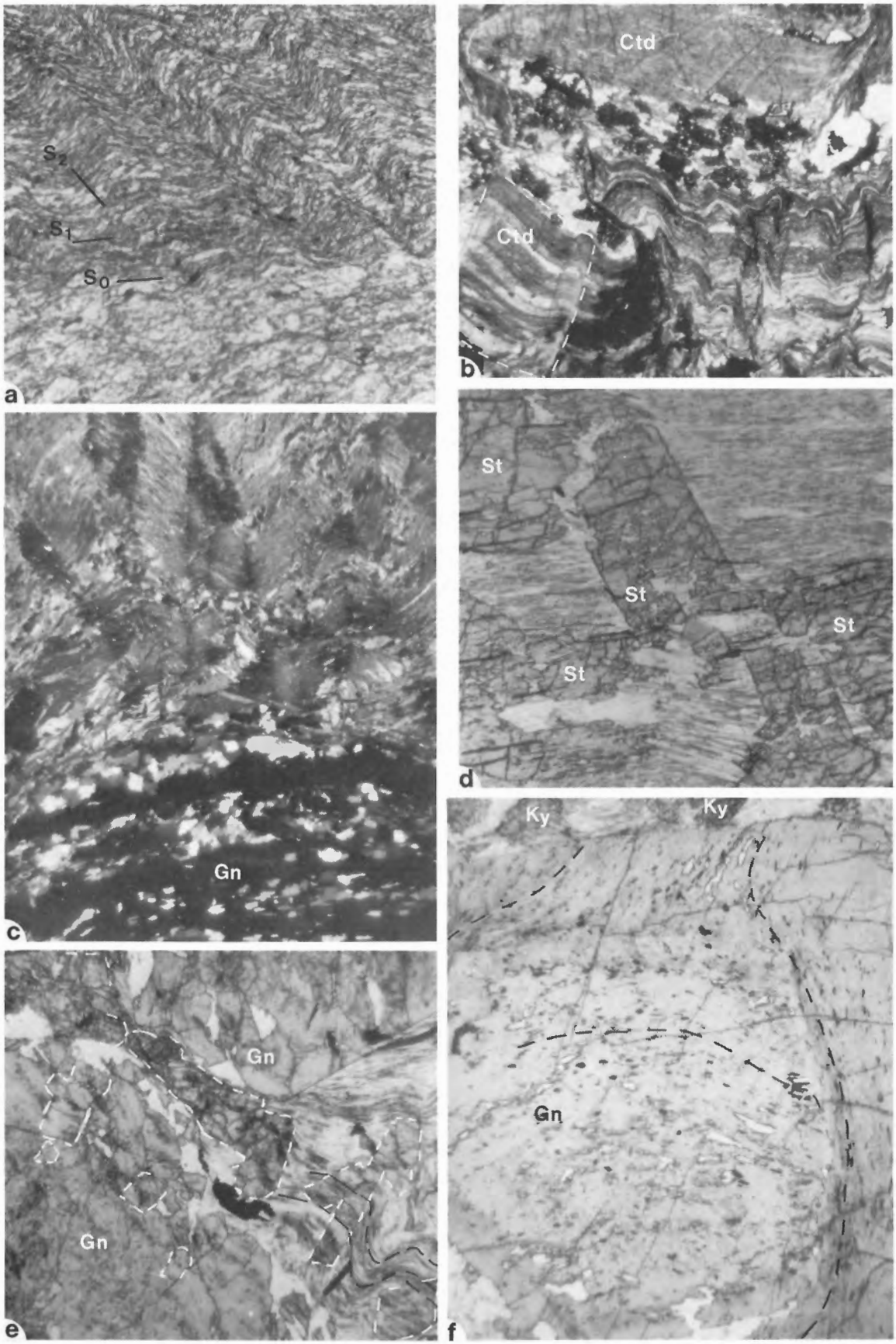
a
S_2
S_1
S_0
b
Ctd
Ctd
c
Gn
d
St
St
St
St
e
Gn
Gn
f
Ky
Ky
Gn

Kyanite-garnet-biotite zone

The zone is marked by the first appearance of **kyanite** with the assemblage **garnet-staurolite-muscovite-biotite-plagioclase-quartz**. All kyanite-bearing schists have the maximum-phase assemblage. It is univariant in P-T space in the ideal pelitic system and is represented on Figure 15 by the curve:

st + mu + qtz + ilm → gn + ky + bi + plag + water. (3)

The change to the AFM diagram is depicted in Figure 13. The persistence of the 7 mineral assemblage over a structural thickness of greater than 600 m may be due to one or more of the minerals being impure with respect to the ideal pelitic system (eg. Zn in staurolite; Mn and Ca in garnet) so that the equilibrium is not strictly univariant. The intersection of the reaction with the kyanite-sillimanite curve restricts the minimum pressure conditions to bathozone 5 or 6, limiting the pressure to greater than about 5.5 kb. In the structurally lowest pelites, orthoamphibole coexists with kyanite, garnet, staurolite, biotite, plagioclase, and quartz. The assemblage is ideally univariant, and the curve:

st + plag + qtz → gn + ky + oa + water (4)

limits pressure to greater than about 6.3 kb and temperature to about 620°C.

The maximum-phase assemblage requires that kyanite coexist with garnet and biotite. In other regions (eg. Carmichael, 1970; Froese and Gasparrini, 1975; St-Onge, 1981;1984a), an Al_2SiO_5-biotite isograd has been mapped at relatively lower grade, based on the discontinuous reaction

ch + st + mu + qtz → Al_2SiO_5 + bi + plag + water. (5)

The reaction was not recognized in Deserters Range because the bulk compositions are not magnesian enough for chlorite to be stable beyond the breakdown of garnet + chlorite.

The schists are strongly crenulated. Garnets are 5 to 8 mm diameter and are either texturally zoned with straight, sigmoidal, or snowball inclusion trails in the core, or are homogeneous, embayed poikiloblasts. The texturally zoned garnets have rims that are either homogeneous or have "wrapped" inclusion trails that indicate flattening of the foliation around garnet cores before garnet-rim growth (Fig. 14f). No chloritoid and only rare staurolite inclusions are preserved in the rims. Staurolite porphyroblasts are coarse, idioblastic, and have straight inclusion trails. In one example staurolite has helicitic inclusions of a kink fold. Kyanite occurs as coarse blades that have been kinked and brittly shuffled. The textures indicate syn-D1 growth of garnet cores, and post-D1, pre-D2 growth of staurolite, kyanite, and garnet rims. These textures are consistent with a single prograde metamorphic event, with the garnet having initially grown under garnet zone conditions, having been slightly resorbed under staurolite-biotite zone conditions by means of reaction (2), and having grown again under kyanite-garnet-biotite zone conditions by means of reaction (3).

Figure 14. Photomicrographs of schists in the Deserters Range. a) Bedding (SO), foliation (S1), and crenulations (S2) in chlorite-sericite phyllite of the chlorite zone. b) Chloritoid with straight inclusion trails and crenulated exterior foliation, from the chlorite zone. c) Straight inclusions in garnet and crenulated exterior foliation, from the garnet zone; 14d straight inclusion trails in staurolite, from the staurolite zone. e) Staurolite inclusions in garnet rim (outlined in white), straight inclusion trails in staurolite in the matrix, and crenulated exterior foliation (foliation traced in black). f) Texturally zoned garnet from the ky-gn-bi zone. The width of a) and d) is 3.6 mm, and the width of b),c),e), and f) is 1.5 mm.

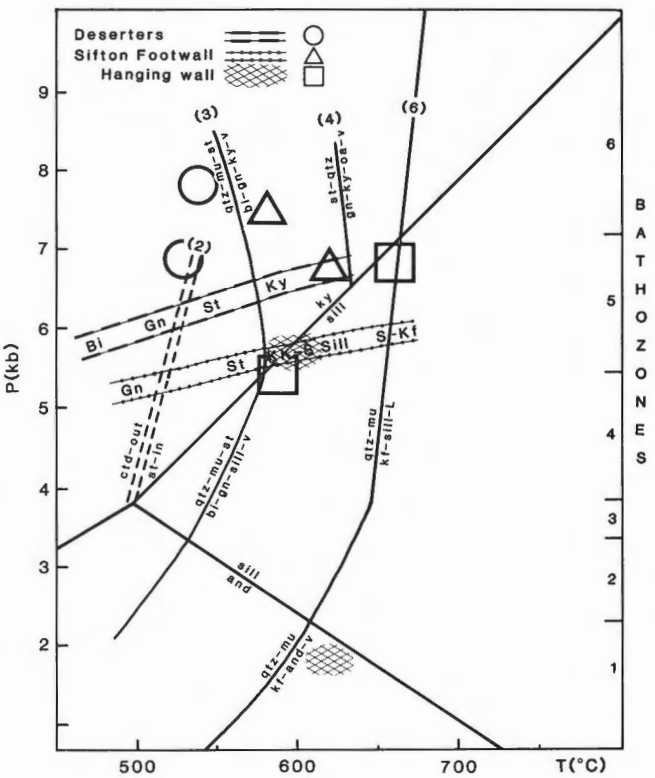

Figure 15. Petrogenetic grid for Deserters and Sifton ranges. The grid is modified from the bathozone grid of Carmichael (*in* Archibald et al., 1983). Curves 2 and 4 are from an unpublished grid devised by D.M. Carmichael; several reactions represented by curve 2 are reviewed by Winkler (1979). Patterned bars show the approximate location of the metamorphic field gradients as deduced from the order and spacing of isograds. Mineral abbreviations represent the corresponding zones for each part of the gradients. Circles, squares and triangles are the P-T conditions determined from geothermobarometry.

Discussion of isograd map-pattern, metamorphic field gradient, and paleo-geothermal gradient

The thin section observations indicate that the D2 crenulations and associated D2 folds are postmetamorphic. Because only one phase of microscopic or mesoscopic folding is recognized, these relationships may be extrapolated to a larger scale, to infer that Deserters Anticline is postmetamorphic and has folded the isograds. Map-scale evidence that the isograds are folded lies in the location of the staurolite isograd at about the same stratigraphic level on the four transects and in the apparent change in dip of the isograd over the Deserters Anticline (Fig. 13). The staurolite isograd cuts gently up-section only at its highest location on Deception Cone. If it is accepted that isograds are close to parallel with stratigraphic layering, well constrained structural cross-sections (Fig. 4c) can be used to determine the spacing of the isogradic surfaces, so as to obtain more restricted estimates of P and T. The kyanite-garnet-biotite isogradic surface ranges from about 1 to 1.5 km from the staurolite-biotite isogradic surface (Fig. 4c). A pressure gradient of 0.3 kb/km corresponds to a P difference of about 0.3 to 0.4 kb between the isograds. The orthoamphibole assemblage is about 1 km up-grade from the kyanite isograd, which corresponds to a P difference of about 0.3 kb. Assuming simultaneous "quenching" of equilibrium, a paleogeothermal gradient can be found between the curves that represent the staurolite-biotite isograd, the kyanite-garnet-biotite isograd, and the orthoamphibole-bearing assemblage, by taking due account of the P differences indicated by the structural thickness between isograds. Such a paleogeothermal gradient is not to be confused with a metamorpic field gradient; it represents the vertical distribution of P-T conditions, not the P-T conditions on any particular part of the erosion surface. It indicates that pressures are probably in the range of 6.1 kb for the staurolite isograd, 6.4 kb for the kyanite-garnet-biotite isograd, and 6.7 kb for the structurally lowest metapelites. The temperature-gradient between each pair of isograds is about 40°C/km and compares with an average paleogeothermal gradient of about 27°C/km between the staurolite-biotite isograd and the paleo-erosion surface.

Summary of metamorphism in Deserters Range

Schists in the Deserters Range are in greenschist and amphibolite facies, at pressures that are inferred to be between 6 and 7 kb. Changes in the topology of the AFM projection illustrate staurolite-biotite and Al_2SiO_5-garnet-biotite reaction isograds that have been previously mapped in lower pressure regions (Carmichael, 1970; Froese and Gasparrini, 1975; St-Onge, 1981, 1984a). The position and spacing of the curves indicate temperature of about 500 to 550°C at 6 kb for the staurolite-biotite isograd, 560-580°C at 6.5 kb for the kyanite-biotite-garnet isograd, and 630°C at a minimum of 6.7 kb for the orthoamphibole-bearing assemblage.

Growth of phyllosilicates is defined as syn-D1. The textures in thin section from each zone suggest that growth of garnet cores was syn-D1 and the growth of other porphyroblasts and garnet rims was postkinematic with respect to D1, indicating that metamorphism outlasted D1. A phase of deformation (D2) after the peak of metamorphism crenulated the phyllosilicates that define the S1 foliation, kinked the kyanites, and folded the isograds along with formation contacts on a large scale.

Metapelites in the Sifton Ranges

Metamorphic grade is lowest (chlorite and garnet zone) west of Spinel Lake and increases to the southeast to the core of the Sifton Antiform (sillimanite zone, Fig. 16). The highest grade isograds are truncated by the Sifton Fault, which has in its immediate hanging wall staurolite zone rocks. Structurally higher units in the hanging wall have assemblages similar to high grade schists in the footwall.

West and east of Spinel Lake

East and west of Spinel Lake, pelitic mineral assemblages define six metamorphic zones separated by a mineral isograd, three reaction isograds, and a fault between the two regions (Fig. 16). The kyanite-sillimanite reaction isograd occurs over a mappable volume and is mapped as a seventh metamorphic zone. A phase of early-, syn-, and/or late metamorphic isoclinal folding of bedding and foliation is defined as D1. An episode of upright folding (D2) is postmetamorphic. The use of the abbreviations D1,D2, is not intended to imply any timing or kinematic relationship between this area and the Deserters Range.

Chlorite zone

The dominant minerals in pelitic assemblages are **muscovite**, **chlorite**, **plagioclase**, and **quartz**. **Biotite** is present in some samples within 500 m of the garnet isograd. Phyllite and psammite are strongly foliated. Foliation is parallel with bedding, and both are commonly crenulated, although crenulation cleavage is rare.

Garnet zone

The garnet isograd (Fig. 16) is marked by the first appearance of garnet in the assemblage **garnet-muscovite-biotite-chlorite-plagioclase-quartz. Margarite** occurs with the assemblage only rarely. Micas and quartz-rich lenses define the foliation. Primary structures are compositional layering and clasts in the metagrits. The foliation is strongly crenulated, and in one thin section an isoclinal fold of foliation is overprinted by the crenulations. Garnet occurs as 2 to 3 mm, fractured poikilitic xenoblasts, partly altered to chlorite and muscovite. Rocks on the east side of the zone are altered metagrits with a strong foliation.

Staurolite-biotite zone

The zone (Fig. 16) is characterized by coexisting **staurolite** and **biotite**, with **garnet**, **muscovite**, **plagioclase** and **quartz** being present as well. Coexisting staurolite and biotite requires a change in the AFM topology (Fig. 16)

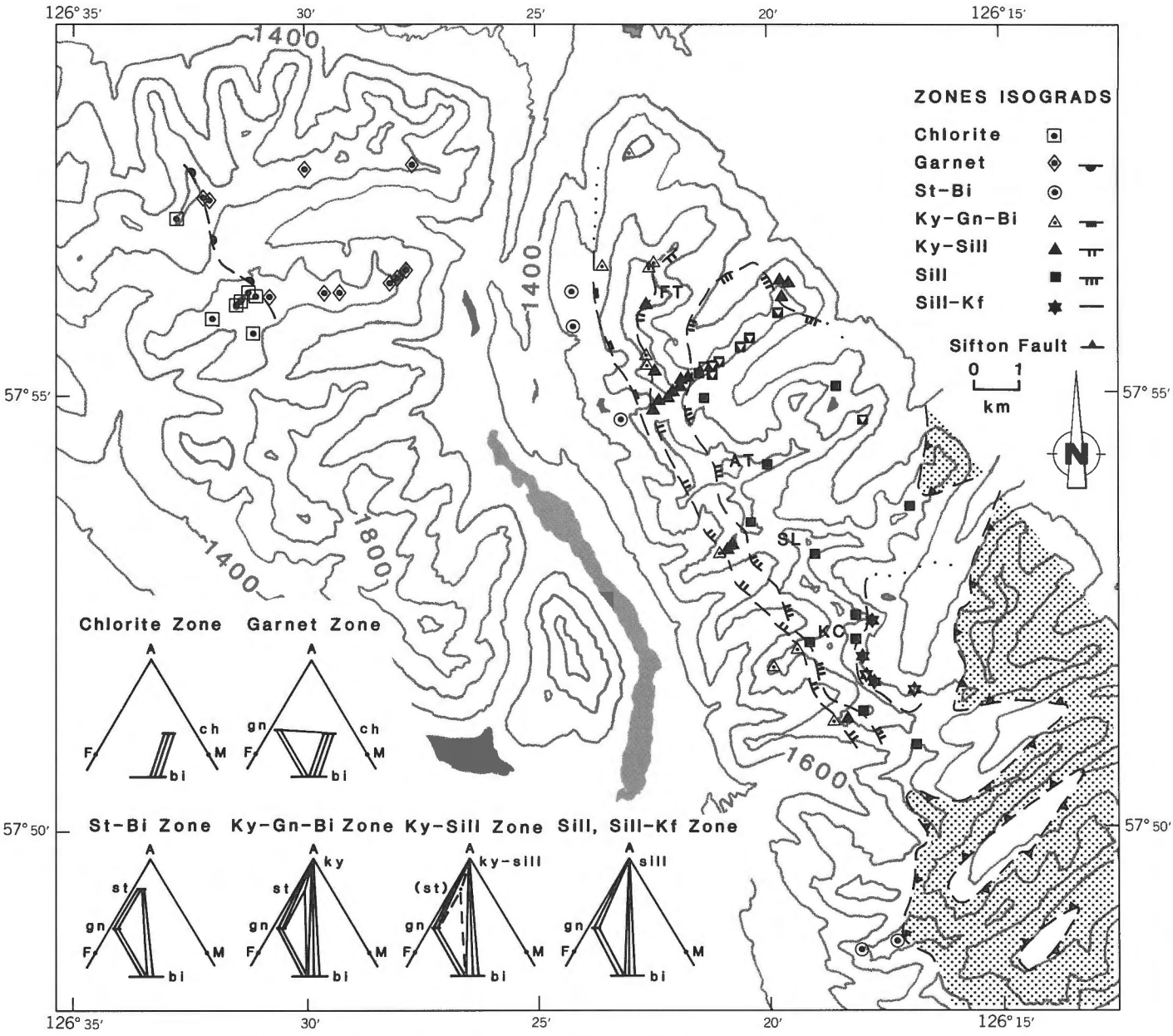

Figure 16. Metamorphic map of Sifton Ranges east and west of Spinel Lake. Ornaments are on the high grade side of the isograds. Points on the map correspond to the maximum-phase assemblages shown on the AFM projection of Thompson (1957), but biotite is not always present, and the absence of garnet in some samples of the sillimanite zone is shown by white triangles. Crossing tie-lines on the AFM projection of Thompson (1957) depict reactions for each isograd. FT, Flat Top Mountain; SL, Mount Slocomb, AT, "Atche Peak", KC, "Kechika Peak", FX, Fox Peak.

from that of the garnet zone, depicted by the reaction:

ch + gn + mu → st + bi + qtz + water (2)

The assemblage occurs along the west flank of the Sifton Ranges and was sampled in two localities, west of Flat Top Mountain and northwest of Fox Peak. Garnet is strongly fractured and embayed and commonly altered to chlorite and muscovite. Snowball texture is rare (Fig. 17a). Staurolite is subidioblastic near Flat Top, but is almost entirely altered to muscovite in the southern locality. In both areas, a proportion of the micas, ranging from 10 to 80 %, is recrystallized to a fine grain size. Quartz is extensively recrystallized to fine subgrains and core-and-mantle textures. Near the Sifton Fault garnet is broken and disaggregated. The high strain in these rocks is probably associated with poorly understood complex structures resulting from faulting along the west flank of the range. In the south, some of the textures may be a result of displacement on the Sifton Fault.

Kyanite-garnet-biotite zone

The zone is marked by the first appearance of kyanite in rocks that already contain garnet and biotite, the common assemblage being **kyanite-garnet-staurolite-muscovite-biotite-plagioclase-quartz**. The reaction is the same one

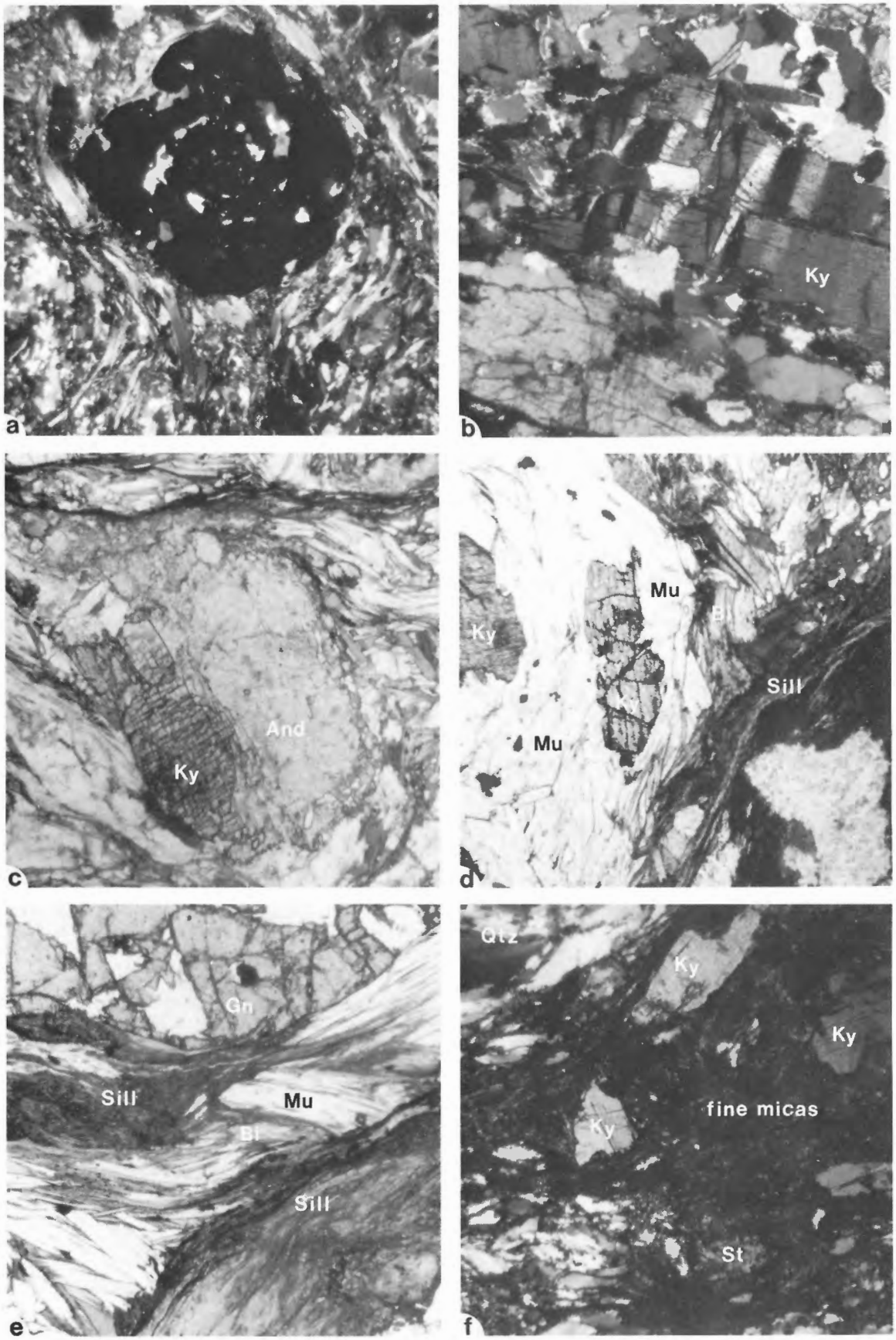
a
b
Ky
c
And
Ky
d
Mu
Ky
Sill
Mu
e
Gn
Sill
Mu
Bi
Sill
f
Qtz
Ky
Ky
fine micas
Ky
St

that marks the kyanite-garnet-biotite zone in Deserters Range. As in the Deserters Range, the assemblage covers a considerable structural thickness (200-300 m) and may indicate that the equilibrium is not strictly univariant. P-T conditions for the zone are about 550 to 580°C and a minimum of 5.5 kb (Fig. 15). In the southernmost occurrence, kyanite is partly replaced by andalusite, which is inferred to indicate continuing recrystallization during lower pressure conditions. Micas are coarse and define a planar fabric that is closely to openly, coarsely crenulated. Plagioclase is commonly partially sericitized. Garnet is 2 to 5 mm in diameter, fractured, embayed and altered with only rare snowball inclusion trails. Much of the staurolite and kyanite is poikiloblastic and embayed. The textures indicate synkinematic (D1) growth of garnet. Open folding of the foliation indicates late or postmetamorphic deformation, probably associated with the late phase of upright folding (F2).

Sillimanite-kyanite zone

The first appearance of sillimanite marks the beginning of a zone over which kyanite and sillimanite coexist and staurolite disappears. The characteristic assemblage is **sillimanite-kyanite-garnet-staurolite-muscovite-biotite-plagioclase-quartz**. Staurolite is abundant in the lower grade part of the zone and is rarely present in the higher grade parts. The 8-phase assemblage corresponds to the intersection of the "univariant" curve for staurolite-muscovite-quartz breakdown with the kyanite-sillimanite univariant curve, and is the "invariant" point that marks the boundary between bathozones 4 and 5. Assuming equilibrium and accurate P-T calibration, it would indicate P and T of about 5.5 kb and 580 to 600°C. Persistence of kyanite and staurolite up to 500 m beyond the isograd is probably due to sluggish rates of dissolution of these minerals (Carmichael, 1979). Staurolite is subidioblastic to xenoblastic and poikilitic, and commonly embayed. It is absent from schist within 100 m of the sillimanite zone. Sillimanite occurs commonly as fibrolitic mats intergrown with biotite, and it increases in abundance up grade. Kyanite is coarse, poikiloblastic, and kinked (Fig. 17b). Garnet is subidoblastic to xenoblastic and embayed. Micas have similar coarsely crenulated habit as in the kyanite-garnet-biotite zone.

Figure 17. Photomicrographs of schists in the Sifton Ranges. a) Snowball texture in garnet from the staurolite zone, footwall of the Sifton Fault. b) Kinked kyanite from the sillimanite-kyanite zone of the footwall. c) Andalusite replacing kyanite, from the sillimanite-kyanite zone of the footwall. d) Kyanite sheathed by muscovite and in textural disequilibrium with sillimanite, from the sillimanite zone of the footwall. e) Typical texture of the sillimanite-zone schists, with fibrolite coexisting with poikilitic, embayed garnet and coarse muscovite and biotite. f) Kyanite and staurolite in a matrix of fine mica and quartz, from near Warner Peak, in the kyanite-garnet-biotite zone of the hanging wall of the Sifton Fault. The width of a) is 3.6 mm, and the width of b),c),d),e), and f) is 1.5 mm.

Kyanite is commonly partly replaced by andalusite at the north end of the range (Fig. 17c). Andalusite replaces only kyanite; it is not found in contact with sillimanite nor spatially associated with sillimanite. Where seen in hand specimen, andalusite occurs with late quartz veins. Its association with late quartz veins and the relatively low pressure it represents compared with the rest of the assemblage attest to its late stage development.

Sillimanite zone

The characteristic assemblage of the zone is **sillimanite-garnet-muscovite-biotite-plagioclase-quartz**. Kyanite is not recognizable in hand specimen. Where it occurs in thin section it is in textural disequilibrium with all other phases and occurs as small xenoblasts surrounded by coarse muscovite (Fig. 17d). There and in the sillimanite-kyanite zone, the textures and the lack of direct replacement of kyanite by sillimanite may be attributed to cation-exchange reactions as invoked by Carmichael (1969). The reactions involve catalysts (eg. muscovite, biotite, quartz) in a net reaction to consume kyanite in one part of the rock and produce sillimanite in another. In one potential reaction, kyanite reacts with quartz to produce muscovite and sillimanite. Muscovite forms a thickening reaction rim between kyanite and quartz that eventually may prevent the reaction from proceeding to completion.

Garnet is commonly subidioblastic or xenoblastic, fractured, embayed, with uncommon, poorly defined snowball inclusion trails. Muscovite, biotite and sillimanite define the foliation, which is coarsly crenulated (Fig. 17e). The assemblage indicates pressures greater than bathozone 1 and less than bathozone 6. As the zone is structurally lower than the sillimanite-kyanite zone, it is inferred to be in bathozone 5.

Sillimanite — K-feldspar zone

A small area in a topographically (and structurally) low area south of Mount Slocomb has the assemblage **sillimanite-garnet-muscovite-biotite-K-feldspar-plagioclase-quartz**. Kyanite is in textural disequilibrium similar to its occurrence in the sillimanite zone. Assuming equilibrium, the assemblage would imply a T and P of about 670°C and 7.2 kb; however, the disequilibrium texture of kyanite would be consistent with a lower P. The assemblage marks the beginning of muscovite breakdown by the anatectic reaction:

$$mu + bi + plag + qtz \rightarrow K\text{-}f + sill + gn + liquid \quad (6)$$

in the model system SiO_2-Al_2O_3-FeO-MgO-Na_2O-CaO-K_2O-H_2O. K-feldspar occurs as 1 to 2 mm porphyroblasts. Textures of the other phases are the same as in the sillimanite zone.

Discussion of isograd pattern

The isograds have been folded after the peak of metamorphism as suggested by 1) the relatively large areal extent of the garnet zone, coincident with the crest of the open anticline west of Spinel Lake; 2) the closure of the

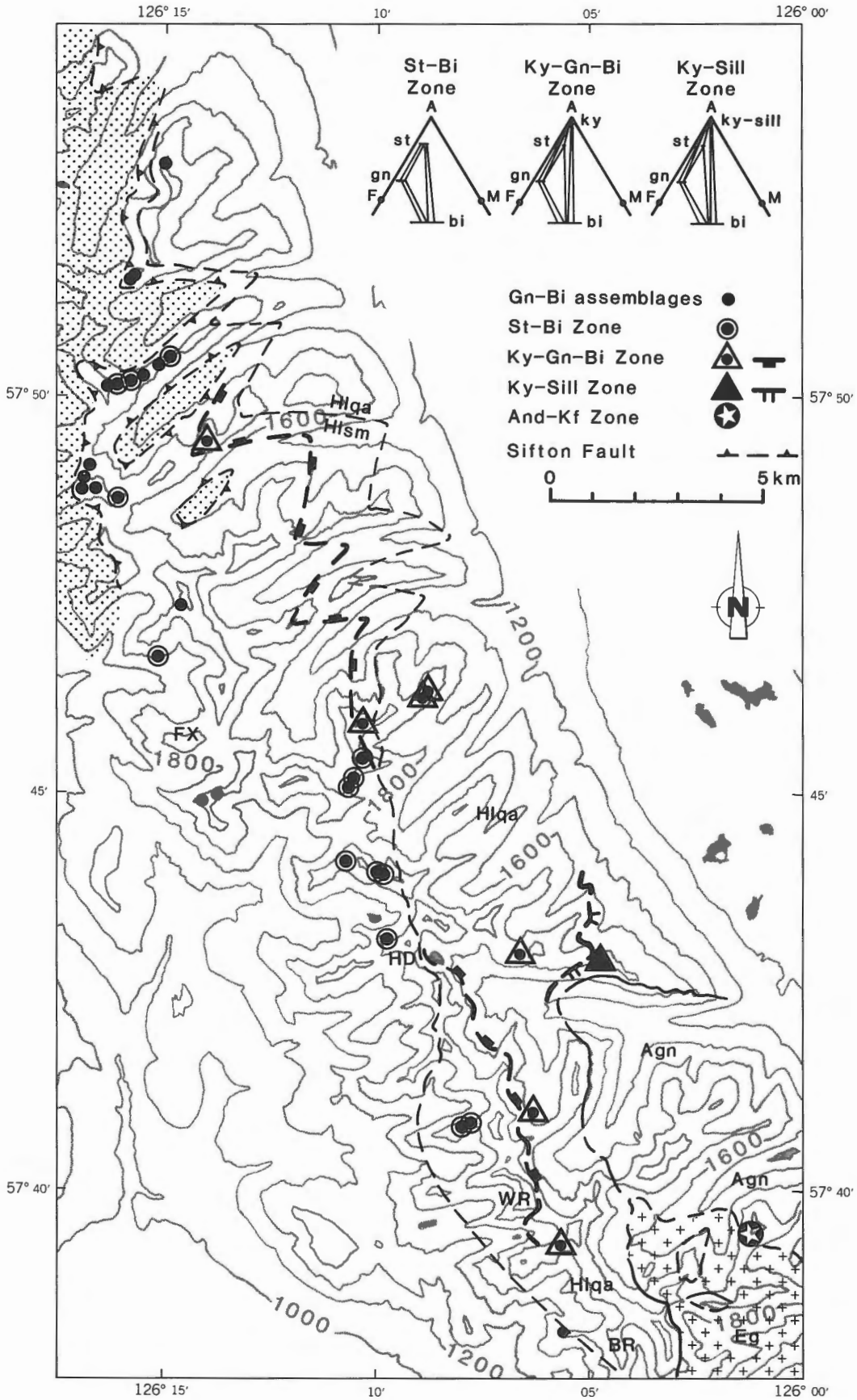

Figure 18. Metamorphic map of hanging wall of the Sifton Fault. Ornaments are on the high grade side of the isograds. Points correspond to maximum-phase assemblages. The assemblage for each zone is shown on the AFM projection of Thompson (1957). HD, Hedges Peak; WR, Warner Peak; BR, Brandon Peak.

sillimanite reaction isograd (Fig. 16) that mimics the closure of formation contacts (Fig. 7); 3) folding of the foliation. Isograds are postulated to be approximately parallel with strata and are extrapolated into the valleys to obtain the structural thickness of the zones and an estimate of the paleogeothermal gradient. By this method the thickness of the kyanite-sillimanite and sillimanite zones combined is about 1.7 km (Fig. 7,16), which corresponds to a P difference of 0.5 kb between the sillimanite and sillimanite — K-feldspar isograds. The close spacing of the isograds requires a thermal gradient of 40°C/km for the muscovite breakdown reaction to be reached. The kyanite-garnet-biotite isograd is less than 500 m from the sillimanite-kyanite zone; the corresponding P difference of about 0.1 kb is consistent with a gently sloping paleogeothermal gradient just above the bathozone 5/4 boundary (Fig. 15). The average T gradient between the kyanite-garnet-biotite isograd and the paleo-erosion surface is 20°C/km.

Summary of metamorphism in the Sifton Ranges

The sequence of isograds east of Spinel Lake indicates a range in temperature and pressure from about 520°C and 5 kb to greater than 650°C and 6 kb. The persistence of staurolite in the kyanite-garnet-biotite and sillimanite-kyanite zones and the extent of kyanite-sillimanite assemblages suggest that the paleogeothermal gradient passes close to the boundary between bathozones 4 and 5 and is at a low or moderate angle to the kyanite-sillimanite curve (Fig. 15).

Poorly defined snowball textures in garnets are a result of synmetamorphic deformation (defined as D1). The phyllosilicates that define the foliation are presumably synmetamorphic, and could be either early-, syn- or late D1. Isoclinal folding and metamorphism were followed by postmetamorphic upright folding (D2) which preceeded displacement on the Sifton Fault. Relatively late replacement of kyanite by andalusite is a result of recrystallization at a pressure at least 2 kb lower than the peak of metamorphism.

Hanging wall of the Sifton Fault

In the hanging wall of the Sifton Fault, four metamorphic zones are defined, one of which is a (late) thermal overprint in the contact aureole of the Balourdet Pluton at the south end of the range. Isograds are not well constrained due to the paucity of pelitic compositions that retain prograde assemblages, and only the kyanite-garnet-biotite and the sillimanite isograds are drawn. Where present, pelitic assemblages are difficult to assess in the field because porphyroblasts are fine and dispersed in a matrix of recrystallized fine quartz and mica (Fig. 17f). In thin section it is rarely possible to demonstrate textural equilibrium, although coarse rather than fine textures are present locally. The presence of coarse quartz inclusions in garnet (protected from grain size reduction associated with faulting), and the truncation of isograds in the footwall of the Sifton Fault support the interpretation that the Sifton Fault postdates the peak of metamorphism. The assemblages reported are inferred to represent the peak of the same metamorphic event that affected the footwall, and therefore the quenching of mineral assemblages appears to be the latest pre-fault marker of the vertical displacement of the hanging wall relative to the footwall. Common accessory minerals are tourmaline, apatite, zircon, opaques, and rarely, sphene and epidote.

Staurolite-biotite zone

The assemblage **garnet-staurolite-muscovite-biotite-plagioclase-quartz** occurs mainly in the schist/marble unit although it also occurs in the wavy schist unit, and rarely in the metaquartzite/amphibolite unit (Fig. 18). The schist near Rocky Peak and Hedges Peak has some of the best preserved coarse textures, although quartz and mica are finely recrystallized. Mica occurs as fine aggregates of flakes about 20 μm across. Chlorite is definitely retrograde in some samples, but the textures are commonly difficult to interpret where chlorite is intergrown with biotite and muscovite. Chlorite may be part of the pre-fault metamorphic assemblage, a syn-fault phase, or a retrograde phase pseudomorphous after biotite. In staurolite-bearing schists, most chlorite appears to be retrograde after biotite. In metaquartzite from this zone, chlorite occurs along the foliation and in pull-aparts of plagioclase and tourmaline, and it was evidently stable in the metaquartzite during faulting. Garnet is commonly broken into clasts 10 to 50 μm in diameter and dispersed into lenses along the foliation. It also occurs as fractured, partially disaggregated porphyroclasts (Fig. 33,35) and uncommonly as 5 to 8 mm subidioblastic porphyroblasts with wavy inclusion trails. Staurolite occurs as coarse porphyroblasts with wavy inclusion trails, and more commonly, as fine subidioblastic clasts less that 1 mm across. Margarite occurs in the assemblage near the Sifton Fault and appears to be stable with all phases. Rare occurrences of andalusite probably formed late relative to other porphyroblasts. The assemblage **garnet-muscovite-biotite-chlorite-quartz** is common in the structurally lowest wavy schist unit. This assemblage may either represent a retrograde (syn-fault) overprint of garnet-zone conditions on the staurolite-biotite zone, or a prograde sub-assemblage of the staurolite-biotite zone.

Kyanite-garnet-biotite zone

Seven occurrences of the assemblage **kyanite-garnet-staurolite-muscovite-biotite-plagioclase-quartz** have been found in the metaquartzite/amphibolite unit, and two occurences in the marble/schist unit (Fig. 18). Kyanite occurs as fine and coarse subidioblastic to xenoblastic grains; in 2 thin sections it is partly altered to andalusite. Other minerals have the same textures as in the staurolite-biotite zone.

As discussed for the zone in the other regions, the assemblage probably indicates peak P and T of greater than 5.5 kb and 580-600°C. North of Warner Peak, the same assemblage lacks muscovite but includes **orthoamphibole** and **cordierite**. Cordierite appears to be a late phase partly replacing kyanite and is inferred to have crystallized during unloading.

Sillimanite-kyanite zone

One locality, representing the structurally and stratigraphically lowest metapelites in the hanging wall, has the assemblage **kyanite-sillimanite-garnet-staurolite-muscovite-biotite-plagioclase-quartz**. The schist has coarse biotite with xenoblastic to subidioblastic garnet less than 0.5 to 3 mm in diameter. Kyanite and sillimanite are relatively coarse and lack reaction rims. Assuming equilibrium, pressure and temperature conditions are on the kyanite-sillimanite curve and on the bathozone 5/4 boundary (Fig. 15).

Tochieka Gneiss and a late thermal overprint

The Tochieka Gneiss generally lacks pelitic assemblages, and consists mainly of **biotite-plagioclase-K-feldspar**, and rarely, **garnet** and **muscovite**. The only metapelite collected is 300 m from an intrusive contact with the Eocene Balourdet Pluton. The assemblage is **andalusite-cordierite-muscovite-biotite-plagioclase-K-feldspar-quartz**. Cordierite is fairly fresh, and andalusite occurs as optically continuous dispersed xenoblastic grains. Both are in textural equilibrium with K-feldspar. Sillimanite(?) occurs as fine needles in one quartz grain. Textures and assemblages are diagnostic of bathozone 1 ($P < 2.3$ kb) and are inferred to reflect a thermal overprint resulting from intrusion of granite at a relatively high crustal level in Eocene times, after substantial post-regional-metamorphic uplift and erosion had taken place.

Isograd pattern

Metamorphic grade is highest in the metaquartzite/amphibolite unit which, overlying the Tochieka Gneiss, is evidently the lowest stratigraphic unit (with pelitic compositions). It is also the highest structural unit in the Sifton Ranges, and its position at least 1 km above the Sifton Fault is an argument for postmetamorphic displacement on the Sifton Fault. Pelitic assemblages are not abundant in the hanging wall. As a consequence, the isograds are poorly constrained, and in regions of considerable relief drawing isograds is difficult because the dip is unknown. In Figure 18, the kyanite-garnet-biotite and sillimanite-kyanite isograds are postulated to be approximately parallel with lithological contacts and foliation. This postulation allows extrapolation of isograds along the foliation in a pattern that is consistent with an interpretation of the postmetamorphic structural history (*see* Structure and tectonics).

The contact between the schist/marble and metaquartzite/amphibolite units is inferred on structural grounds to be a postmetamorphic fault. Three kilometres north of Rocky Peak, in the footwall of this fault the presence of kyanite-garnet-biotite zone schists in a position structurally above the staurolite-biotite zone suggests inversion of the metamorphic zones below the fault. The apparent inversion may be a result of either folding in the footwall of the nearby fault, or by structural interleaving of the zones by faulting. In the units above the fault, the metamorphic grade appears to decrease structurally upwards from the basement. Following that pattern, the kyanite-garnet-biotite isograd between Warner and Hedges peaks is drawn so as to dip gently southwest, consistent with the structures in that area. This approach depicts an interpretation of the general form of the metamorphic isograds, although probably not their exact location.

Summary of metamorphism of the hanging wall of the Sifton Fault

Hanging wall assemblages indicate maximum conditions in bathozone 5. Poorly preserved snowball textures in garnet are a result of synmetamorphic deformation, which is constrained only to pre-Eocene in the study area. The timing of metamorphism is postulated to be mid-Mesozoic by comparison with other parts of the core zone of the Omineca Belt that have been dated. Movement on the Sifton Fault does not appear to have resulted in significant overprint of new mineral assemblages in schists except for the presence of chlorite with equivocal textures. The dominant effect of faulting is textural, including extensive recrystallization of quartz and micas to a finer grain size, and cataclasis of garnet to a finer grain size and dispersal of it along the foliation.

Metamorphic grade is generally lower in the west and higher in the east. The change is roughly conformable with the inferred structural and stratigraphic levels, and is considered to be in part of postmetamorphic tectonic origin. Mineral assemblages in both the footwall and hanging wall of the Sifton Fault are characteristic of bathozone 5/4 and 5, and indicate that both regions were metamorphosed at about the same pressure and temperature.

Geothermobarometry

Well constrained pressure estimates are desirable for a more comprehensive interpretation of the tectonic history than could be deduced by a structural analysis alone. Garnet-kyanite-biotite-plagioclase schists were collected from the Deserters Range, and the footwall and hanging wall of the Sifton Fault, with the purpose of obtaining P — T determinations using electron microprobe analyses of those minerals and calibrated mineral equilibria. Thin sections with univariant mineral assemblages (in the model pelitic system) were chosen as a further constraint on the P — T estimates. Geothermometry is based on the garnet — biotite exchange reaction calibrated by Ferry and Spear (1978). Geobarometry is based on the grossular — anorthite equilibrium (Kretz, 1959,1964; Ghent, 1976; Ghent et al., 1979) as calibrated by Newton and Haselton (1981). These calibrations were chosen because they have been found by workers in well studied areas to yield pressures and temperatures that are the most internally consistent with other geothermobarometric methods and with structural/metamorphic interpretations of the areas (eg. Ghent et al., 1979; Ferry, 1980; Hodges and Spear, 1982; St-Onge, 1984b).

Approach

Garnet, plagioclase and biotite were analyzed in two thin sections from each of the Deserters Range, the footwall, and the hanging wall of the Sifton Fault. Sample locations are shown in Figure 19. In each thin section domains around three different garnets were chosen for analysis.

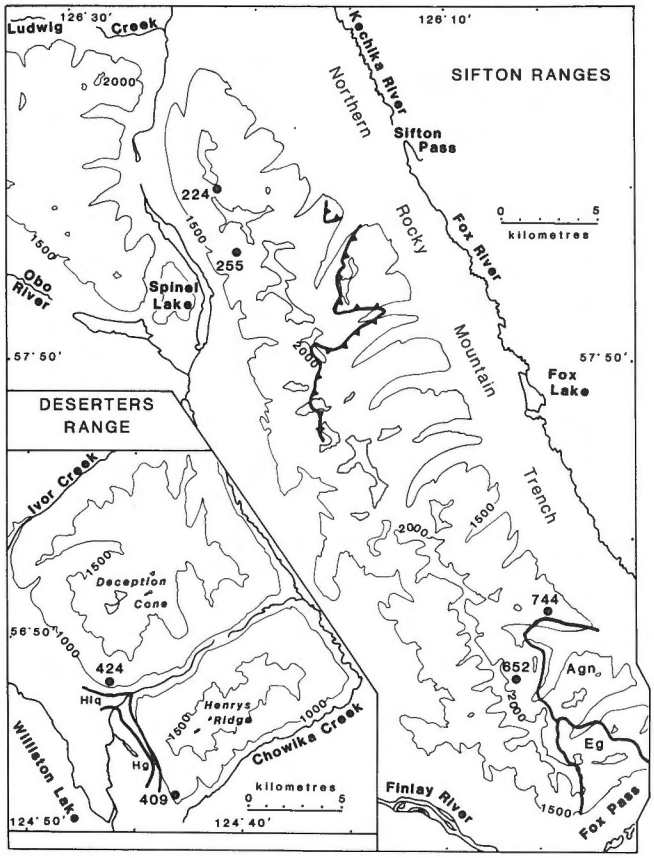

Figure 19. Location of samples used for geothermobarometry.

Each domain consists of the garnet, and a biotite and plagioclase within 2 mm of the garnet. In most domains a biotite in contact with garnet and a biotite in the matrix of the schist were analyzed. One or two plagioclase grains were analyzed for each domain. Most garnets in the sections chosen are zoned; one and commonly two rim spots, an interior spot, and a core spot were analysed. Three analyses at each spot were averaged. The analytical procedure, treatment of precision and accuracy, and the averaged analyses and structural formulae are given in the Appendix.

Garnet — biotite geothermometry

The partitioning of Fe and Mg between garnet and biotite is largely a temperature-dependent equilibrium (Thompson, 1976; Goldman and Albee, 1977; Ferry and Spear, 1978). Ferry and Spear (1978) calibrated the equilibrium:

phlogopite + almandine = annite + pyrope

$$KMg_3Si_3AlO_{10}(OH)_2 + Fe_3Al_2Si_3O_{12} = KFe_3Si_3AlO_{10}(OH)_2 + Mg_3Al_2Si_3O_{12}$$

with synthetic end-members. The resulting log-Kd curves are close to isothermal, with experimental error of ±50°C.

Grossular — anorthite — Al_2SiO_5 — quartz geobarometry

Newton and Haselton (1981) based the calibration of the equilibrium:

anorthite = grossular + kyanite + quartz

$$3CaAl_2Si_2O_8 = Ca_3Al_2Si_3O_{12} + 2Al_2SiO_5 + SiO_2$$

on an experimental determination of the end-member reaction. The advantage of this calibration over the calibration of Ghent (1976) and Ghent et al. (1979) is that it employs the free energy interaction parameter (W), to correct for the nonideality of the garnet and plagioclase solid solutions. Newton and Haselton suggested that the geobarometer not be used for garnets rich in Mn because $W_{Ca\text{-}Mn}$ is unknown. Using an APL program composed by D.M. Carmichael, the equilibrium equation has been solved simultaneously with the equation for the garnet-biotite equilibrium to obtain a P and T at the intersection of the log-Kd curves. Garnet rims in each domain are combined with the plagioclase, and the matrix and contact biotites for the domain to calculate several P and T estimates for each domain. The calculated P and T are listed in Table 3, and shown on Figure 20.

Mineral chemistry and geothermobarometry

Garnet zoning

A common problem in using garnet in geothermobarometry is assessing the role of zonation in the garnets. Most Deserters Range and footwall garnets are 'normally' zoned (Hollister 1966), that is, they have cores enriched in Ca and Mn and depleted in Fe and Mg, relative to the rims. They lack the rim of 'reverse' zoning ascribed by Tracy et al. (1976) to retrograde continuous reactions. The zoning results in substantially lower T and P for garnet cores and variably lower T and P for garnet interiors (within 0.1 to 0.5 mm of the rim). The lack of a retrograde rim permits the inference that garnet rims yield peak temperatures, and only garnet rims are used in the P-T determinations (Table 3, Fig. 20). Domain 255-2, in a section from the Sifton Ranges, is an exception in that it is unzoned. Homogeneous garnet and the high T's for this domain are consistent with the proposal by Woodsworth (1977) that volume diffusion in garnet results in homogenization at about 600°C. Domain 255-3 also yields T's above 600°C, but the garnets are normally zoned. All garnets in the hanging wall domains are unsystematically zoned. In section 652, Mg shows normal zoning and Fe is either homogenous or reversely zoned, indicating that originally zoned garnets in 652 are partly homogenized. Similar unsystematic zoning is described by Ghent et al. (1982). In 744, no elements show normal zoning; Mg and Mn show homogenization in all domains and Fe is homogeneous or has weak reverse zoning. This pattern may be a result of complete homogenization at greater than 600°C followed by partial re-equilibration at lower grade.

Tracy et al. (1976) suggested that late continuous reactions may involve biotite. To test the within-sample homogeneity of biotite, grains in the matrix of the schist, and at garnet rims were analyzed; matrix biotites do not have consistently higher or lower Fe/Fe+Mg than the biotites at garnet rims. Single biotite grains are homogeneous. Plagioclase in Deserters Range and the footwall of the Sifton Fault fall in the range of $An_{18\text{-}25}$, and plagioclase in the hanging wall is $An_{30\text{-}36}$. Plagioclase analyses include

Table 3. Geothermobarometry results. Three garnets in each thin section were chosen for analysis. The domains (D), indicated by numbers 1 to 5, are defined by a garnet, and biotite and plagioclase grains within 2 mm of the garnet. Within each domain two areas on the rim of the garnet (G) and different grains of the biotite (B) and plagioclase (Pl) were used for the calculations, and are represented by a letters. In domains where a mineral is not represented by a letter, only one grain was analysed. For each domain, the pressure (P, in kilobars) and temperature (T, in °C) are calculated for all combinations of the three minerals. The data are plotted in Fig. 20.

G	B	Pl	T	P
			Section 409	
1	a	a	523	6.3
		b	515	6.1
	c	a	524	7.0
		b	516	6.8
2	c	b	506	6.1
		a	520	6.4
5	a	b	543	7.8
		a	498	6.7
		c	520	7.2
	b	b	520	7.3
		a	478	6.2
		c	499	6.7
			Section 424	
1	a	b	a 526	8.0
			b 525	7.8
		a	a 558	8.8
			b 557	8.6
	b	b	a 536	7.0
			b 536	6.8
		a	a 569	7.8
			b 568	7.6
2	a	b	535	8.5
		a	548	8.8
		d	586	9.8
	b	b	578	9.6
		a	592	10.0
		d	635	11.2
3	c	b	a 616	9.8
	b		616	9.9.
		a	a 603	9.5
			b 603	9.5
	b	b	a 625	10.4
			b 625	10.5
		a	a 612	10.1
			b 612	10.2

G	B	Pl	T	P
			Section 224-3	
1	a	b	a 535	7.4
			b 535	7.5
		a	a 534	7.3
			b 534	7.4
	d	b	a 603	8.5
			b 604	8.6
		a	a 602	8.5
			b 602	8.6
2	d	a	a 588	6.2
		b	588	6.1
			c 590	6.6
		b	a 584	6.1
			b 584	6.0
			c 586	6.5
		c	a 586	6.1
			b 586	6.0
			c 588	6.6
	e	a	a 597	6.1
			b 597	5.9
			c 599	6.5
		b	a 593	6.0
			b 593	5.9
			c 595	6.4
		c	a 595	6.0
			b 595	5.9
			c 597	6.5
3	a	b	a 513	8.1
			b 511	7.3
		a	a 510	8.0
			b 507	7.2
		c	a 506	7.8
			b 503	7.1
	d	b	a 655	11.0
			b 651	10.0
		a	a 650	10.8
			b 646	9.9
		c	a 644	10.7
		c	a 644	10.7
			b 641	9.8

G	B	Pl	T	P
			Section 255	
1	a		591	6.0
	d		595	5.7
2	a	a	634	7.7
		b	639	7.8
	c	a	600	7.0
		b	604	7.1
3	a	b	617	5.9
		a	623	6.1
	d	b	645	6.7
		a	652	6.8
			Section 744	
1	a	c	637	6.0
		b	698	7.2
	b	c	612	4.7
		b	669	5.7
2	a	c	672	7.1
		a	674	7.2
		b	635	6.4
	b	c	683	8.2
		a	685	8.3
		b	645	7.4
3	a	a	a 532	4.1
			b 532	4.1
	c	a	a 562	4.4
			b 562	4.4
			Section 652	
1	a	c	a 551	4.4
			a 622	5.8
			b 592	5.2
	d	c	563	4.3
		a	637	5.6
		b	606	5.1
2	a	b	513	4.7
		a	570	5.9
	c	b	542	4.7
	c	b	542	4.7
		a	603	5.9
			a 628	6.3
	b	b	676	9.1
		a	655	8.7

core and rim spots and zoning was not detected. An exception is 652 which has weak zoning, and in this case the interior spots were averaged.

Deserters Range

The two samples in Deserters Range are from the kyanite-garnet-biotite zone of the metaquartzite/amphibolite unit (Fig. 19). Section 409 is from about 250 m above the metaquartzite contact in Chowika Creek, and 424 is about 150 m above the metaquartzite contact in Police Creek. They both contain the assemblage kyanite-staurolite-garnet-biotite-muscovite-plagioclase-quartz. The graph of P's and T's (Fig. 20) shows a wide range in T along the garnet/plagioclase isopleths. If all data are averaged, sections 409 and 424 yield T's and P's of 515°C /6.7 kb and 580°C/9.1 kb respectively. The pressure difference of 2.4 kb between the two samples is high considering the similar structural level inferred for the samples. In 409 most matrix biotites give higher T whereas in 424 most matrix biotites give lower T. Matrix biotite temperatures from both are preferred because they have less within-sample spread in data, and because they yield a more reasonable difference in pressure between the two samples. Excluded also are domains 424-3 and 424-2b, which have much higher P and T as a result of the anomalously low Fe/Fe + Mg in garnet relative to biotite. If 424-2b and 424-3 are extrapolated along the garnet/

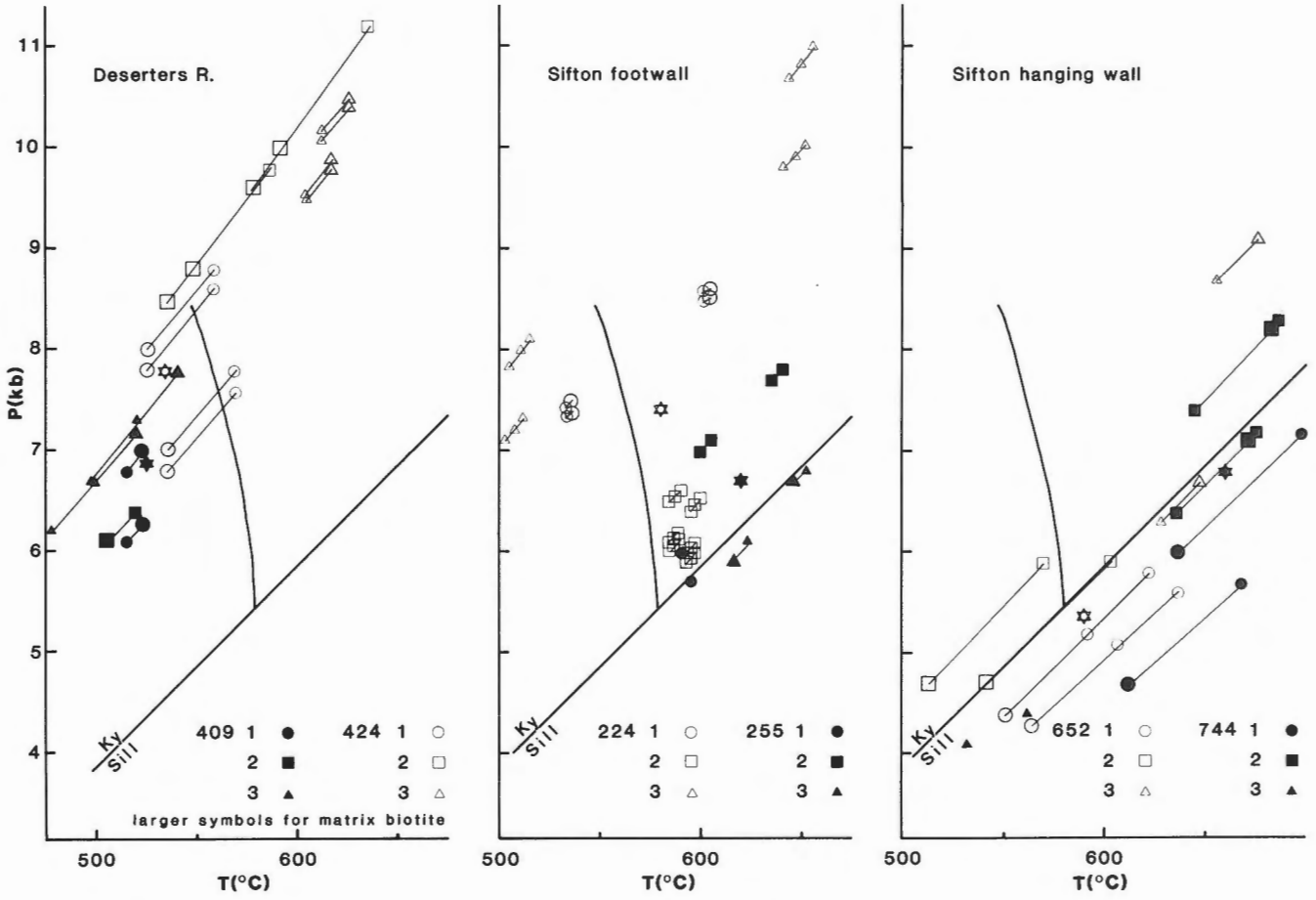

Figure 20. Graphs of geothermobarometry results. Domains in each thin section are distinguished by different symbols. The combination of analyses of different grains of the 3 minerals within each domain are plotted. Lines join biotites that are combined with the same garnet analysis, and larger symbols denote results from matrix biotite. Stars are the average P and T of selected data for each sample.

plagioclase isopleths to the lower temperatures of the other points, they fall into the same range of pressure.

The selection of data results in temperatures and pressures of 525 (standard deviation (s.d.) 15)°C and 6.7 (s.d. 0.7) kb, and 535 (s.d. 10)°C and 7.8 (s.d. 0.8) kb for sections 409 and 424 respectively. The averages are 30 to 40°C below the univariant curve that represents the assemblage (Fig. 15). The position of the curve is not well known, but estimates of experimental error of ±50°C for the geothermometer (Ferry and Spear, 1978) encompass the temperature of the curve as given by Carmichael (*in* Archibald et al., 1983).

Footwall of the Sifton Fault, Sifton Ranges

The footwall sections are from the kyanite-garnet-biotite zone of the prominent pelitic schist unit HIps and contain the assemblage kyanite-staurolite-garnet-biotite-muscovite-plagioclase-quartz. The different biotites from all domains yield within-domain differences of 10°C. The combination of different plagioclase results in a range of pressure of 0.8 kb within domain 224-3; 0.5 kb for the three plagioclases of domain 224-2; and less than 0.1 kb for the two plagioclases in domain 224-1. Data averaged for all domains in each section yields T and P of 580°C/7.4 kb for section 224, and 620°C/6.7 kb for section 255. Domain 224-1 has a spread of 70°C and 1.2 kb, and 224-3 has a spread of 140°C and 2.6 kb. The greatest source of the spread in temperature in 224-1,3 and 255-2,3 is the variation of Fe/Fe+Mg in garnet relative to biotite between different garnet rim spots of the same garnet. Pressure differences between domains in 224 are due largely to the variation of X_{Ca} in garnet. The combination of analyses from 2 garnets, 3 plagioclases, and 3 biotites for domain 224-2 yield a strong cluster of points at about 590°C and 6.3 kb. Only one biotite in 255-1 was analyzed; it gives points close to the group of points for 224-2.

The average T and P of all data of 255 is not significantly different from 224-2, or from the average of all 224 points. The data indicate an average T and P of 620 (s.d. 20)°C/6.7 (s.d. 0.7) kb (section 255), and 580 (s.d. 45)°C/7.4 (s.d. 1.5) kb (section 224), for the kyanite-garnet-biotite zone in the footwall of the Sifton Fault.

Hanging wall of the Sifton Fault, Sifton Ranges

Both samples are from the metaquartzite/amphibolite unit (Fig. 19). Section 744 is from schists that are inferred to have been the structurally lowest pelites during

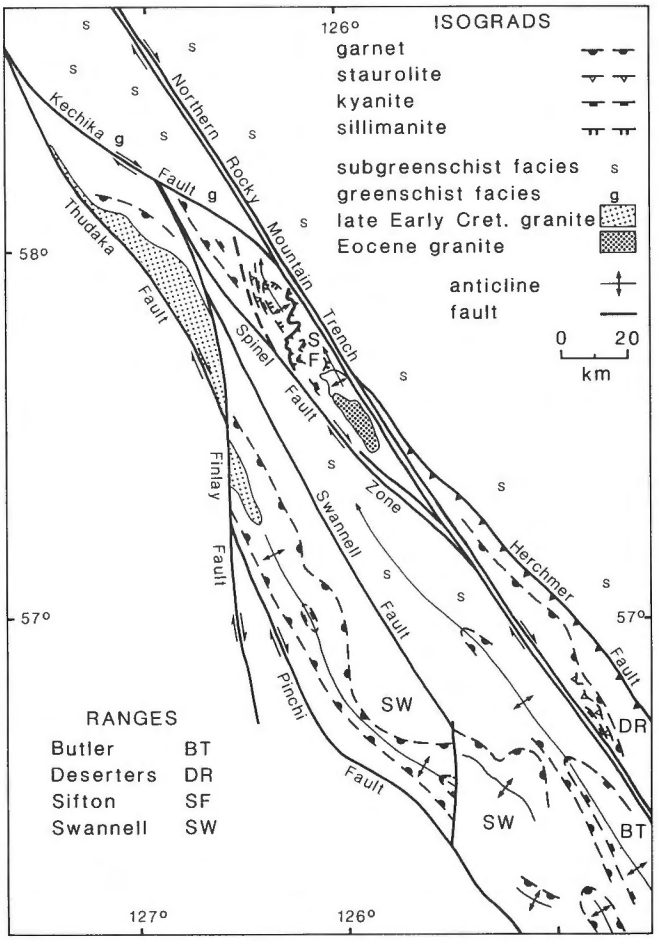

Figure 21. Regional metamorphic setting of the Deserters and Sifton ranges. The map shows the coincidence of metamorphic culminations with regional anticlinoria, and the relatively high grade of the Deserters and Sifton ranges. Ornaments are on the high grade side of the isograds. Compiled from Gabrielse et al. (1977a), Gabrielse, (1975), and personal communications.

metamorphism. It has the assemblage sillimanite-kyanite-staurolite-garnet-biotite-muscovite-plagioclase-quartz and the average of all data is 630°C and 6.1 kb. Homogenization of garnet in section 744 is consistent with the temperatures of greater than 600°C (Woodsworth, 1977) but has resulted in a great spread (4 kb) of pressures. Temperatures have about the same variation in T (60°C) as for unzoned garnets of the Deserters Range. 744-3 is excluded due to the anomalously low Fe/Fe+Mg; if projected along the log-Kd curves for garnet/plagioclase to the temperature range of 744-1 and 2, it is in the same range of pressure. The average of domains 1 and 2 in 744 is 660 (s.d. 30)°C and 6.8 (s.d. 1.1) kb.

Section 652 is from about mid-structural level in the unit and has the assemblage kyanite-staurolite-garnet-orthoclase-biotite-plagioclase-quartz, with late cordierite. Garnets are partially homogenized, with Fe evenly distributed (domain 2) or retrograde (domains 1,3). The average of all data in 652 yield 600°C and 5.9 kb. A large part of the spread in data is the within-domain temperatures from different biotites, and the high X_{Ca} in garnet of domain 652-3b. Exclusion of domain 652-3b, which gives significantly higher T and P, yields 590 (s.d. 40)°C and 5.4 (s.d. 0.8) kb.

The selection of data yields T's and P's for 744 and 652 that can be compared with their mineral assemblages. The results for 744 are consistent with proximity to the kyanite-sillimanite curve as indicated by coexisting kyanite and sillimanite in thin section, but the temperatures are higher than expected if staurolite was in equilibrium with the other minerals. The range of P and T for 652 is consistent with both the univariant assemblage kyanite-staurolite-garnet-biotite, and the relatively low pressures suggested by coexisting (late) cordierite with orthoamphibole. As for the other samples, consistency with the mineral assemblage does not mean that the P-T estimates are accurate. The mineral assemblage is not invariant, and greater pressures for any of the samples could also be consistent with the mineral assemblage. In addition, the position of the staurolite-muscovite-quartz breakdown curve is not accurately known. The zoning of garnets is a suggestion that the P-T estimates need not be inferred to represent peak P-T conditions, even though they are consistent with the mineral assemblage.

Summary of geothermobarometry

Mineral assemblages in each range give fairly well constrained temperature estimates of the peak of metamorphism because the dehydration curves are steep, but the pressure estimates are not as well constrained. For tectonic studies, **relative** pressure and temperature estimates obtained from calibrated geothermobarometers are useful for providing a comparison of the postmetamorphic uplift of terranes. These data are probably more reliable than absolute P and T determinations considering the discrepancies between different calibrations and the uncertainties inherent in them. Temperature and pressure estimates for the Deserters Range and footwall of the Sifton Fault are inferred to represent approximate peak metamorphic conditions because the garnets are 'normally' zoned and the points are within the stability field of the mineral assemblage. In contrast, hanging wall garnets are either homogeneous with some retrograde zoning (744), or are partially homogenized and retrograded (652). These relationships suggest that the T and P may reflect reequilibration at lower-than-peak conditions. The temperature for 652 is consistent with the stability field of the mineral assemblage, but for 744 it is higher than expected if staurolite was stable. Considering the high strain in the hanging-wall schists, and as a result, the difficulty in demonstrating textural equilibrium, the consistency of the data is better than was expected, but the results from the hanging wall are probably less accurate than those for the footwall and Deserters Range. In all cases, consistency with the mineral assemblage is not necessarily an indication of accuracy of the data. The results of the geothermobarometric study are as follows:

	T(°C)	P(kb)
Deserters Range	409 525 s.d. 15	6.9 s.d. 0.7
	424 535 s.d. 10	7.8 s.d. 0.8
Sifton Fault footwall	224 580 s.d. 45	7.4 s.d. 1.5
	255 620 s.d. 20	6.7 s.d. 0.7
Sifton Fault hanging wall	744 660 s.d. 30	6.8 s.d. 1.1
	652 590 s.d. 40	5.4 s.d. 0.8

Errors reported are 1 standard deviation errors derived from the distribution of the selected apparent P and T values for each sample. Ferry and Spear (1978) estimated an experimental error of $\pm 50°C$ for the geothermometer, and Hodges and Spear (1982) estimated an error of ± 1.5 kb for the geobarometer. A large amount of the variation in temperature and pressure is probably not due to analytical uncertainty, but to disequilibrium, as noted by Pigage and Greenwood (1982) for geothermometry of schist in the Azure Lake area of the Cariboo Mountains. Disequilibrium may be a result of inhomogeneous (re)equilibration during cooling. The hanging wall of the Sifton Fault yields pressures that are not significantly different than the footwall.

Regional metamorphic setting of Deserters and Sifton ranges

The Deserters Range has the highest grade rocks in the northern Rocky Mountains. The relatively high grade reflects a culmination in postmetamorphic uplift. The Sifton Ranges has some of the highest grade metapelites in the northern Omineca Belt. Figure 21 is a map of metamorphic grade compiled from regional reports and discussion with H. Gabrielse. The garnet isograd emphasizes the regional style of antiformal isograds, which in the Sifton Ranges is inferred to be a result of postmetamorphic upright folding. The antiformal pattern may have been acquired in mid-Cretaceous time by uplift of the core of the Swannell Ranges to result in K-Ar ages for biotite and muscovite of 90 Ma, whereas ages on the flanks (140 Ma) retain the record of earlier postmetamorphic cooling of the region (*see* Fig. 46). Kyanite is the Al_2SiO_5-polymorph in the Swannell and Butler ranges. The Horseranch Range in McDame map area (Gabrielse, 1963; Fig. 3) is the only range other than the Sifton Ranges that has the assemblage sillimanite — K-feldspar (collections made by the author in 1983). These two ranges have in common the greatest amount of postmetamorphic uplift in the northern Omineca Belt, and also Eocene K-Ar ages, that indicate that some of the uplift was as late as Eocene. These two features can be more fully appreciated after the tectonic evolution of the Sifton Ranges is considered.

Summary and Conclusions of Metamorphism

The variety of metamorphic grade and distribution of isograds in the Deserters and Sifton ranges is inferred to be largely the result of postmetamorphic upright folding which provides structural and metamorphic relief. Thin sections from both ranges contain evidence of syn-metamorphic and postmetamorphic deformation. Folded isograds in the footwall of the Sifton Fault are truncated by the fault. Mineral assemblages indicate that the maximum pressure reached is bathozone 5 or 6 (Carmichael, 1978) in Deserters Range and bathozone 5 or 5/4 in the Sifton Ranges. The geothermobarometric study yields approximately the same P-T conditions as the mineral assemblage and both suggest that the Deserters Range may have been metamorphosed at a greater pressure than the Sifton Ranges, although the difference in pressure from the geothermobarometry is not great enough to be conclusive. The mineral assemblages and geothermobarometric study do not restrict the range in pressure enough to determine the relative vertical displacement on the Sifton Fault.

STRUCTURE AND TECTONICS

Orientation data on several different types of fabric elements were recorded in the field and are used to determine the macroscopic geometry of map units. Macroscopic geometry is illustrated by maps of the distribution of fabric elements and by serial cross-sections. The maps show an average attitude of a fabric element for each square kilometre where linear fabrics, or poles to planar fabrics, define a point maximum (eg. Fig. 22). Poles to girdles (pi poles) are shown where the fabrics are folded on a small enough scale with respect to the square kilometre to define a great-circle girdle. Planes indicate relative consistency of data, and the pi poles may indicate regions of folding. Computer programs used to manipulate and display the structural data are given by R.D. McMechan (1981). Macroscopic geometry and observations of mesoscopic and microscopic fabric relationships are used to interpret the kinematic history.

Radiometric dating of metamorphic minerals forming the foliations in the Wolverine Complex constrains syn- and post-metamorphic deformation to Mesozoic and younger (Parrish, 1979). Any pre-Mesozoic deformation has been obliterated or is not geometrically distinct from the Mesozoic deformation.

Deserters Range

Macroscopic geometry of fabric elements

Bedding and foliation

Primary structures are rare, and bedding is recognized mainly by changes in rock type. Bedding measurements are sparse in homogeneous rocks such as phyllite and psammite. Foliation is defined by planar arrays of platy and elongate minerals in schist and phyllite, and by compositional layering in amphibolite.

Bedding and foliation in rocks overlying the Deserters Gneiss have generally a similar distribution of attitudes and are folded on a relatively local scale throughout much of the area (Fig. 22). Poles to girdles consistently plunge gently to the northwest north of Deception Cone and to the southeast in the southeast. The only area of consistent dips is on the southwest flank of "Henry's Ridge" where metaquartzite is folded over the crest of an anticline. This is in accord with the field observations that the metaquartzite is generally only warped whereas less competent and thinner-layered rocks are crenulated or folded into chevron folds and kinks of all scales (Fig. 23). Open to tight folds in metaquartzite were found only on cliffs in Police Creek.

For the purposes of structural analysis, the area has been subdivided into two relatively homogeneous structural domains based on the orientations of axial surfaces of folds (Fig. 24). Bedding and foliation are grouped into the

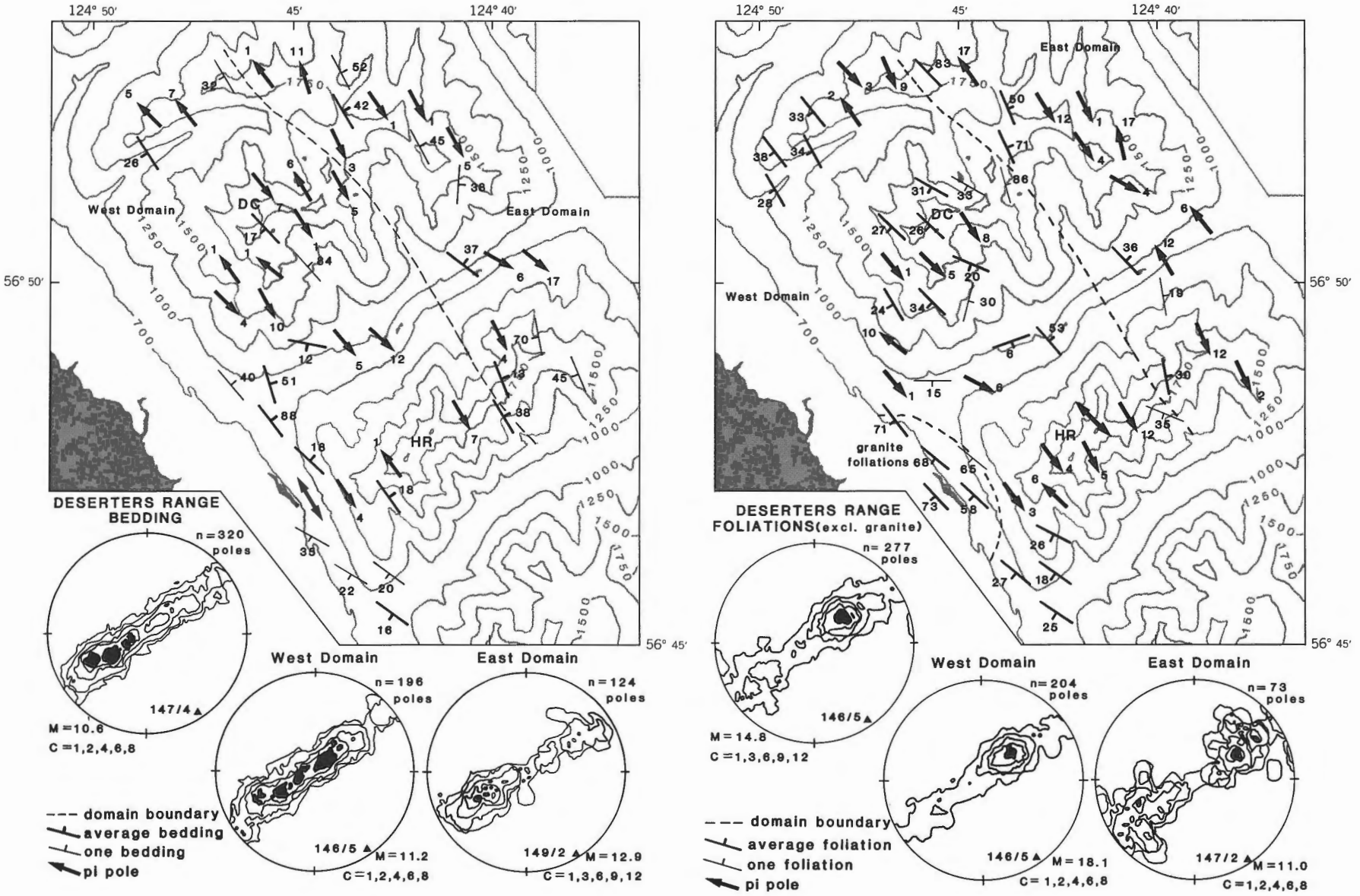

Figure 22. Maps of average bedding and foliation attitudes in the Deserters Range. The maps show the average attitude (or pi pole) for the surrounding square kilometre. Stereographic projections are lower hemisphere and equal area. Contours are in % per 1 % area. DC, Deception Cone; HR, "Henry's Ridge".

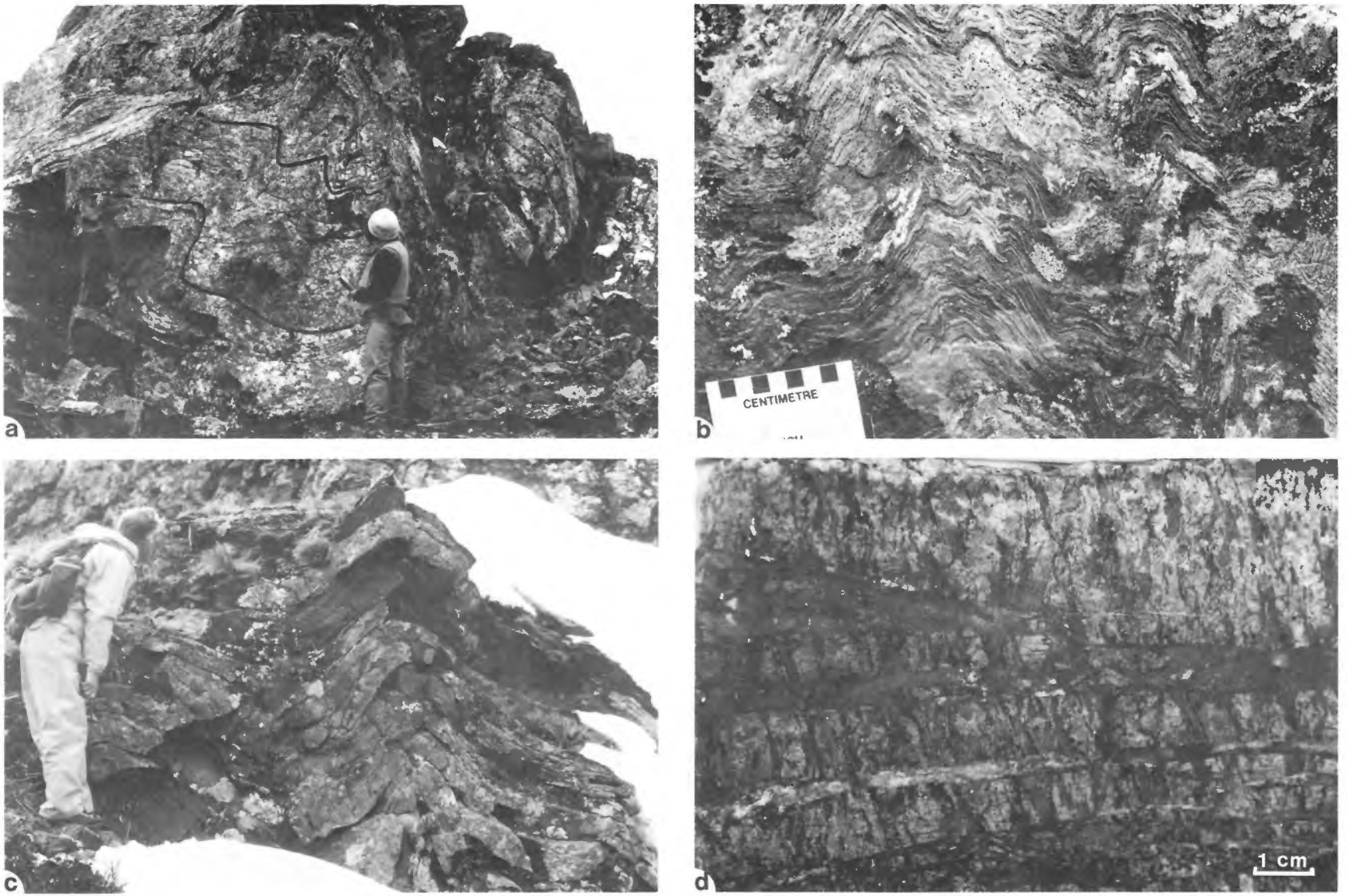

Figure 23. Structures in the Deserters Range. a) View NW of folded amphibolite with narrow hinge and moderately SW dipping axial surfaces, from the peak 1 km SW of Deception Cone summit (west domain) (GSC 404483-B). b) View SW of chevron folds of laminated metaquartzite (HMs) with steep axial surfaces, from 1.5 km east of Deception Cone summit (east domain) (GSC 204483-C). c) View NW of upright folds of metaquartzite (HMs) on "Henry's Ridge" (GSC 204483-D). d) Veins of ultracataclasite cutting the foliation in the Deserters Gneiss, from the SW slopes of "Henry's Ridge", top is to the NW. (GSC 204483-E)

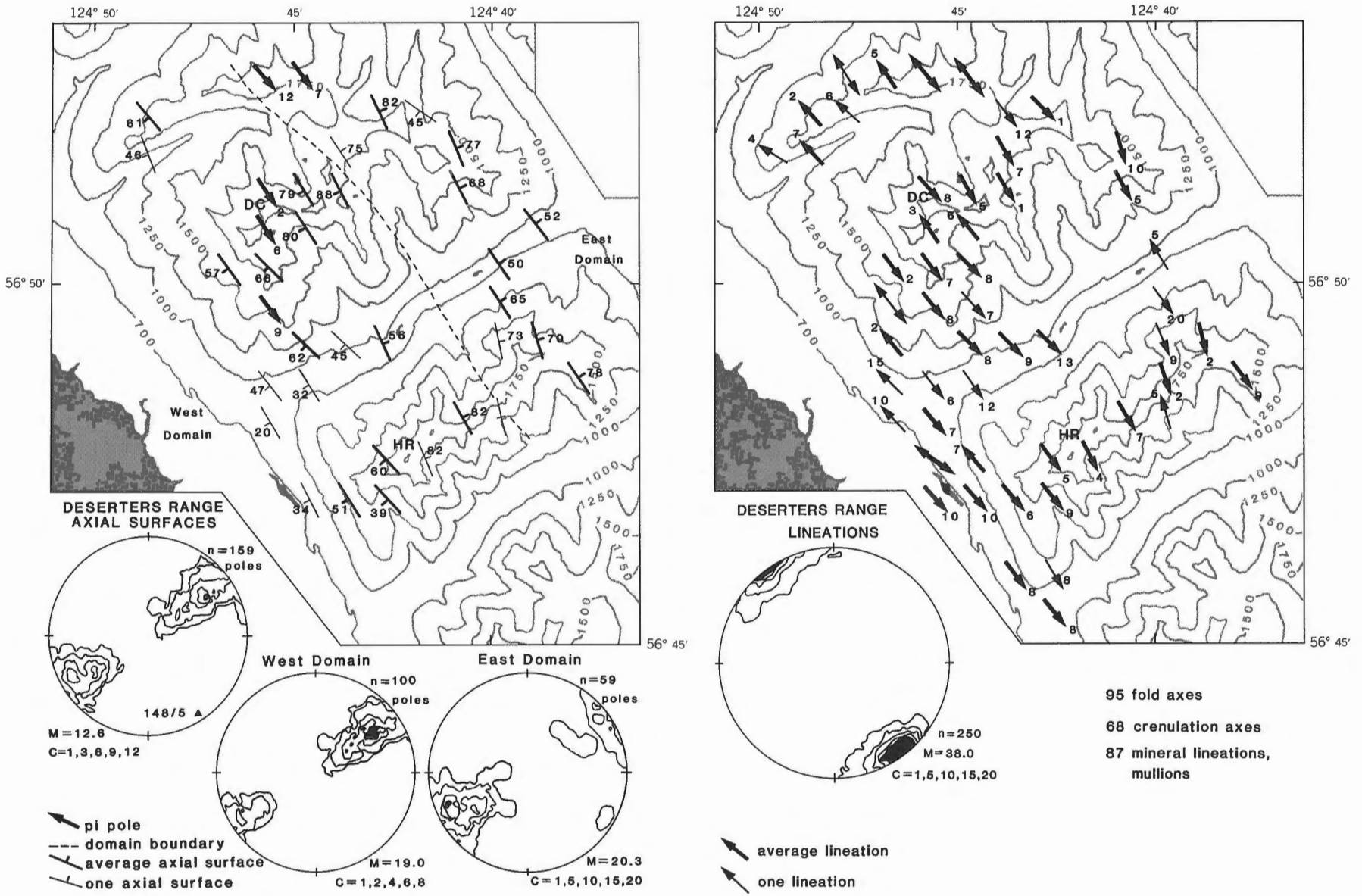

Figure 24. Maps of average linear elements and axial surface attitudes in the Deserters Range. The maps show the average attitude (or pi pole where appropriate) for the surrounding square kilometre. Stereographic projections are lower hemisphere and equal area. Contours are in % per 1 % area. DC, Deception Cone, HR, "Henry's Ridge".

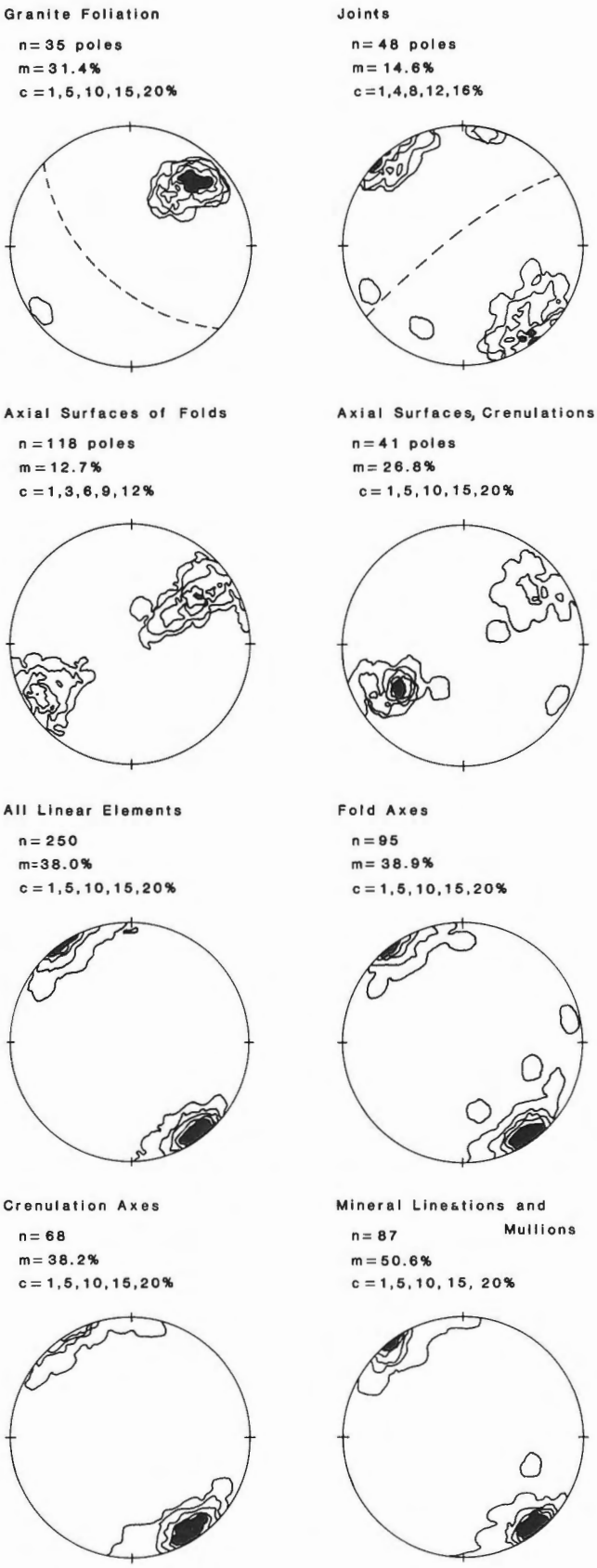

Figure 25. Stereograms of fabrics in the Deserters Range that are not shown on the maps of fabrics. Stereographic projections are lower hemishpere and equal area. Contours are in % per 1 % area.

same two domains, although the local scale of folding does not permit a clear separation of homogeneous fabric domains. Bedding and foliation have a weak concentration of gentle to moderate dips in the west, and moderate to steep dips in the east (Fig. 22), which suggests that in the west domain the long limbs of folds dip gently to moderately, and in the east domain long limbs dip moderately to steeply. This pattern is consistent with the field observations (Fig. 23a), and with the map pattern (Fig. 4) as shown by the fairly abrupt change from gently dipping units in the west to steeply dipping in the east.

Foliation in the Deserters Gneiss is defined by lenses up to 2 cm long of fine biotite, and by lenses of quartz. Foliation strikes northwest and consistently dips steeply to the southwest (Fig. 25). It is mylonitic and probably associated with transcurrent faulting in the Northern Rocky Mountain Trench. The foliation is cut by undeformed brittle extension fractures which dip steeply southeast and are filled with ultracataclasite (Fig. 23d). The fractures are perpendicular to the extension direction of a dextral shear couple parallel with the trench, and are interpreted as extensional fractures related to late (brittle) dextral faulting in the trench.

Fold axes and axial surfaces

Folds of bedding and foliation (F2) are coaxial with mineral lineations and mullions in metaquartzite (Fig. 25), and accordingly, all linear elements are plotted together in Figure 24. The map of lineations (Fig. 24) shows consistent northwest trends which are parallel with pi poles of bedding and foliation. Most of the deviations from the mean occur in a southeast region of more southerly trends. The map also illustrates a structural culmination near Deception Cone, defined by northwesterly plunges in the northwest and southeasterly plunges in the southeast. The culmination coincides with the regional zone of maximum postmetamorphic uplift, as expressed by exposure of the highest metamorphic grade and lowest stratigraphic level in the northern Rocky Mountains. Folds are cylindrical, and both harmonic and disharmonic types are common. The strongly foliated and anisotropic character of the assemblage has resulted in the development of angular, open to closed folds, chevron and kink folds in thinly-layered rocks, and rounded similar folds in thickly-layered rocks (Fig. 23).

Axial surfaces of crenulations are everywhere parallel with the axial surfaces of mesoscopic (F2) folds (Fig. 25). The attitudes of both these structures are plotted together in Figure 24. The map shows that the west domain has mainly steep southwesterly-dipping axial surfaces, with dips ranging from gently southwest through the vertical to steeply northeast; no gentle to moderate northeast dips are present. The east domain has mainly steep northeast dips that range from moderately northeast through the vertical to moderately southwest; no gentle southwest dips are present. Therefore, in the west domain, where bedding and foliation dip gently, the axial surfaces dip moderately and steeply southwest (Fig. 23a). In the east domain, where bedding and foliations dip moderately to steeply the axial surfaces dip steeply northeast (Fig. 23b). This pattern

results from the gentle convergent upwards fanning of F2 axial surfaces across the moderately southwest-dipping axial surface of Deserters Anticline (Gabrielse, 1975). In outcrop in the west domain, axial surfaces of minor folds on the limbs of larger folds are locally perpendicular to bedding and foliation. These relationships suggest that before the Deserters Anticline formed, bedding and foliation were subparallel. Minor folds developed in the strongly anisotropic layering by compression parallel with the layering and the buckling of relatively competent layers in a less competent matrix, producing axial surfaces at a high angle to bedding and foliation. As the Deserters Anticline and large-scale kinks formed, the earlier folds were rotated.

Summary of macroscopic geometry

The macroscopic geometry is shown in a detailed cross-section of "Henry's Ridge" (Fig. 4b), and in serial cross-sections of the range (Fig. 4c). The sections are drawn through regions of good ground control, and the projection and geometry of contacts are based on outcrop observations and map-scale trends of bedding, foliation, and lineations. Bedding, foliation parallel with bedding, and isograds are folded into a map-scale inclined anticline, the Deserters Anticline. Open to closed folds trend consistently northwest with gentle northwest plunges in the northwest, and gentle southeast plunges in the southeast, forming a gentle structural and metamorphic culmination.

Microscopic fabric elements and the relationship of metamorphism to deformation

Details of mineral assemblages and textural relationships were described earlier (*see* Metamorphism). A strong planar fabric (S1) defined by phyllosilicates is parallel with compositional layering (S0). Both are strongly crenulated, with a lack of mineral growth in the axial surfaces (S2) of crenulations or folds. The presence of rare snowball texture in the cores of garnets indicates syn-D1 growth of porphyroblasts. Garnet rims, staurolite and kyanite are post-D1, but predate the strong D2 crenulation. Quartz is granoblastic with undulose extinction and sutured grain boundaries.

The data indicate that the earliest deformation recognized is synmetamorphic. The lack of minor folds associated with the S1 foliation, however, inhibits generalizations about the kinematics of the deformation. Staurolite, kyanite, and garnet rims are posttectonic with respect to the S1 foliation, indicating that metamorphism outlasted deformation. Chevron and kink folding of foliation and of kyanite crystals, and the lack of axial surface foliation to F2 folds, indicate that folding postdates the peak of metamorphism. Accordingly, on the regional scale, the deformation producing the mesoscopic folds and the map pattern is interpreted to be postmetamorphic. The strong mineral lineation is inferred to have formed during the synmetamorphic deformation, and postmetamorphic folding was either fortuitously coaxial, or was governed by the strongly linear fabric already present.

Regional geological and tectonic implications

In metamorphic belts a schistosity representing a flattening plane is commonly observed to be parallel with the axial surface of folds of a phase of deformation (Turner and Weiss, 1963). Examples of schistosity in the axial surfaces of minor folds allow extrapolation of minor structures to a larger scale. In Deserters Range no isoclinal folds, nor folds with axial surface schistosity were found. Two tight folds in marble have axial surfaces parallel with the foliation in nearby schistose rocks. One of the folds verges east and the other verges west. The axis that could be measured is parallel with other lineations in the area. The entire map area is within a single stratigraphically upright panel. Although the stratiform foliation and mineral lineation are indicative of intense strain, no structural evidence of large-scale recumbent fold nappes or thrust nappes was found. However, mineral assemblage and geothermobarometric data suggest that the strata were metamorphosed at a relatively high pressure (6 to 8 kb), and tectonic thickening during D1 is inferred to have been substantial.

There are few constraints on the timing of deformation. Synmetamorphic deformation may be mid-Mesozoic, as suggested by early Cretaceous cooling ages of schist of the Misinchinka Group in the hanging wall of the Herchmer Fault (on the Hart Highway, Wanless et al., 1979). In Mesozoic times the Deserters Range was probably several hundred kilometres northwest of presently adjacent parts of the Omineca Belt, and its present location is a result of subsequent dextral transcurrent faulting along the Northern Rocky Mountain Trench (Gabrielse, 1985). It is reasonable to postulate that in the Mesozoic the Deserters Range was marginal to the Omineca Belt and was involved in regional northeast compression by folding or thrusting, or both.

The postmetamorphic history may be related to eastward contraction of the Foreland Belt in the Late Cretaceous and Early Tertiary, in part by thrusting on the Herchmer Fault. Early Cretaceous cooling ages in the hanging wall (Wanless et al., 1979) reflect uplift, but the relationship of the uplift to movement on the Herchmer Fault is unknown. Final cooling of the study area was in the Eocene, as indicated by Eocene K-Ar ages of biotite and hornblende (Wanless et al., 1974,1978), and may reflect the development of an Eocene thermal and related structural culmination associated with transcurrent movement in the Northern Rocky Mountain Trench. According to Gabrielse (1985) the culmination may have included the southern Sifton Ranges, offset 125 km dextrally along the trench since the Early Eocene.

Sifton Ranges: east and west of Spinel Lake

Macroscopic geometry

Two areas of distinctive geology in the Sifton Ranges are characterized by cylindrical folding and coherent internal stratigraphy, features which discriminate them from the hanging wall of the Sifton Fault. They are referred to as east and west of Spinel Lake rather than the footwall of the Sifton Fault because it is not apparent that the region west of Spinel Lake was ever overlain by the Sifton Fault.

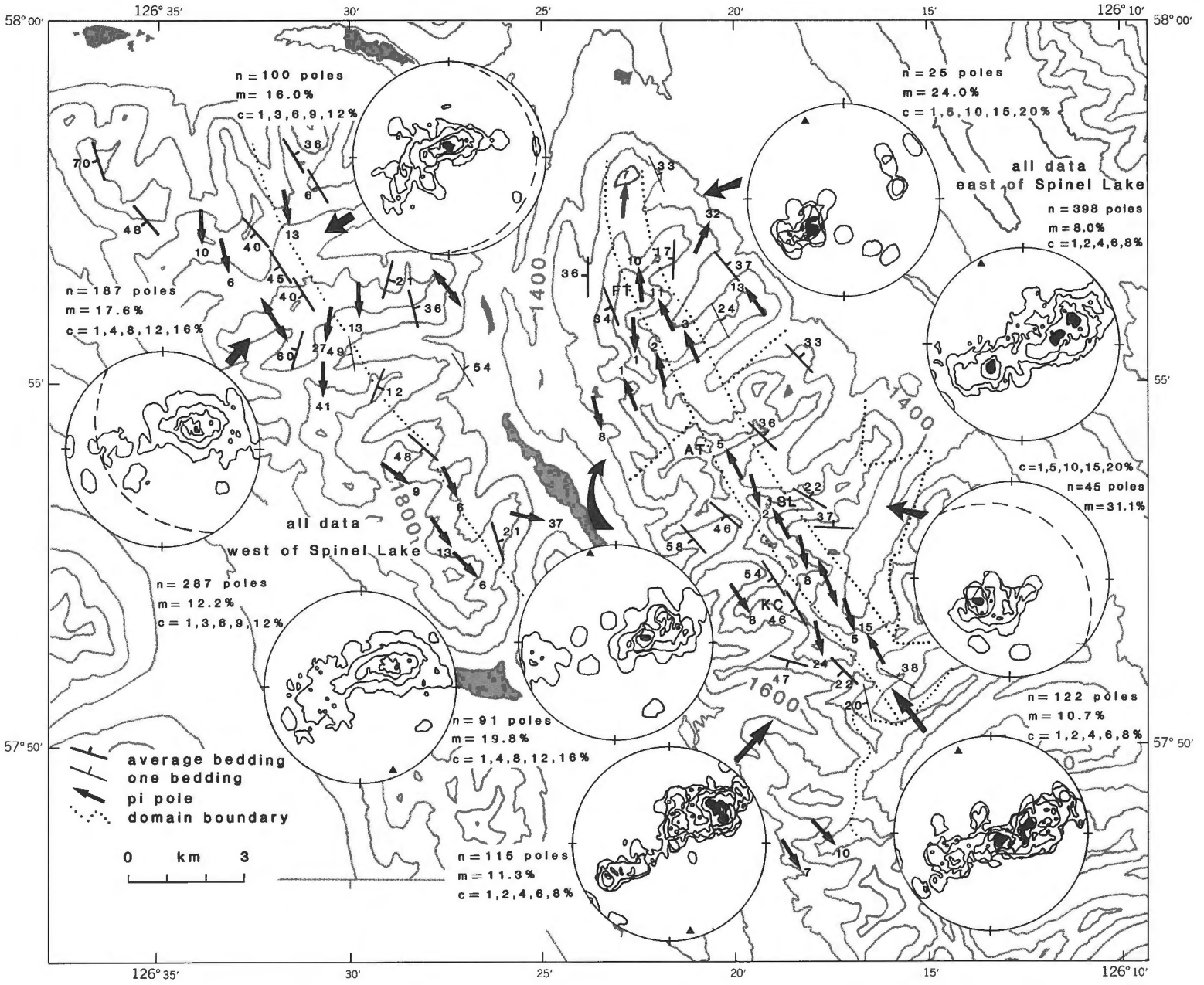

Figure 26. Map of average bedding attitudes in the Sifton Ranges. The map shows the average attitude (or pi pole) of bedding for the surrounding square kilometre. Stereographic projections are lower hemisphere and equal-area. Contours are in % per 1 % area. FT, Flat Top Mountain; SL, Mount Slocomb, AT, "Atche Peak"; KC, "Kechika Peak".

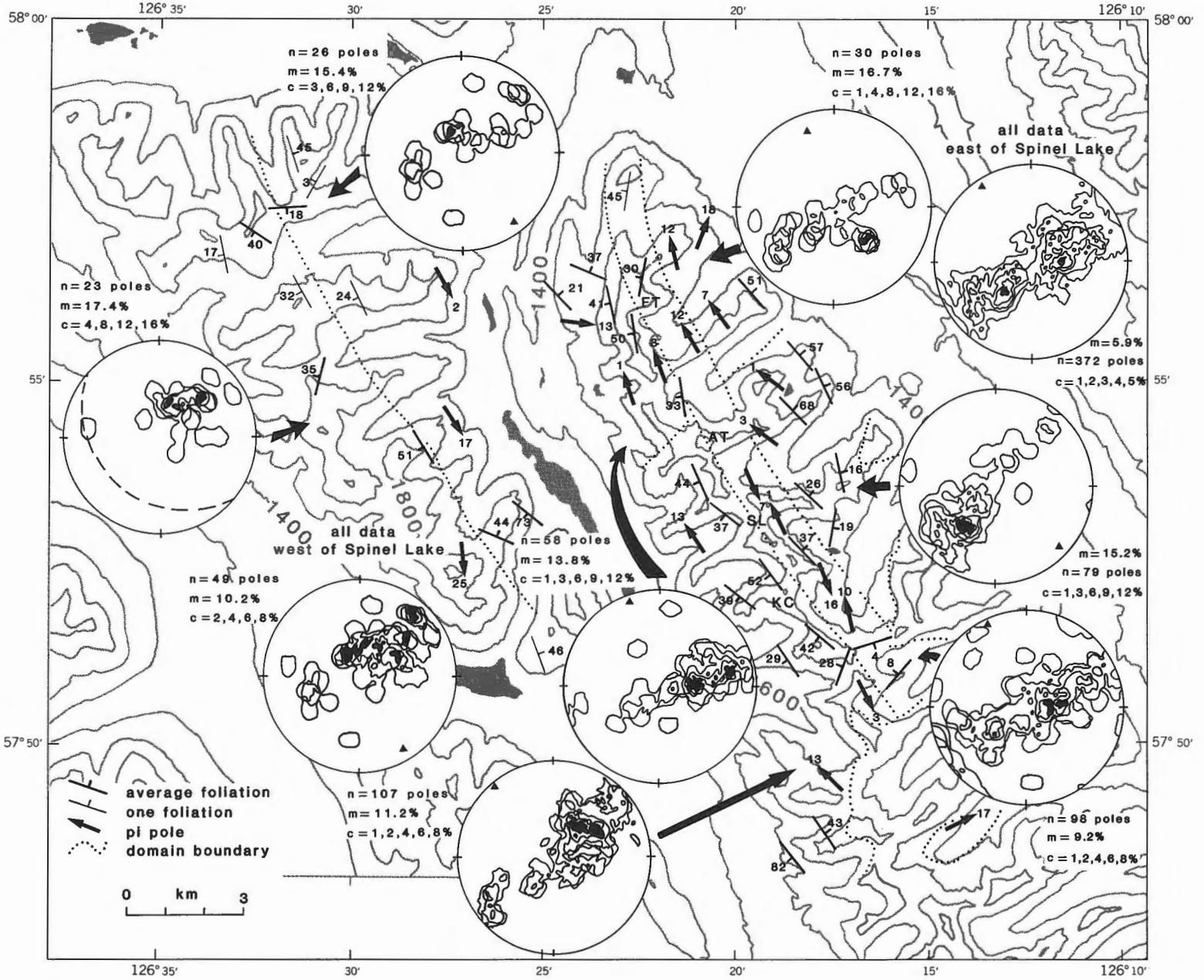

Figure 27. Map of average foliation attitudes in the Sifton Ranges. The map shows the average attitude (or pi pole) of foliation for the surrounding square kilometre. Stereographic projections are lower hemisphere and equal area. Contours are in % per 1 % area. FT, Flat Top Mountain; SL, Mount Slocomb, AT, "Atche Peak"; KC, "Kechika Peak".

Bedding and foliation

The range in orientation of bedding (Fig. 26) is generally the same as that of foliation (Fig. 27), consistent with the outcrop observations that the two are in most cases parallel. East and west of Spinel Lake, bedding and foliation are folded into two steeply inclined and gently plunging open anticlines with curved axial surface traces that can be seen on the map pattern and in Figure 26. The late curving of the axial surface trace requires dividing the limbs of the anticlines into several domains, so as to achieve more homogeneous fabric domains of bedding and foliation.

Bedding and foliation are isoclinally folded. The most common isoclinal folds are folds of foliation which do not have an axial surface foliation; rarely, folds of bedding have an axial surface foliation. Considering the likelihood of folding a foliation that developed during the same progressive deformation, isoclinal folds of foliation are not inferred to represent two episodes of folding. The syn- to late-metamorphic phase of deformation is defined as D1. A "late" episode of upright folding is referred to as D2. Five examples of crenulation cleavage in the axial surfaces of late upright folds were found.

On the moderately dipping limbs of the F2 anticlines and antiforms, F1 and F2 folds cannot always be distinguished because their geometry may be the same (eg. Fig. 28a). The best evidence of early (F1) structures is in the hinges of the late anticlines and antiforms, because the overprinting of late upright structures on recumbent structures is unambiguous (Fig. 28b). This evidence is of three types:

1) At three localities, foliation was observed to crosscut bedding along the axial surfaces of early folds. These are: northwest of Spinel Lake in rare west-verging tight to isoclinal folds of bedding and foliation; 3 km southeast of Mount Slocomb in a stack of recumbent F1 isoclines of metaquartzite (Fig. 28c); and on the west ridge of Mount Slocomb. Nowhere was it possible to determine stratigraphic facing in outcrop, and therefore the relationship of the structures to larger-scale ones is unknown.

2) The large-scale fold exposed on Mt. Slocomb (Fig. 28e) is one of the few examples of a large-scale F1 closure. The geometry in Figure 28e requires one phase of isoclinal folding to form the closure outlined by marble, and a phase of upright folding (F2) to fold the axial surface and limbs of the F1 closure. Because no marble is exposed structurally above the closure, either the limb of an east-verging fold was faulted off, or the early structure is west-verging.

3) A less well defined example of large-scale F1 folding occurs in unit HIg on the northernmost ridges, which expose the highest structural levels. A change in vergence of minor folds from mainly west-verging folds south of Flat Top Mountain (Fig. 7b,28d) to east-verging in the structurally higher zone to the north indicates a closure to the east of unknown vergence. The change in vergence occurs in the structurally highest unit of the F2 closure, and therefore its significance to large-scale geometry, is unknown.

The greater thickness of paragneiss on the east limb of the Sifton Antiform (Fig. 7b,c) may also be a relic of the early F1 folding event. Many changes in vergence of minor structures occur within units, but no markers were found in the critical areas to delineate structures or stratigraphic facing, and the changes are too numerous relative to the scale of mapping to locate major fold axial surfaces.

Fold axes and axial surfaces

All linear elements are combined in Figure 29 because it was generally not possible to distinguish with confidence the different phases of folds. An exception is found east of Spinel Lake in the hinge zone of the Sifton Antiform, where late upright folds can be distinguished from early recumbent folds and can be shown to be coaxial (Fig. 30). Figure 29 illustrates the consistent northwesterly trends and gentle plunges within the domains, and the curve in the axial surface trace of the major F2 antiform (the Sifton Antiform). West of Spinel Lake, non coaxial conjugate kink folds are present; their axes are irregular and have been excluded from Figure 29. This fold style may have formed as a result of the lower metamorphic grade and greater planar anisotropy in the Stelkuz Formation.

Figure 31 of axial surfaces is intended to show F1 folds throughout the area. However, in areas of moderately-to steeply-dipping strata some of the upright F2 folds that have the same geometry have probably been included inadvertently. Only in the F2 hinge zone east of Spinel Lake do the axial surfaces of definite F1 and F2 folds constitute two distinct subsets (Fig. 30); only early folds are shown in the hinge zone. Axial surfaces of noncoaxial conjugate kink folds west of Spinel Lake are omitted from the map of axial surfaces. These maps show the reorientation of F1 axial surfaces so as to be almost parallel with the axial surface of the upright F2 Sifton antiform. An exception is the area immediately east of the bend in Spinel Lake, where the attitudes of axial surfaces may be associated with poorly understood structures along the west flank of the range and east of Spinel Lake.

Lamprophyre dykes

Undeformed lamprophyre dykes 0.2 to 1 m wide occur throughout the Sifton Ranges (Fig. 32), and according to Gabrielse et al. (1977b), lamprophyre dykes are almost restricted to the Sifton Ranges. West of Spinel Lake, the majority dip steeply east-northeast or west-southwest (Fig. 32). Their orientation indicates brittle ENE extension. In the footwall and hanging wall of the Sifton Fault they have a weak concentration of steep northwest and southeast dips, their orientation being indicative of brittle SE extension. Southeast extension corresponds to the direction of maximum extension for dextral shear along the trench. The gentle to moderate dips occur only in the hanging wall, where their orientation is probably controlled by the strong gently-dipping planar fabric. K-Ar (biotite) ages of 37.8 $\pm$ 1.7 and 43.2 $\pm$ 0.7 Ma (Wanless et al., 1979; J.C. Roddick pers comm., 1985) indicate intrusion during late episodes of faulting in the Northern Rocky Mountain Trench and Spinel Fault Zone (C.J. Dodds, *in* Wanless et al., 1979, p.11). The ENE extension in the area west of Spinel Lake may be associated with normal faulting in the Spinel Fault Zone. Regional relationships indicate transcurrent displacement for the Spinel Fault Zone (Gabrielse, 1985), but no detailed studies have been done in the fault zone to exclude a period of normal faulting.

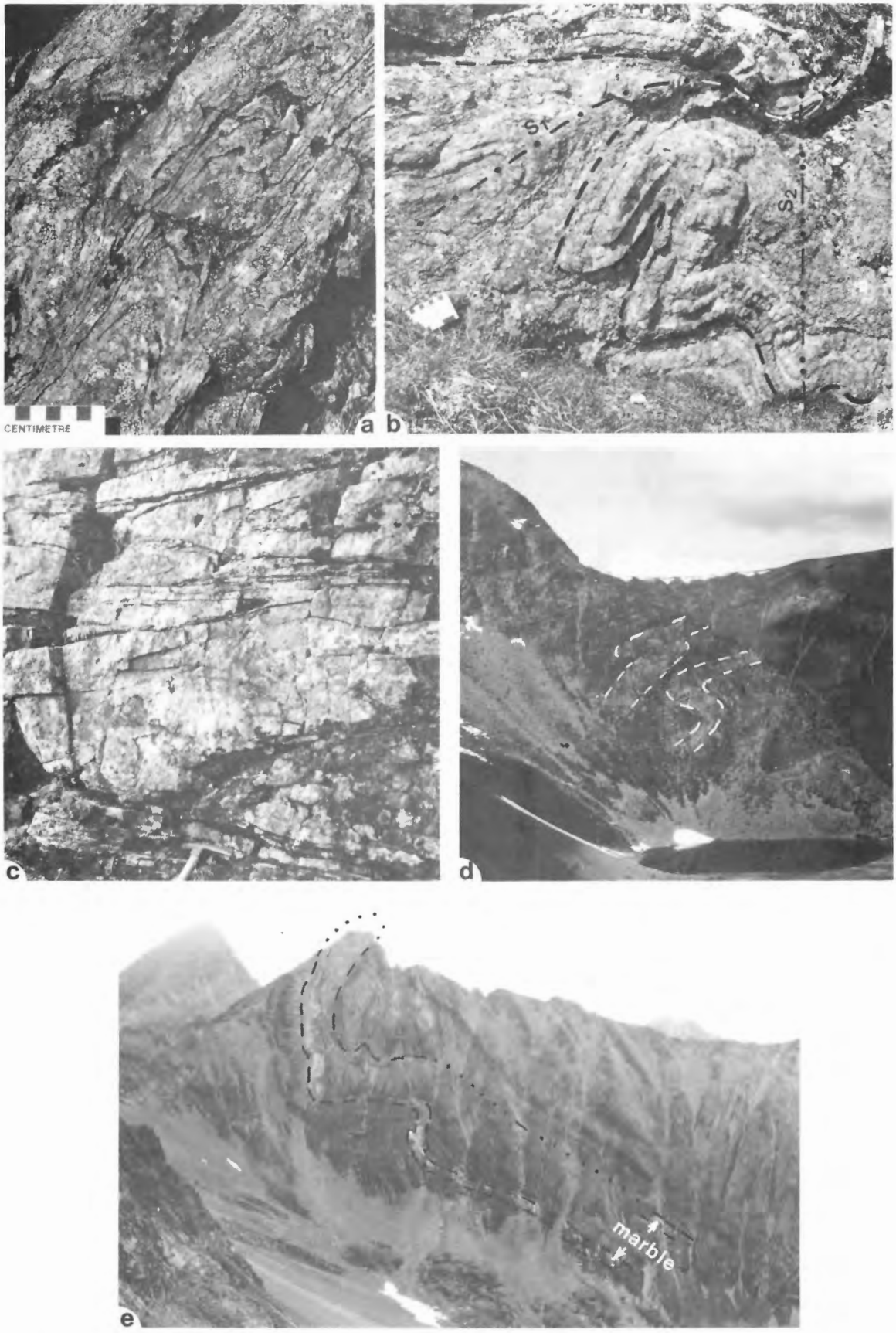

Figure 28. Structures in the footwall of the Sifton Fault. a) View NW of folds on the west limb of the Sifton Antiform, 2 km west of Mount Slocomb (GSC 204483-F). b) View NW of overprinting of upright F2 folds on tight F1 fold, 1.5 km NE of "Atche Peak" (GSC 204483-G). c) Isoclinally folded metaquartzite (Hlq) with axial surface foliation, 1.6 km SE of "Kechika Peak" (GSC 204483-M). d) View NW of large-scale folds of bedding 1 km south of Flat Top Mountain (GSC 204483-I). e) View NW of folded marble beds that mark a large-scale F1 closure on the south face of Mount Slocomb. (GSC 204483-J)

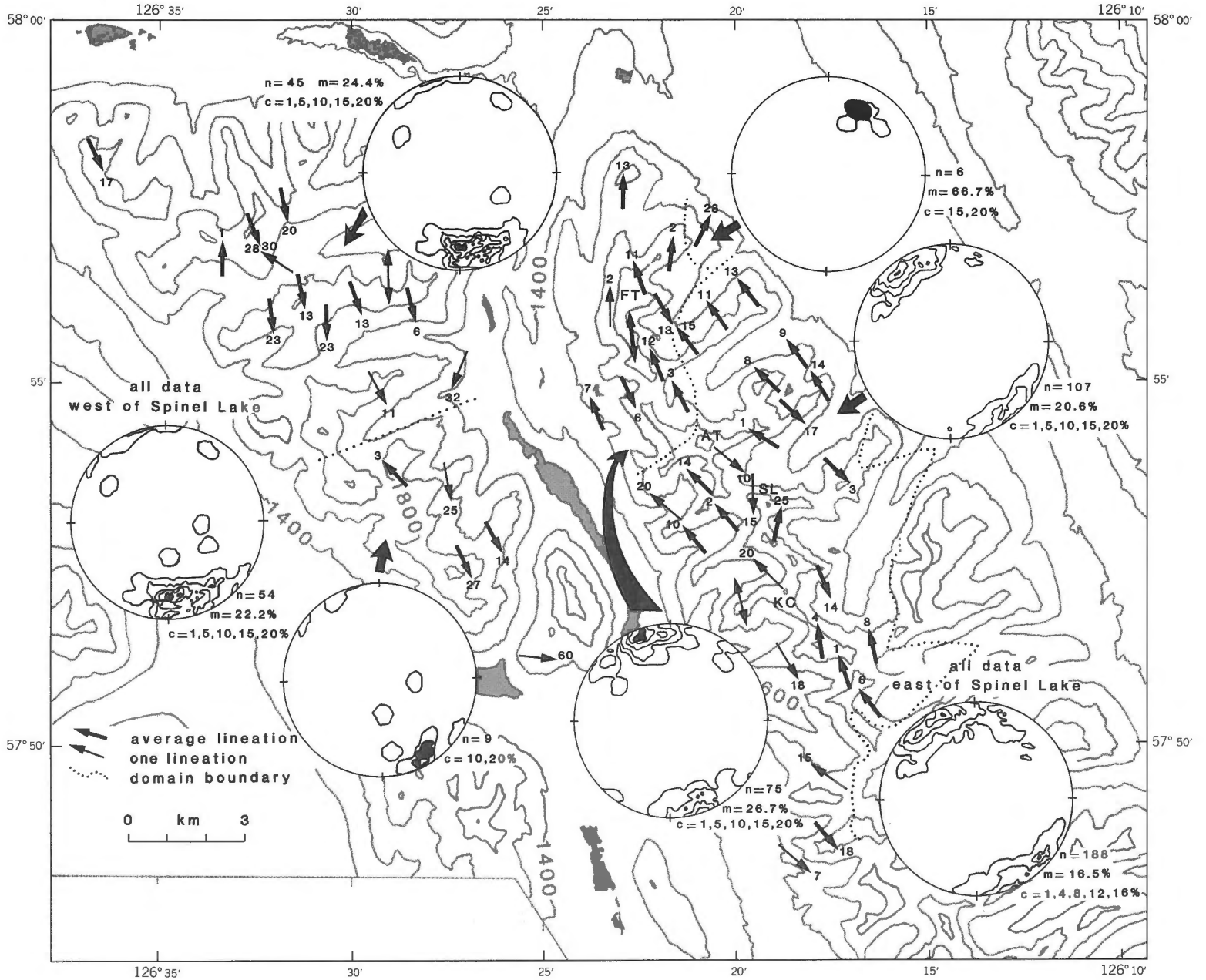

Figure 29. Map of average linear element attitudes in the Sifton Ranges. The map shows the average attitude of linear elements for the surrounding square kilometre. Stereographic projections are lower hemisphere and equal area. Contours are in % per 1 % area. FT, Flat Top Mountain; SL, Mount Slocomb; AT, "Atche Peak"; KC, "Kechika Peak".

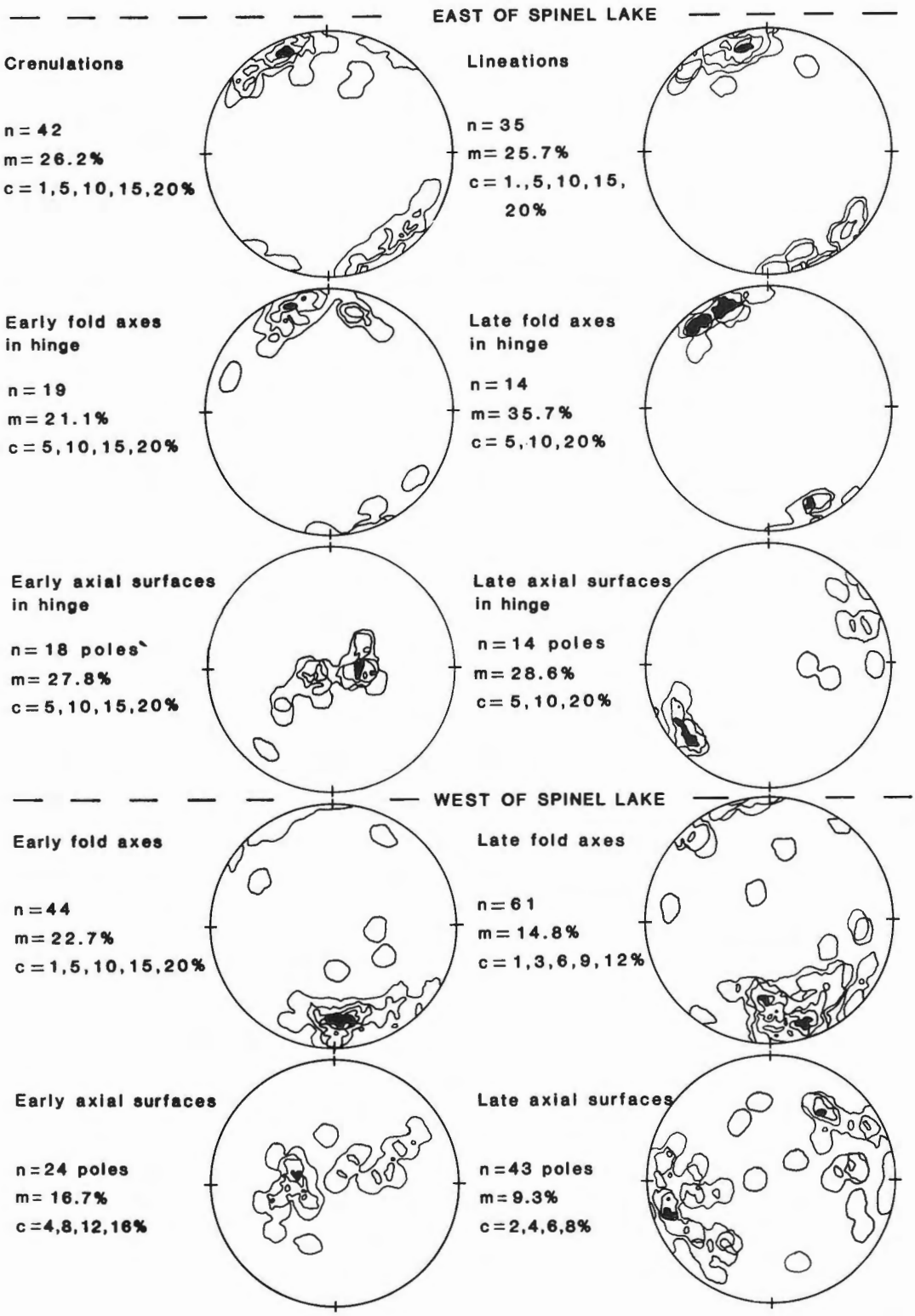

Figure 30. Stereograms of fabrics in the Sifton Ranges that are not shown on the maps of fabrics. Stereographic projections are lower hemishpere and equal area. Contours are in % per 1 % area.

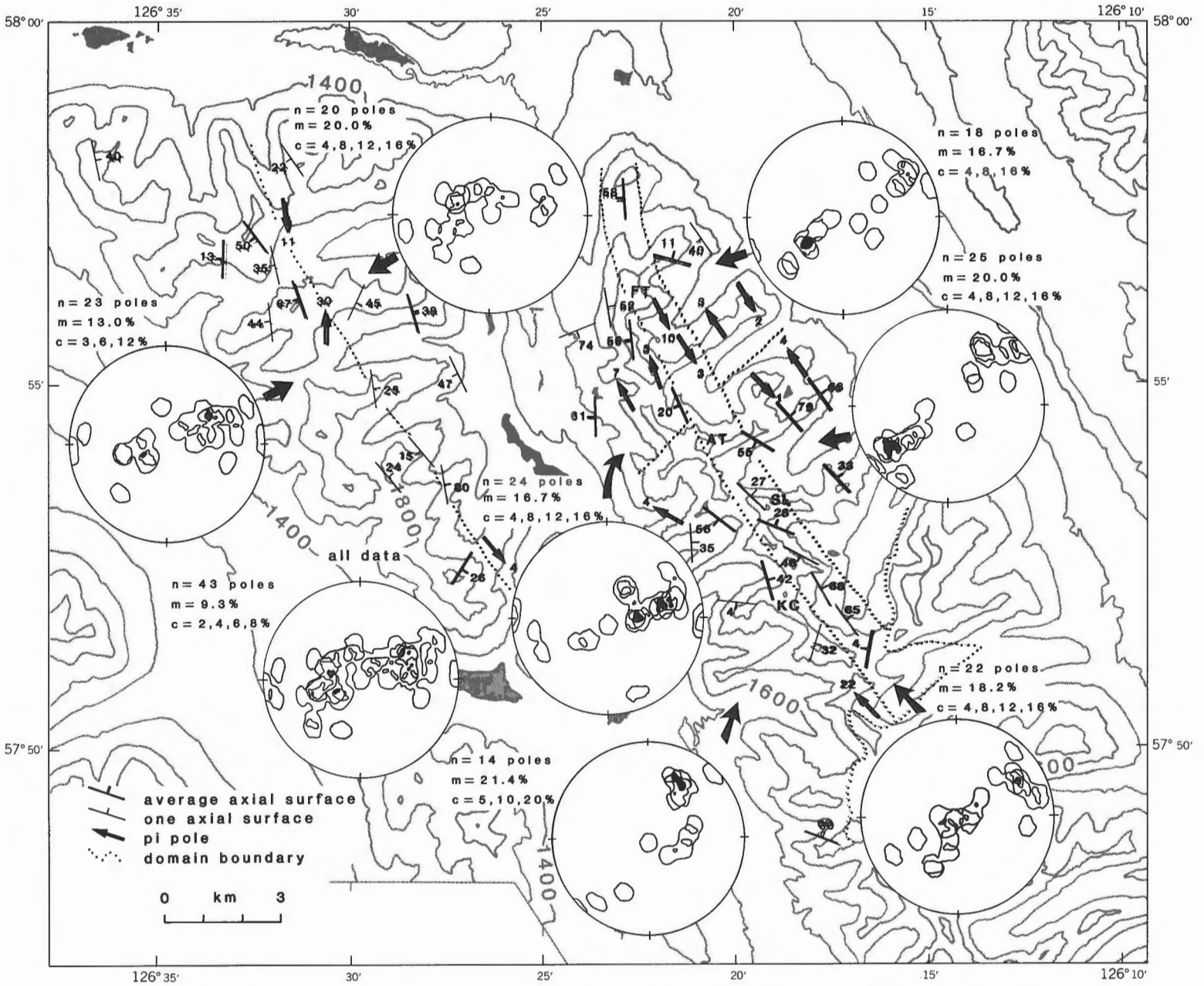

Figure 31. Map of average axial surface attitudes in the Sifton Ranges. The map shows the average attitude (or pi pole) of axial surfaces for the surrounding square kilometre. Stereographic projections are lower hemisphere and equal area. Contours are in % per 1 % area. FT, Flat Top Mountain; SL, Mount Slocomb; AT, "Atche Peak"; KC, "Kechika Peak".

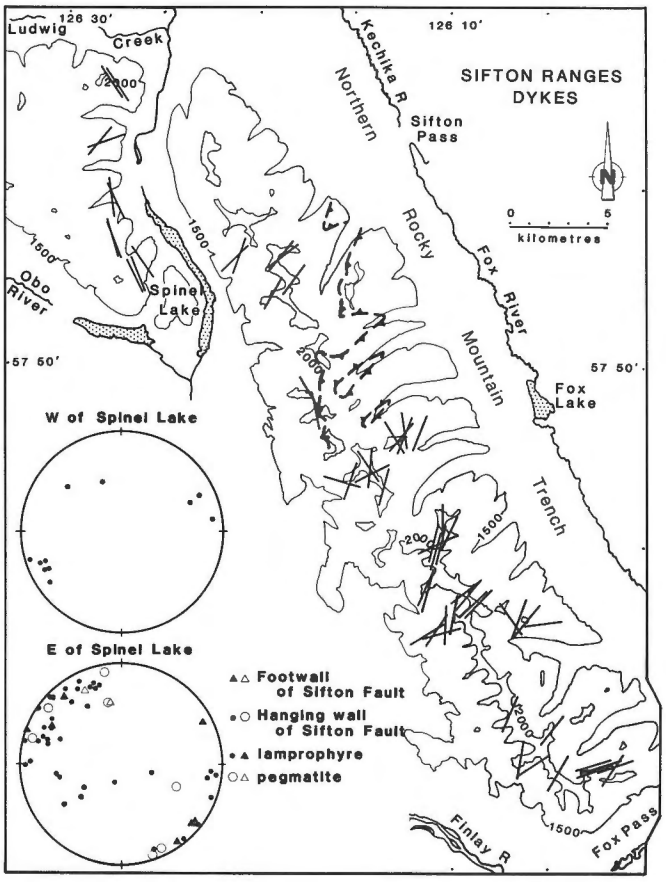

Figure 32. Location and orientation of dykes in the Sifton Ranges. Only lamprophyre dykes are shown on the map. Stereographic projections are lower hemisphere and equal area.

Summary of macroscopic geometry east and west of Spinel Lake

Intense early deformation (D1) has resulted in transposition of bedding, folds of bedding, foliation, and folds of the foliation prior to a phase of upright folding (F2) which produced the variation from gentle to steep inclination of bedding, foliation, and F1 folds. Recumbent isoclinal F1 folds are overprinted by upright F2 folds in the hinge zone of the F2 antiform east of Spinel Lake (Sifton Antiform). The only map-scale structures are open, gently plunging antiforms (F2) of bedding and foliation (Fig. 7b,c). The F1 folds have no map-scale expression because the level of erosion is entirely within a single, structurally upright panel.

Microscopic fabric elements

Details of textures in thin section were described earlier (*see* Metamorphism). A strong preferred orientation of foliation (S1) is parallel with bedding (S0). The most prominent structure in thin section is a coarse crenulation (S2) of the foliation (and kyanite), which lacks mineral growth along the axial surface. Snowball texture in garnet attests to synmetamorphic deformation. In rare examples from west of Spinel Lake, isoclinal microfolds of S1 foliation are overprinted by crenulations; this corroborates the outcrop observations that an early episode of deformation was overprinted by a second.

Regional geological and tectonic implications

An early phase of isoclinal folding (D1) was associated with foliation development (synmetamorphic) and folding of the S1 foliation. Isoclinal folding of the foliation indicates that D1 was syn- and/or late-metamorphic. Considering the relatively high pressures indicated by the metamorphic studies, tectonic thickening during D1 is inferred to have been substantial. The pattern of isograds east of Spinel Lake indicates that upright folding (D2) postdates the quenching of isograds (the approximate peak of metamorphism). Vergence of D1 is not well defined, but may be to the west (assuming that the footwall strata are upright).

Other parts of the core zone of the northern Omineca Belt have a strong foliation parallel with bedding, but little evidence for nappes has been reported, except near Chase Mountain in the Wolverine Complex (Parrish, 1976). There, two phases of synmetamorphic tight to isoclinal folds are overprinted by northwest-trending upright open folds. The second phase of isoclinal folding verges northeast, and no reversal of vergence was found. Large-scale west-verging folds occur in the cover rocks of the Omineca Belt northwest of the Sifton Ranges (H. Gabrielse, pers. comm., 1985). Late upright antiforms are common in the core zone of the northern Omineca Belt (eg. Gabrielse, 1975; Parrish, 1976; Gabrielse et al., 1977a). In one of the antiforms, the Swannell Ranges, K-Ar ages are younger in the centre (90 Ma) than on the flanks (140 Ma). As explained earlier, the pattern of ages may date the upright folding and, by extrapolation, the upright F2 structures in the Sifton Ranges as mid-Cretaceous.

Sifton Ranges: hanging wall of Sifton Fault

Macroscopic geometry

The Sifton Fault is a gently dipping surface with an overall northerly trace. The contrasting stratigraphy of the footwall and hanging wall, and the truncation of the Sifton Antiform in the footwall by the lowest unit in the hanging wall, provide ample evidence that the Sifton Fault is a major, map-scale structure (Fig. 7). Although it is evident at map scale, it is not easily identified at the outcrop scale because schists near the fault have few features diagnostic of either the footwall or the hanging wall. The fault, as mapped here, is the surface below which there are no strata that unequivocally belong in the hanging-wall. Criteria used to distinguish footwall from hanging-wall rocks are as follows.

1) Map units that can be traced from the coherent stratigraphy of the footwall towards the Sifton Fault are included in the footwall;

2) At map-scale, a zone of relatively low grade pelitic schists of the hanging wall truncates high grade isograds of the footwall (Fig. 16,18), so that in the vicinity of the fault (as identified at the map scale) sillimanite-bearing schists are assigned to the footwall.

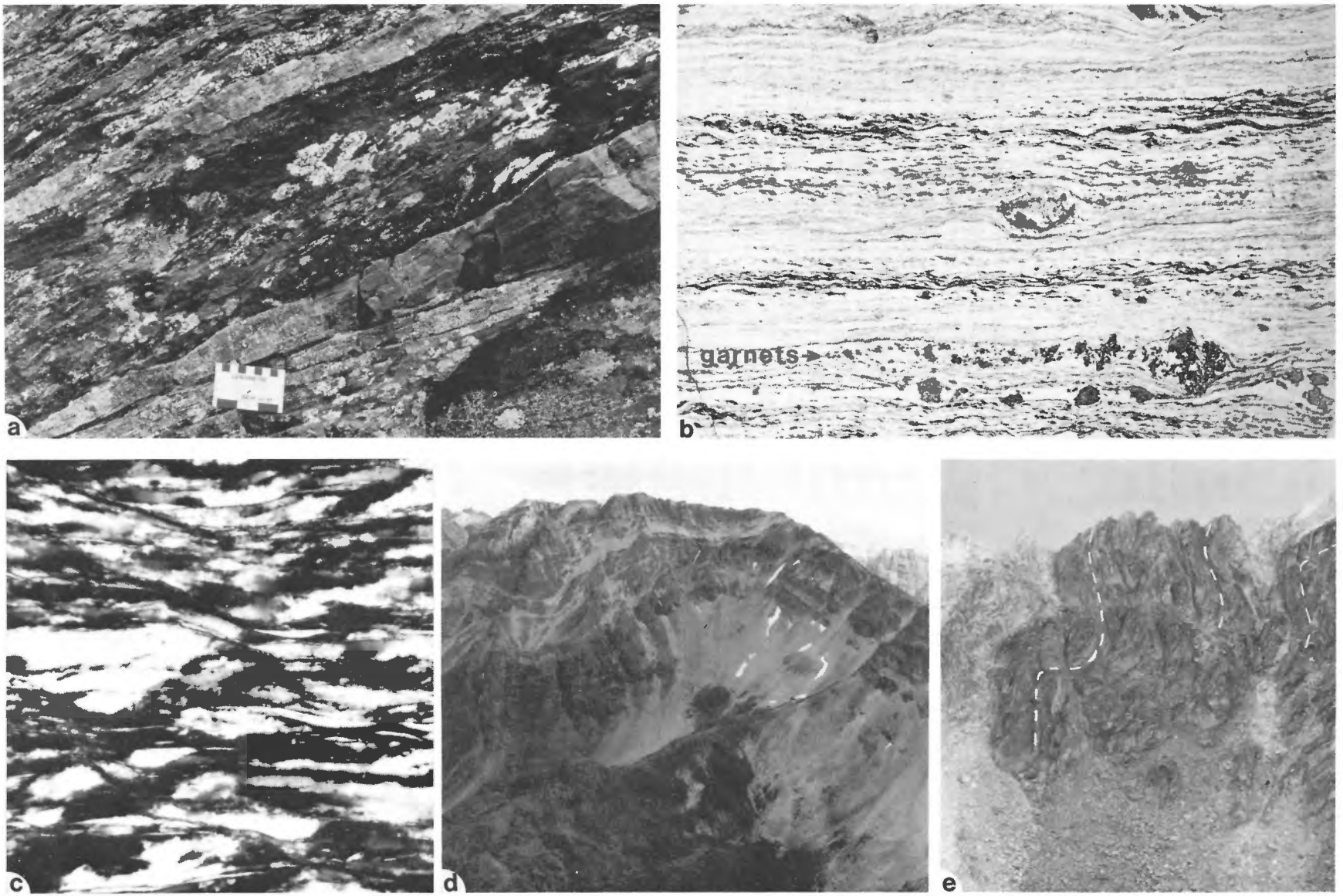

Figure 33. Foliation in the hanging wall of the Sifton Fault. a) Strongly foliated metaquartzite and amphibolite in unit HIqa (viewed to the east)(GSC 204483-K). b) Photomicrograph of compositional layers defining the foliation, note the layer of fine garnets that appear to have broken off the large garnet at lower right. Left side of the photograph is to the south (width is 2.3 cm). c) Ribbons of quartz defining the foliation (width is 1 mm). d) View south to the large scale late antiform 2 km SE of Fox Peak. (GSC 204483-L) e) View SE to late inclined kink folds on the SW flank of the Sifton Ranges, 1.5 km west of Hedges Peak. (GSC 204483-M)

3) Rocks that are unlike those found in the northern part of the footwall are considered part of the hanging wall. These include a) isolated (house-size and larger) blocks of marble surrounded by schist, that may have originated in the footwall but are not stratigraphically continuous with footwall strata, and b) "wavy", rusty weathering schist (Fig. 10c) that is typical of the structurally lowest unit that (at map scale) truncates the Sifton Antiform in the footwall.

The hanging wall consists of metamorphic rocks with a variety of textures and structures found in shear zones, and as a result, the hanging wall is considered to be a shear zone. The base of the fault zone is referred to as the Sifton Fault. A search for kinematic indicators in the vicinity of the fault revealed that they are consistent with those found in the hanging wall and therefore structures in the hanging wall are inferred to be a result of displacement on the Sifton Fault.

Foliation and shear bands

The foliation ranges from schistosity to a variety of mylonitic fabrics. Gneissosity in amphibolite and compositional layering in all units is parallel with the foliation in outcrop (Fig. 33a). The mylonitic foliation is defined by quartz ribbons and lenses, and compositional layers of fine micas, feldspar, garnet and opaques (Fig. 33b,c). The foliation is commonly wavy where it is cut at a low angle by a cleavage.

The variation in orientation of foliation is shown in Fig. 34. On the northeast flank of the Sifton Ranges, the foliation dips gently and consistently northeast. East of Hedges Peak it is folded into an open antiform, and the east limb coincides with the east-dipping flank of the range. The central region and west flank have variable gentle to moderate dips dispersed in a great circle as a result of late open folding about gently northwest-plunging fold axes (Fig. 33,d,e). The Sifton Fault truncates the Sifton Antiform in its footwall, and therefore upright folds in the hanging wall cannot be related to folds in the footwall. However, it is likely that at least some of the upright folding that affected the hanging wall also affected the footwall. A domain northwest of Mount Brandon with steep dips and northwest strikes is probably related to movement on the steeply-dipping Spinel Fault Zone.

The cleavage offsets and warps limited segments of the mylonitic foliation which are asymptotic with the cleavage in the regions of offset, and accordingly, it is inferred to have been ductile. The appearance of the cleavage that warps the mylonitic foliation (Fig. 35a,b,c,d) is the same as shear bands that have been described in shear zones (Platt and Vissers, 1980; Berthe et al., 1979; White et al., 1980; Gapais and White, 1982; Simpson, 1984; Weijermars and Rondeel, 1984). Independent kinematic indicators from those zones confirm that shear bands have a consistent angular relationship with the mylonitic foliation and can be used as a kinematic indicator (White et al., 1980; Simpson and Schmid, 1983). At a larger scale, Weijermars and Rondeel (1984) have demonstrated that in the Truchas shear zone (Spain) the shear bands have an angular relationship with the shear zone boundary that is consistent with relationships at the mesoscopic scale. More than 55 examples of mesoscopic shear bands were found throughout the hanging wall of the Sifton Fault; the orientation of the shear bands is at an acute angle clockwise (looking east) from the mylonitic foliation (Fig. 35a). Eight oriented thin sections cut perpendicular to the foliation and parallel with the lineation have shear bands, and their orientation with respect to the foliation is consistent with the mesoscopic observations (Fig. 35b,c). The orientation of the shear bands relative to mylonitic foliation indicates that the hanging wall moved southerly over the footwall. This interpretation is consistent with the analysis of folds in the hanging wall.

Lineations

A prominent mineral lineation is defined by quartz rods and amphibole crystals which lie in the plane of the foliation. A central domain constituting a large part of the hanging wall has a strong maximum of gently NNW-plunging lineations (Fig. 36). The east flank of the range consists of several domains of more northerly-trending gentle plunges. The area of steep foliation northwest of Mount Brandon has gently WNW-plunging lineations that are inferred to be related to strike-slip movement on the Spinel Fault Zone. Four examples of tremolite fibers in ENE-striking, steeply dipping, extension fractures (1 to 5 cm wide) in marble are parallel with quartz and amphibole mineral lineations. In general, elongation lineations are parallel with the finite maximum extension direction. As strain increases in a zone of predominantly simple shear, newly formed and pre-existing linear elements rotate to closer to the direction of shear, at large strains becoming nearly parallel with the shear zone walls (Ramsay, 1967,1980). Accordingly, the mean lineation in each domain of the hanging wall is inferred to be a good indication of the slip line.

Cylindrical folds and sheath folds

In outcrop nearly all folds are cylindrical, but five strongly noncylindrical, or sheath folds were found. On the regional scale, the fold axes are dispersed so as to define a gently-dipping great circle (Fig. 36).

Hansen (1967) recognized that for fold axes with a planar preferred orientation, the line contained within the separation angle between folds of opposing vergence may be inferred to be a slip line. This analysis has been applied to the regional orientation of fold axes to determine the slip line (Hansen, 1971; Barton, 1975; Davis, 1983). Several workers (Escher and Watterson, 1974; Roberts, 1977; Bell, 1978; Williams, 1978) recognized that the regional reorientation of fold axes is associated with fault zones with a large component of simple shear. Mesoscopic sheath folds occur in ductile fault zones and are thought to form by the progressive rotation of pre-existing and newly formed fold axes towards the direction of maximum elongation in shear zones with a large component of simple shear (Rhodes and Gayer, 1977; Quinquis et al., 1978; Henderson, 1981). However, the variation of the fold axes over the entire shear zone is generally not attributed to the development of sheath folds. Both scales of fold geometry can be used to determine the sense of displacement of a fault zone.

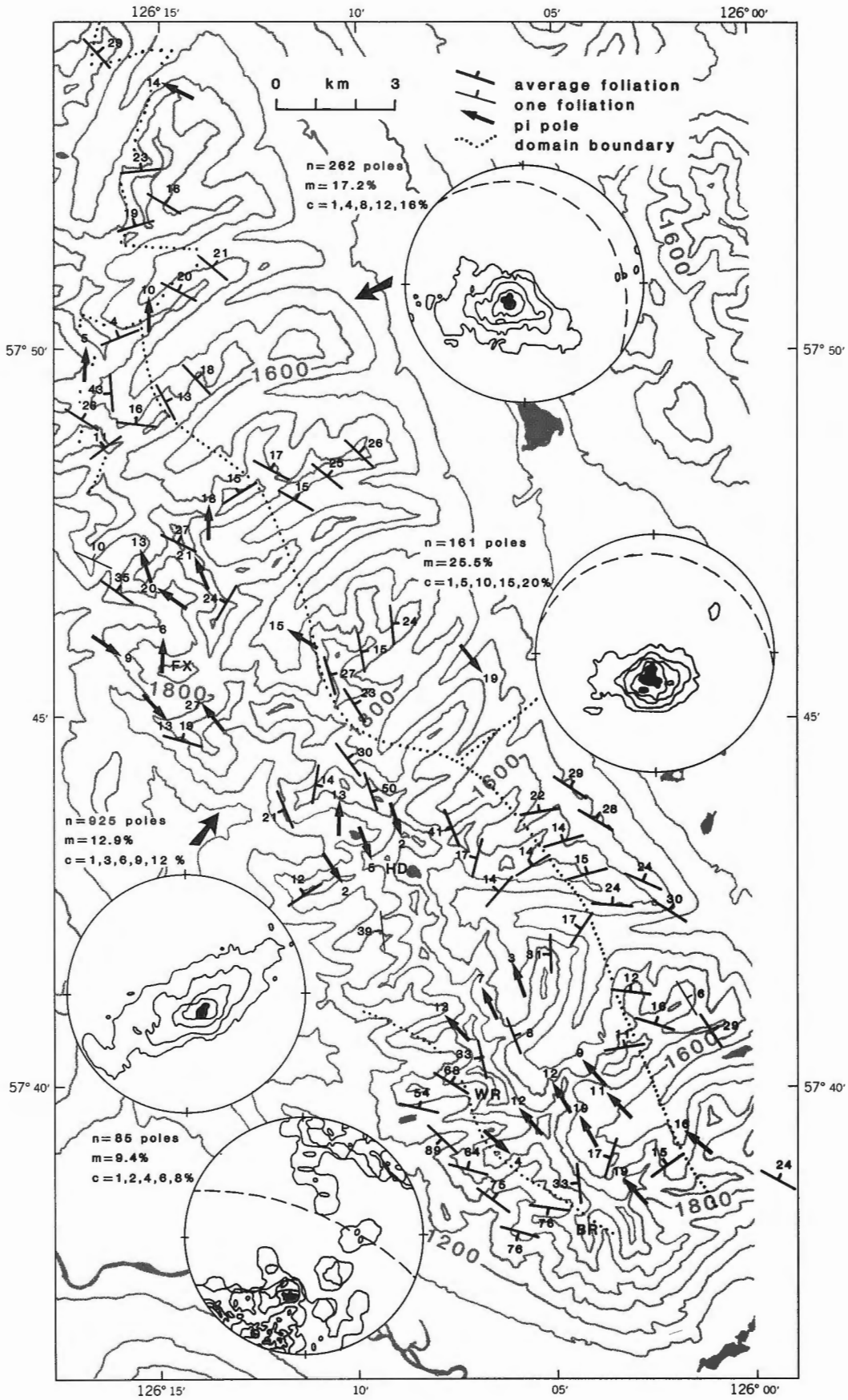

Figure 34. Map of average foliation attitudes in the hanging wall of the Sifton Fault. The map shows the average attitude (or pi pole) of foliation for the surrounding square kilometre. Stereographic projections are lower hemisphere and equal area. Contours are in % per 1 % area. FX, Fox Peak; HD, Hedges Peak; WR, Warner Peak; BR, Brandon Peak.

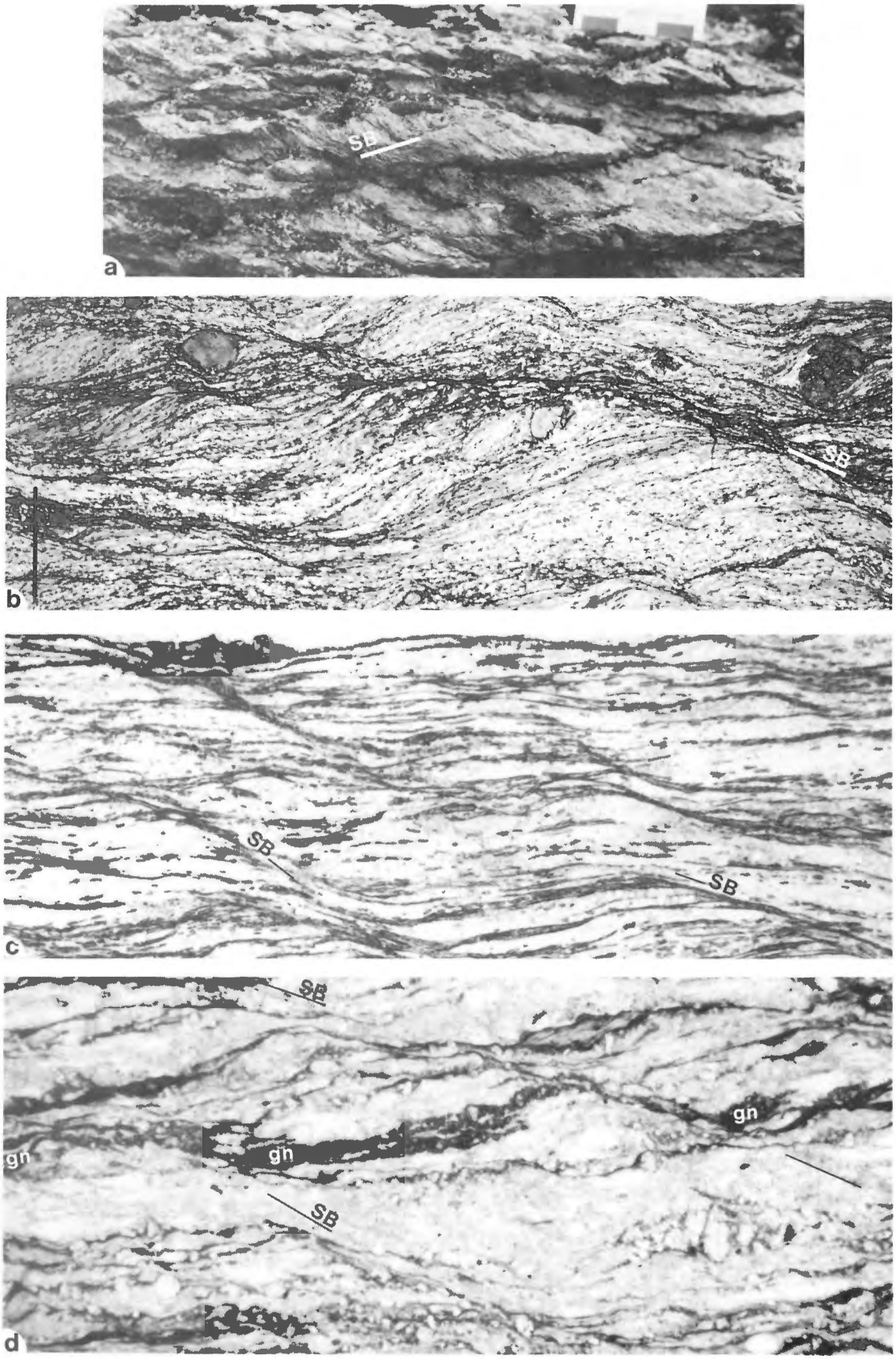

Figure 35. Shear bands (SB) in the hanging wall of the Sifton Fault; a) is viewed to the west; and b) and c) to the east; all indicate top-to-the-south displacement (top-to-the-left in a), top-to-the-right in b) and c) a) Shear bands in psammitic schist (unit Hlsm) (GSC 204483-N). b) Shear bands in pelitic schist (width is 1.7 cm). c) Shear bands in metaquartzite, chlorite is parallel with the foliation and in pull-aparts of tourmaline (top left; width is 2.1 mm). d) Garnets that are dispersed along the foliation define a layer that is offset by shear bands (width is 5.1 mm).

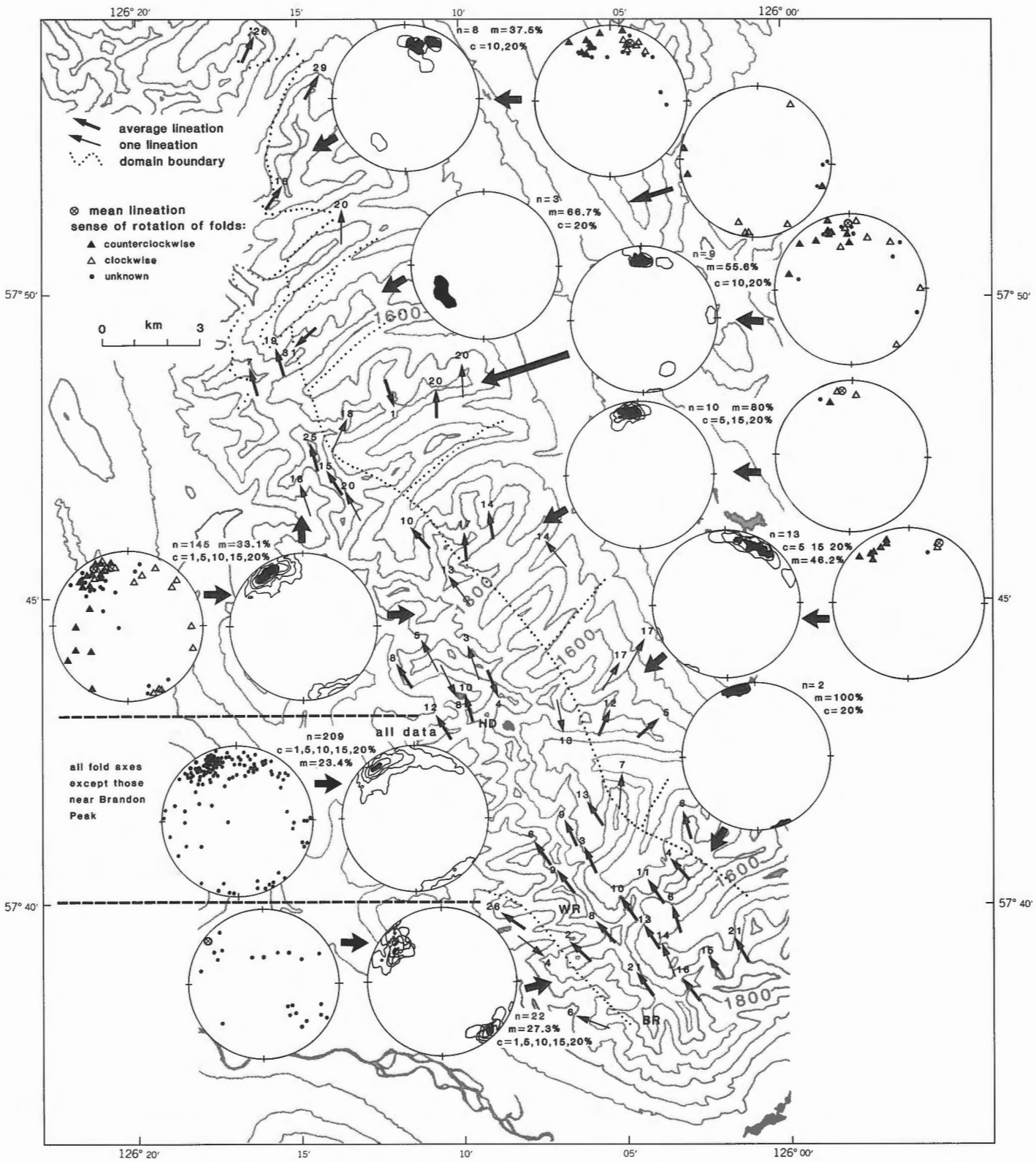

Figure 36. Map of average mineral lineation attitudes, and orientations of fold axes in the hanging wall of the Sifton Fault. The map shows the average attitude of mineral lineations for the surrounding square kilometre. Corresponding contoured stereograms for each domain show lineation data, and the neighbouring stereograms are plots of fold axes for the domains. Stereographic projections are lower hemisphere and equal area. Contours are in % per 1 % area. FX, Fox Peak; HD, Hedges Peak; WR, Warner Peak; BR, Brandon Peak.

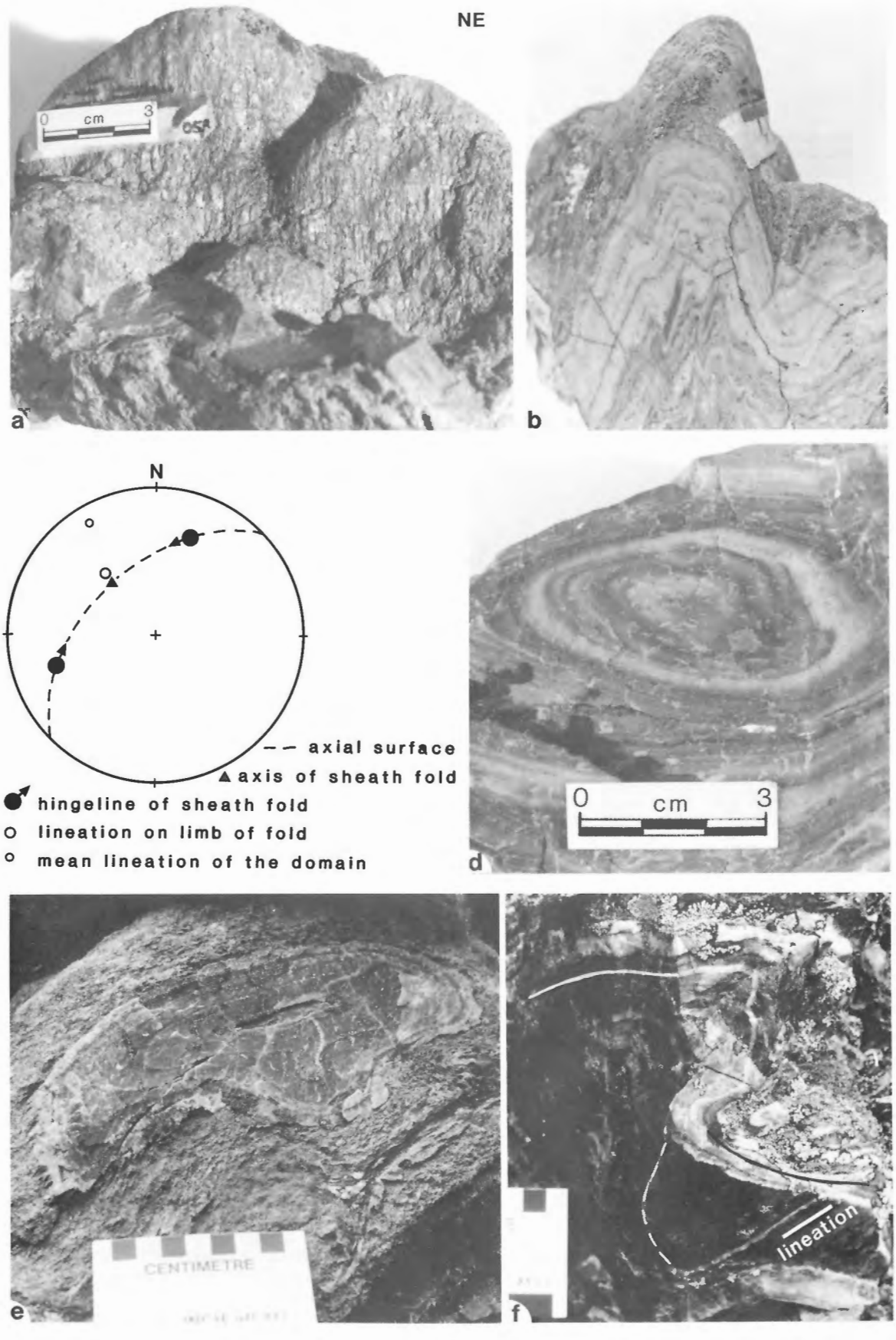
NE
0 cm 3
a
b
N
axial surface
axis of sheath fold
hingeline of sheath fold
lineation on limb of fold
mean lineation of the domain
0 cm 3
d
CENTIMETRE
e
lineation
f

Fold geometry in the hanging wall of the Sifton Fault can be studied at two scales of observation. The oriented mesoscopic sheath fold in Figure 37a,b,c has fold axes dispersed through an angle of 110° within the axial surface. The stretching lineation is measured on the limb of an early stage sheath fold that is not isoclinal, and hence it is not exactly parallel with the axis of the sheath. The lineation is oblique to the hinge line that folds it, and the asymmetry of the fold indicates that the hanging wall moved southerly. In Figure 37d,e, compositional layering defines concentric ovals that are the cross-section of a sheath fold. The stretching lineation in this sample is parallel with the axis of the fold and both are indicators of the slip line. It is clear from these examples and from Figure 37f that the formation of sheath folds results in dispersion of fold axes into a great circle that is parallel with the foliation and axial surface. Folds of opposing vergence (viewed down-plunge) occupy two mutually exclusive segments of the great circle that are separated by the slip line, as described by Hansen (1967). The sense of displacement is determined from the sense of rotation of the folds.

A limitation of the Hansen analysis is that the method of plotting fold axes requires that a set of folds must always be viewed in the same direction, a condition that is met only in dip-slip faults by the convention of viewing down-plunge. When folds in strike-slip faults are viewed down-plunge, all have the same sense of rotation, and hence no separation angle can be identified by the method of plotting folds as described by Hansen. A problem arises in oblique-slip faults where a separation angle can be found, but it need not be parallel with the slip line because the convention of viewing down-plunge violates the rule of viewing the fold set in the same direction. The consequence is that the method of plotting data as described by Hansen cannot be used to determine the slip line. However, the same **principle** can be applied to strike-slip or oblique-slip faults by using an alternative method of plotting the sense of rotation of folds. If the slip line can be determined independently, the Hansen method can be applied to dip-slip faults to derive the sense of displacement. The slip line may be identified by the axis of sheath folds, by lineations that are inferred to be kinematically related to the fault, or by markers offset by the fault.

Figure 37. Sheath folds in the hanging wall of the Sifton Fault. a) Sheath fold viewed parallel to the plane of the axial surface to show the curvature of the hinge line, note strong lineation that is parallel with the axis of the sheath (GSC 204483-O). b) View along hinge line of the fold in Figure 37a)(GSC 204483-P). c) Lower hemisphere stereographic projection of measured features of the oriented fold in Figure 46a), b. d), e) View northerly to cross-sections of sheath folds (also parallel with mineral lineation) (GSC 204483-Q,R). f) View NNE to sheath fold showing the approximate coincidence of foliation (compositional layering), axial surface of sheath fold, and the plane that contains the hinge line; the white dashed line is the hinge line, and the solid lines show a layer that outlines the fold geometry. (GSC 204483-S)

Cylindrical fold axes in large domains of the study area are dispersed into great circles (Fig. 36). The cylindrical folds may, but need not be the limbs of large-scale sheath folds; only those folds that nucleate perpendicular to the slip line will become sheath folds. In the central domain, the great circle of mesoscopically cylindrical folds dips gently north-northwest, approximately parallel with the foliation, and in the east domains the poorly defined great circles are also close to the foliation (Fig. 34,36). Within each of the domains, the great circle can be divided into two well-defined segments of clockwise and counterclockwise sense of rotation (looking down-plunge). The axes of sheath folds and the strong concentration of lineations in each domain determine tightly constrained slip lines. The coincidence of these fabrics with the separation point determined from the sense of rotation of cylindrical folds confirms that the method of plotting folds as described by Hansen is valid for determining the sense of displacement on the Sifton Fault. The sheath folds, lineations, and sense of rotation of folds collectively indicate southerly displacement of the hanging wall relative to the footwall. The orientation of axial surfaces of cylindrical folds are shown in Figure 38.

West of Fox Lake, a macroscopic fold of marble has a north-plunging fold axis and clockwise sense of rotation (Fig. 39a,b,c). This large-scale fold is consistent with smaller scale folds in its domain, where folds plunging more northerly than about azimuth 330° have clockwise sense of rotation. Other macroscopic folds are exposed in the hanging wall (Fig. 39d,e), but in few cases is it possible to determine both the fold axis and sense of rotation.

The slip line and sense of rotation of the folds at mesoscopic and macroscopic scales indicate south-southeast displacement of the hanging wall over the footwall for much of the area, with more southerly displacement indicated for the east domains.

Map pattern

The distribution of map units indicates that they dip northeast on the east flank of the range, and dip gently in the central region. East of Hedges Peak, an antiform of Tochieka Gneiss and the overlying metaquartzite is well defined. The units appear to be gently dipping sheets parallel with the foliation (Fig. 7), but their geometry is complicated by two relationships. The first is that the metaquartzite unit overlies gneiss in the south, and overlies the schist/marble unit in the north. This geometry may be the result of either folding or faulting of the formations described earlier (*see* Stratigraphy). Because the folds are noncylindrical they cannot be used to determine large-scale geometry by down-plunge projection. Lenticular and sheet-like bodies are seen in outcrop, and because it is likely that if a large-scale fold formed in the shear zone the limbs would be faulted, a faulting model is preferred. The possibility of associated folding is not ruled out. Figure 7c portrays a contraction fault separating the Tochieka Gneiss and unit HIqa from the underlying schist/marble unit.

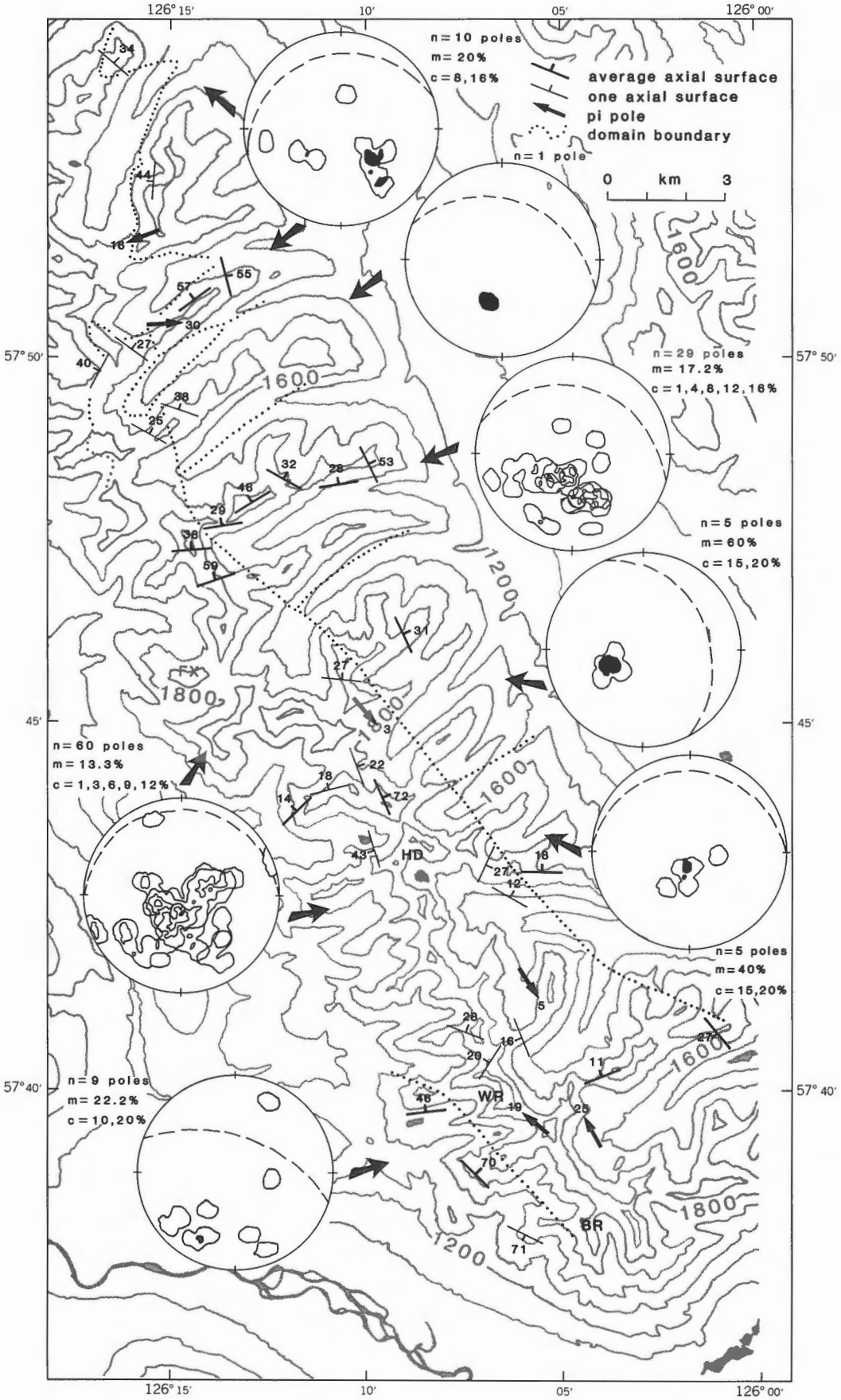

Figure 38. Map of average axial surface attitudes in the hanging wall of the Sifton Fault. The map shows the average attitude (or pi pole) of axial surfaces for the surrounding square kilometre. Stereographic projections are lower hemisphere and equal area. Contours are in % per 1 % area. FX, Fox Peak; HD, Hedges Peak; WR, Warner Peak; BR, Brandon Peak.

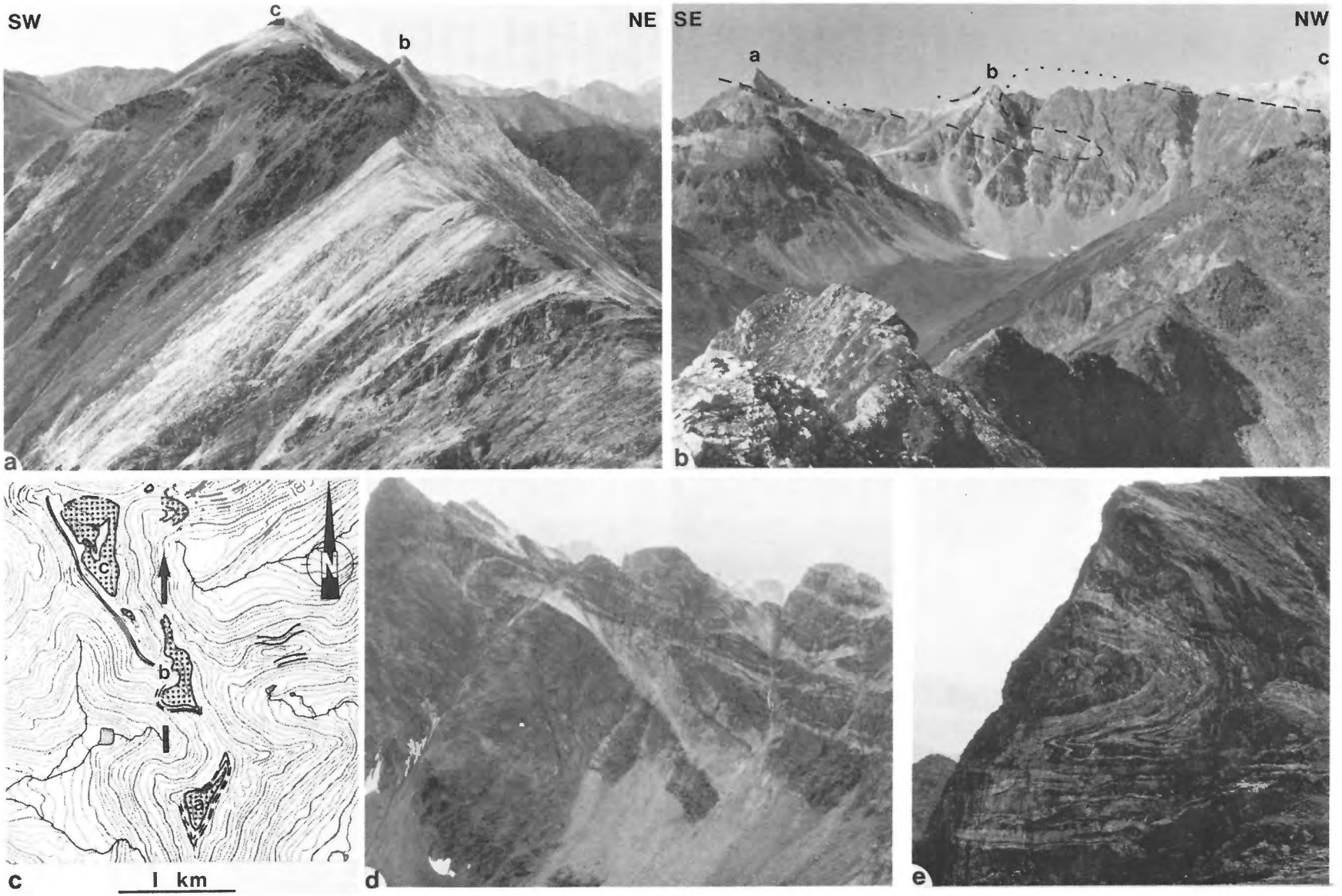

Figure 39. Macroscopic folds in the hanging wall of the Sifton Fault. a) View NNW (down-plunge) along the ridge shown in Figure 39b. The folded marble layer has clockwise sense of rotation (GSC 204483-T). b) View WSW of the same fold showing the closure and northerly plunge of the fold (GSC 204483). c) Map of the same marble layer (patterned) in Figure 39 a and b showing the northerly trend of the fold. d) View south to folded marble 1 km SSE of Hedges Peak (GSC 204483-V). e) View SSE to folded metaquartzite and amphibolite 2 km SSE of Hedges Peak. The height of the cliff exposure is about 50 m. (GSC 204483-W)

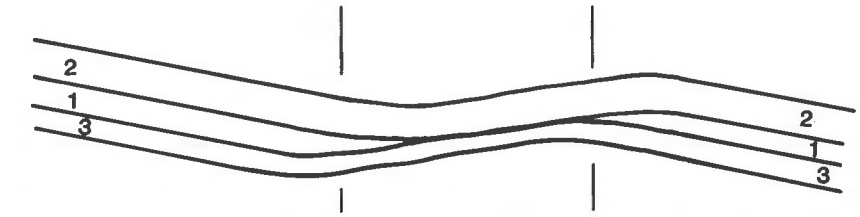

a

b

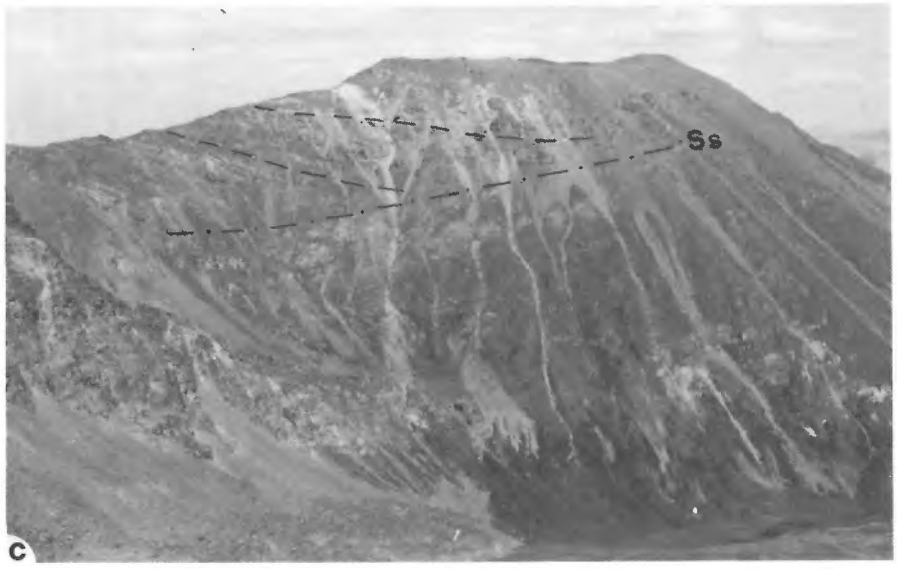

c

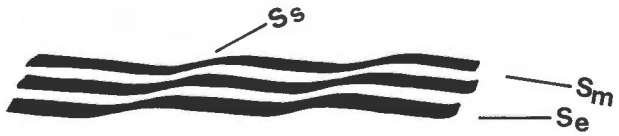

d

Figure 40. Macroscopic "shear bands" in the hanging wall of the Sifton Fault. All figures are viewed to the west and indicate top-to-the-south (left) displacement. a) Schematic diagram (cross-section) to show how the hanging wall may be a macroscopic "shear band" (the area between the vertical lines corresponds to the hanging wall; numbers refer to map units on Fig. 7c,d). b) View SW to mesoscopic "shear band" of metaquartzite and amphibolite in unit Hlqa, 3.5 km east of Hedges Peak. (GSC 204483-X) c) View west to macroscopic "shear band" geometry 3 km east of "Kechika Peak". The print was exposed backwards so as to be looking in the same direction as a,b,and d. The plateau at the bottom of the photograph is the Sifton Fault (GSC 204483-Y). d) Illustration of how shear bands (Ss) result in the discordance between the enveloping surface of a foliation (Se) and the foliation away from the shear bands (Sm).

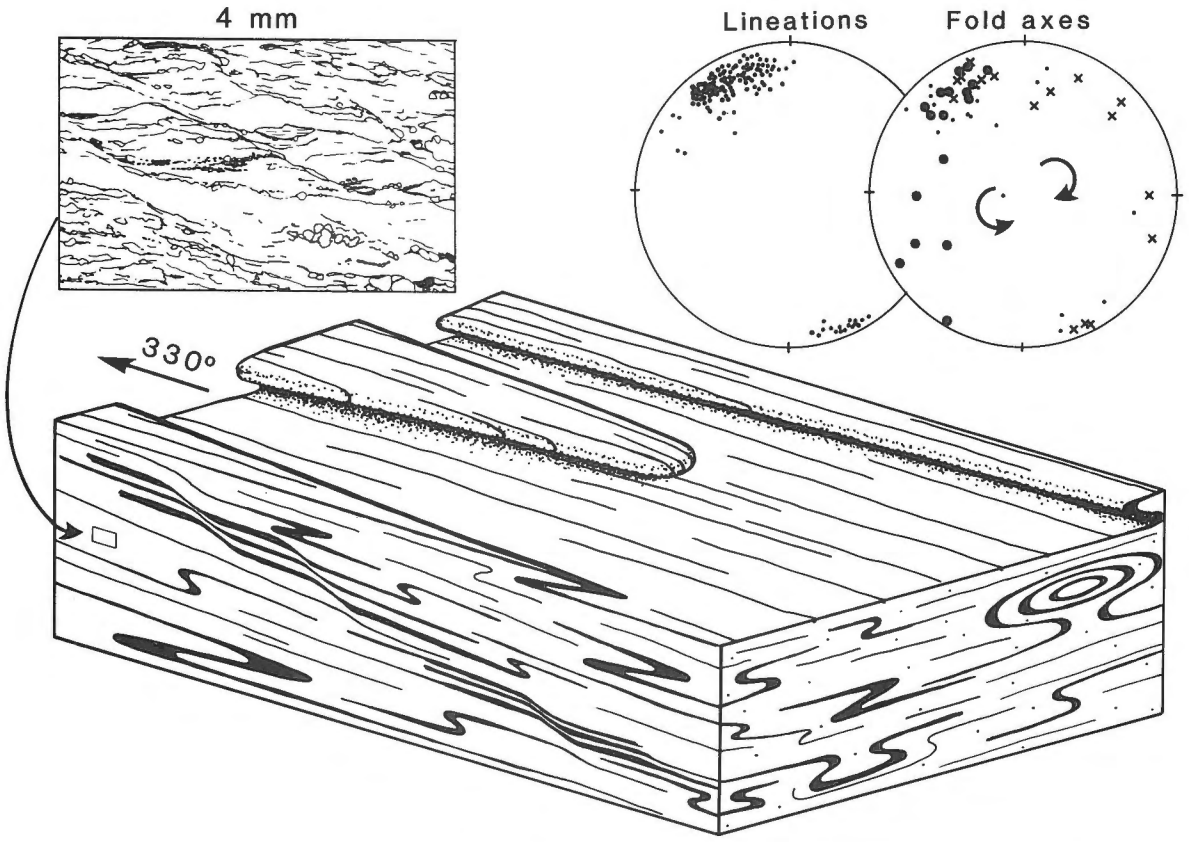

Figure 41. Kinematic indicators in the hanging wall of the Sifton Fault. A strong lineation plunges consistently NNW. Shear bands at microscopic and mesoscopic scales are on the surface parallel with the lineation and perpendicular to the foliation, and indicate top-to-the-SSE displacement. Mesoscopic sheath folds have axes parallel with the lineation and appear as "eyes" on the surface perpendicular to the lineation; their sense of rotation indicates top-to-the-SSE displacement. Cylindrical folds are dispersed (at map-scale) into a great circle parallel with the foliation, and the point separating folds with opposing senses of rotation is parallel with the mean lineation. The sense of rotation of the folds indicates top-to-the-SSE displacement.

The second complication is that the foliation is mesoscopically parallel with the compositional layering and with contacts between mappable units, but at map scale the foliation is discordant to the contacts of units, as shown by a longitudinal cross-section (Fig. 7d). The discordance can be explained if the hanging wall of the Sifton Fault is considered to be a map-scale shear band or series of shear bands of any scale (eg. Fig. 40a) with the same sense of displacement as observed in outcrop. Shear bands and shear-band-like geometries have been observed on all scales from microscopic to possibly mountain-side scale (Fig. 35,40b,c), and result in an enveloping surface of foliations that is discordant to the foliation, as depicted in Figure 40d.

Microscopic fabrics

Quartz occurs commonly as equant subgrains and new grains, 30-40 μm diameter, and as ribbons. It has undulose extinction and sutured grain boundaries. In some quartzitic rocks coarse recrystallized quartz has grown over an excellent foliation defined by micas. Feldspar is commonly undeformed, with only rare undulose extinction, core and mantle texture, or pull-aparts. Micas are either sigmoidal bundles of coarse muscovite and biotite, or are very fine grained. Garnet is fractured. Small (50 μm) xenoblastic grains of garnet appear to have broken off of larger fractured garnets and are now dispersed along the foliation (shear plane), or occur as lenses of disaggregated bits of garnet (Fig. 33b,35d).

The dominant microstructure used as a kinematic indicator is the relationship between the mylonitic foliation and shear bands. Excellent examples of shear bands occur in oriented thin sections cut perpendicular to the foliation and parallel with the lineation (Fig. 35). They indicate a sense of shear the same as mesoscopic shear bands: hanging wall to the south-southeast. Rotated augen are rare, and C/S fabrics (Berthe et al., 1979) are absent. Chlorite occurs in pull-aparts of tourmaline and plagioclase, and along the mylonitic foliation and shear bands (Fig. 35c).

Summary of macroscopic geometry and kinematic interpretation

The southeastern half of the Sifton Ranges is a gently-dipping fault zone characterized by a variety of

metamorphic rocks, including ductile fault rocks. The sole fault is referred to as the Sifton Fault, and the overlying fault zone as the hanging wall. The antiform of bedding, foliation and isograds in the footwall is truncated by the fault, and none of the structures characteristic of the fault zone are found in the footwall, although some finely recrystallized quartz occurs locally in schist in the south. No clearly pre-fault structures are present in the hanging wall, and no structures may be related in any way to footwall or Deserters Range structures. Post-fault structures are open folds and crenulations of the mylonitic fabric.

The structures relevent to the kinematic interpretation are summarized in Figure 41. The angular relationship between shear bands and the foliation and the sense of offset on the shear bands suggest that the hanging wall moved southerly over the footwall. Strong lineations are interpreted to be parallel with the slip lines of the Sifton Fault. In each domain they are parallel with the separation angle between two concentrations of fold axes inferred to have formed by the progressive rotation of hinge lines towards the direction of finite elongation. The analysis of folds and lineations results in tightly constrained slip lines which plunge gently to the north-northwest. The sense of rotation of the folds indicates that the hanging wall was displaced south-southeasterly over the footwall, consistent with observations of mesoscopic sheath folds. Analysis of structures at micro — meso — and macro-scopic scales indicates south-southeast displacement of the hanging wall over the footwall.

Summary of metamorphic conditions and timing of faulting

As discussed by Sibson (1977), ductile fabrics indicate at least greenschist facies conditions during faulting. Temperatures of at least 300°C are required for quartz to deform plastically, which, at normal geothermal gradients, corresponds to depths of 10 to 15 km (Sibson, 1977). The mineral assemblages that in part define the mylonitic foliation, lineation, and shear bands are: chlorite-biotite-muscovite in schists; hornblende-quartz-plagioclase in mafic rocks; and tremolite fibres in extension fractures in marble. These assemblages indicate that conditions during faulting were about low amphibolite facies.

The Sifton Fault truncates isograds in the footwall and therefore postdates the peak of metamorphism (mid-Jurassic(?)). It also truncates the Sifton Antiform in the footwall, a structure that is similar in form to anticlines elsewhere in the core zone of the Omineca Belt. The mid-Cretaceous cooling ages in the core of the Swannell Range may date the development of the anticlinoria, and if so, the Sifton Fault may be post mid-Cretaceous. Geochronological data on rocks in the Sifton Ranges are listed in Figure 46. Hanging-wall rocks are cut by undeformed intrusive rocks (granite, lamprophyre dykes, and pegmatite dykes) with K-Ar ages of 38 to 51 Ma (Wanless et al., 1979; J.C. Roddick pers comm., 1985), that limit the timing of the Sifton Fault to pre mid-Eocene. K-Ar ages of micas from metamorphic rocks in the hanging wall and footwall range from 40 to 53 Ma (Wanless et al., 1979; Stevens et al., 1982) and are an indication of pre — or mid-Eocene tectonic and/or thermal activity. K-Ar ages of hornblende from the hanging wall are 58 to 60 Ma and indicate that the hanging wall cooled from a relatively high temperature (about 530°C, *see* Fig. 46) in the Late Paleocene. The young K-Ar ages indicate relatively high temperature for the region following displacement on the Sifton Fault, and are in agreement with the relatively high temperature during displacement that is indicated by the mineral assemblages.

Tectonic significance of the Sifton Fault

The inferred south-southeast displacement of the hanging wall of the Sifton Fault leads to the following questions pertinent to the tectonic evolution of the region. 1) Is the Sifton Fault a contraction fault, or is it an extension fault similar to low-angle detachments recognized in the southern Cordillera in recent years 2) Is the displacement on the Sifton Fault compatible with what is already known about the tectonic evolution of the region 3) Can the Sifton Fault shed some light on poorly understood aspects of the regional geology?

Extension or contraction fault?

The Sifton Fault in its present orientation is a normal fault in the sense that displacement is obliquely down-dip. However, it may be either an extension fault or a contraction fault that has been rotated so as to reverse its dip direction. The presence of 1) basement gneiss in the hanging wall, and 2) mylonite in the hanging wall over a footwall unaffected by faulting, indicate that deeper-seated (and more ductile) rocks were displaced over higher ones. Accordingly, the Sifton Fault is inferred to be a thrust fault that has since been tilted southwards so as to have "normal" displacement. The most recent pre-fault indication of structural level is given by the metamorphic mineral assemblages. These were shown earlier (*see* Metamorphisme) to be not significantly different; both the footwall and the hanging wall are in bathozone 5 (Carmichael, 1978). The geothermobarometric investigation, although it should be capable of resolving pressure differences of the order of a kilobar within a single bathozone, indicates only that the two domains were within a few kilometres of the same structural level during equilibration and does not resolve their relative vertical displacement. The similar metamorphic grade may be explained by either a late southward tilt that may have lowered the hanging wall by the same amount that it was raised by thrusting (both relative to the footwall), or by extension (shear band-like) faults associated with late displacement on the Sifton Fault.

The SSE contraction postulated for the Sifton Fault is compatible with the other structural features of the region. The swarm of major NNW-striking dextral transcurrent faults, a dominant feature of the northern Omineca Belt, is kinematically consistent with shortening in a southerly direction. North of Kechika Fault, a series of en echelon folds with easterly axial surface traces provides local evidence for southerly compression associated with the dextral transcurrent displacement (Gabrielse, 1985). No

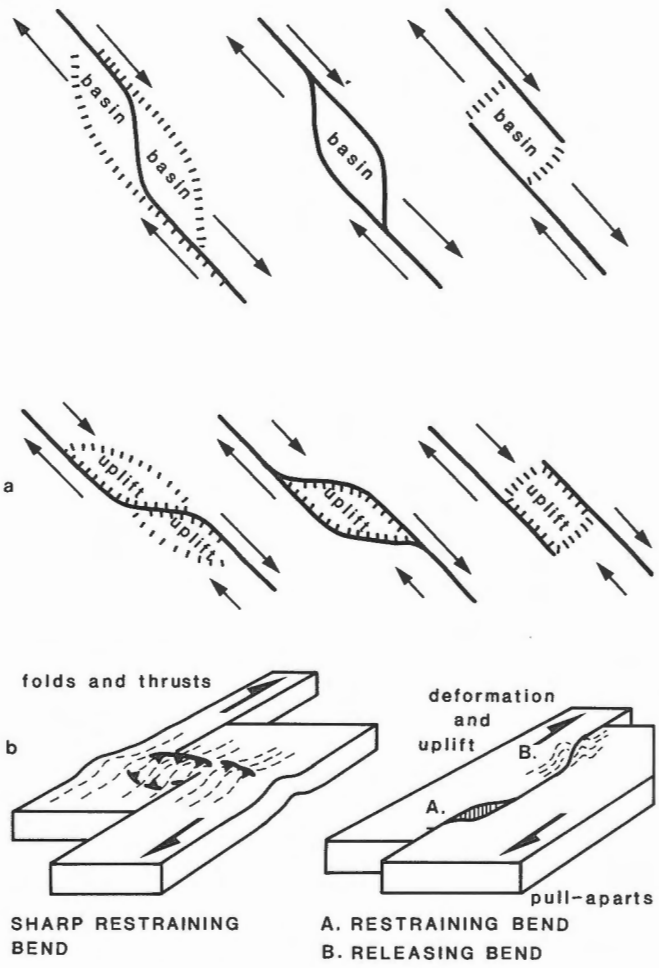

Figure 42. Structures associated with bends in transcurrent faults. a) Basins and uplifts formed by tension and compression respectively along strike slip fault zones (modified after Dibblee, 1977). b) Block diagrams showing deformation at "restraining bends" (modified after Crowell, 1974b).

local or regional structures that may be related to the alternative interpretion of south-southeast extension have been observed in the Cassiar or Omineca mountains. The following section will show that a model of south-southeast thrusting can explain several regional features and is entirely consistent with the known tectonics for Cretaceous and Eocene times.

A model relating the Sifton Fault to dextral transcurrent faults

Several relationships unique to the region may be used to develop a conceptual model for south-southeast contraction on the Sifton Fault: 1) the slip lines for most of the area are parallel with the Northern Rocky Mountain Trench; 2) the Sifton Ranges lie immediately south-southeast of a left-stepping bend in the Kechika Fault, a dextral transcurrent fault which splays from the Northern Rocky Mountain Trench near the junction of the Sifton Fault and the trench; 3) the Sifton Fault must be rooted to the north if it is a contraction fault; 4) the Sifton Fault probably moved at about the same time as the Kechika Fault (timing of Kechika Fault from Gabrielse, 1985). These relationships suggest that the Sifton Fault may be related to transcurrent faulting, and in particular, to the Kechika Fault.

Compression associated with transcurrent faults may be caused by simple parallel wrenching (Wilcox et al., 1973; Harding, 1973,1974), oblique convergence (transpression, Harland, 1971; Lowell, 1972; Wilcox et al., 1973; Sylvester and Smith, 1976), or by bends in simple parallel faults (Crowell, 1974a,b; Dibblee, 1977; Rodgers, 1980; Aydin and Page, 1984). Bends in transcurrent faults, or linkage between en echelon faults, result in oblique divergence or convergence on the joining segment, depending on the direction of the bend relative to the sense of displacement on the transcurrent fault (Fig. 42). These situations are commonly analyzed with reference to the strain ellipse and the simple shear model. The majority of the literature deals with extensional zones and the basins resulting from bends (eg. Crowell, 1974a,b; Rodgers, 1980). Convergence zones have recieved far less attention and existing discussions of them are inadequate because: 1) they are commonly referred to simply as zones of convergence or uplift and the mechanism is not considered (eg. Fig. 42a); 2) there has been little or no description of detailed structures found or to be expected in the zones; 3) the sense of displacement is commonly shown or inferred to be in a direction oblique to the transcurrent fault zone (a concept inherited from the simple shear model); 4) in attempts to show the geometry of the convergent zones in three dimensions, the displacement on transcurrent faults shown by the ends of block diagrams cannot be balanced with the shortening that must occur in the zones that join the transcurrent faults (Fig. 42b). The following model addresses these problems.

Figure 43a is a conceptual model of a fault surface which permits the amount of shortening across a bend in a transcurrent fault to balance with the amount of displacement on the transcurrent fault. The result is a thrust fault curving into an oblique strike-slip fault with a reverse component, which joins two segments of a transcurrent fault. The direction of the slip line on the thrust segment is parallel with the transcurrent faults, a geometrical requirement if they are one fault surface. The surface trace to be expected is shown by the top of the model in Figure 43a. The magnitude of displacement on the fault is the length of the thrust segment measured parallel with the slip line. In this model, the Sifton Fault is the gently dipping thrust segment that joins two transcurrent segments; the Kechika Fault and Northern Rocky Mountain Trench. As in the model, slip lines in the hanging wall are parallel with the faults in the Northern Rocky Mountain Trench. The extent of exposure of hanging wall rocks is shown in Fig. 43.

A Californian analogy

In a recent paper dealing with transcurrent faults in California, Aydin and Page (1984) have applied the simple shear model to the San Andreas and related faults, in an attempt to explain the structures in the San Francisco Bay area (Fig. 44). They give an explanation for faults and

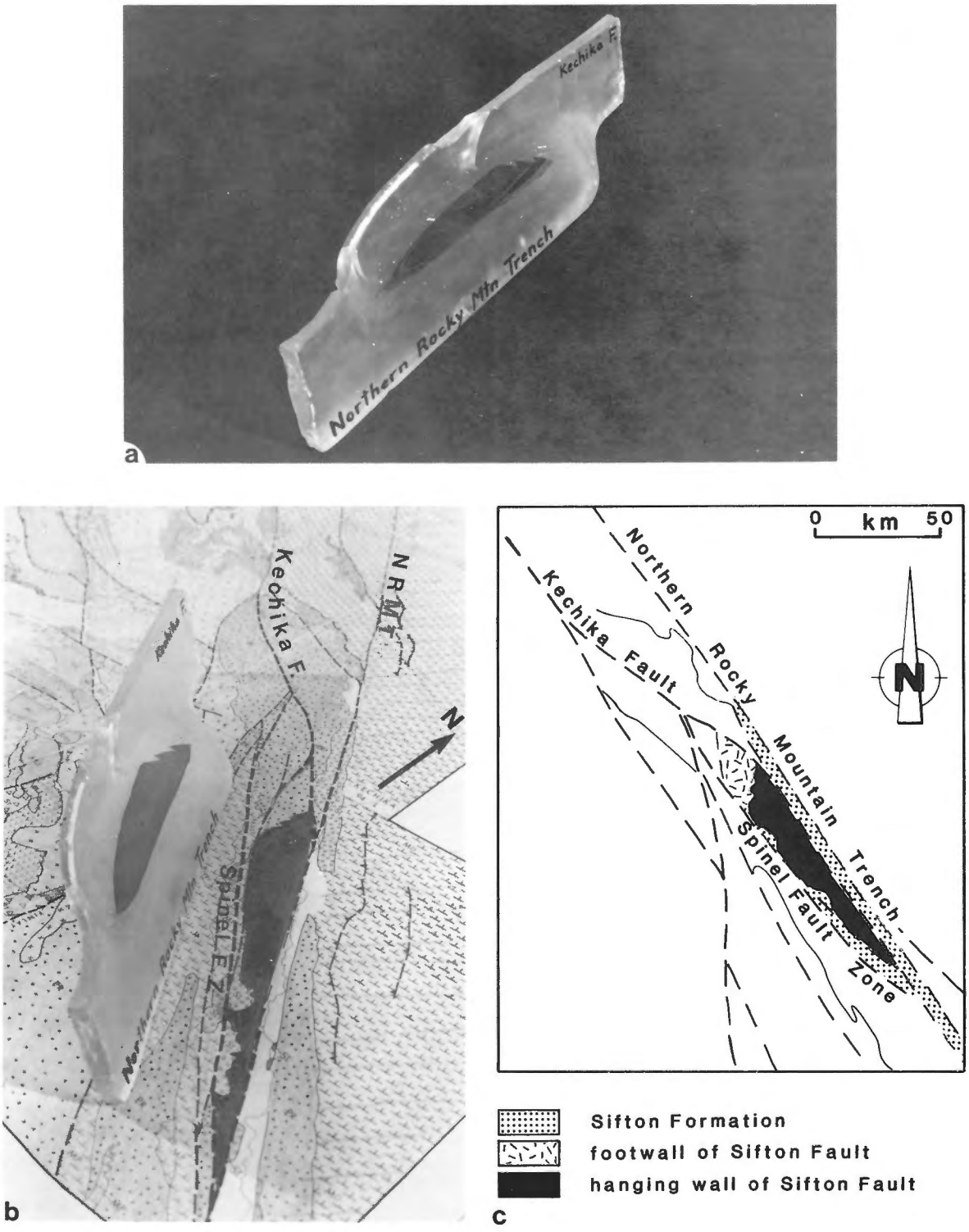

Figure 43. Conceptual model of the Sifton Fault surface. a) The model shows a gently dipping fault (the Sifton Fault) that joins two segments of a transcurrent fault so that the Sifton Fault, the Kechika Fault, and faults in the Northern Rocky Mountain Trench are one fault surface with the same direction and amount of displacement. The top of the model is the hypothetical surface trace prior to erosion. b),c) Map of the regional geology (H. Gabrielse, unpublished map), showing the relationship of features on the model to those on the ground. The dark area on the model is the present extent of hanging wall rock, and the area to the NW of it is now eroded so that the footwall is exposed. The Sifton Formation occurs in valleys SW and NE of the Sifton Ranges.

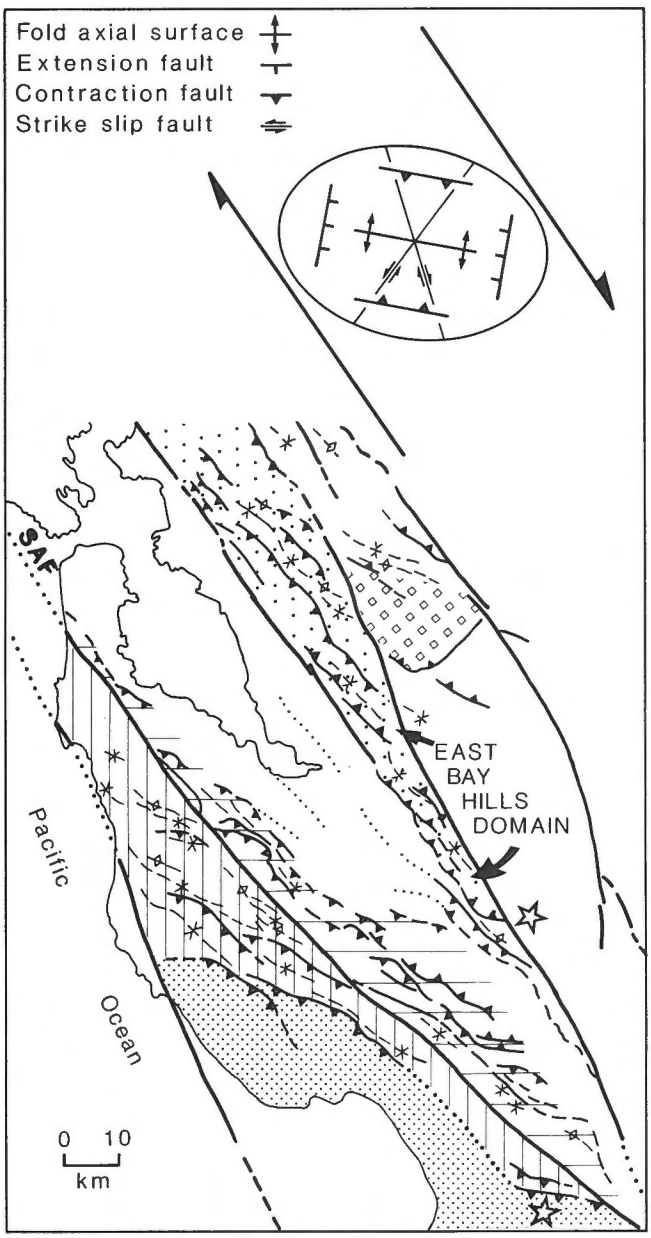

Figure 44. Structural features in the San Francisco Bay area (modified after Aydin and Page, 1984). The map was compiled by Aydin and Page to show the relationship of structures to the San Andreas (SAF) and related faults. The strain ellipse is modified after Harding, 1974.

folds oriented in the shortening direction (easterly traces, near stars in Fig. 44), but conclude that their analysis has no explanation for the thrusts and oblique thrusts that are subparallel with the major transcurrent faults (eg. the SW boundary of the East Bay Hills domain). The model in Figure 43a predicts the pattern of fault traces exposed in the San Francisco Bay area; thrust faults with easterly traces curve into large segments of oblique thrusts that are parallel with the transcurrent faults and eventually become transcurrent faults. According to the model, the segment of oblique thrust may be a measure of the extent of a gently dipping fault at depth. The fact that the type of surface trace predicted by the Sifton model has developed in association with such a well-studied, currently active wrench-fault system is evidence in support of the model, but independent evidence for oblique slip in the California thrust faults has not been documented.

The simple shear model as applied by Aydin and Page (1984) predicts displacement on a thrust fault in a direction oblique (south) to the transcurrent fault (southeast). Because the direction of displacement between two rigid rock masses is constant, regardless of the orientation of the fault, any displacement on the thrust fault must be in a direction parallel with the displacement on the transcurrent fault. In the Sifton model, the fault may initiate in the direction predicted by the simple-shear model (Ramsay, 1967,1980) and as shown by clay model experiments (Wilcox et al., 1973). However, once the thrust fault is established, the domain between the transcurrent faults need no longer be a region of simple shear, and further displacement is governed by (and therefore parallel with) the displacement on the bounding faults. If the domain between the transcurrent faults remains a region of simple shear, then folds and faults that initiate at 45° to the bounding faults will rotate towards parallelism with the bounding faults within a region of steeply dipping structures. This is clearly not the case for the Sifton Fault because all structures are gently dipping and the footwall is (internally) unaffected by transcurrent fault displacement.

Flower structures

The Sifton model differs markedly from "flower structures" (also called "palm-tree structures") that have been described in recent fault zones (Lowell, 1972; Sylvester and Smith, 1976; Harding and Lowell, 1979). Flower structures are sets of high-level oblique thrust faults which splay upwards and outwards from transcurrent faults at depth. They accommodate upward displacement, essentially extrusion of material up and out of the fault zone, which allows oblique convergence at depth. Such structures obviously can develop only at high structural levels; application of this concept to deep-level fault zones (eg. Lund, 1984) would result in severe geometrical problems of extending the faults to the surface.

Regional implications of the Sifton Fault model

If the Sifton Fault is a contraction fault, an easterly-trending fault trace with major stratigraphic throw should outcrop somewhere to the south, and hanging wall strata should be found in a north-dipping panel somewhere to the north. The Sifton Ranges are entirely fault-bounded within a system of faults of poorly understood timing and displacement. Some of the faults have substantial dip-slip as well as strike-slip displacement, so it is not a simple matter to look either south or north for extensions of the Sifton Fault, which may by now be far removed laterally, totally eroded, or still deeply buried. The rocks to the north are low grade and part of the Windermere Supergroup (Gabrielse, 1962a; pers. comm., 1984). Greater uplift of the Sifton Ranges with respect to the area north of the Kechika Fault inhibits attempts to correlate strata from the hanging wall to north of the Kechika Fault.

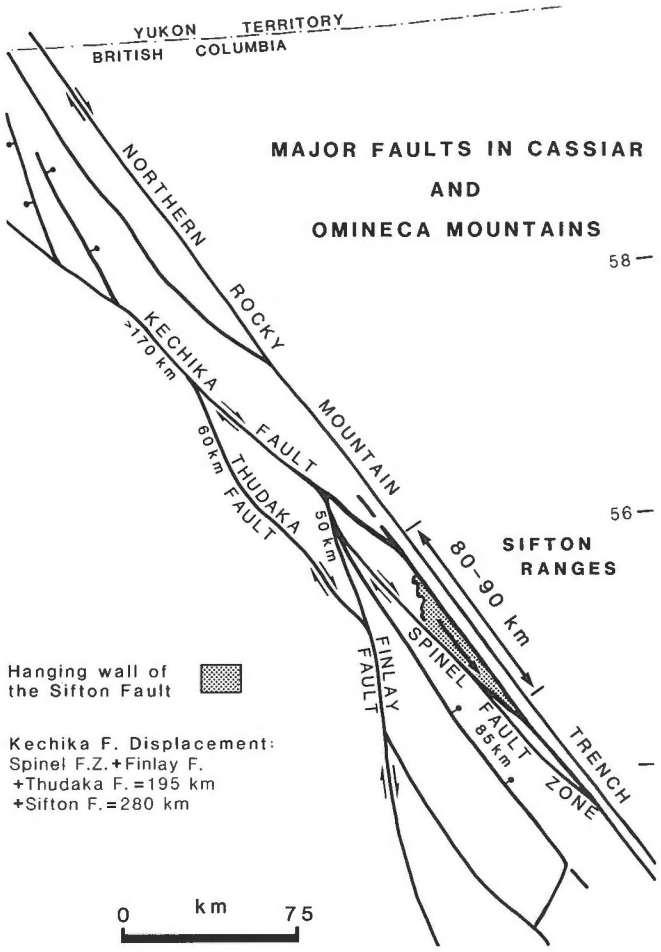

Figure 45. Displacement on major faults in the Cassiar and Omineca mountains. The map shows the magnitude of displacement on faults related to the Sifton Ranges (modified after Gabrielse, 1985).

According to the model, the distance measured along the slip lines from the Kechika Fault to the southernmost exposures of hanging-wall rocks is the minimum displacement on the Sifton Fault. The regional mapping of Gabrielse et al. (1977a) determined that the Cormier Range (the region of the Sifton Ranges south of Fox Pass) consists of rock types similar to those of the hanging wall. Similar structures were observed in the central Cormier Range during a brief visit as part of this study. The amount of overlap of hanging wall on footwall measured along the slip line and including the Cormier Range is 80 to 90 km (Fig. 45).

Displacement on the Sifton Fault of 80 to 90 km in a south-southeast direction places constraints on the regional analysis of offsets on the transcurrent faults. However, depending on the timing and interaction of the Sifton Fault with other faults, at least three interpretations may be tenable.

1) In a recent synthesis of the dextral transcurrent faults in the northern Cordillera, Gabrielse (1985) estimated the displacement on the Spinel Fault Zone to be 85 km (late Eocene to Oligocene), on the basis of offset conglomerate; and the displacement on the Kechika Fault to be more than 170 km (mid-Cretaceous to Oligocene) on the basis of offset structural style. Displacement on the Spinel Fault Zone (85 km) must have occurred also on that part of the Kechika Fault northwest of their junction (Fig. 45). This leaves 85 km of Kechika Fault displacement for the segment between Spinel Fault and the trench, which in the model becomes the Sifton Fault (*see* Fig. 43a). This is compatible with the magnitude of minimum displacement on the Sifton Fault determined from overlap, and with the timing postulated by Gabrielse (1985).

2) If similar arguments are used for determining displacement on the Kechika Fault, by summing the displacement on all faults which splay from it, then the displacement on the Kechika Fault is 195 km before the Sifton Fault is considered (Fig. 45). If 85 km of displacement for the Sifton Fault is added, a minimum displacement of 280 km is obtained for the Kechika Fault; a better estimate of the minimum displacement than the 170 km determined by Gabrielse (1985) from the offset of structural markers on the fault.

3) The Spinel Fault Zone may represent the oblique-strike-slip segment of the model. In this case the displacement on the Spinel Fault Zone should equal that on the Sifton Fault, because it is part of the same fault surface (Fig. 43a). The minimum displacement of 80 to 90 km for the Sifton Fault is compatible with the 85 km of displacement on the Spinel Fault Zone. This model requires the Sifton Fault and Spinel Fault Zone to be contemporaneous. Undeformed Eocene granite in Sifton Ranges limits the Sifton Fault to mid-Eocene or older, and the Spinel Fault Zone offsets Eocene sediments which limit the age of strike-slip displacement on it to Late Eocene or Oligocene (Gabrielse, 1985). The timing relationships indicate that this interpretation is untenable only if there was no displacement on the Spinel Fault Zone prior to the Late Eocene; the amount (if any) of pre — Late Eocene displacement is unknown. The geometrical consequence of the Sifton and Spinel faults being one surface is that the part of the Spinel Fault Zone that is north of where it diverges from the Sifton Fault either has no displacement, or it is a fault not related to the Sifton-Spinel fault. Structures in that region of the Spinel Fault Zone have not been examined.

"Metamorphic core complexes"

Cordilleran metamorphic core complexes of the western United States and Canada are culminations of metamorphic rocks with gently-dipping foliation, a well developed lineation, and Cenozoic K-Ar dates on metasedimentary rocks. They are associated with low-angle faults in which brittle structures are overprinted on ductile ones, and they are inferred to be largely a result of crustal extension (reviewed by Coney, 1980; and Armstrong, 1982). The geology of the Sifton Ranges differs markedly from those areas in the following ways: 1) the absence of brittle structures; 2) a lack of significant change in metamorphic grade across the fault; 3) the lineations and inferred displacement direction are parallel with the length of the range rather than across its width, as would be expected in simple crustal extension, and as is observed in "metamorphic core complexes"; 4) the Sifton Fault is inferred to be a contraction fault.

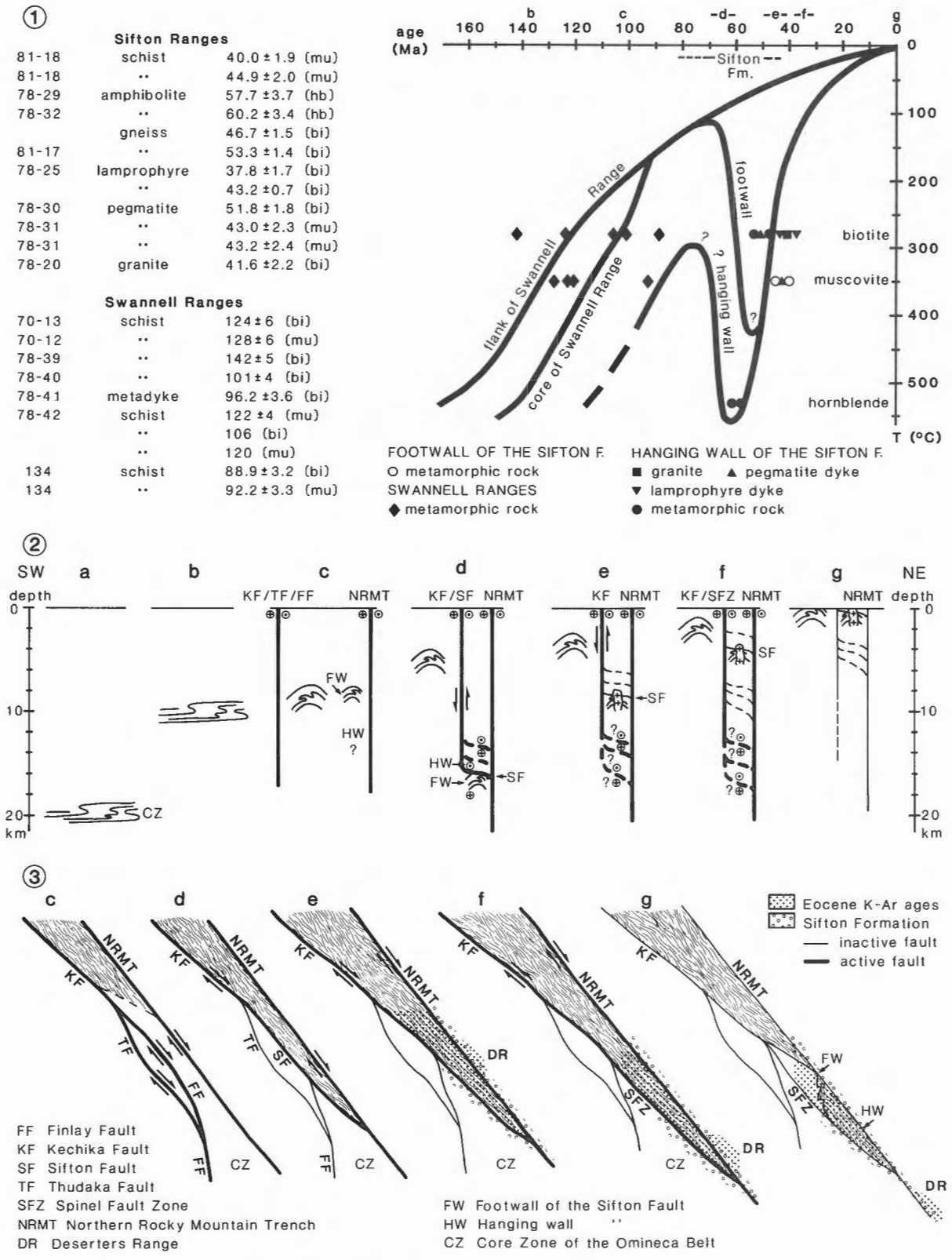

Figure 46. Geochronological data and structural and thermal history for the Sifton Ranges. 46-1) The time/temperature curves are obtained by plotting the K-Ar ages of rocks against their blocking temperatures. Ages are from Wanless et al., 1971,1979; Parrish, 1976,1979 (sample 134 and unpublished GSC data for the Swannell Ranges); Stevens et al., 1982. Blocking temperatures are from Harrison and McDougall, 1980,1982. 46-2) The blocking temperatures for all data are converted to kilometres of depth to show the structural level of the different geological elements for the times that the data represent (indicated by lower case letters in Fig. 46-1,2,3). 46-3) The corresponding map view for each of those times.

Summary of the structural and thermal history of the Sifton Ranges

Geochronological data may be used to constrain the timing of structural events in the Sifton Ranges, which will facilitate a more comprehensive regional structural synthesis. K-Ar data for the Sifton and Swannell ranges are displayed on a time/temperature plot that depicts the time when hornblende, muscovite, and biotite cooled through their blocking temperatures (Fig. 46-1). The blocking temperatures are converted to kilometres of depth in Figure 46-2 by assuming a geothermal gradient of 35°C/km. In this way the approximate depth of the rocks (presently exposed) can be shown on a cross section for a particular time. The maps below the sections (Fig. 46-3) illustrate which of the transcurrent faults were active during those times.

Mid-Mesozoic crustal thickening associated with recumbent isoclinal folding, at the relatively high pressure indicated by the metamorphic studies, is shown in Figure 46-2a. In the Swannell Ranges, the core zone of the Omineca Belt cooled through the blocking temperatures of muscovite and biotite beginning at 140 Ma (Fig. 46-1,2b), and subsequent relative uplift in the cores of anticlinoria resulted in ages of around 100 Ma (Fig. 46-1,2c, Wanless et al., 1971,1979; Parrish, 1976,1979). The footwall of the Sifton Fault has a similar structural style and roughly similar grade of metamorphism to that of the core zone of the Omineca Belt, and accordingly it is assumed to have had a similar mid-Mesozoic history. Mid-Mesozoic deformation in rocks that became the hanging wall of the Sifton Fault is poorly known because the structures (if any) were obliterated during faulting. The grade of metamorphism is roughly the same as for the footwall, and because the fault is interpreted to be a contraction fault, the hanging wall is assumed to have been at a greater depth than the footwall (Fig. 46-2c). In the mid Mesozoic, however, it would have been farther to the northwest. Displacement on the Kechika Fault prior to the Late Cretaceous was accommodated by the Thudaka and Finlay faults (Fig. 46-2c,3c, Gabrielse, 1985).

In the Late Cretaceous, transcurrent displacement on the Kechika Fault transferred to faults in the Northern Rocky Mountain Trench, and the Sifton Fault developed as a result of the local transpression (Fig. 46-2d,3d). Overlap and loading of the hanging wall on footwall, and perhaps similar transpressional structures at a higher level, resulted in burial and heating of the hanging wall to above the blocking temperature of hornblende, and of the footwall to at least above the blocking temperature of muscovite. Subsequent rapid uplift, perhaps aided by transpressional structures at depth, resulted in cooling and resetting of the K-Ar ages in mid-Eocene time (Fig. 46-1,2e,3e; Wanless et al., 1979; Stevens et al., 1982). The pre-Eocene path of the hanging wall (Fig. 46-1) is speculative. Geobarometry suggests that the throw on the Sifton Fault is less than about 5 km, so a path is choosen that mimics the footwall, but at greater depth. This interpretation requires less throw on the Sifton Fault than if the Eocene K-Ar dates in the hanging wall are a result of the first cooling through the blocking temperature of hornblende since the peak of mid-Mesozoic metamorphism. The undeformed Balourdet Pluton intrudes the hanging wall of the Sifton Fault in the southern Sifton Ranges. It has an Eocene K-Ar age which indicates that displacement on the Sifton Fault had ceased by about 40 Ma (Fig. 46-1,2e). Intrusion of the granitic body may also have been related to the early Tertiary tectonic activity. The relatively high grade mineral assemblages and the ductile fabrics in the mylonites attest to the high temperature during faulting. Uplift restricted to the area of overlap may have contributed to the abrupt increase in metamorphic grade across the Kechika Fault (Fig. 21), and to the exceptional thickness of the Late Cretaceous to Eocene coarse clastic sediments (Sifton Formation) in areas surrounding the Sifton Ranges (Fig. 3, 43b, 46-3e). Late Eocene to Oligocene displacement on the Kechika Fault (Gabrielse, 1985) was accommodated by the Spinel Fault Zone, which at depth may have joined faults in the trench in a way similar to the Sifton Fault, and resulted in further uplift of the Sifton Ranges (46-2f,3f). Continued dextral displacement on faults in the Northern Rocky Mountain Trench displaced the Deserters Range (also with Eocene K-Ar ages) from the east side of the Sifton Ranges to its present location 125 km to the southeast (Fig. 46-3g; Gabrielse, 1985).

CONCLUSIONS

Complexly deformed greenschist and amphibolite facies metasediments in the Deserters and Sifton ranges are assigned to the Upper Proterozoic Windermere Supergroup. Precambrian basement gneiss, dated by U-Pb zircon geochronology, occurs in both areas. An age of 1.85 Ga for orthogneiss basement in the Sifton Ranges indicates that Middle and possibly some Upper Proterozoic rocks were removed by uplift and erosion in pre-and early-Windermere time. Detrital zircons with inherited U-Pb ages of about 2 Ga in metasediments of the Yukon Tanana Terrane (Alaska), and in feldspathic grits of the Windermere Supergroup in the Cassiar-Omineca and Cariboo mountains suggest widespread exposure of Early Proterozoic gneiss in the Late Proterozoic; the gneiss may have been a major source for the Windermere Supergroup. Granitic basement (728 Ma) east of the Northern Rocky Mountain Trench, in Deserters Range, is overlain nonconformably by the Windermere Supergroup. In the northern Rocky Mountains, swarms of northerly-trending diabase dykes of probable early Windermere age cut thick pre-Windermere strata and demonstrate Late Proterozoic extension. These data support a model of Late Proterozoic uplift, rifting, sedimentation, and volcanic activity at least locally (in Deserters Range) younger than 728 Ma.

Metamorphism during the mid Mesozoic was at relatively high pressure in both ranges. The pelitic mineral assemblages suggest that the maximum pressures attained were in bathozone 5 or 6 in the Deserters Range, and in bathozone 5 in the Sifton Ranges. Pressure estimates from a geothermobarometric study are between 6 and 8 kb for the Deserters Range, and 5 and 7 kb for the Sifton Ranges. Isograds in the Deserters Range and in the footwall of the Sifton Fault were folded by postmetamorphic inclined and upright folding. The folded isograds in the footwall of the Sifton Fault are truncated by the fault, indicating that the Sifton Fault postdated the peak of metamorphism. Mineral

assemblage and geothermobarometric data indicate that the hanging wall was metamorphosed at about the same depth as the footwall. The tectonic loading associated with the Sifton Fault may have contributed to the net post-metamorphic uplift and may provide an explanation for why some of the highest grade rocks in the northern Omineca Belt are found in the Sifton Ranges.

The study area is characterized by two distinct structural styles, which can be interpreted as indicating approximately orthogonal directions of compression. In Deserters and parts of Sifton ranges, cylindrical folds of compositional layering and penetrative fabric have northwest-trending axes, indicative of the northeasterly shortening that is typical of the Foreland and Omineca belts. In Deserters Range, the folds are open to closed and appear to represent mainly one episode of deformation. In the Sifton Ranges, two episodes of deformation associated with northeast shortening are evident. Tight to isoclinal synmetamorphic F1 folds are refolded by coaxial, open, upright F2 folds. A third episode of deformation in the Sifton Ranges, is indicated by the truncation of the large-scale F2 open anticline by the gently dipping Sifton Fault. The simplest interpretation of the structural style in the hanging wall of the Sifton Fault is that the mylonitic foliation, lineation, sheath folds, and shear bands developed as a result of progressive simple shear in a gently-dipping shear zone that displaced the hanging wall south-southeast relative to the footwall. The displacement is interpreted as south-southeasterly shortening, a direction of compression anomalous to the Omineca Belt. The gently-dipping fault zone can be related geometrically and kinematically to major dextral transcurrent faults which dissect the region. The suggested model involves two segments of a left-stepping transcurrent fault zone that are joined via a gently-dipping thrust fault with displacement in a direction parallel with the transcurrent fault.

The Sifton Fault model satisfies both local and regional geological constraints and has led to a refinement of the estimates of the displacement on the major transcurrent faults in the northern Omineca Belt. It gives an explanation for the distribution of Eocene K-Ar dates and clastic sediments which are almost restricted to this region. In addition, it provides an alternative to the "crustal extension" model of metamorphic core complexes for the development of elongate ranges with gently dipping (and fault-related) foliations. Other high-standing core-zone anticlinoria with Eocene cooling ages such as the Horseranch and Butler ranges should be examined in light of both of these models.

REFERENCES

Albee, A.L. and Ray, L.
1970: Correction factors for electron microanalysis of silicates, oxides, carbonates, phosphates and sulfates; Analytical Chemistry, v.42, p. 1408-1414.

Archibald, D.A., Glover, J.K., Price, R.A., Farrar, E., and Carmichael, D.M.
1983: Geochronology and tectonic implications of magmatism and metamorphism, southern Kootenay Arc and neighbouring regions, southeastern British Columbia. Part 1: Jurassic to mid-Cretaceous; Canadian Journal of Earth Sciences, v.20, p.1891-1913.

Armstrong, R.L.
1982: Cordilleran metamorphic core complexes — from Arizona to southern Canada; Annual Review of Earth and Planetary Sciences, v.10, p.129-154.

Armstrong, R.L., Eisbacher, G.H., and Evans, P.D.
1982: Age and stratigraphic — tectonic significance of Proterozoic diabase sheets, Mackenzie Mountains, northwestern Canada; Canadian Journal of Earth Sciences, v.19, p.316-323.

Aydin, A. and Page, B.M.
1984: Diverse Pliocene-Quaternary tectonics in a transform environment, San Francisco Bay region, California; Geological Society of America, Bulletin, v.95, p.1303-1317.

Bally, A.W., Gordy, P.L., and Stewart, G.A.
1966: Structure, siesmic data, and orogenic evolution of southern Canadian rocky mountains; Canadian Petroleum Geologists Bulletin, v.14, p.337-381.

Barton, C.M.
1975: Mt. Olympos, Greece: new light on an old window; Geological Society of London, Journal, v.131, p.389-396.

Bell, T.H.
1978: Progressive deformation and reorientation of fold axes in a ductile mylonite zone: the Woodroffe Thrust; Tectonophysics, v.44, p.285-320.

Bence, A.E. and Albee, A.L.
1968: Empirical correction factors for the electron microanalysis of silicates and oxides; Journal of Geology, v.76, p.382-403.

Berthe, D., Choukroune, P., and Gapais, D.
1979: Orientations préférentielles du quartz et orthogneissification progressive en régime cisaillant: l'exemple du cisaillement sudarmoricain; Bulletin de Minéralogie, v.102, p.265-272.

Bond, G.C. and Kominz, M.A.
1984: Construction of tectonic subsidence curves for the early Paleozoic miogeocline, southern Canadian Rocky Mountains: implications for subsidence mechanisms, age of break-up and crustal thinning; Geological Society of America, Bulletin, v.95, p.155-173.

Campbell, R.B., Mountjoy, E.W., and Young, F.G.
1973: Geology of McBride map-area, British Columbia; Geological Survey of Canada, Paper 72-35.

Carmichael, D.M.
1969: On the mechanism of prograde metamorphic reactions in quartz-bearing pelitic rocks; Contributions to Mineralogy and Petrology, v.20, p.244-267.
1970: Intersecting isograds in the Whetstone lake area, Ontario; Journal of Petrology, v.11, p.147-181.
1978: Metamorphic bathozones and bathograds: a measure of the depth of post-metamorphic uplift and erosion on the regional scale; American Journal of Science, v.278, p.769-797.
1979: Some implications of metamorphic reaction mechanisms for geothermobarometry based on solid solution equilibria: *in* Geological Society of America, Abstracts with Programs, v.11, no. 7, p.398.

Coney, P.J.
1980: Cordilleran metamorphic core complexes: an overview; Geological Society of America Memoir 153, p.7-31.

Coney, P.J., Jones, D.L., and Monger, J.W.H.
1980: Cordilleran suspect terranes; Nature, v.288, p.329-333.

Crowell, J.C.
1974a: Sedimentation along the San Andreas fault, California; *in* Modern and Ancient Geosynclinal Sedimentation: ed. R.H. Dott and R.H. Shaver Society of Economic Paleontologists and Mineralogists, Special Publication 19, p.292-303.
1974b: Origin of late Cenozoic basins in southern California; *in* Tectonics and Sedimentation, ed. W.R. Dickinson; Society of Economic Paleontologists and Mineralogists, Special Paper 22, p.190-204.

Davis, G.H.
1983: Shear-zone model for the origin of metamorphic core complexes; Geology, v.11, p.342-347.

Devlin, W.J., Bond, G.C., and Brueckner, K.
1984: Geologic and geochemical evidence for late Proterozoic — early Cambrian rifting and continental separation, southeast British Columbia and northeast Washington; *in* Geological Society of America, Abstracts with Programs, v.16, no.6, p.487.
1985: An assessment of the age and tectonic setting of volcanics near the base of the Windermere Supergroup in northeastern Washington: implications for latest Proterozoic — earliest Cambrian continental separation; Canadian Journal of Earth Sciences, v.22, p.829-837.

Dibblee, T.W., Jr.
1977: Stike-slip tectonics of the San Andreas fault and its role in Cenozoic basin evolvement; *in* Late Mesozoic and Cenozoic Sedimentation and Tectonics in California, ed. T.H. Nilsen; San Joaquin Geological Society, Bakersfield, California, p.26-38.

Dolmage, V.
1928: Finlay River District, British Columia; Geological Survey of Canada, Summary Report 1927, Part A, 1928.

Eisbacher, G.H.
1972: Tectonic overprinting near Ware, Northern Rocky Mountain Trench; Canadian Journal of Earth Sciences, v.9, p.903-913.
1974: Sedimentary history and tectonic evolution of the Sustut and Sifton basins, north-central British Columbia; Geological Survey of Canada, Paper 73-31.
1981: Sedimentary tectonics and glacial record in the Windermere Supergroup, Mackenzie Mountains, northwestern Canada; Geological Survey of Canada, Paper 80-27.

Escher, A. and Watterson, J.
1974: Stretching fabrics, folds and crustal shortening; Tectonophysics, v.22, p.223-231.

Evenchick, C.A.
1983: Nonconformity at the base of upper Proterozoic Misinchinka Group, Deserters Range, northern Rocky Mountains; *in* Current Research, Part A, Geological Survey of Canada, Paper 83-1A, p.475.

Evenchick, C.A., Parrish, R.R., and Gabrielse, H.
1984: Precambrian gneiss and late Proterozoic sedimentation in north-central British Columbia; Geology, v.12, p.233-237.

Ferry, J.M.
1980: A comparative study of geothermometers and geobarometers in pelitic schists from south-central Maine; American Mineralogist, v.65, p.720-732.

Ferry, J.M. and Spear, F.S.
1978: Experimental calibration of the partitioning of Fe and Mg between biotite and garnet; Contributions to Mineralogy and Petrology, v.66, p.113-117.

Fritz, W.H.
1972: Cambrian biostratigraphy, western Rocky Mountains, British Columbia; *in* Report of Activities, Part A, Geological Survey of Canada, Paper 72-1A, p.209-211.
1980: Two new formations in the Lower Cambrian, Atan Group, Cassiar Mountains, north-central British Columbia: *in* Current Research, Part B, Geological Survey of Canada, Paper 80-1B, p. 217-225.
1984: Uppermost Precambrian and Lower Cambrian strata, northern Omineca Mountains, north-central British Columbia; *in* Current Research Part B, Geological Survey of Canada, Paper 84-1B, p.245-254.

Froese, E. and Gasparrini, E.
1975: Metamorphic zones in the Snow Lake area, Manitoba; Canadian Mineralogist, v.13, p.162-167.

Gabrielse, H.
1962a: Kechika, British Columbia; Geological Survey of Canada, Map 42-1962.
1962b: Rabbit River, British Columbia; Geological Survey of Canada, Map 46-1962.
1963: McDame map-area, Cassiar District, British Columbia; Geological Survey of Canada, Memoir 319.
1972: Younger Precambrian of the Canadian Cordillera; American Journal of Science, v. 272, p.521-536.
1975: Geology of Fort Grahame east-half map-area, British Columbia; Geological Survey of Canada, Paper 75-33.
1985: Major dextral transcurrent displacements along the Northern Rocky Mountain Trench and related lineaments in north-central British Columbia; Geological Society of America, Bulletin, v.96, p.1-14.

Gabrielse, H. and Taylor G.C.
1983: Geological maps and cross-sections of the northern Canadian Cordillera from southwest of Fort Nelson, British Columbia to Gravina Island, southeastern Alaska; Geological Survey of Canada, Open File 864.

Gabrielse, H., Dodds, C.J. and Mansy, J.L.
1977b: Operation Finlay, British Columbia; *in* Current Research, Part A, Geological Survey of Canada, Paper 77-1A, p.243-246.

Gabrielse, H., Dodds, C.J., Mansy, J.L., and Eisbacher, G.H.
1977a: Geology of Toodoggone River (94E) and Ware west-half (94F W-half) map-areas; Geological Survey of Canada, Open File 483.

Gapais, D. and White, S.H.
1982: Ductile shear bands in a naturally deformed quartzite; Textures and Microstructures, v.5, p.1-17.

Ghent, E.D.
1976: Plagioclase-garnet-Al_2SiO_5-quartz: a potential geobarometer-geothermometer; American Mineralogist, v.61, p.710-714.

Ghent, E.D., Robbins, D.B., and Stout, M.Z.
1979: Geothermometry, geobarometry, and fluid compositions of metamorphosed calc-silicates and pelites, Mica Creek, British Columbia; American Mineralogist, v.64, p.874-885.

Ghent, E.D., Knitter, C.C., Raeside, R.P., and Stout, M.Z.
1982: Geothermometry and geobarometry of pelitic rocks, upper kyanite and sillimanite zones, Mica Creek area, British Columbia; Canadian Mineralogist, v.20, p.295-305.

Goldman, D.S. and Albee, A.L.
1977: Correlation of Mg/Fe partitioning between garnet and biotite with O^{18}/O^{16} partitioning between quartz and magnetite; American Journal of Science, v.277, p.750-767.

Hansen, E.
1967: Methods of deducing slip-line orientations from the geometry of folds; Annual Report of the Director, Geophysical Laboratory, 1965-1966, Carnegie Institution of Washington, p.387-405.
1971: Strain Facies; Springer-Verlag, 208p.

Harding, T.P.
1973: Newport-Inglewood trend, California-an example of wrenching style of deformation; American Association of Petroleum Geologists, Bulletin, v.58, p.97-116.
1974: Petroleum traps associated with wrench faults; American Association of Petroleum Geologists, Bulletin, v.58, p.1290-1304.

Harding, T.P. and Lowell, J.D.
1979: Structural styles, their plate-tectonic habitats, and hydrocarbon traps in petroleum provinces; American Association of Petroleum Geologists, Bulletin, v. 63, p.1016-1058.

Harland, W.B.
1971: Tectonic transpression in Caledonian Spitzbergen; Geological Magazine, v.197, p.27-42

Harms, T.A.
1984: Structural style of the Sylvester Allochthon, northeastern Cry Lake map area, British Columbia; *in* Current Research, Part A, Geological Survey of Canada, Paper 84-1A, p.109-112.

Harrison, T.M. and McDougall, I.
1980: Investigations of an intrusive contact, northwest Nelson, New Zealand — 1. Thermal, chronological, and isotopic constraints; Geochimica et Cosmochimica Acta, v.44, p.1985-2003.
1982: The thermal significance of potassium feldspar K-Ar ages inferred from $^{40}Ar/^{39}Ar$ age spectrum results; Geochimica et Cosmochimica Acta, v.46, p.1811-1820.

Hedley, M.S. and Holland, S.S.
1941: Reconnaissance in the area of Turnagain and upper Kechika Rivers, northern British Columbia; British Columbia Department of Mines, Bulletin no. 12.

Henderson, J.R.
1981: Structural analysis of sheath folds with horizontal X-axes, NE Canada; Journal of Structural Geology, v.3, p.203-210.

Hodges, K.V. and Spear, F.S.
1982: Geothermometry, geobarometry and the Al_2SiO_5 triple point at Mt. Moosilauke, New Hampshire; American Mineralogist, v.67, p.1118-1134.

Hofmann, H.J., Mountjoy, E.W., and Teitz, M.W.
1985: Ediacaran fossils from the Miette Group, Rocky Mountains, British Columbia, Canada; Geology, v.13, p.819-821.

Hollister, L.S.
1966: Garnet zoning: an interpretation based on the Rayleigh Fractionation model; Science, v.154, p.1647-1651.

Irish, E.J.W.
1970: Halfway River map-area, British Columbia; Geological Survey of Canada, Paper 69-11.

Irving, E., Woodsworth, G.J., Wynne, P.J., and Morrison, A.
1985: Paleomagnetic evidence for displacement from the south of the Coast Plutonic Complex, British Columbia; Canadian Journal of Earth Sciences, v. 22, p.584-598.

Kretz, R.
1959: Chemical study of garnet, biotite, and hornblende from gneisses of southwestern Quebec, with emphasis on distribution of elements in coexisting minerals; Journal of Geology, v.67, p.371-402.
1964: Analysis of equilibrium in garnet-biotite-sillimanite gneisses from Quebec; Journal of Petrology, v.5, p.1-20.

Leclair, A.D.
1983: Stratigraphy and structural implications of central Kootenay Arc rocks, southeastern British Columbia; *in* Current Research, Part A, Geological Survey of Canada, Paper 83-1A, p.235-240.

Leonard, R.
1984: Metamorphism, structure, and stratigraphy around the Mount Blackman Gneiss, British Columbia; *in* Current Research, Part A, Geological Survey of Canada, Paper 84-1A, p.121-127.

Lowell, J.D.
1972: Spitsbergen Tertiary orogenic belt and the Spitsbergen fracture zone; Geological Society of America, Bulletin, v.83, p.3091-3102.

Lund, K.
1984: The continent-island arc juncture in west-central Idaho — a missing link in Cordilleran tectonics; *in* Geological Society of America, Abstracts with Programs, v.16, no.6, p.580.

Mansy, J.L.
1980: La Cordillère canadienne au Nord et au centre de la Colombie Britannique (Canada); Revue de géologie dynamique et de géographie physique, v. 22, p.233-254.

Mansy, J.L. and Gabrielse, H.
1978: Stratigraphy, terminology and correlation of upper Proterozoic rocks in Omineca and Cassiar mountains, north-central British Columbia; Geological Survey of Canada, Paper 77-19.

McConnell, R.G.
1896: Report on exploration of Finlay and Omineca Rivers; Geological Survey of Canada, Annual Report v.7, 1894, p.6-40c.

McDonough, M.R. and Simony, P.S.
1984: Basement gneisses and Hadrynian metasediments near Bulldog Creek, Selwyn Range, British Columbia; *in* Current Research, Part A, Geological Survey of Canada, Paper 84-1A, p.99-102.

McMechan, R.D.
1981: Stratigraphy, sedimentology, structure and tectonic implications of the Oligocene Kishenehn Formation, Flathead Valley Graben, southeast British Columbia; unpublished Ph.D. thesis, Queen's University at Kingston, Kingston, Ontario, 327p.

Miller, F.K., McKee, E.H., and Yates, R.G.
1973: Age and correlation of the Windermere Group in northeastern Washington; Geological Society of America,Bulletin, v.84, p.3723-3730.

Monger, J.W.H., Price, R.A., and Tempelman-Kluit, D.J.
1982: Tectonic accretion and the origin of the two major metamorphic and plutonic welts in the Canadian Cordillera; Geology, v.10, p.70-75.

Muller, J.E.
1961: Pine Pass map-area, British Columbia; Geological Survey of Canada, Map 11-1961.

Newton, R.C. and Haselton, H.T.
1981: Thermodynamics of the garnet-plagioclase-Al_2SiO_5 — quartz geobarometer; *in* Thermodynamics of Minerals and Melts, ed. R.C. Newton and others; Springer-Verlag, New York, p.131-147.

Oke, C.
1982: Structure and metamorphism of Precambrian basement and its cover in the Mount Blackman area, British Columbia; unpublished M.Sc. thesis, University of Calgary, Calgary, Alberta, 115 p.

Oke, C. and Simony, P.S.
1981: Basement gneisses of the western Rocky Mountains, Hugh Allen Creek area, British Columbia; *in* Current Research, Part A, Geological Survey of Canada, Paper 81-1A, p.181-184.

Parrish, R.R.
1976: Structure, metamorphism, and geochronology of the northern Wolverine Complex, near Chase Mountain, Aiken Lake map-area, British Columbia; unpublished M.Sc. thesis, University of British Columbia, Vancouver, British Columbia, 89p.
1979: Geochronology and tectonics of the northern Wolverine Complex, British Columbia; Canadian Journal of Earth Sciences, v.16, p.1428-1438.

Parrish, R.R. and Armstrong, R.L.
1983: U-Pb zircon ages and tectonic significance of gneisses in structural culminations of the Omineca Crystalline Belt, British Columbia; Geological Society of America Abstracts with Programs, v.15, p.324.

Pigage, L.C. and Greenwood, H.J.
1982: Internally consistent estimates of pressure and temperature: the staurolite problem; American Journal of Science, v.282, p.943-969.

Platt, J.P. and Vissers, R.L.M.
1980: Extensional structures in anisotropic rocks; Journal of Structural Geology, v.2, p.397-410.

Poulton, T.P. and Simony, P.S.
1980: Stratigraphy, sedimentology, and regional correlation of the Horsethief Creek Group (Hadrynian, late Precambrian) in the northern Purcell and Selkirk mountains, British Columbia; Canadian Journal of Earth Sciences, v.17, p.1708-1724.

Price, R.A.
1981: The Cordilleran foreland thrust and fold belt in the southern Canadian Rocky Mountains; *in* Thrust and Nappe Tectonics, ed. by N.J. Price and K.C. McClay; Geological Society of London, Special Volume 9, p.427-448.

Price, R.A. and Mountjoy, E.W.,
1970: Geologic structure of the Canadian Rocky Mountains between Bow and Athabasca rivers, a progress report; Geological Association of Canada, Special Paper 6, p.7-26.

Quinquis, H., Audren, C., Brun, J.P., and Cobbold, P.R.
1978: Intense progressive shear in the Ile de Groix blueschists and compatibility with subduction; Nature, v.273, p. 43-45.

Ramsay, J.G.
1967: Folding and Fracturing of Rocks; McGraw-Hill, New York, 568p.
1980: Shear zone geometry: a review; Journal of Structural Geology, v.2, p.83-99.

Rhodes, S. and Gayer, R.A.
1977: Non-cylindrical folds, linear structures in the X-direction and mylonite developed during translation of the Caledonian Kalak Nappe Complex of Finnmark; Geological Magazine, v.114, p.329-408.

Roberts, J.L.
1977: Allochthonous origin of the Jotunheim Massif in south Norway: a reconnaissance study along its northwest margin; Geological Society of London, Journal, v.134, p.351-362.

Rodgers, D.A.
1980: Analysis of basin development produced by en echelon strike slip faults; *in* Sedimentation at Oblique-Slip Margins, ed. P.F. Ballance and H.G. Reading; International Association of Sedimentologists, Special Publication 4, Oxford, England, p.27-41.

Roots, E.F.
1954: Geology and mineral deposits of Aiken Lake map-area, British Columbia; Geological Survey of Canada, Memoir 274.

Rutter, N.W. and Taylor, G.C.
1968: Bedrock geology along Ingenika and Finlay rivers, Peace River Reservoir area, British Columbia; Geological Survey of Canada, Bulletin 186.

St-Onge, M.R.
1981: Metamorphic conditions of the low-pressure internal zone of north-central Wopmay Orogen, Northwest Territories, Canada; unpublished Ph.D. thesis, Queen's University at Kingston, Kingston, Ontario, 240p.
1984a: The muscovite-melt bathograd and low-P isograd suites in north-central Wopmay Orogen, Northwest Territories, Canada; Journal of Metamorphic Geology, v.2, p.315-326.
1984b: Geothermometry and geobarometry in pelitic rocks of north-central Wopmay Orogen (early Proterozoic) Northwest Territories, Canada; Geological Society of America Bulletin, v.95, p.196-208.

Sibson, R.H.
1977: Fault rocks and fault mechanisms; Geological Society of London, Journal, v.133, p.191-213.

Silberling, N.J. and Jones, D.L.
1984: Lithotectonic terrane maps of the North America Cordillera; United States Geological Survey, Open File Report 84-523.

Simpson, C.
1984: Borrego Springs-Santa Rosa mylonite zone: a Late Cretaceous west-directed thrust in southern California; Geology, v.12, p.8-11.

Simpson, C. and Schmid, S.M.
1983: An evaluation of criteria to deduce the sense of movement in sheared rocks; Geological Society of America Bulletin, v.94, p.1281-1288.

Slind, O.L. and Perkins, G.D.
1966: Lower Paleozoic and Proterozoic sediments of the Rocky Mountains between Jasper, Alberta and Pine River, British Columbia; Canadian Petroleum Geologists, Bulletin, v.14, p.442-468.

Stevens, R.D., Delabio, R.N., and Lachance, G.R.
1982: Age Determinations and Geological Studies: K-Ar Isotopic Ages, Report 16; Geological Survey of Canada, Paper 82-2.

Stott, D.F., McMechan, M.E., Taylor, G.C., and Muller, J.E.
1983: Geology of Pine Pass (Mackenzie) map area, NTS 93O, British Columbia; Geological Survey of Canada, Open File 925.

Streckeisen, A.
1979: Classification and nomenclature of volcanic rocks, lamprophyres, carbonatites, and melilitic rocks: recommendations and suggestions of the IUGS Subcommission on the Systematics of Igneous Rocks; Geology, v.7, p.331-335.

Sylvester, A.G. and R.R. Smith
1976: Tectonic transpression and basement-controlled deformation in San Andreas fault zone, Salton Trough, California; American Association of Petroleum Geologists Bulletin, v.30, p.2081-2102.

Taylor, G.C. and Stott, D.F.
1973: Tuchodi Lakes map-area, British Columbia (94K); Geological Survey of Canada, Memoir 373.

Taylor, G.C., Cecile, M.P., Jefferson, C.W., and Norford, B.S.
1979: Stratigraphy of Ware (East half) map-area, northeastern British Columbia; *in* Current Research, Part A, Geological Survey of Canada, Paper 79-1A, p.227-231.

Thompson, A.B.
1976: Mineral reactions in pelitic rocks: Prediction and calculation of P-T-X (Fe-Mg) relations; American Journal of Science, v.276, p. 401-454.

Thompson, J.B. Jr.
1957: The graphical analysis of mineral assemblages in pelitic schists; American Mineralogist, v.42, p.842-858.

Thompson, R.I.
1978: Geological maps of the Halfway River map-area (94B), 1:250 000 and 1:50 000; Geological Survey of Canada, Open File 536.

Tracy, R.J., Robinson, P., and Thompson, A.B.
1976: Garnet composition and zoning in the determination of temperature and pressure of metamorphism, central Massachusetts; American Mineralogist, v.61, p.762-775.

Turner, F.J.
1981: Metamorphic Petrology. Mineralogical, Field and Tectonic Aspects, second edition; McGraw-Hill, New York, 524p.

Turner, F.J. and Weiss, L.E.
1963: Structural Analysis of Metamorphic Tectonites; McGraw-Hill Book Company, New York, 545p.

Wanless, R.K.,Stevens, R.D., Lachance, G.R., and Delabio, R.N.
1971: Age Determinations and Geochronological Studies: K-Ar Isotopic Ages; Geological Survey of Canada, Paper 71-2.
1974: Age Determinations and Geochronological Studies: K-Ar Isotopic Ages, Report 12; Geological Survey of Canada, Paper 74-2.
1978: Age Determinations and Geochronological Studies: K-Ar Isotopic Ages, Report 13; Geological Survey of Canada, Paper 77-2.
1979: Age Determinations and Geochronological Studies: K-Ar Isotopic Ages, Report 14; Geological Survey of Canada, Paper 79-2.

Weijermars, R. and Rondeel, H.E.
1984: Shear band foliation as an indicator of sense of shear: field observations in central Spain; Geology, v.12, p.603-606.

White, S.H., Burrows, S.E., Carreras, J., Shaw, N.D., Humpreys, F.J.
1980: On mylonites in ductile shear zones; Journal of Structural Geology, v.2, p.175-187.

Wilcox, R.E., Harding, T.P., and Seely, D.R.
1973: Basic wrench tectonics; American Association of Petroleum Geologists, Bulletin, v.57, p.74-96.

Williams, G.D.
1978: Rotation of contemporary folds into the X direction during overthrust processes in Laksefjord, Finnmark; Tectonophysics, v.48, p.29-40.

Winkler, H.G.F.
1979: Petrogenesis of Metamorphic Rocks, fifth edition; Spinger-Verlag, New York, 348p.

Woodsworth, G.J.
1977: Homogenization of zoned garnets from pelitic schists; Canadian Mineralogist, v.15, p.230-242.

Yeo, G.M.
1981: The late Proterozoic Rapitan Glaciation in the northern Cordillera; *in* Proterozoic Basins of Canada, ed. F.H.A. Campbell; Geological Survey of Canada, Paper 81-10, p.27-46.

Young, F.G., Campbell, R.B., and Poulton, T.P.
1973: The Windermere Supergroup of the southeastern Canadian Cordillera; *in* Belt Symposium 1973, Vol. 1: Department of Geology, University of Idaho and Idaho Bureau of Mines and Geology, Moscow, Idaho, p.181-203.

Young, G.M., Jefferson, C.W., Delaney, G.D., and Yeo, G.M.
1979: Middle and late Proterozoic evolution of the northern Canadian Cordillera and Shield; Geology, v.7, p. 125-128.

APPENDIX

Microprobe analyses and analytical procedure

Analytical procedure

Ten-oxide analyses of garnet, biotite, and plagioclase were done on the ARL-SEMQ electron micoroprobe at Queen's University. EDS operating conditions were with an accelerating voltage of 15 kv, beam current of 75 nA, beam diameter fo 2 μm and a spectra collecting time of 200 seconds. Apparent concentrations were corrected on-line for matrix effects using programs written by P.L. Roeder (Queen's University) that incorporate the Bence and Albee (1968) corrections as modified by Albee and Ray (1970).

Structural formalae were calcultated from the microprobe analyses using programs written by D.M. Carmichael. The ferric iron content in garnet is estimated by assuming stoichiometry and satisfying cationic charge constraints, and if possible, site constraints (assuming a total cationic charge of 24 and that all cations occupy 8 sites). For biotite, the ferric iron content cannot be estimated by this method because of the large octahedral vacancies. Total iron is calculated as FeO, and H_2O is calculated assuming full hydroxyl site occupancy. The structural formulae of garnet show that ferric iron is generally less than 2 % of the ferrous iron content; total iron is given as FeO.

Precision and accuracy

Ten analyses of NBS-K412 glass (S 204) were done with the same operating conditions over a period of about two weeks in June 1984. The mean, standard deviation, range of analyses, and accepted values are listed in the following table.

	Mean	Standard deviation	Range	Accepted value
SiO_2	45.30	.11	45.07-45.43	45.35
AL_2O_3	9.28	.11	9.12- 9.44	9.27
FeO	9.97	.15	9.73-10.20	9.96
MgO	19.20	.05	19.13-19.27	19.33
CaO	15.25	.10	15.14-15.42	15.25

Analyses

Three domains in each thin section were chosen for analysis. The domains are defined by a garnet (garn), and biotite (bi) and plagioclase (plag) grains within 2 mm of the garnet. Within each domain 3 or 4 areas of the garnet were analyzed, and are labeled a to d, commonly a core spot (cor), an interior spot (int) and two rim spots (rim). In most domains two biotite grains were analyzed, one in contact with the garnet (cont), and one in the marix of the schist (matr). In section 424 domain 2, 'clos' refers to a biotite that is close to, but not in contact with garnet. In section 744 domain 1, 'bi-a core' is an analysis of biotite from the core of the garnet. In many domains only one plagioclase grain was analyzed and in those cases it is not given a lower case letter. Data used for the calculation of pressure and temperature in Table 3 are identified by the same lower case letters.

Analyses of section 409, domain 1

	garn cor-d	garn int-b	garn rim-a	garn rim-c	bi-a matr	bi-b cont	plag
SiO_2	37.70	37.70	37.71	37.83	36.64	36.80	63.90
Al_2O_3	22.26	22.32	22.29	22.50	20.31	20.30	24.12
TiO_2	0.00	0.00	0.00	0.10	1.36	1.60	0.02
FeO	30.24	33.64	34.61	34.19	17.07	17.03	0.04
MgO	1.04	2.97	3.31	3.25	11.11	11.26	0.00
MnO	4.02	0.20	0.24	0.35	0.00	0.04	0.00
CaO	6.88	4.73	3.03	3.62	0.11	0.16	4.24
Na_2O	0.03	0.00	0.00	0.00	0.10	0.18	9.23
K_2O	0.00	0.00	0.01	0.00	8.69	8.36	0.02
Cr_2O_3	0.10	0.06	0.00	0.03	0.00	0.05	0.05
H_2O	0.00	0.00	0.00	0.00	4.03	4.05	0.00
Total	102.27	101.62	101.21	101.87	99.42	99.83	101.61
Si	2.965	2.961	2.974	2.962	2.727	2.722	2.777
$Al^{(iv)}$	0.035	0.039	0.026	0.038	1.273	1.278	1.223
$Al^{(vi)}$	2.028	2.027	2.046	2.039	0.508	0.492	0.013
Ti	0.000	0.000	0.000	0.006	0.076	0.089	0.001
Fe^{3+}	0.015	0.010	0.000	0.003	0.000	0.000	0.000
Fe^{2+}	1.972	2.198	2.283	2.236	1.062	1.053	0.001
Mg	0.122	0.348	0.389	0.379	1.233	1.242	0.000
Mn	0.268	0.013	0.016	0.023	0.000	0.003	0.000
Ca	0.580	0.398	0.256	0.304	0.009	0.013	0.197
Na	0.005	0.000	0.000	0.000	0.014	0.026	0.778
K	0.000	0.000	0.001	0.000	0.825	0.789	0.001
Cr	0.006	0.004	0.000	0.002	0.000	0.003	0.002
O	12.000	12.000	12.000	12.000	10.000	10.000	8.000
OH,F	0.000	0.000	0.000	0.000	2.000	2.000	0.000
F/F+M	0.942	0.864	0.854	0.855	0.463	0.457	
X_{Alm}	0.672	0.744	0.775	0.760			
X_{Pyr}	0.041	0.117	0.132	0.129			
X_{Spes}	0.091	0.004	0.005	0.008			
X_{Gros}	0.196	0.134	0.087	0.103			
X_{An}							0.203

Analyses of section 409, domain 2

	garn cor-b	garn int-a	garn rim-c	bi-b matr	bi-a cont	plag
SiO_2	37.36	37.24	37.60	35.94	36.19	64.15
Al_2O	22.14	22.05	22.46	19.76	19.84	23.64
TiO_2	0.03	0.05	0.04	1.39	1.41	0.00
FeO	30.55	34.32	35.12	18.25	18.24	0.08
MgO	1.39	2.22	2.93	10.96	10.48	0.00
MnO	3.53	0.12	0.47	0.08	0.00	0.00
CaO	6.96	5.10	2.92	0.04	0.06	3.87
Na_2O	0.00	0.00	0.00	0.17	0.00	9.32
K_2O	0.00	0.00	0.03	7.48	7.41	0.00
Cr_2O_3	0.00	0.00	0.00	0.00	0.00	0.04
H_2O	0.00	0.00	0.00	3.96	3.96	0.00
Total	101.95	101.16	101.60	98.03	97.59	101.11
Si	2.916	2.954	2.963	2.716	2.741	2.798
$Al^{(iv)}$	0.018	0.046	0.037	1.284	1.259	1.202
$Al^{(vi)}$	2.019	2.015	2.049	0.476	0.512	0.013
Ti	0.002	0.003	0.002	0.079	0.081	0.000
Fe^{3+}	0.017	0.021	0.000	0.000	0.000	0.002
Fe^{2+}	1.975	2.253	2.314	1.154	1.155	0.001
Mg	0.162	0.262	0.344	1.235	1.183	0.000
Mn	0.233	0.008	0.031	0.005	0.000	0.000
Ca	0.582	0.434	0.247	0.004	0.005	0.181
Na	0.000	0.000	0.000	0.025	0.000	0.788
K	0.000	0.000	0.003	0.722	0.716	0.000
Cr	0.000	0.003	0.002	0.000	0.000	0.001
O	12.000	12.000	12.000	10.000	10.000	8.000
OH,F	0.000	0.000	0.000	2.000	2.000	0.000
F/F+M	0.925	0.897	0.871	0.483	0.494	
X_{Alm}	0.671	0.764	0.788			
X_{Pyr}	0.055	0.088	0.117			
X_{Spes}	0.078	0.003	0.010			
X_{Gros}	0.196	0.146	0.084			
X_{An}						0.186

Analyses of section 409, domain 5

	garn cor-c	garn rim-a	garn rim-b	bi-b matr	bi-a cont	bi-a cont	plag
SiO_2	37.80	37.97	37.95	36.56	36.79	36.62	63.96
Al_2O_3	22.26	22.58	22.51	20.47	19.90	20.07	24.18
TiO_2	0.08	0.13	0.03	1.51	1.94	1.73	0.00
FeO	31.05	34.06	34.50	17.22	15.93	16.73	0.05
MgO	1.08	3.38	3.17	11.10	11.78	11.54	0.00
MnO	3.09	0.13	0.11	0.05	0.07	0.08	0.00
CaO	7.15	3.95	4.04	0.11	0.13	0.16	4.26
Na_2O	0.00	0.00	0.04	0.24	0.12	0.22	9.10
K_2O	0.00	0.00	0.02	8.60	8.80	8.22	0.02
Cr_2O_3	0.03	0.02	0.01	0.00	0.08	0.07	0.03
H_2O	0.00	0.00	0.00	4.04	4.05	4.04	0.00
Total	102.55	102.23	102.36	99.91	99.59	99.48	101.60
Si	2.965	2.960	2.960	2.710	2.723	2.716	2.779
$Al^{(iv)}$	0.035	0.040	0.040	1.290	1.277	1.284	1.221
$Al^{(vi)}$	2.023	2.034	2.028	0.498	0.460	0.471	0.017
Ti	0.005	0.008	0.002	0.084	0.108	0.096	0.000
Fe^{3+}	0.001	0.000	0.019	0.000	0.000	0.000	0.000
Fe^{2+}	2.035	2.220	2.228	1.068	0.986	1.038	0.002
Mg	0.127	0.393	0.368	1.227	1.300	1.276	0.000
Mn	0.205	0.008	0.007	0.003	0.005	0.005	0.000
Ca	0.601	0.330	0.338	0.009	0.011	0.013	0.198
Na	0.000	0.000	0.006	0.034	0.018	0.032	0.767
K	0.000	0.000	0.002	0.813	0.831	0.777	0.001
Cr	0.002	0.001	0.000	0.000	0.005	0.004	0.001
O	12.000	12.000	12.000	10.000	10.000	10.000	8.000
OH,F	0.000	0.000	0.000	2.000	2.000	2.000	0.000
F/F+M	0.941	0.850	0.859	0.465	0.431	0.449	
X_{Alm}	0.686	0.752	0.759				
X_{Pyr}	0.043	0.133	0.124				
X_{Spes}	0.069	0.003	0.002				
X_{Gros}	0.202	0.112	0.114				
X_{An}							0.205

Analyses of section 424, domain 1

	garn cor-c	garn rim-a	garn rim-b	bi-b mat	bi-a cont	plag mat-b	plag con-a
SiO_2	38.08	38.17	38.53	36.63	36.51	64.34	64.50
Al_2O_3	22.46	22.63	22.83	20.30	21.14	24.73	24.70
TiO_2	0.00	0.00	0.00	2.14	1.78	0.03	0.04
FeO	32.59	33.45	34.60	17.83	18.11	0.08	0.08
MgO	0.95	2.90	3.14	10.62	9.83	0.00	0.00
MnO	2.07	0.38	0.53	0.08	0.03	0.02	0.00
CaO	7.28	5.30	3.76	0.05	0.18	4.69	4.77
Na_2O	0.00	0.00	0.00	0.13	0.00	8.95	8.61
K_2O	0.03	0.03	0.04	8.51	8.06	0.03	0.03
Cr_2O_3	0.10	0.06	0.00	0.05	0.03	0.00	0.04
H_2O	0.00	0.00	0.00	4.05	4.04	0.00	0.00
Total	103.57	102.90	103.43	100.39	99.71	102.87	102.78
Si	2.961	2.959	2.973	2.707	2.709	2.764	2.769
$Al^{(iv)}$	0.039	0.041	0.027	1.293	1.291	1.236	1.231
$Al^{(vi)}$	2.020	2.027	2.048	0.475	0.558	0.015	0.019
Ti	0.000	0.000	0.000	0.119	0.099	0.001	0.001
Fe^{3+}	0.017	0.014	0.000	0.000	0.000	0.000	0.000
Fe^{2+}	2.101	2.153	2.232	1.102	1.124	0.003	0.003
Mg	0.110	0.335	0.361	1.170	1.087	0.000	0.000
Mn	0.137	0.025	0.035	0.005	0.002	0.001	0.000
Ca	0.607	0.440	0.311	0.004	0.014	0.216	0.219
Na	0.000	0.000	0.000	0.019	0.000	0.746	0.717
K	0.003	0.003	0.004	0.802	0.763	0.001	0.002
Cr	0.006	0.003	0.000	0.003	0.002	0.000	0.001
O	12.000	12.000	12.000	10.000	10.000	8.000	8.000
OH,F	0.000	0.000	0.000	2.000	2.000	0.000	0.000
F/F+M	0.951	0.866	0.861	0.485	0.508		
X_{Alm}	0.713	0.730	0.759				
X_{Pyr}	0.037	0.113	0.123				
X_{Spes}	0.046	0.008	0.012				
X_{Gros}	0.204	0.148	0.106				
X_{An}						0.234	0.224

Analyses of section 424, domain 2

	garn cor-d	garn rim-a	garn rim-b	bi-b matr	bi-a clos	bi-d cont	plag
SiO_2	37.49	37.89	37.96	36.54	35.63	35.90	64.60
Al_2O_3	22.14	22.49	22.44	19.81	20.52	20.48	24.70
TiO_2	0.05	0.00	0.00	1.97	1.31	1.67	0.03
FeO	30.74	33.17	33.07	19.27	19.76	18.51	0.00
MgO	0.90	2.72	3.06	10.60	9.43	9.82	0.00
MnO	3.81	0.30	0.18	0.03	0.13	0.03	0.03
CaO	6.97	5.55	5.52	0.13	0.21	0.14	4.67
Na_2O	0.03	0.00	0.00	0.06	0.10	0.22	9.26
K_2O	0.01	0.00	0.00	8.30	8.13	8.50	0.00
Cr_2O_3	0.14	0.07	0.05	0.08	0.13	0.05	0.06
H_2O	0.00	0.00	0.00	4.05	3.97	3.99	0.00
Total	102.28	102.19	102.29	100.83	99.31	99.31	103.36
Si	2.954	2.958	2.957	2.705	2.688	2.695	2.764
$Al^{(iv)}$	0.046	0.042	0.043	1.295	1.312	1.305	1.236
$Al^{(vi)}$	2.011	2.028	2.016	0.434	0.512	0.508	0.009
Ti	0.003	0.000	0.000	0.109	0.074	0.094	0.001
Fe^{3+}	0.025	0.012	0.023	0.000	0.000	0.000	0.000
Fe^{2+}	1.998	2.153	2.128	1.193	1.246	1.162	0.000
Mg	0.105	0.317	0.356	1.170	1.060	1.099	0.000
Mn	0.254	0.020	0.012	0.002	0.009	0.002	0.001
Ca	0.589	0.465	0.461	0.010	0.017	0.012	0.214
Na	0.004	0.000	0.000	0.008	0.014	0.032	0.768
K	0.001	0.000	0.000	0.784	0.782	0.814	0.000
Cr	0.009	0.005	0.003	0.004	0.008	0.003	0.002
O	12.000	12.000	12.000	10.000	10.000	10.000	8.000
OH,F	0.000	0.000	0.000	2.000	2.000	2.000	0.000
F/F+M	0.951	0.872	0.858	0.505	0.540	0.514	
X_{Alm}	0.681	0.730	0.722				
X_{Pyr}	0.035	0.107	0.119				
X_{Spes}	0.085	0.007	0.004				
X_{Gros}	0.198	0.157	0.115				
X_{An}							0.218

Analyses of section 424, domain 3

	garn cor-d	garn int-a	garn rim-b	garn rim-c	bi-b matr	bi-a cont	plag b	plag a
SiO_2	37.66	37.76	37.95	37.95	36.07	36.30	63.67	63.93
Al_2O_3	22.18	22.36	22.44	22.48	20.31	20.66	24.38	24.50
TiO_2	0.03	0.03	0.03	0.00	2.11	2.12	0.02	0.00
FeO	32.88	33.39	33.49	33.60	18.57	17.91	0.00	0.00
MgO	1.27	2.21	3.40	3.35	9.89	9.84	0.00	0.00
MnO	0.95	0.40	0.24	0.35	0.09	0.10	0.00	0.05
CaO	7.18	6.09	4.78	4.31	0.14	0.09	4.49	4.55
Na_2O	0.00	0.00	0.00	0.00	0.14	0.30	9.21	9.18
K_2O	0.00	0.04	0.00	0.00	8.66	8.63	0.05	0.02
Cr_2O_3	0.08	0.09	0.12	0.11	0.02	0.00	0.08	0.00
H_2O	0.00	0.00	0.00	0.00	4.01	4.03	0.00	0.00
Total	102.24	102.37	102.44	102.15	100.03	99.99	101.91	102.23
Si	2.960	2.953	2.951	2.960	2.692	2.699	2.763	2.764
$Al^{(iv)}$	0.040	0.047	0.049	0.040	1.308	1.301	1.237	1.236
$Al^{(vi)}$	2.015	2.014	2.008	2.027	0.478	0.510	0.010	0.013
Ti	0.002	0.002	0.002	0.000	0.118	0.119	0.001	0.000
Fe^{3+}	0.018	0.029	0.030	0.008	0.000	0.000	0.000	0.000
Fe^{2+}	2.142	2.152	2.145	2.183	1.159	1.113	0.000	0.000
Mg	0.149	0.258	0.394	0.390	1.100	1.090	0.000	0.000
Mn	0.063	0.027	0.016	0.023	0.006	0.006	0.000	0.002
Ca	0.605	0.511	0.399	0.360	.011	0.007	0.209	0.211
Na	0.000	0.000	0.000	0.000	0.021	0.044	0.775	0.770
K	0.000	0.004	0.000	0.000	0.824	0.818	0.003	0.001
Cr	0.005	0.006	0.007	0.007	0.001	0.000	0.003	0.000
O	12.000	12.000	12.000	12.000	10.000	10.000	8.000	8.000
OH,F	0.000	0.000	0.000	0.000	2.000	2.000	0.000	0.000
F/F+M	0.935	0.894	0.847	0.849	0.513	0.505		
X_{Alm}	0.726	0.733	0.729	0.739				
X_{Pyr}	0.050	0.087	0.132	0.132				
X_{Spes}	0.021	0.009	0.005	0.008				
X_{Gros}	0.203	0.172	0.134	0.121				
X_{An}							0.212	0.215

Analyses of section 255-3, domain 1

	garn cor-c	garn int-b	garn rim-a	garn rim-d	bi matr	plag
SiO_2	37.44	38.03	37.76	37.42	36.21	65.89
Al_2O_3	22.24	22.52	22.33	22.16	20.54	23.93
TiO_2	0.07	0.00	0.00	0.00	2.58	0.00
FeO	29.32	34.53	33.21	32.74	18.30	0.05
MgO	2.08	4.02	2.98	2.97	8.98	0.00
MnO	6.04	0.96	3.84	4.28	0.20	0.00
CaO	4.65	2.35	1.76	1.59	0.12	3.57
Na_2O	0.07	0.00	0.00	0.00	0.24	8.06
K_2O	0.02	0.00	0.00	0.02	8.72	0.03
Cr_2O_3	0.08	0.03	0.00	0.00	0.00	0.08
H_2O	0.00	0.00	0.00	0.00	4.01	0.00
Total	102.01	102.45	101.87	101.19	99.89	101.61
Si	2.905	2.960	2.974	2.941	2.703	2.836
$Al^{(iv)}$	0.040	0.026	0.000	1.297	1.164	
$Al^{(vi)}$	2.034	2.026	2.047	2.053	0.509	0.050
Ti	0.004	0.000	0.000	0.000	0.145	0.000
Fe^{3+}	0.000	0.014	0.000	0.000	0.000	0.000
Fe^{2+}	1.903	2.232	2.188	2.152	1.142	0.002
Mg	0.241	0.466	0.349	0.348	0.999	0.000
Mn	0.397	0.063	0.256	0.285	0.013	0.000
Ca	0.387	0.196	0.149	0.134	0.009	0.165
Na	0.010	0.000	0.000	0.000	0.035	0.673
K	0.002	0.000	0.000	0.002	0.830	0.002
Cr	0.005	0.002	0.000	0.000	0.000	0.003
O	12.000	12.000	12.000	12.000	10.000	8.000
OH,F	0.000	0.000	0.000	0.000	2.000	0.000
F/F+M	0.888	0.828	0.862	0.861	0.533	
X_{Alm}	0.650	0.756	0.744	0.737		
X_{Pyr}	0.082	0.157	0.119	0.119		
X_{Spes}	0.136	0.021	0.087	0.098		
X_{Gros}	0.132	0.066	0.051	0.046		
X_{An}						0.196

Analyses of section 255-3, domain 2

	garn cor-b	garn rim-a	garn rim-c	bi a	bi b	plag
SiO_2	37.87	37.78	38.06	36.39	36.03	65.98
Al_2O_3	21.94	22.10	22.23	21.22	20.39	23.21
TiO_2	0.00	0.00	0.00	2.49	2.38	0.03
FeO	32.81	33.53	32.28	19.35	19.94	0.14
MgO	3.38	3.33	2.96	9.58	9.77	0.00
MnO	3.61	3.00	4.48	0.22	0.20	0.00
CaO	2.25	2.08	2.09	0.08	0.10	3.37
Na_2O	0.00	0.00	0.00	0.12	0.13	8.34
K_2O	0.00	0.02	0.00	7.88	8.26	0.00
Cr_2O_3	0.00	0.00	0.00	0.04	0.04	0.04
H_2O	0.00	0.00	0.00	4.08	4.05	0.00
Total	101.87	101.84	102.10	101.44	101.28	101.11
Si	2.979	2.974	2.975	2.669	2.666	2.855
$Al^{(iv)}$	0.021	0.026	0.000	1.331	1.334	1.145
$Al^{(vi)}$	2.014	2.024	2.048	0.504	0.445	0.038
Ti	0.000	0.000	0.000	0.137	0.132	0.001
Fe^{3+}	0.007	0.008	0.000	0.000	0.000	0.000
Fe^{2+}	2.152	2.198	2.111	1.187	1.234	0.005
Mg	0.397	0.390	0.345	1.048	1.078	0.000
Mn	0.240	0.200	0.297	0.013	0.012	0.000
Ca	0.190	0.176	0.175	0.006	0.008	0.156
Na	0.000	0.000	0.000	0.017	0.018	0.700
K	0.000	0.002	0.000	0.737	0.780	0.000
Cr	0.000	0.000	0.000	0.002	0.003	0.001
O	12.000	12.000	12.000	10.000	10.000	8.000
OH,F	0.000	0.000	0.000	2.000	2.000	0.000
F/F+M	0.845	0.850	0.860	0.531	0.534	
X_{Alm}	0.723	0.742	0.721			
X_{Pyr}	0.133	0.131	0.118			
X_{Spes}	0.080	0.067	0.101			
X_{Gros}	0.064	0.059	0.060			
X_{An}						0.183

Analyses of section 255-3, domain 3

	garn cor-c	garn int-b	garn rim-a	garn rim-d	bi-b matr	bi-a cont	plag b
SiO_2	37.98	38.23	38.12	38.09	35.97	35.96	66.22
Al_2O_3	22.57	22.69	22.66	22.81	20.51	21.23	24.02
TiO_2	0.00	0.00	0.00	0.00	2.75	1.71	0.00
FeO	29.01	34.53	35.03	34.67	20.71	21.18	0.03
MgO	0.91	3.23	3.10	3.28	9.33	9.40	0.00
MnO	8.35	0.73	3.72	3.60	0.18	0.21	0.00
CaO	5.76	4.01	1.48	1.56	0.04	0.07	3.43
Na_2O	0.00	0.00	0.00	0.00	0.19	0.00	8.00
K_2O	0.00	0.00	0.00	0.00	7.81	7.66	0.03
Cr_2O_3	0.10	0.05	0.00	0.02	0.04	0.00	0.00
H_2O	0.00	0.00	0.00	0.00	4.06	4.05	0.00
Total	104.69	103.47	104.11	104.03	101.58	101.47	101.72
Si	2.888	2.912	2.906	2.895	2.653	2.657	2.842
$Al^{(iv)}$	0.000	0.000	0.000	0.000	1.347	1.343	1.158
$Al^{(vi)}$	2.023	2.037	2.036	2.043	0.437	0.505	0.058
Ti	0.000	0.000	0.000	0.000	0.152	0.095	0.000
Fe^{3+}	0.000	0.000	0.000	0.000	0.029	0.000	0.000
Fe^{2+}	1.845	2.199	2.233	2.203	1.247	1.309	0.001
Mg	0.103	0.367	0.352	0.371	1.026	1.035	0.000
Mn	0.538	0.047	0.240	0.232	0.011	0.013	0.000
Ca	0.470	0.327	0.121	0.127	0.003	0.006	0.158
Na	0.000	0.000	0.000	0.000	0.027	0.000	0.666
K	0.000	0.000	0.000	0.000	0.735	0.722	0.002
Cr	0.006	0.003	0.000	0.001	0.002	0.000	0.000
O	12.000	12.000	12.000	12.000	10.000	10.000	8.000
OH,F	0.000	0.000	0.000	0.000	2.000	2.000	0.000
F/F+M	0.947	0.857	0.864	0.856	0.554	0.558	
X_{Alm}	0.624	0.748	0.758	0.751			
X_{Pyr}	0.034	0.125	0.119	0.126			
X_{Spes}	0.182	0.016	0.081	0.079			
X_{Gros}	0.159	0.111	0.041	0.043			
X_{An}							0.191

Analyses of section 224-3, domain 1

	garn cor-c	garn int-b	garn rim-a	garn rim-d	bi-b matr	bi-a cont	plag b	plag a
SiO_2	37.54	37.42	37.69	37.74	35.36	35.65	62.98	62.91
Al_2O_3	22.05	22.25	22.26	22.24	20.59	20.70	24.83	24.87
TiO	0.00	0.03	0.07	0.00	2.32	1.89	0.03	0.00
FeO	26.38	31.91	30.74	32.25	18.71	19.06	0.00	0.03
MgO	0.91	1.40	2.26	2.87	9.09	9.29	0.00	0.00
MnO	7.52	2.85	4.03	2.13	0.19	0.22	0.00	0.04
CaO	7.62	6.35	4.89	4.07	0.16	0.17	5.22	5.29
Na_2O	0.00	0.00	0.00	0.00	0.20	0.20	8.67	8.50
K_2O	0.03	0.00	0.02	0.03	9.03	8.65	0.11	0.11
Cr_2O_3	0.00	0.14	0.02	0.02	0.03	0.08	0.03	0.05
H_2O	0.00	0.00	0.00	0.00	3.98	3.99	0.00	0.00
Total	102.04	102.35	101.98	101.35	99.66	99.89	101.87	101.78
Si	2.960	2.943	2.964	2.974	2.662	2.674	2.738	2.737
$Al^{(iv)}$	0.040	0.057	0.036	0.026	1.338	1.326	1.262	1.263
$Al^{(vi)}$	2.009	2.006	2.027	2.040	0.488	0.503	0.011	0.012
Ti	0.000	0.002	0.004	0.000	0.132	0.107	0.001	0.000
Fe^{3+}	0.034	0.038	0.003	0.004	0.000	0.000	0.000	0.000
Fe^{2+}	1.702	2.056	2.018	2.121	1.178	1.195	0.000	0.001
Mg	0.107	0.164	0.264	0.338	1.020	1.038	0.000	0.000
Mn	0.502	0.190	0.268	0.142	0.012	0.014	0.000	0.001
Ca	0.644	0.535	0.412	0.343	0.013	0.013	0.243	0.246
Na	0.000	0.000	0.000	0.000	0.029	0.029	0.731	0.717
K	0.003	0.000	0.002	0.003	0.867	0.828	0.006	0.006
Cr	0.000	0.009	0.001	0.001	0.002	0.005	0.001	0.002
O	12.000	12.000	12.000	12.000	10.000	10.000	8.000	8.000
OH,F	0.000	0.000	0.000	0.000	2.000	2.000	0.000	0.000
F/F+M	0.942	0.927	0.884	0.863	0.536	0.535		
X_{Alm}	0.581	0.702	0.682	0.721				
X_{Pyr}	0.036	0.055	0.089	0.115				
X_{Spee}	0.168	0.064	0.090	0.048				
X_{Gros}	0.215	0.179	0.139	0.116				
X_{An}							0.248	0.254

Analyses of section 224-3, domain 2

	garn cor-c	garn int-b	garn rim-d	garn rim-e	bi a	bi b	bi c	plag a	plag b	plag c
SiO_2	37.63	37.67	37.56	35.21	35.68	35.73	63.62	63.43	63.97	
Al_2O_3	22.19	22.28	22.33	22.23	20.02	21.51	20.23	24.84	25.06	24.26
TiO	0.03	0.00	0.00	0.03	1.71	1.88	2.36	0.06	0.00	0.02
FeO	28.01	33.32	32.02	32.34	20.48	18.92	19.88	0.14	0.03	0.12
MgO	1.07	2.07	2.54	2.64	9.01	8.42	8.79	0.00	0.00	0.00
MnO	6.42	0.91	4.93	4.70	0.21	0.30	0.23	0.00	0.05	0.00
CaO	6.87	5.99	2.45	2.25	0.11	0.13	0.12	5.10	5.27	4.54
Na_2O	0.00	0.00	0.00	0.00	0.05	0.08	0.12	8.74	8.69	8.87
K_2O	0.02	0.00	0.00	0.00	9.17	8.78	8.73	0.04	0.14	0.10
Cr_2O_3	0.00	0.03	0.02	0.00	0.04	0.09	0.02	0.08	0.04	0.02
H_2O	0.00	0.00	0.00	0.00	3.95	4.00	3.99	0.00	0.00	0.00
Total	102.15	102.23	101.96	101.76	99.97	99.77	100.21	102.61	102.71	101.91
Si	2.958	2.952	2.970	2.968	2.667	2.674	2.682	2.745	2.737	2.773
$Al^{(iv)}$	0.042	0.048	0.030	0.032	1.333	1.326	1.318	1.255	1.263	1.227
$Al^{(vi)}$	2.019	2.011	2.045	2.039	0.455	0.573	0.472	0.008	0.011	0.013
Ti	0.002	0.000	0.000	0.002	0.097	0.106	0.133	0.002	0.000	0.001
Fe^{3+}	0.023	0.036	0.000	0.001	0.000	0.000	0.000	0.000	0.000	0.000
Fe^{2+}	1.821	2.146	2.111	2.137	1.298	1.187	1.248	0.005	0.001	0.004
Mg	0.126	0.242	0.299	0.311	1.018	0.941	0.984	0.000	0.000	0.000
Mn	0.428	0.061	0.329	0.315	0.013	0.019	0.015	0.000	0.002	0.000
Ca	0.580	0.504	0.207	0.191	0.009	0.010	0.010	0.236	0.244	0.211
Na	0.000	0.000	0.000	0.000	0.008	0.011	0.018	0.731	0.727	0.746
K	0.002	0.000	0.000	0.000	0.886	0.840	0.836	0.002	0.008	0.006
Cr	0.000	0.002	0.001	0.000	0.003	0.005	0.001	0.003	0.001	0.001
O	2.000	12.000	12.000	12.000	10.000	10.000	10.000	8.000	8.000	8.000
OH,F	0.000	0.000	0.000	0.000	2.000	2.000	2.000	0.000	0.000	0.000
F/F+M	0.936	0.900	0.876	0.873	0.560	0.558	0.559			
X_{Alm}	0.632	0.730	0.717	0.724						
X_{Pyr}	0.041	0.081	0.101	0.105						
X_{Spee}	0.139	0.020	0.112	0.107						
X_{Gros}	0.188	0.169	0.070	0.065						
X_{An}								0.243	0.249	0.219

Analyses of section 224-3, domain 3

	garn cor-c	garn int-b	garn rim-a	garn rim-d	bi-b matr	bi-a cont	bi-c cont	plag a	plag b
SiO_2	37.68	38.00	37.97	37.92	35.37	35.21	35.21	63.14	61.91
Al_2O_3	22.18	22.38	22.39	22.44	20.10	20.50	20.36	23.70	24.41
TiO_2	0.00	0.03	0.06	0.00	2.57	2.41	2.32	0.00	0.00
FeO	29.54	32.15	33.13	32.68	20.09	19.60	19.06	0.02	0.05
MgO	1.06	1.51	2.03	2.96	8.85	8.73	8.60	0.00	0.00
MnO	5.06	1.91	0.98	2.00	0.19	0.10	0.21	0.00	0.00
CaO	6.66	6.72	5.57	4.31	0.09	0.16	0.11	4.27	5.05
Na_2O	0.00	0.00	0.00	0.00	0.31	0.26	0.23	9.02	8.49
K_2O	0.03	0.01	0.02	0.05	9.12	9.27	8.73	0.09	0.10
Cr_2O_3	0.03	0.04	0.07	0.03	0.00	0.10	0.03	0.05	0.02
H_2O	0.00	0.00	0.00	0.00	3.99	3.98	3.94	0.00	0.00
Total	102.25	102.74	102.22	102.37	100.68	100.31	98.80	100.29	100.04
Si	2.967	2.968	2.973	2.960	2.655	2.649	2.675	2.781	2.740
$Al^{(iv)}$	0.033	0.032	0.027	0.040	1.345	1.351	1.325	1.219	1.260
$Al^{(vi)}$	2.025	2.029	2.040	2.024	0.434	0.466	0.498	0.011	0.013
Ti	0.000	0.002	0.003	0.000	0.145	0.136	0.133	0.000	0.000
Fe^{3+}	0.014	0.001	0.000	0.022	0.000	0.000	0.000	0.000	0.000
Fe^{2+}	1.930	2.100	2.170	2.109	1.262	1.233	1.211	0.001	0.002
Mg	0.125	0.175	0.237	0.344	0.990	0.979	0.974	0.000	0.000
Mn	0.337	0.126	0.065	0.132	0.012	0.006	0.013	0.000	0.000
Ca	0.562	0.562	0.467	0.360	0.007	0.013	0.009	0.202	0.240
Na	0.000	0.000	0.000	0.000	0.045	0.038	0.033	0.770	0.729
K	0.003	0.001	0.002	0.005	0.874	0.890	0.846	0.005	0.005
Cr	0.002	0.002	0.004	0.002	0.000	0.006	0.002	0.002	0.001
O	12.000	12.000	12.000	12.000	10.000	10.000	10.000	8.000	8.000
OH,F	0.000	0.000	0.000	0.000	2.000	2.000	2.000	0.000	0.000
F/F+M	0.940	0.923	0.902	0.861	0.560	0.557	0.554		
X_{Alm}	0.655	0.709	0.738	0.718					
X_{Pyr}	0.042	0.059	0.081	0.116					
X_{Spee}	0.114	0.043	0.022	0.044					
X_{Gros}	0.189	0.190	0.159	0.121					
X_{An}								0.206	0.246

Analyses of section 652-6, domain 1

	garn cor-c	garn int-b	garn rim-a	garn rim-d	bi-c matr	bi-a cont	bi-b cont	plag
SiO_2	38.25	38.93	39.04	38.79	38.58	38.48	38.55	63.24
Al_2O_3	22.43	22.84	22.94	22.96	18.06	18.68	17.67	26.45
TiO_2	0.00	0.00	0.04	0.00	1.98	1.31	1.59	0.02
FeO	33.43	32.67	32.32	32.28	14.11	15.60	15.30	0.04
MgO	3.57	5.33	5.84	6.07	15.50	14.15	14.98	0.00
MnO	0.44	0.13	0.40	0.48	0.00	0.04	0.00	0.00
CaO	4.40	3.13	2.42	2.14	0.11	0.09	0.09	6.46
Na_2O	0.00	0.00	0.00	0.00	0.16	0.17	0.31	6.42
K_2O	0.01	0.00	0.04	0.00	7.47	7.21	7.50	0.02
Cr_2O_3	0.05	0.09	0.03	0.03	0.00	0.05	0.00	0.00
H_2O	0.00	0.00	0.00	0.00	4.14	4.11	4.11	0.00
Total	102.59	103.12	103.08	102.76	100.11	99.89	100.11	102.65
Si	2.968	2.974	2.975	2.965	2.792	2.802	2.808	2.713
$Al^{(iv)}$	0.032	0.026	0.025	0.035	1.208	1.198	1.192	1.287
$Al^{(vi)}$	2.019	2.030	2.037	2.034	0.332	0.406	0.324	0.051
Ti	0.000	0.000	0.002	0.000	0.108	0.072	0.087	0.001
Fe^{3+}	0.011	0.002	0.000	0.006	0.000	0.000	0.000	0.000
Fe^{2+}	2.158	2.084	2.060	2.057	0.854	0.950	0.932	0.001
Mg	0.413	0.607	0.663	0.692	1.672	1.536	1.626	0.000
Mn	0.029	0.008	0.026	0.031	0.000	0.002	0.000	0.000
Ca	0.366	0.256	0.198	0.175	0.009	0.007	0.007	0.297
Na	0.000	0.000	0.000	0.000	0.023	0.024	0.044	0.534
K	0.001	0.000	0.004	0.000	0.690	0.670	0.697	0.001
Cr	0.003	0.006	0.002	0.002	0.000	0.003	0.000	0.000
O	12.000	12.000	12.000	12.000	10.000	10.000	10.000	8.000
OH,F	0.000	0.000	0.000	0.000	2.000	2.000	2.000	0.000
F/F+M	0.840	0.775	0.757	0.749	0.338	0.382	0.364	
X_{Alm}	0.729	0.705	0.699	0.697				
X_{Pyr}	0.139	0.205	0.225	0.234				
X_{Spes}	0.010	0.003	0.009	0.010				
X_{Gros}	0.123	0.087	0.067	0.059				
X_{An}								0.357

Analyses of section 652-6, domain 2

	garn cor-b	garn rim-a	garn rim-c	bi-b matr	bi-a cont	plag
SiO_2	38.42	38.94	38.86	38.80	38.20	60.89
Al_2O_3	22.69	22.94	22.95	18.87	18.76	25.52
TiO_2	0.00	0.00	0.00	1.62	1.51	0.00
FeO	32.25	31.65	31.76	12.84	14.71	0.04
MgO	3.56	5.63	6.21	15.77	15.25	0.00
MnO	1.23	0.47	0.60	0.03	0.08	0.02
CaO	5.10	2.93	2.49	0.05	0.05	6.27
Na_2O	0.00	0.00	0.00	0.37	0.13	7.55
K_2O	0.01	0.02	0.01	7.33	7.74	0.05
Cr_2O_3	0.00	0.00	0.02	0.09	0.03	0.00
H_2O	0.00	0.00	0.00	4.16	4.14	0.00
Total	103.26	102.58	102.90	99.94	100.60	100.35
Si	2.957	2.979	2.963	2.792	2.762	2.691
$Al^{(vi)}$	0.043	0.021	0.037	1.208	1.238	1.309
$Al^{(iv)}$	2.016	2.048	2.025	0.392	0.362	0.020
Ti	0.000	0.000	0.000	0.088	0.082	0.000
Fe^{3+}	0.030	0.000	0.012	0.000	0.002	0.000
Fe^{2+}	2.044	2.025	2.011	0.773	0.887	0.001
Mg	0.408	0.642	0.706	1.691	1.644	0.000
Mn	0.080	0.031	0.039	0.002	0.005	0.001
Ca	0.421	0.240	0.204	0.004	0.004	0.297
Na	0.000	0.000	0.000	0.051	0.018	0.647
K	0.001	0.002	0.001	0.673	0.714	0.003
Cr	0.000	0.000	0.001	0.005	0.002	0.000
O	12.000	12.000	12.000	10.000	10.000	8.000
OH,F	0.000	0.000	0.000	2.000	2.000	0.000
F/F+M	0.836	0.759	0.741	0.314	0.351	
X_{Alm}	0.695	0.689	0.681			
X_{Pyr}	0.137	0.219	0.238			
X_{Spes}	0.268	0.011	0.013			
X_{Gros}	0.141	0.082	0.069			
X_{An}						0.314

Analyses of section 652-6, domain 3

	garn cor-d	garn int-c	garn rim-a	garn rim-b	bi-b matr	bi-a cont	plag
SiO_2	37.47	37.47	37.99	38.03	38.08	37.43	62.56
Al_2O_3	22.19	22.21	22.36	22.41	17.74	18.01	26.14
TiO_2	0.00	0.00	0.03	0.00	1.41	0.95	0.00
FeO	33.76	32.70	31.93	30.61	16.96	17.16	0.14
MgO	3.65	4.40	5.60	5.61	14.12	14.73	0.00
MnO	0.32	0.22	0.35	0.25	0.00	0.00	0.02
CaO	3.38	3.24	2.44	3.73	0.08	0.13	6.53
Na_2O	0.00	0.00	0.00	0.00	0.35	0.18	7.72
K_2O	0.00	0.00	0.00	0.01	7.52	6.93	0.00
Cr_2O_3	0.07	0.07	0.00	0.00	0.07	0.00	0.00
H_2O	0.00	0.00	0.00	0.00	4.09	4.08	0.00
Total	100.84	100.31	100.70	100.65	100.41	99.60	103.12
Si	2.961	2.960	2.968	2.964	2.789	2.746	2.691
$Al^{(iv)}$	0.039	0.040	0.032	0.036	1.211	1.254	1.309
$Al^{(vi)}$	2.028	2.028	2.027	2.023	0.321	0.302	0.017
Ti	0.000	0.000	0.002	0.000	0.077	0.051	0.000
Fe^{3+}	0.007	0.011	0.015	0.017	0.000	0.153	0.000
Fe^{2+}	2.223	2.149	2.070	1.976	1.039	0.883	0.005
Mg	0.430	0.518	0.652	0.652	1.542	1.610	0.000
Mn	0.021	0.014	0.023	0.017	0.000	0.000	0.001
Ca	0.286	0.274	0.204	0.311	0.006	0.010	0.301
Na	0.000	0.000	0.000	0.000	0.050	0.026	0.644
K	0.000	0.000	0.000	0.001	0.703	0.648	0.000
Cr	0.005	0.004	0.000	0.000	0.004	0.000	0.000
O	12.000	12.000	12.000	12.000	10.000	10.000	8.000
OH,F	0.000	0.000	0.000	0.000	2.000	2.000	0.000
F/F+M	0.838	0.807	0.762	0.753	0.402	0.392	
X_{Alm}	0.752	0.728	0.703	0.670			
X_{Pyr}	0.145	0.175	0.220	0.219			
X_{Spes}	0.007	0.005	0.008	0.006			
X_{Gros}	0.096	0.092	0.069	0.105			
X_{An}							0.319

Analyses of section 744, domain 1

	garn cor-d	garn int-c	garn rim-a	garn rim-b	bi-c matr	bi-b cont	bi-a core
SiO_2	37.58	37.42	37.55	37.64	36.24	36.56	35.74
Al_2O_3	22.10	22.07	22.17	22.27	19.99	18.95	19.22
TiO_2	0.00	0.00	0.00	0.00	2.19	1.67	1.50
FeO	32.14	32.47	30.86	31.30	17.87	19.66	20.36
MgO	4.17	3.42	3.80	3.65	10.64	10.22	9.30
MnO	2.73	3.42	3.98	4.64	0.25	0.17	0.31
CaO	2.09	1.94	2.08	1.69	0.13	0.09	0.09
Na_2O	0.00	0.00	0.00	0.00	0.23	0.15	0.26
K_2O	0.04	0.01	0.00	0.03	8.30	8.31	8.14
Cr_2O_3	0.00	0.00	0.02	0.02	0.00	0.00	0.05
H_2O	0.00	0.00	0.00	0.00	4.03	3.99	3.93
Total	100.86	100.75	100.48	101.25	99.88	99.78	98.92
Si	2.967	2.972	2.976	2.970	2.697	2.745	2.721
$Al^{(iv)}$	0.033	0.028	0.024	0.030	1.303	1.255	1.279
$Al^{(vi)}$	2.024	2.038	2.047	2.041	0.451	0.422	0.446
Ti	0.000	0.000	0.000	0.000	0.122	0.094	0.086
Fe^{3+}	0.017	0.000	0.000	0.000	0.000	0.000	0.000
Fe^{2+}	2.104	2.156	2.045	2.066	1.112	1.235	1.296
Mg	0.490	0.404	0.449	0.430	1.181	1.144	1.056
Mn	0.183	0.230	0.267	0.310	0.016	0.011	0.020
Ca	0.177	0.165	0.177	0.143	0.011	0.007	0.008
Na	0.000	0.000	0.000	0.000	0.033	0.021	0.039
K	0.004	0.001	0.000	0.003	0.788	0.796	0.791
Cr	0.000	0.000	0.001	0.001	0.000	0.000	0.003
O	12.000	12.000	12.000	12.000	10.000	10.000	10.000
OH,F	0.000	0.000	0.000	0.000	2.000	2.000	2.000
F/F+M	0.812	0.842	0.820	0.828	0.485	0.519	0.551
X_{Alm}	0.714	0.730	0.696	0.701			
X_{Pyr}	0.165	0.137	0.153	0.146			
X_{Spes}	0.062	0.078	0.091	0.105			
X_{Gros}	0.060	0.056	0.060	0.048			

Analyses for section 744, domain 2

	garn cor-c	garn rim-a	garn rim-b	bi-c matr	bi-b cont	bi-a cont
SiO_2	37.80	37.57	37.45	36.14	36.46	36.68
Al_2O_3	22.28	22.09	22.13	20.26	21.06	20.11
TiO_2	0.00	0.06	0.02	2.01	1.40	1.96
FeO	31.32	31.07	31.09	18.53	17.83	17.63
MgO	4.98	3.96	4.02	10.60	10.15	11.02
MnO	2.29	3.57	2.78	0.19	0.22	0.22
CaO	2.48	2.36	2.88	0.16	0.10	0.13
Na_2O	0.03	0.03	0.00	0.37	0.39	0.29
K_2O	0.02	0.00	0.02	8.20	8.17	8.01
Cr_2O_3	0.00	0.07	0.03	0.00	0.00	0.02
H_2O	0.00	0.00	0.00	4.04	4.04	4.05
Total	101.20	100.77	100.42	100.58	99.83	100.12
Si	2.956	2.968	2.965	2.679	2.706	2.712
$Al^{(iv)}$	0.044	0.032	0.035	1.321	1.294	1.288
$Al^{(vi)}$	2.010	2.025	2.030	0.449	0.549	0.465
Ti	0.000	0.003	0.001	0.112	0.078	0.109
Fe^{3+}	0.040	0.013	0.005	0.000	0.000	0.000
Fe^{2+}	2.004	2.038	2.054	1.149	1.107	1.090
Mg	0.581	0.466	0.475	1.171	1.123	1.214
Mn	0.152	0.239	0.186	0.012	0.014	0.014
Ca	0.208	0.200	0.244	0.012	0.008	0.010
Na	0.004	0.005	0.000	0.054	0.057	0.042
K	0.002	0.000	0.002	0.775	0.774	0.755
Cr	0.000	0.004	0.002	0.000	0.000	0.001
O	12.000	12.000	12.000	10.000	10.000	10.000
OH,F	0.000	0.000	0.000	2.000	2.000	2.000
F/F+M	0.779	0.815	0.812	0.495	0.474	0.496
X_{Alm}	0.685	0.694	0.695			
X_{Pyr}	0.195	0.158	0.160			
X_{Spes}	0.051	0.081	0.063			
X_{Gros}	0.070	0.068	0.082			

Analyses of section 744, domain 3

	garn cor-b	garn int-d	garn rim-a	garn rim-c	bi-a cont	plag a	plag b
SiO_2	38.25	38.02	37.76	37.83	36.34	60.49	60.53
Al_2O_3	22.32	22.42	22.28	22.40	21.21	25.18	24.80
TiO_2	0.00	0.07	0.06	0.00	1.70	0.00	0.00
FeO	31.61	31.81	30.80	31.45	16.32	0.00	0.05
MgO	4.81	4.68	3.19	3.56	10.84	0.00	0.00
MnO	2.30	2.26	5.24	4.67	0.17	0.00	0.00
CaO	2.37	2.44	2.30	2.14	0.09	6.02	5.95
Na_2O	0.00	0.00	0.00	0.00	0.29	7.72	7.63
K_2O	0.01	0.00	0.00	0.02	7.72	0.09	0.01
Cr_2O_3	0.00	0.06	0.00	0.03	0.03	0.07	0.05
H_2O	0.00	0.00	0.00	0.00	4.03	0.00	0.00
Total	101.67	101.76	101.64	102.10	98.73	99.39	99.02
Si	2.979	2.963	2.972	2.963	2.701	2.700	2.709
$Al^{(iv)}$	0.021	0.037	0.028	0.037	1.299	1.300	1.291
$Al^{(vi)}$	2.027	2.022	2.039	2.031	0.559	0.014	0.016
Ti	0.000	0.004	0.004	0.000	0.095	0.000	0.000
Fe^{3+}	0.005	0.005	0.004	0.009	0.000	0.000	0.000
Fe^{2+}	2.053	2.067	2.024	2.050	1.014	0.000	0.002
Mg	0.559	0.543	0.374	0.415	1.201	0.000	0.000
Mn	0.152	0.149	0.350	0.310	0.011	0.000	0.000
Ca	0.197	0.204	0.194	0.179	0.007	0.288	0.285
Na	0.000	0.000	0.000	0.000	0.041	0.668	0.662
K	0.001	0.000	0.000	0.002	0.732	0.005	0.001
Cr	0.000	0.004	0.000	0.002	0.002	0.003	0.002
O	12.000	12.000	12.000	12.000	10.000	8.000	8.000
OH,F	0.000	0.000	0.000	0.000	2.000	0.000	0.000
F/F+M	0.786	0.792	0.844	0.832	0.458		
X_{Alm}	0.694	0.698	0.688	0.695			
X_{Pyr}	0.188	0.183	0.127	0.140			
X_{Spes}	0.051	0.050	0.119	0.105			
X_{Gros}	0.066	0.069	0.066	0.060			
X_{An}						0.300	0.301